Development and control of a robotic system for no-scar surgery

Antonio de Donno

UNIVERSITÉ DE STRASBOURG

ÉCOLE DOCTORALE ED 269 – Mathématiques, Sciences de l'Information et de l'Ingénieur

CNRS - ICube, Equipe AVR (Automatique, Vision et Robotique)

THÈSE présentée par :

Antonio DE DONNO

soutenue le : **13 décembre 2013**

pour obtenir le grade de : **Docteur de l'université de Strasbourg**

Discipline/ Spécialité : Robotique

Development and control of a robotic system for no-scar surgery

THÈSE dirigée par :

M DE MATHELIN Michel	Professeur, Université de Strasbourg

RAPPORTEURS :

Mme MENCIASSI Arianna	Professeur, Scuola Superiore Sant'Anna, Pise (Italie)
M SZEWCZYK Jérôme	Professeur, Polytech Paris - UPMC

AUTRES MEMBRES DU JURY :

M CINQUIN Philippe	Professeur, Faculté de Médecine, CHU Grenoble
M NAGEOTTE Florent	Maître de Conférences, Université de Strasbourg

Development and control of a robotic system for no-scar surgery

Antonio DE DONNO

Development and control of a robotic system for no-scar surgery

Résumé

La chirurgie sans cicatrices, visant à réaliser des opérations chirurgicales sans cicatrices visibles, est l'avant-garde dans le domaine de la chirurgie mini-invasive. L'absence d'instruments adéquats est l'un des freins à son utilisation en routine clinique. Dans ce contexte, nous introduisons un nouveau robot chirurgical téléopéré, composé d'un endoscope et de deux instruments flexibles, avec 10 DDL motorisés. Cette thèse explore les différentes façons de contrôler le système. La cinématique du robot est analysée et différentes stratégies de contrôle maître/esclave, allant du contrôle articulaire au Cartésien, sont proposées. Ces stratégies ont été testés sur un simulateur virtuel ainsi que sur le système réel en laboratoire et en ex-vivo. Les résultats montrent qu'un seul utilisateur est capable de contrôler le robot et d'effectuer des tâches complexes en utilisant deux interfaces haptiques.

Mots-clés: robotique chirurgicale, téléopération, interfaces haptiques, simulation virtuelle.

Résumé en anglais

No-scar surgery, which aims at performing surgical operations without visible scars, is the vanguard in the field of Minimally Invasive Surgery (MIS). The lack of adequate instrumentation is one of the issues to its clinical routine use. In this context, we introduce a novel teleoperated surgical robot, consisting of an endoscope and two flexible instruments, with 10 motorized DOFs. This thesis investigates the possibilities to control the system. The robot kinematics is analyzed, and different master/slave control strategies, ranging from joint to Cartesian control, are proposed. These strategies have been tested on a specifically developed virtual simulator and on the real system in laboratory and ex-vivo experiments. The results show that a single user is capable to control the robotic system and to perform complex tasks by means of two haptic interfaces.

Keywords: surgical robotics, teleoperation, haptic interfaces, virtual simulation.

Ciao, Nonni.

Acknowledgments

Obtaining the highest academic degree is an achievement that makes me proud and happy: after years of university studies, I feel that an important chapter of my life is now concluded, and the celebration of my doctorate represents the crowning of one of my big ambitions.

But, as usually, an achieved success should and must be shared with those who collaterally contributed to it, making it possible or actively participating in its development. For this reason, I will use the next few lines to thank all the persons involved in this event, apologizing in advance with those who I will involuntarily forget to mention.

First of all, I have to express my gratitude to the members of my jury: prof. Philippe Cinquin, prof. Arianna Menciassi and prof. Jérôme Szewczyk. I appreciated their involvement in the evaluation of my work, and it was an honor for me to be judged by some of the most expert researchers in the field of Medical robotics.

I am deeply grateful to my thesis director, prof. Michel de Mathelin, for allowing me to participate in such interesting project and to constantly accompanying and guiding me during the last three years. Since our first contact, he always demonstrated me trust and esteem, and I hope that the results of our collaboration made him pleased of his choice.

I would like to sincerely thank my thesis supervisor, Florent Nageotte: I learned a lot working with him, and I had the possibility to discover his many positive sides, both professionals and personals. His support during my first phase of adaptation was very important for me, and I also appreciated the freedom he left me in exploring different and new tracks throughout my PhD work.

I cannot imagine that I would obtained the results presented in this thesis without the fundamental contribution of Philippe Zanne and Lucile Zorn. They always had the proper answer for each problem, and their patience and kindness were the added values to their professional skills. Together with Florent, they form a strong work group capable of impressive results, and I am delighted that I had the opportunity to work with them.

A big thank you goes to all the members of the equipe, both permanents and PhD students, for the good atmosphere that they were able to create in the lab. It

was very nice to know each of them and to share good moments together. I want to thank Laurent Goffin for all his work done on the first version of the simulator, but also for the interesting discussions we often had. Thanks to all the PhD students, former (Bérengère, Mathieu, Lennart, Houssem, Salih, Xavier, Fadi, Julien) and current (sorry guys, you are too much to cite each of you!), with whom I passed enjoyable moments inside and outside the lab. Let me tell good luck to the students of my promotion, Markus, Laure and Ryad, for their upcoming defenses: it is your turn!

During these years in Strasbourg I met many nice and interesting persons, and it is also thank to them if these years passed well! Particularly, I am very thankful to Julie for all the support, material and personal, that she was able to give me. Her presence was very important, especially during some difficult periods, and I am also glad to met a person internally so rich.

Non ringrazierò mai a sufficienza i miei genitori per tutto ciò che hanno fatto, fanno e continueranno a fare per me. Anche se siamo lontani geograficamente, riescono sempre a trasmettermi il loro affetto incondizionato e il loro sostegno in ogni decisione che prendo. Per me rappresentano un punto di riferimento fisso, e se sono arrivato fin qui gran parte del merito è anche loro. Spero che questo ulteriore traguardo li possa rendere orgogliosi di me. Vi voglio bene.

Questa tesi è dedicata alla memoria dei miei nonni, Domenico e Maria, che dopo una vita trascorsa insieme hanno deciso di continuare a vegliare su di me da qualche altro luogo. Mi mancate moltissimo, vi porto nel mio cuore.

Contents

Part I

Main Thesis

1

Preface

After many years of experiments and skepticism between late 1980s and 1990s, nowadays Minimally Invasive Surgery (MIS) is the *de facto* standard in surgical procedures. The improved surgical expertise, together with specifically developed tools, allowed the advancement of MIS procedures: operations such as cholecystectomy, nissen fundoplication and appendectomy are now performed routinely with the use of laparoscopic techniques [172]. The advantages of a minimally invasive approach are several, mainly focused on the patient: compared to laparotomies procedures, the equivalent laparoscopic interventions reduce the trauma of the surgical scars, decrease the volume of blood loss during the operation, reduce the post-operative pain related to the cicatrization and allow shorter hospitalization times and faster rehabilitations. On the contrary, MIS procedures force surgeons to deal with new constraints: there is no longer a direct contact between the surgeon and the patient, being the manual palpation of organs and tissues substituted by their manipulation by means of instruments. Moreover, the vision of anatomical structures is achieved with bidimensional images, captured by a miniaturized camera inserted inside the body and sent to a monitor. In the last 25 years, surgeons have learned how to operate with a MIS approach, where instruments and imaging systems are inserted through several skin incisions, vision is provided by an endoscopic camera and there is no haptic feedback that could guide the surgeon gesture.

Mastery of these procedures has led to the development of more complex laparoscopic approaches, nowadays referred as *no-scar surgery*, that have the aim to reduce as much as possible the surgical invasiveness. The idea to perform surgeries with no violation of the externally visible body skin is the next frontier in MIS. This ambitious goal is becoming possible also thanks to two new surgical approaches:

- NOTES (Natural Orifice Transluminal Endoscopic Surgery), which exploits the natural orifices of the human body as access ports for the internal cavities: in this case, no external incisions are performed, and the only scar is inside the body.
- LESS (Laparo-Endoscopic Single-site Surgery), in which a single access port is used to insert the whole instrumentation set: the access port is chosen in a

hidden part of the body (typically the umbilicus) in such a manner that the performed scar is not visible after the operation.

Compared to standard laparoscopy, both techniques involve an additional advantage for the patient, consisting in the better aesthetic result after the operation. On the contrary, the new constraints imposed to minimize the invasiveness of the surgical operation make its execution harder: triangulation, dexterity and sizes of instruments are largely limited by the single (transluminal or not) access port.

New instrumentation is therefore needed, which has to take account of the particular features of no-scar surgery approaches and, if possible, to try to overcome the inner limitations. Ideally, the perfect instruments for no-scar surgery should be able to pass from a narrow port, reach the target point (which could be located tens of centimeters away from the access port) and then reconfigure themselves for performing the operation. This implies that some compromises should be taken. First, instruments must be as flexible as necessary to adapt their shapes to the anatomical constraints, but rigid enough to properly transmit forces. Moreover, according to the chosen access port, instruments lengths could vary and be longer than those of laparoscopic instruments (especially in transluminal operations), therefore a proper actuation mean capable to transparently transfer the user motion to the instrument tips has to be used. Dexterity could be gained implementing flexible sections in the instruments structures, trying to obtain tools that are highly adaptable to tortuous environments. But, the more complex the instruments design is, the more their user interfaces become complicated in the use.

Nowadays, robotics is pervading many working and social fields, helping or substituting humans in performing procedures that could be strenuous, dangerous, tiring or phisically not feasible. The advantages in using robotics are several: compared to the manual procedure, a task can be performed with more precision, repeatability and ergonomics when using robotics assistance. Except for the case of mobile robots, a robot is typically confined in a bounded space, in order not to be dangerous when in movement, and it could be pre-programmed or numerically controlled, according to the task that it has to execute.

Surgery is a field that is going to exploit the potential benefits of robotics: from the first trials in which a robot served as an instrument steady holder, nowadays a surgical robot could intervene by guiding the surgeon hands, in order to avoid tools motions in zones considered unsafe, filtering their movements, to reduce or magnify the gesture and to compensate the natural hands tremor, and replicating the surgeon commands. Rather than operating upright and, sometimes, with poor ergonomics, a surgical robot could offer an ergonomic interface, specifically conceived to control the robot motions without physical efforts and in an intuitive way.

Starting from mid 1990s, several robotics prototypes have been proposed for laparoscopic surgery, and nowadays mature commercial solutions exist for this kind of surgeries. Robotics system for no-scar surgery, instead, are still in the experimental phase: the first prototypes appeared in early 2000s, after the initial attempts with manual instrumentation, but so far a complete, functional and commercial solution for no-scar surgeries still does not exist for multiple reasons.

NOTES and LESS are two techniques common in the approach, but very different in the execution: while in LESS rigid instrumentation could be used if the access port is near the zone to be treated, NOTES forcedly requires long and flexible instrumentation. Moreover, size and shape of a NOTES platform should be adapted to the particular orifice used as access port.

In this context, we are proposing a novel flexible robot, named STRAS (Single access and Transluminal Robotic Assistant for Surgeons), specifically developed for LESS or close transluminal operations. STRAS is a flexible endoscopic guide that permits to introduce two flexible instruments (a grasper and an electric hook) inside the body passing through a single access port. Endoscope and instruments are provided with flexible articulated distal sections that allow their deflection movements, thus enlarging the system workspace and offering more dexterity. The instruments are inserted inside the main endoscope from its proximal side and, thanks to two foldable flaps implemented on the endoscope head, their channels are deviated on the distal side in order to obtain triangulation. STRAS has a total of 10 actuated Degrees Of Freedom (DOFs), organized as follows:

- 3 DOFs from the main endoscope, which can translate forward and backward, and its actuated distal section can be bent in two orthogonal directions;
- 3 DOFs from each instrument, which can translate, rotate and deflect in one direction;
- one additional DOF for the opening and closing of the grasper.

For how it is composed, STRAS has a tree-like architecture, with the instruments positions that depend on the endoscope movements. The presence of flexible continuum sections does not allow a kinematics description of the system with standard methods, therefore a particular modeling should be adopted.

We developed STRAS as a teleoperated robot, in which the robotized endoscope and instruments are the slave system. The master manipulator, instead, is composed by two haptic interfaces that offer 7 DOFs each. The first issue to be addressed, therefore, is to find a proper mapping between master and slave systems, since they have different kinematics. This problematic is strictly linked to the choice of a control strategy scheme for the slave robot, *i.e.* the control law that permits to transform the desired references, given from the user by means of the master interfaces, in low-level references for the robot actuators. Several choices for both mappings and control strategy schemes are possible, and their suitability for the practical use largely depends on the tasks that have to be performed and on the users experience.

In this case, a virtual environment in which testing the various solutions can be advantageous, since it could permit to study the system behavior in several different conditions. Moreover, a virtual simulator of the system can represent a good training tool for the final users, which can train on the different control strategies proposed and choose their preferred. They can also better understand the system features and improve their skills before using the real robot. But in order to be effective, a virtual simulator must closely replicate the behavior of the simulated system, including its non-linearities and the interactions with the surrounding environment. On the other hand, the complexity of the system model employed in the virtual simulator should be proportionate to the computational

capacities of the computer that runs the simulator. Therefore, a proper compromise between level of realism and computational load must be found.

The purpose of this manuscript is to present the work performed by the author between October 2010 and October 2013 in the Equipe AVR (Automatique, Vision et Robotique) of the ICube laboratory at the University of Strasbourg, France. This work, led under the direction of Prof. Michel de Mathelin and supervised by Florent Nageotte, ascribes inside the ISIS project. This project, proposed in conjunction with industrial (Karl Storz Gmbh, Tuttlingen, Germany) and medical (IRCAD, Strasbourg, France) partners and with the financial support of the Alsace Biovalley Cluster (Illkirch, France), aims at developing a novel flexible robot for no-scar surgery.

The following chapters will be organized as follows:

- In chapter 2 a presentation of the medical context will be proposed. First, an historical introduction will present the milestones in the development and evolution of endoscopy, laparoscopy and, finally, no-scar surgery techniques. Afterwards, a discussion about the most important requirements that instruments developed for no-scar surgery should have will be proposed, before introducing the state of the art of surgical instrumentation. In this review, the commercial and experimental systems for no-scar surgery hitherto proposed will be analyzed, trying to summarize their current limitations.
- In chapter 3 we will discuss about the introduction of robotics in surgery. After introducing the most known and accepted taxonomies of surgical robots, the historical evolution of robotics applications in surgery will be briefly presented. This evolution will be concluded by the state of the art of robotic systems proposed for no-scar surgery, including the main experimental platforms presented in the last years by research groups worldwide. The chapter will end with a detailed discussion about STRAS (Single access and Transluminal Robotic Assistant for Surgeons), the novel flexible robot developed in our lab. In this discussion, we will show its main components, the work done to robotize the system and the proposed user workstation.
- Chapter 4 will be consecrated to the kinematic description of STRAS. Unlike standard robotic manipulators, STRAS is composed by flexible sections that could not be described kinematically with standard methods: we will introduce, therefore, a specific modelization for continuum sections and we will show how the kinematic model of STRAS is computed. The workspace analysis and the study of the system singularities will conclude the first part of the chapter. The teleoperation of STRAS is the main topic of the second part: we will present the proposed control strategies for the slave robot and the master/slave mappings, together with some solutions for the execution of automatic movements that could help surgeons during the system use.
- In chapter 5 we will present the work done for the development of a virtual simulator for STRAS. After an introduction about the existing simulators in medicine and surgery, we will focus on the challenges to address when implementing a virtual simulator for the training in no-scar surgery techniques. The initial aim when developing our virtual simulator was to have a kinematic replica of STRAS: the first version of the simulator allowed us to perform as-

sessment experiments in which we compared the proposed control strategies and we analyzed the corresponding system behavior. Further development toward the aim of implementing a training simulator led to the second version, which includes physical interactions and reproduce typical tasks of surgical training.

- In chapter 6 the experimental results obtained both with the virtual simulators and STRAS will be presented. Together with the first experiments aimed at assessing the proposed control strategies, we will present a comparison between STRAS and its manual version ANUBISCOPE®. A brief discussion about preliminary *ex vivo* tests performed with STRAS will conclude the chapter.
- Chapter 7 will conclude this manuscript discussing about the obtained results, the current system limitations and pointing out the potential perspectives for the further development of STRAS.

2

Medical Context

Contents

2.1 Introduction

Before being anglicized, the original form of the word "Surgery" was *Cheirourgia*. This term, which comes from the ancient Greek (it is composed by *cheir*, "hand", and *ergon*, "work"), indicates the origins of this particular branch of medicine that deals with diseases or pathological processes of different nature (injuries, traumas, scares, fractures, etc.) for the treatment of which it is necessary to intervene with therapeutic methods.

Since humans first learned to make and handle tools, they have employed their talents to develop surgical techniques, each time more sophisticated than the last ones, with the aim to reduce more and more the three principal obstacles that plagued the medical profession from its infancy: bleeding, pain and infection. A better knowledge of the human anatomy and physiology, together with all the technological advancements introduced in surgery, have transformed surgery from a risky "art" into a scientific discipline capable of treating many diseases and conditions. Particularly in the last two centuries, massive changes and improvements in the surgery field led to what we call today *modern surgery*, which encompasses all the surgical techniques that aim to minimize their invasiveness while improving their efficacy. Between mid 1800s and early 1900s, physicians started to discover anaesthesia and sterilization techniques, reducing dramatically the high mortality of surgeries at that period. The other big breakthrough happened in mid 1900s, with the progressive passage from *laparotomy* (from the greek *lapara*, "flank", and

tome, "cut"), generally called "open surgery", to *laparoscopy* (*scopos*, "look at") or, more in general, *endoscopy*. While in laparotomy the surgeon performs a large incision through the abdominal wall to gain access into the abdominal cavity, in endoscopy a small camera and the instrumentation are inserted inside the body through skin incisions or a natural orifice. Laparotomy, normally used for exploration in severely injured patients or for organ transplant, permits to directly see and palpate the internal organs, and represents a very good diagnostic tool with an immediate possibility to treat the disease. On the contrary, as well as for the aesthetic results, the large performed scar leads to massive blood loss during surgery, requires long recovery time and produces an important post-operative pain during the cicatrization phase. All these side effects could be almost completely overcome by reducing the wound size, in other words passing to a minimally invasive approach, in which the surgeon does not have a direct and visual contact with the anatomic zone to be treated, but he/she can see the internal human body only by means of an endoscope.

In this chapter, an introduction of the medical context in which this thesis work ascribes is presented. In sections 2.2 and 2.3 an historical survey (which does not pretend to be exhaustive in all the possible details) will introduce the evolution from the first surgical attempts to the state of the art in minimally invasive surgery. This historical review is a personal revision of several good sources [164] [126] [118] [44]. Every technological evolution needs to be supported by the appropriate tools, so in surgery: the boost towards a minimally invasive approach requests an effort in the development of new and more appropriate instrumentation. In section 2.4, an analysis of the main requirements for minimally invasive instrumentation and an overview of commercially available tools is presented.

2.2 Historical evolution of endoscopy

It is very difficult, if not impossible, to precisely find the first ever endoscopy performed on a human being. Hippocrates (460-375 BC) first described a rectal speculum around 400 BC (see fig. 2.1), and a three-bladed vaginal speculum, dated around 70 BC, was found in the ruins of Pompei, Italy (see fig. 2.2), demonstrating that primitive endoscopic tools were used in Roman medicine [152]. At that time nothing but ambient light was used, so the internal body exploration was mostly limited by the illumination problem.

To find a real advancement in endoscopy it is necessary to wait eighteen centuries: in 1806 Philipp Bozzini (1773-1809), a German physician and obstetrician, published the description of his *Lichtleiter* [18] (literally "Light conductor", from German), a primitive endoscope that permitted to inspect ear, mouth, nasal cavity, rectum and bladder. It was basically an elongated thin funnel with a beeswax candle attached on its proximal end (see fig. 2.3).

Although it was the first attempt to use artificial light in endoscopy, the illumination carried by the candle was insufficient, and there were safety problems for both physician and patient. Moreover, at that period Bozzini's invention was criticized for "undue curiosity" [66]. Unfortunately, Bozzini was not able to improve his Lichtleiter because he died few years later. Anyway, his work inspired other physicians of those days that tried to overcome the first encountered problems. Pierre

Fig. 2.1. Left: Hippocrates. Right: rectal speculum (courtesy of Historical Collections and Services of the Health Sciences Library, University of Virginia).

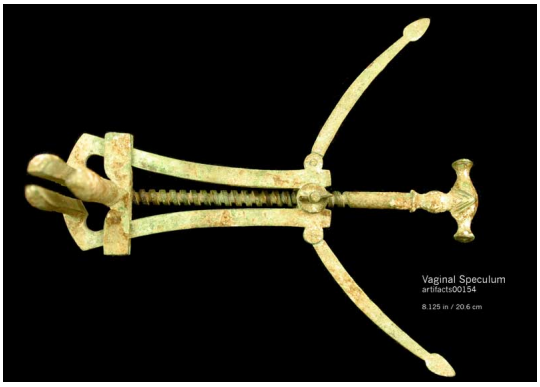

Fig. 2.2. Vaginal speculum found in the ruins of Pompei, Italy (courtesy of Historical Collections and Services of the Health Sciences Library, University of Virginia).

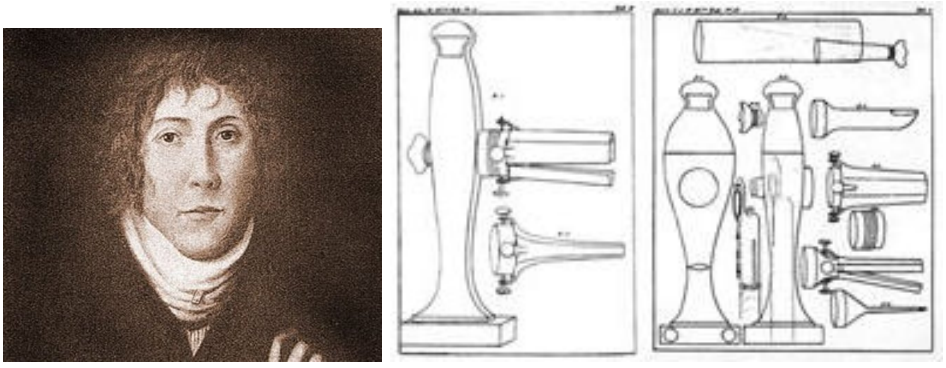

Fig. 2.3. Philipp Bozzini and his Lichtleiter.

Salomon Ségalas (1792-1874), a French urologist, tried to improve the illumination making the funnel of highly polished silver and using mirrors in the light path. He called it *speculum urethro-cystique* [162], because it was mainly designed for inspecting urethra and the interior of bladder. An advancing step was performed in 1853 by Antonin Jean Desormeaux (1815-1894), another French urologist, when

he presented at the *Académie des Sciences* in Paris an improved endoscope that used a kerosene lamp (burning a mixture of alcohol and turpentine) and a concave mirror with a central hole used to reflect the light into the organ (see fig. 2.4). Though Desormeaux's innovations were not big deviations from the design princi-

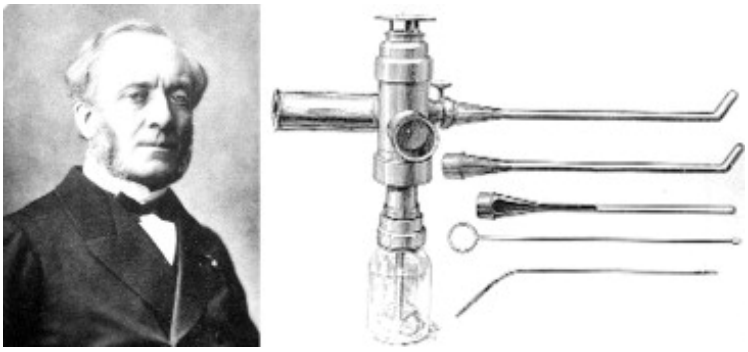

Fig. 2.4. Antonin Jean Desormeaux and his endoscope.

ples established by earlier pioneers, he is credited with coining the word *endoscopy* (originally *endoscopie*, from French) and with constructing the first functional endoscope used into a patient (he removed a papilloma from the patient urethra). This first result proved to the scientific community the value of such instrument as an effective diagnostic tool, but also demonstrated its promising therapeutic possibilities.

The next major breakthrough in the history of endoscopy came with the discovery of electricity and the invention of the electric bulb by Edison. Maximilian Carl-Fredrich Nitze (1848-1906), a German urologist, was the first to place an electrically heated water-cooled platinum wire into the rectum to visualize the transilluminated bladder [146], realizing that "to light up a room one must carry the lamp inside" [74]. His work was promising, but there still were problems related to the poor illumination, limited by the diameter of the funnel, and to the burns caused by the electrical heating. Therefore, he began working in collaboration with optical technicians at the University of Berlin first, then in Vienna with Joseph Leiter, a well-known instrument maker, with the clever ideas to miniaturize a telescope, in order to improve the visibility, and to use the Mignon lamp, a small vacuum lamp derived from the incandescent light bulb, as light source. These two improvements led in 1879 to the Nitze-Leiter cystoscope [129], an improved scope that no longer required cooling system and permitted to easily locate and remove bladder stones (see fig. 2.5). Using his new invention, Nitze became the first to coagulate a bladder papilloma using hot, galvanized wire loops and to take endoscopic photographs [119].

With the advent of the industrial revolution in the early 1900s, several scientists tried to improve the Nitze cystoscope design, and there were the first attempts to produce a commercial endoscope in the United States [148]. Big improvements were achieved for the endoscopic optical system when William K. Otis, an American urologist who visited Nitze in Berlin, produced a new optical system: the *spherical*

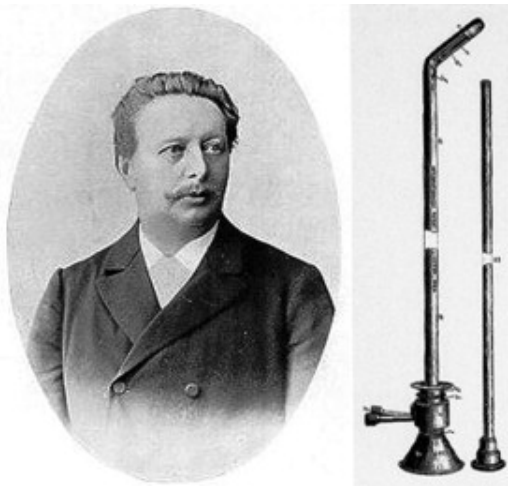

Fig. 2.5. Maximilian Carl-Fredrich Nitze and his endoscope.

prism. This system, patented in 1902, resulted in wide-angle lens cystoscopes that started to be commercialized in 1905 by Reinhold Wappler [134]. The drawback with this new optical technique was the inversion of the image, so in 1907 Zeiss, a Swiss company, developed a prism, still used in many European instruments, which solved this problem and, in addition, produced a vertical, sharp image brighter than before [5].

With the improvements in vision and lighting, physicians were now limited in the human body exploration by the shape and the rigidity of their new endoscopes. In 1881 Jan Mikulicz-Radecki (1850-1905, see fig. 2.7), a Polish-Austrian surgeon, was the first to develop the electric oesophagoscope-gastroscope, a particular endoscope designed with the anatomy of the human finger in mind [117]. It was composed of vertebrated segments of hollow tubes covered with rubber, the tip of which could be angulated or pulled straight controlled by a system of wires located proximally (noted F, see fig. 2.6). This oesophagoscope was then improved by Georg Kelling (1866-1945, see fig. 2.7), a German surgeon credited for the first endoscopic procedure performed on a living dog who had the abdominal cavity insufflated with filtered air [96]. Moreover, Kelling is considered the inventor of the *trocar*, the common access port used in laparoscopy, because in his experiments he inserted the scope in the dog through a small incision in the abdominal wall, while with a second self-made port he established pneumoperitoneum [160]. Between 1901 and 1923, Kelling performed many endoscopic procedures on living human patients in his private clinic, reporting his clinical experience in a 1923 article. Kelling mentioned that his increased use of the scope's diagnostic capabilities was partly influenced by the poor economic situation of Germany after the First World War that made the cost of laparotomies, which required long hospital stay and anaesthesia, prohibitively expensive [73]. Indeed, Kelling came closer than any other practitioner of his days to achieve progresses in the three areas in which laparatomies were then dominating: providing definitive diagnoses, finding and stopping internal haemorrhaging and treating pathologies in the most complete

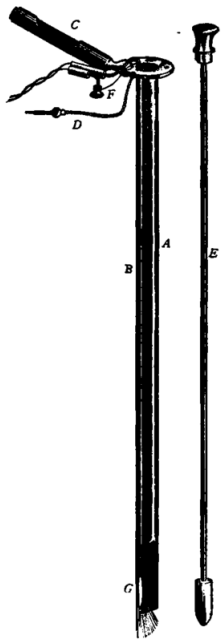

Fig. 2.6. The Oesophagoscope. A: Hollow metal tube, B: Longitudinal groove, C: Handle, D: Plug, E: Obturator, F: Carrier with wires, G: Lamp (reprinted from [48]).

possible way. Though Kelling's work did not completely reach these three objectives, he provided some of the most crucial and groundbreaking insights towards understanding how such goals might be attained endoscopically. In particular, his idea of a flexible oesophagoscope, though ineffective in his own day, was in fact adopted late in the 20th century after fiber optics made such a design concept feasible.

Fig. 2.7. Left: Jan Mikulicz-Radecki. Middle: Georg Kelling. Right: Hans Christian Jacobaeus.

Aware of technology limitations, Kelling unfortunately perceived little future for endoscopic techniques and did not pursue his studies further. From the first trials in 1901 to his last publication in 1923 he did not produce any clinical account about his surgeries, while other physicians were actively involved in exploring new endoscopic procedures. Particularly, Hans Christian Jacobaeus (1879-1937, see fig. 2.7), a Swedish professor of internal medicine, performed in 1910 the world's first thoracoscopic therapeutic procedure in a living human patient [87]. He believed to have performed the world's first laparoscopic case, not still being aware of Kelling's trials (Kelling's report appeared two months later in the same journal). However, Jacobaeus' techniques were quite different from Kelling's ones, because he did not establish pneumoperitoneum before surgeries. One year later he coined the term *laparoscopy* (originally "laparothorakoskopie" from German), recognizing deserving credits to Kelling for the underlying idea, but criticizing him for not having proved practical applications of his method [88]. In general, Jacobaeus produced much more publications than Kelling about laparoscopic procedures he performed, and he established a gold standard in thoracoscopy procedure that lasted at least for the next 15 years.

Although surgeries performed from a natural orifice access are becoming more common only nowadays, the first attempts in this particular field are very dated. Dmitry Oskarovic von Ott (1855-1929), a Russian gynaecologist, is considered the first surgeon in the history of endoscopy (before Kelling by a few months) to successfully view the pelvic organs by the vaginal route in a living human patient using endoscopic principles. He utilized a standard incandescent light bulb with a reflector for gynaecological operations: the light, placed in front of an adjustable mirror, was fastened to the forehead with a band. His technique was based on the principles of posterior colpotomy (from the Greek *kolpos*, "womb", and *tome*, "cut"), a well-known blind procedure in which the surgeon incises the wall of the vagina in order to reach the appendix or the gallbladder. Ott's modified version, which he called *ventroscopy* [194], was presented for the first time in 1901 during the meeting of the Gynaecology and Obstetricial Society in St. Peterburg, Russia. Despite Kelling, Ott used an endoscope without optical lenses. In 1909 he published his first endoscopic inspection of the abdominal cavity with a minilaparotomy technique [195], *i.e.* a laparotomy performed with a reduced incision. Ott is credited also for the first endoscopic procedure performed with the patient in Trendelenburg position, where the body is laid flat on the back (supine position) with the feet higher than the head by 15-30 degrees (it allows better access to the pelvic organs as gravity pulls the intestines away from the pelvis). A part of the surgical community refused to recognize these new procedures as endoscopic, claiming that they all were "a disguised laparotomy" [122]. Also if Ott's work is still far from the modern endoscopic procedures, his visionary mind in this field should be recognized, as he largely contributed to the advancements of minimally invasive surgical techniques.

Within just a few years of Kelling's, Jacobaeus' and Ott's groundbreaking successes, a growing number of physicians from multiple disciplines all across the world were enthusiastic about this promising surgical method. A new generation of American gynaecologists took inspiration from pioneers' works to develop endoscopic techniques toward operative procedures. In 1911, Bertram Moses Bernheim

(1880-1958), an assistant surgeon at John Hopkins University Hospital (Baltimore, MD, USA), performed the first laparoscopy in the United States. Before learning of both Kelling's and Jacobaeus' prior work, Bernheim published his experiences, naming the procedure *organoscopy* [14]. Bernheim was fascinated about this new technique, so he started to report his experiences, also when he met negative outcomes. In one case, he was not able to see a pancreatic carcinoma because of the limited angle of vision imposed by the use of a cystoscope. Despite this, Bernheim reported that the overall diagnostic success rate was very high for laparoscopy. His superiors at the hospital were not convinced about this and encouraged him to abandon the idea. Moreover, the First World War came, medical priorities drastically changed and Bernheim, drifted away from his initial enthusiasm, focused his activity instead on vascular biology.

Since more endoscopic procedures started to be performed, technique limitations and rising deaths rates became especially apparent. The lack of adequate training or equipment, inexperience and improper instrumentation largely influenced efficacy and safety of endoscopy. As well, problems with limited visualization, inability to detect or stop intra-operative haemorrhaging, deaths caused by unpredictable insufflation complications, burns caused by electrocautery, bowel perforations and injuries to major blood vessels still served to scare off would-be practitioners from attempting endoscopic techniques for the first time or investing in their further development. For all these reasons, the efforts in the development of endoscopic techniques during the 1920s decade were concentrated in finding potential solution to these complications.

In 1920, Benjamin Henry Orndoff (1881-1971), an American radiologist, developed a sharp pyramidal tip on the laparoscopic trocar (of the kind still in use today) to facilitate puncture and to minimize damages caused by initial trocar entry [132]. During a surgical procedure, Orndoff was used to switch from looking both into the scope and to an X-ray screen in order to guide his actions, a groundbreaking method precursor of what we call today *interventional radiology*. A year later, the first needle for pneumoperitoneum was introduced by R. Korbsch [100], and Otto Goetze (1886-1957), a German surgeon, published the details of his novel device, the *insufflator* [65]. In 1929, Heinrich Otto Kalk (1895-1973), a German hepatologist and gastroenterologist, solved the field of vision problem, which had been one of the longest standing difficulties afflicting endoscopy (cfr. Bernheim problems in detecting a pancreatic carcinoma). Although a forward-viewing instrument with a viewing angle of 135 degrees had been already introduced two years earlier, Kalk was able to adapt this existing technology into a more practicable and succesful instrument, broading the scope's usefulness and allowing more operative and diagnostic procedures impossible to be performed before [93]. In 1935, Kalk described a dual-trocar technique that facilitated instruments manipulation [91]: though again he was not the first to invent this technique, he was one of the earliest to routinely apply it, as well as to make certain refinements that increased its safety. At that time, an endoscopic biopsy presented a high risk of mortality, because it could only be performed in a nearly blind state using still dangerous electrocauterizing tools. Surgeons of the day believed that only by thoroughly palpating the organs during an exploratory laparotomy one could come to discover the deeply-embedded cancer nodules. Kalk became one of the first ever to

introduce a safe and accurate method for endoscopic liver, gallbladder and kidney biopsies. In 1951 he published one of the largest series of laparoscopic surgeries at that time, reporting on 2000 laparoscopic procedures performed under local anesthesia and, apparently, without a single mortality [92]. These good results moved many surgeons much closer to abandoning exploratory laparotomies and to adopt more and more endoscopic approaches.

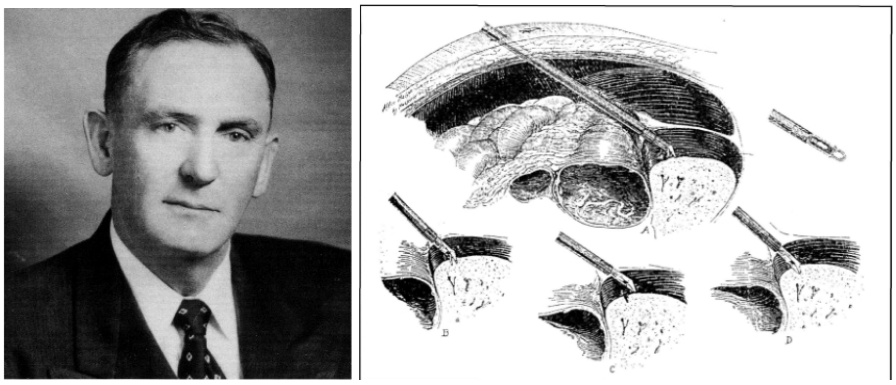

Fig. 2.8. Left: John Caroll Ruddock. Right: picture of a peritoneoscopic biopsy performed by Ruddock (reprinted from [106]).

In the 1930s, Kalk gave a big contribute to the development of endoscopy, largely influencing the surgical techniques in Germany and, more in general, in Europe. At that time, overseas communications were not well developed yet, therefore the American surgeons were not aware of the European progresses. In the same period as Kalk, John Caroll Ruddock (1891-1964), an American internist, is considered the biggest driving force behind laparoscopy's progress and acceptance in the United States. He reported a significant amount of procedures, performing in his lifetime about 5000 laparoscopies, all with low levels of morbidity and mortality [156]. He was also involved in the improvement of endoscopic tools, since he recognized the inner limitations of cystoscopes used in that period. Cystoscopes were designed with optics and other features adapted to the contours of a urethra entry point, so they were not very suitable for abdominal explorations. In 1934, Ruddock modified a cystoscope applying a new optic system, referred as *foreblique visual system*, that allowed for a greater viewing area of abdominal and peritoneal cavities. Ruddock termed his device *peritoneoscope*, and published its description with a clinical set of 200 successful cases [154]. Although Ruddock was not exactly the first to invent this type of optics system (cfr. Kremer and Kalk versions in 1927 and 1929 respectively), he deserves credits for recognizing these disparate technologies and bringing them together into one operative unit. Ruddock realized that a laparoscope with a 45 degrees viewing angle was far superior than the standard with 90 degrees angle found in the optics of cystoscopes. In 1937, Ruddock plugged in a photographic unit to his laparoscope, becoming one of the earliest to experiment with laparoscopic photography. Moreover, he implemented built-

in biopsy forceps to his peritoneoscope, capable of both cutting and coagulating thanks to a bipolar electro-cautery unit [155] (see fig. 2.8).

In the following 20 years, instruments design would remain essentially unchanged, apart from slight variations that several physicians performed on available endoscopes to adapt them to their needs. During these years there were few technology advancements, while the number of procedures impressively increased. Unfortunately, some cases of mortality during endoscopic procedures were reported, enhancing the skepticism of those who always considered endoscopic procedures dangerous. A well-reported problem was due to air embolism caused by insufflation complications. Tolerable pressure, speed of insufflation and constant air volume in the abdomen were concepts still not known, and in many cases established with empirical attempts. An important advance in this particular field occurred in 1938, when Janos Veress (1903-1979), an Hungarian internist, developed a particular needle for the creation of the pneumoperitoneum [192] (see fig. 2.9). The needle had initially been conceived to perform therapeutic pneumothorax in patients suffering from tubercolosis. However, laparoscopists quickly realized its potential as a safer method for creating pneumoperitoneum. The main safety feature was the spring-loaded obturator, which allowed safe insertion and insufflation of the peritoneal cavity: an inner stylet automatically converted the sharping cutting edge to a rounded end incorporating a side hole. The Veress needle, with few minor technological improvements, is still in use today and represents the oldest and most traditional technique to establish the primary port entry in laparoscopy.

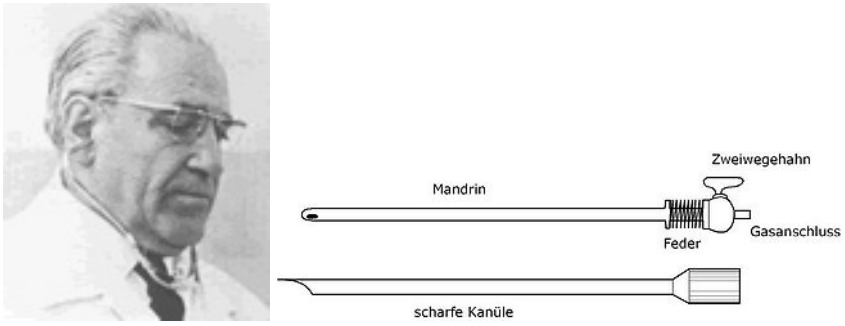

Fig. 2.9. Left: Janos Veress. Right: the Veress needle, composed by a bladed cannula (*scharfe Kanüle*) that contains the stylet (*Mandrin*). At the stylet top, a spring (*Feder*) controls its retraction and a two-way cock (*Zweiwegehahn*) regulates the gas insufflation from the connection (*Gasanschluss*) (reproduction from `http://en.wikipedia.org`).

In the 1950s the illumination was still one of the biggest problems affecting endoscopy. In 1952, Max Fourestier (1907-1986), a French physician, together with A. Gladu and J. Vulmiere introduced the use of a quartz light rod to replace the distal lamp in the bronchoscope [55]. This was the first documented use of fiberglass light source (called "cold light" because the amount of heat transmitted to the tip was very low compared to incandescent light bulbs) in endoscopy. Despite its utility, the quartz rod exhibited several limitations, including high price, fragility and the need to position the light source close to the external eyepiece.

Two years later, Harold Horace Hopkins (1918-1994, see fig. 2.10), a British physicist actively involved in optics research [82], reported about the transmission of recognizable images through a flexible fiber optic bundle made of a tube of glass with thin lenses of air [83]. Hopkins' work was improved few years later by Basil Isaac Hirschowitz (1925-2013), an American gastroenterologist, that used a highly transparent optical quality glass to give birth to the first useful flexible fiberoptic endoscope [79] (see fig. 2.10). Indeed, the subsequent introduction of fiberoptic technology, combined with the development of flexible-tip instruments, initiated a renaissance of laparoscopy.

Fig. 2.10. Left: Harold Horace Hopkins. Middle, right: Basil Isaac Hirschowitz and his flexible endoscope.

Hopkins patented his lens system in 1959. Seeing this as a promising system, Karl Storz (1911-1996, see fig. 2.11), a German engineer who founded his company in 1945 to produce instruments and headlamps for ENT (Ear, Nose and Throat) specialists, bought the patent and, in 1967, began to produce endoscopes with the Hopkins rod lens. At that time, Storz realized that fiber bundles, initially recruited to transmit images only, could also be used to transmit cold light source. Hence, he developed the first working endoscope with both Hopkins lens and the re-engineered fiber optics bundles, obtaining the most precise and clear images ever achieved. This innovation enabled, for the first time, high resolution films and photographs to be captured: many images had been made prior to Storz' discovery, but since the light sources were either too hot or too weak, the consequent poor resolution of the captured images simply rendered these nascent technologies mere novelties. As well, patient safety was vastly improved, since then the reliable extracorporeal light source could replace old heater and poorer systems.

In the 1970s, endoscopy was a known and even more accepted alternative to laparotomy to treat several pathologies, mainly in gynaecology and gastroenterology. Many surgeons were enthusiastic about this new clinical tool, but they recognized also the drawbacks in performing an endoscopic procedure from their point of view. For instance, looking through the scope presented inherent disadvantages of back strain for the operating physician and poor visualization of the peritoneal

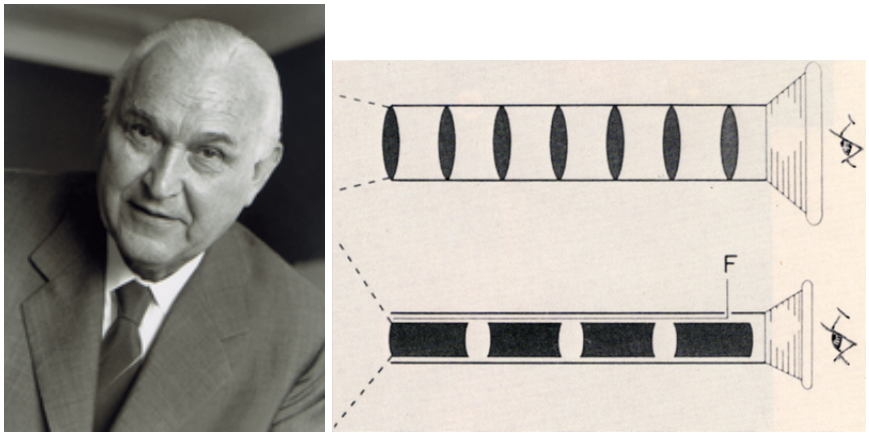

Fig. 2.11. Left: Karl Storz. Right: Hopkins rod lens system (reproduction from `http://www.karlstorz.de`).

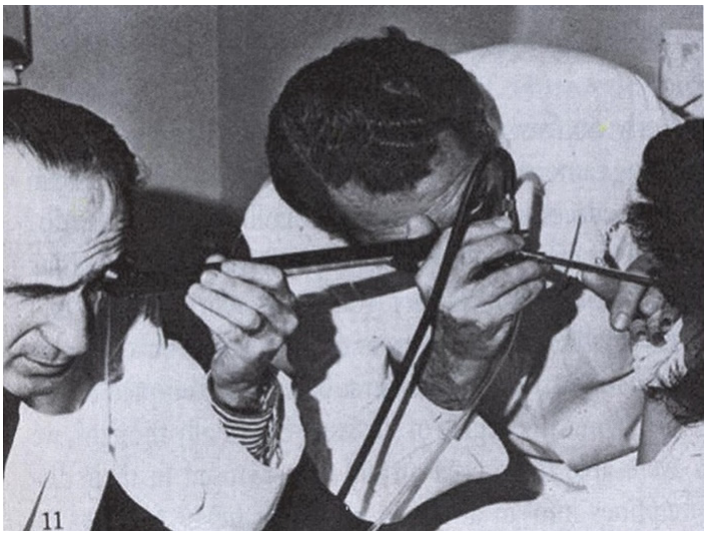

Fig. 2.12. Prior to videolaparoscopy, the old method of performing laparoscopy required that doctors bend over and peer through the laparoscope's eyepiece (reproduction from `http://www.nezhat.org`).

structure, due to the use of one eye through a narrow aperture (see fig. 2.12). Furthermore, each procedure normally performed with a laparotomy had to be re-invented, and there were essentially no textbooks or protocols established yet which would have demonstrated how to make these procedures laparoscopically. A common solution to both issues was proposed in this decade with the advent of *video-laparoscopy*, an evolution of standard laparoscopic technique in which a video camera is attached to the endoscope and the endoscopic images are sent to a monitor. The idea was not new: the advent of cinematography in 1930s pushed some physicians to apply this new technique in endoscopy. TV and film technolo-

gies started to be used more often in surgery after World War II: in 1952, Uji, Fukami and Suginara, Japanese pioneers from Hayashida Hospital (Kitakyushu, Fukuoka Prefecture, Japan) developed one of the earliest endoscopic cameras that they called *gastrocamera* [189]. One year later, Cohen and Guterman introduced their *Cameron cavicamera*, which was capable of filming and photography [27]. The debut of the world's first television and color film broadcasts in 1955 gave the opportunity to Raoul Palmer (1904-1985), a French gynaecologist, to present the first live endoscopy. In the same year, the world first television broadcasts of live bronchoscopies were achieved separately by the French bronchoscopists A. Soulas and J. M. Dubois de Montreynaud [176] (see fig. 2.13).

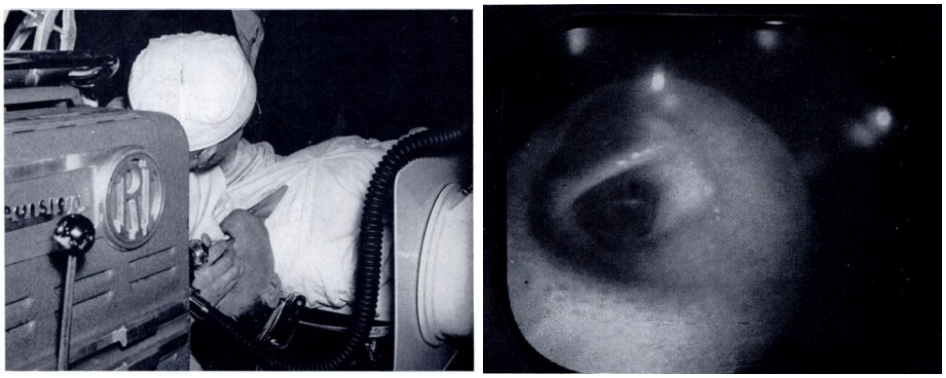

Fig. 2.13. A. Soulas performing a videobronchoscopy. Left: a standard bronchoscope, with a television camera plugged in on its proximal side, is placed in the patient's trachea. Rather than seeing through the eyepiece, Soulas is looking to a screen. Right: picture extracted from the videobonchoscopy procedure (reprinted from [176]).

All of these imaging systems were borrowed from the cinematography field, hence they were definitely not designed for being used in an operating room. While some of the technological rudiments to support video-laparoscopy had been in existence from at least 40 years, the conceptual idea of combining these technologies and adapting them to endoscopy had been entirely overlooked until Nezhat's contribution. Camran Nezhat (1947-), an Iranian-born American laparoscopic surgeon considered the "founding father" of operative video-laparoscopy, was the first to operate off the monitor in the late 1970s ("operating off the monitor" refers to the method of performing endoscopic surgeries while viewing a video monitor in an upright position, instead of looking directly at the patient). He was capable to perform advanced gynaecological procedures never done before with the laparoscope, such as the treatment of extensive endometriosis, demonstrating the safety and feasibility of complicated surgeries performed laparoscopically [127]. Nezhat's idea was still too advanced for being supported by the available technology: at that time, operating off the monitor was barely feasible, because the early generation of optics and video systems did not yet produce sufficient resolution. Moreover, despite the superior illumination afforded by the most recent fiber optics and lens systems, the quality of light had not advanced to a level where images could be ef-

ficiently sent to the monitor. Finally, laparoscopic procedures normally took much more time than the equivalent open surgeries: this added time factor was not helping in convincing that the video-laparoscopy method was better or safer than open surgery (because of the longer times compared to laparotomy, laparoscopy was even called "foreveroscopy") [171]. This is the reason why so many surgeons were initially against the idea: it was quite disorienting to view barely discernible images emanating from a low-resolution, two-dimensional screen positioned far away from both surgeon and patient, and to not have a direct contact with the patient.

Fig. 2.14. Willard Sterling Boyle and George Elwood Smith, winners of the 2009 Nobel prize in Physics for the invention of the CCD sensor (courtesy of Alcatel-Lucent/Bell Labs).

To overcome these inherent deficiencies standing in the way of the new video-laparoscopy technique, it was necessary to find a relationship of collaboration between laparoscopic surgeons and surgical instruments manufacturers, in order to improve the current state of the art in the fields of cameras and light sources and to develop customized devices for operative video-laparoscopy. The big breakthrough that marked the passage to modern laparoscopy was the introduction of charge-coupled device (CCD) digital cameras in endoscopy. The charge-coupled device was invented in 1969 at AT&T Bell Labs by Willard Sterling Boyle and George Elwood Smith [17] (see fig. 2.14). The original idea was to develop a shift register with the ability to transfer charges along the surface of a semiconductor from one storage capacitor to the next. Nowadays, CCDs are essentially used as memory modules, delay lines or for imaging devices. By 1971, a team of Bell researchers, led by Michael F. Tompsett, was able to capture images with simple linear devices. They were the first to reproduce black and white text and a gray scale picture with a CCD composed of 96 elements [185].

The first attempts to use CCDs in video-laparoscopic surgery began only in the next decade. In 1985, Erich Muhe (1938-2005, see fig. 2.15), a German surgeon,

performed the first laparoscopic cholecystectomy in less than two hours using an instrument he designed himself (which he called *galloscope*) and relying on the images that came from the endoscopic camera. By 1987, Muhe performed 97 laparoscopic cholecystectomies all with good results, giving himself reason to call the procedure "like magic" [107]. However, that was not what the German Surgical Society thought: Muhe's 1986 presentation to the German Surgical Society Congress detailing what he had achieved was met with great skepticism. His work was called into question by German authorities, which led to a full censure for "improper surgical actions". The result was that no Muhe's lectures about his work were published, therefore the scientific world outside Germany was not aware of these results. In the same period, Philippe Mouret (1938-2008, see fig. 2.15), a French gynaecologist, was actively working on the development of laparoscopy. In 1987 he performed the first video-assisted laparoscopic cholecystectomy using standardized instrumentation for gynaecological laparoscopy. Likewise Muhe, Mouret's work was not initially regarded as a crucial contribution too, perhaps because of his principal role as a private surgeon (he was not affiliated with any university) and his choice not to publish. Anyway, Mouret started some collaborations with other French surgeons, constituting what was called "the French connection" and contributing to the widespread of the laparoscopic technique [108]. One year later, two American surgeons, McKernan and Saye, performed the first laparoscopic cholecystectomy in the United States. In 1989, the Second International Symposium in Endoscopic Surgery, held in Atlanta, Georgia, represented the moment when general surgeons became convinced of operative laparoscopy as the future of surgery.

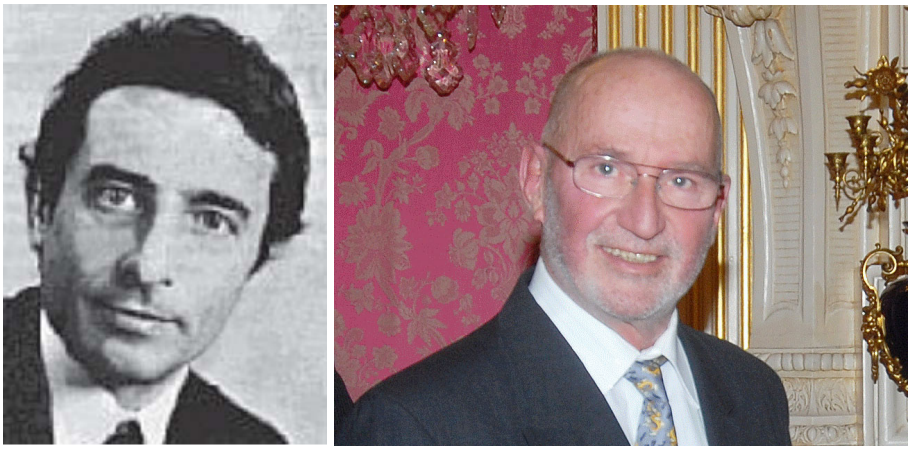

Fig. 2.15. Left: Erich Muhe. Right: Philippe Mouret.

An impressive increase of laparoscopic applications occurred in the 1990s: many of the gynaecological, gastroenterological, abdominal, thoracical and general surgeries performed to date with an open access started to be converted in a laparoscopic way by the first enthusiastic surgeons. There were several advantages in adopting this new approach: the surgical treatment became less invasive and more

cost-efficient, the patient recovery was faster and the hospitalization time was drastically reduced. Anyway, a part of the surgical community did not agree with this revolution, referred to as "experimental surgery" for the few data to support its efficacy, and criticized the less-skilled and less-experienced surgeons that performed these procedures. A significant complication rate was found for some of the first laparoscopic procedures, and this was probably related to the surgeons inexperience [173]. However, these initial problems did not block the evolution and diffusion of the laparoscopic technique: the increasing number of reports, publications and lectures held by laparoscopic surgeons, together with the technological advancements in instrumentation, led laparoscopic surgery to what it is today: a *de facto* standard in surgical operations.

2.3 Toward surgery without scars

The term *Minimally Invasive Surgery* (MIS), coined in 1987 by the British urologist John E. A. Wickham [201], refers to all the surgical approaches that try to reduce as much as possible the operation invasiveness. Benefits for the patients are the driving force behind the need of a minimal invasive technique: rather than a large scar as in open surgery, the smaller incisions allow to reduce blood loss during the surgery, shorten recovery time and decrease post-operative pain. It is possible to distinguish four main approaches in MIS [193] (see fig. 2.16):

1. **Extraluminal access**: instruments of 5-10 mm in diameter are introduced inside the body cavity through small skin incisions. Typically, 3 or 4 incisions are performed: the first port is used to establish pneumoperitoneum and to introduce the camera, while the others are for instruments (see fig. 2.17). Laparoscopy and thoracoscopy are two common example of surgical techniques that use this access route. A recent evolution of extraluminal techniques, which has the aim to reduce even more the invasiveness, is represented by LESS (Laparo -Endoscopic Single-site Surgery), in which all the instruments are inserted from a single incision. For better aesthetic results, umbilicus is typically chosen as incision point, because the final scar remains hidden.
2. **Intraluminal access**: the operation site is inside a tubular anatomical structure, as oesophagus, colon or urethra. These structures are reachable from natural orifices, so there is no need to perforate their luminal boundaries. Intravascular operations are a particular case of intraluminal procedures where the operation site is reached by means of a percutaneous puncture of a major blood artery (the most common examples are angioplasty or stent placement, in which a catheter is inserted from the femoral artery, see fig. 2.17).
3. **Transluminal access**: in order to enlarge the limited workspace of an intraluminal access, a transluminal approach consists in reaching the internal abdomen cavity by a controlled breach of a luminal barrier. This technique, known as NOTES (Natural Orifice Translumenal Endoscopic Surgery), consists in passing instrumentation through a natural orifice (mouth, urethra, anus, vagina) then through an internal incision in the stomach, bladder, colon or vagina, thus avoiding any external incision or scar (see fig. 2.18).

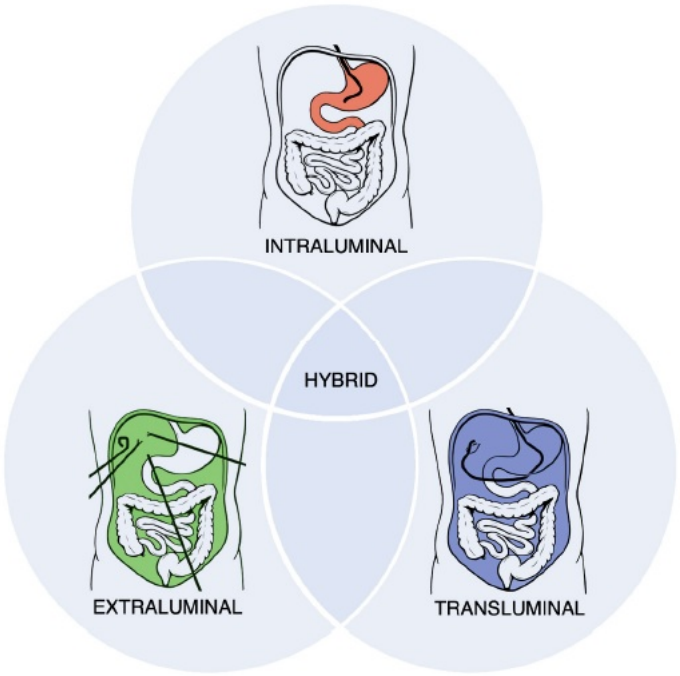

Fig. 2.16. Main approaches in minimally invasive surgery (reprinted from [193]).

4. **Hybrid approach**: it consists in combining the previous approaches during a surgical operation, in order to overcome the inner limitations of each access route.

If the introduction of laparoscopy revolutionized the common way of doing surgery when laparotomy was largely accepted ("Big surgeon, big incision" was the axiom in surgery at that time), nowadays natural orifice surgery represents perhaps the "Holy Grail" of minimally invasive surgical techniques: extirpative and reconstructive surgeries performed with no violation of the externally visible body skin.

Natural orifices were already used for intraluminal explorations in surgical specialities such as gynaecology or gastroenterology, but nobody before the year 2000 tried an transluminal gastric approach, *i.e.* to reach the peritoneal or thoracic cavities starting from a gastric access. The first documented transgastric NOTES procedure is credited to Anthony Kalloo (1955-), an American surgeon that in 2000 reported a peritoneoscopy in a survival porcine model. In this initial approach, finally published in 2004 [94], access to the peritoneal cavity was gained with a flexible videogastroscope inserted through the mouth: once in the stomach, Kalloo performed a needle-knife puncture and balloon dilatation of the stomach anterior wall in order to enter in the abdominal cavity. In 2004, N. Reddy and P. Rao, two Indian surgeons, reported on the first human transgastric NOTES ap-

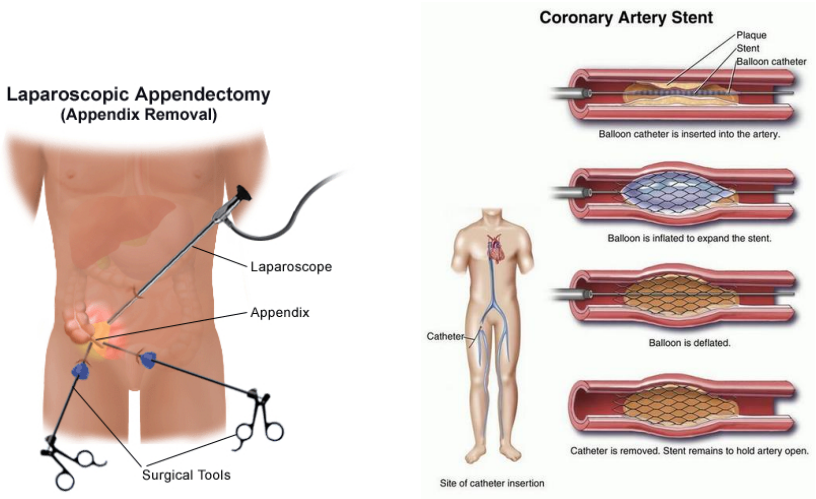

Fig. 2.17. Left: Typical port placement for a laparoscopic appendectomy. Right: Intraluminal coronary artery stent (reproductions from U.S. National Library of Medicine, National Institutes of Health (NIH)).

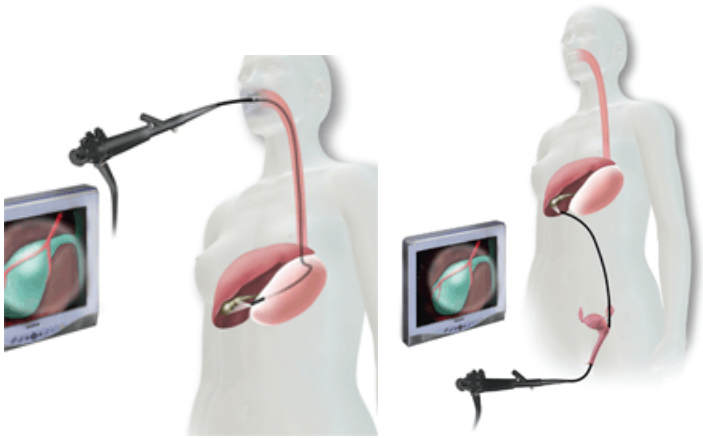

Fig. 2.18. Transgastric (left) and transvaginal (right) routes for NOTES cholecystectomy.

pendectomy [147]. After these initial attempts, the interest in NOTES increased and numerous procedures were performed, mainly on pigs of various breeds.

Although most of these experiments were technically successful, procedures were long and tedious, and did not allow immediate translation for clinical practice. In most cases, laparoscopic assistance was deemed necessary by the surgeons, thus invalidating the concept of no-scar surgery. Moreover, the transgastric route required specific instruments, larger than a normal gastroscope, with increased push force, wider freedom of movement and variable rigidity [58]. Finally, the ap-

plied gastric viscotomy (*i.e.* the incision of the stomach anterior wall) could lead to issues, such as risk of infections or leakage of gastric fluids.

For all these reasons, in the second half of the 2000s decade the interest for the transvaginal route gained importance. Although it excludes male patients to benefit from the NOTES technique, transvaginal access was well established and accepted since many years. It had been already used in the 20th Century by gynaecologists for diagnostic and therapeutic purposes (cfr. Dmitry Oskarovic von Ott in 1901, see section 2.2). In addition, it allows to extract large specimens after laparoscopic procedures, which was a great issue in transgastric procedures. In 2007, Ricardo Zorron, a Brasilian surgeon, reported the first transvaginal hybrid (because laparoscopically assisted) NOTES cholecystectomy [207]. A few months later, Jacques Marescaux, a French surgeon, published the first "pure" NOTES transvaginal cholecystectomy without any laparoscopic assistance [113] (see fig. 2.19). Following these major achievements, first series of NOTES procedures were published the following years, trying to evaluate the complication rate and to establish if NOTES could be a safe alternative to some laparoscopic procedures.

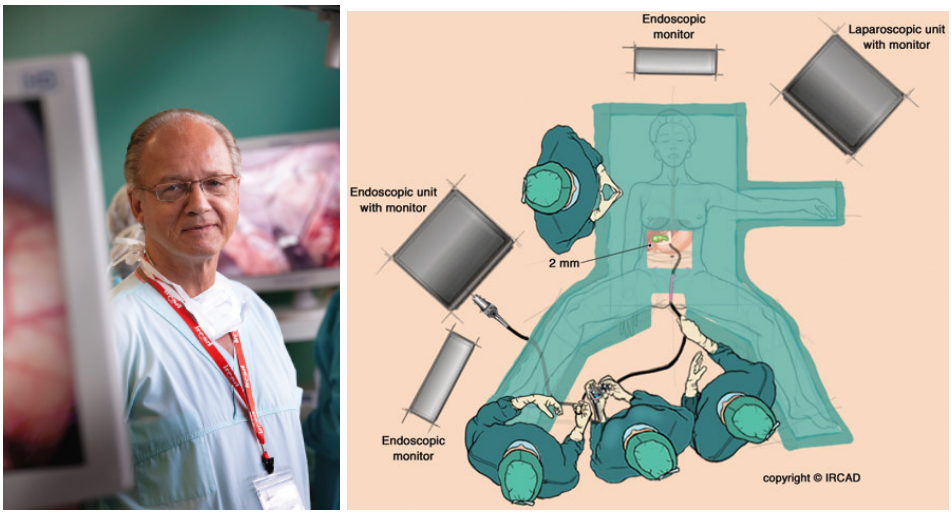

Fig. 2.19. Jacques Marescaux and his first NOTES transvaginal cholecystectomy (reprinted from [113]).

Although proven feasible for some procedures, limitations in current technology and instrumentation have kept NOTES away from the everyday surgical practice. A compromise between traditional laparoscopic surgery and NOTES could be represented by transumbilical or, more generally, single port surgery. The umbilicus port is not strictly a natural orifice, however transumbilical surgery clearly benefits from the advances of NOTES. In this case, the scar left after the operation is inside the umbilicus, so it is not visible (see fig. 2.20). The advantage of the single port technique with respect to NOTES is evident in abdominal surgeries, because the entry point is closer to the operating field, thus instruments could be shorter and,

in some cases, rigid. On the contrary, NOTES necessarily requires long and flexible instruments that must adapt their shapes to anatomical constraints.

In 2008, innovative leaders in the field of minimally invasive surgery gathered to establish a universally applied terminology for single-site surgical techniques. The Laparo-Endoscopic Single-site Surgery Consortium for Assessment and Research (LESSCAR) agreed upon LESS (Laparo-Endoscopic Single-site Surgery) as the accepted nomenclature for this field of surgery [153]. This consolidation brought together many denominations that appeared after the first attempts, as Single-Site Access (SSA) surgery [186], Single-Port Access (SPA) surgery [29], Single Trocar Access (STA) surgery [161], Single-Incision Laparoscopic Surgery (SILS) [24], Minimally Invasive Single-Site (MISS) surgery [40], Natural Orfice Transumbilical Surgery (NOTUS) [28], One-Port Umbilical Surgery (OPUS) [144], Transumbilical Endoscopic Surgery (TUES) [205] or Transumbilical Laparoscopic-Assisted (TULA) surgery [135]. This was done in an effort to unify rather than fragment this evolving field, consolidate research efforts, improve educational training programs and universalize reporting in the literature. Nowadays, LESS encompasses many forms of minimally invasive surgery, all with the concerted aim to minimize or eliminate the incisions needed for operative access.

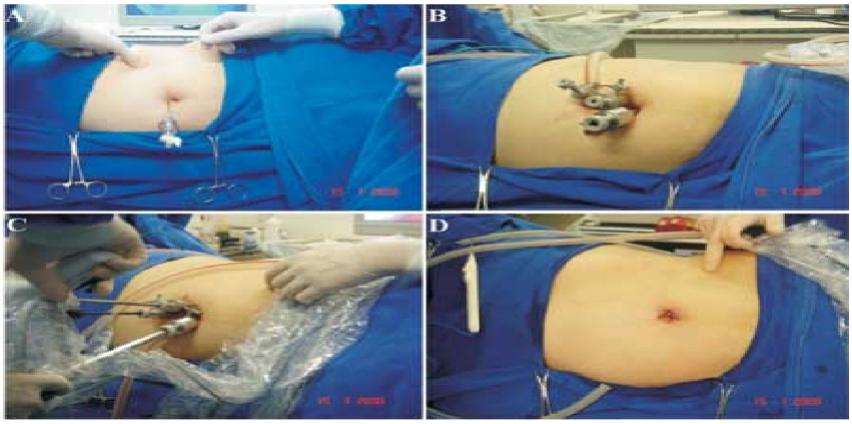

Fig. 2.20. Typical LESS phases. A: Port incision and CO_2 insufflation. B: Trocar placement. C: Operation. D: Final aesthetic results (reprinted from [19]).

The earliest cases of LESS date back to 1960s, several decades before the initial publications describing modern laparoscopy. First procedures were performed via a single trocar, accomodating a laparoscope and a working instrument immediately adjacent to it. The initial reports of operative LESS centered on needle biopsies performed under laparoscopic visualization [140] and female sterilization [149]. These first procedures are still performed today with the same techniques, but with modern instrumentation. After these first attempts, surgeons tried to treat more complex operative cases laparoscopically, but they found more practical to use an additional trocar. Traditional laparoscopy was arising, so first attempts in LESS remained without much consideration.

A new interest in LESS, in tandem with NOTES, was expressed in 2000s under the idea of minimizing the surgical invasiveness. Some of the earliest cases of modern LESS date back to 2005, when urologists from Japan reported one of the first adrenalectomies performed with this technique [76]. In 2007, a group of American urologists performed nephrectomies on pigs using a single incision through which 5 mm trocars were inserted. Once the technique was perfected in the porcine model, nephrectomy was successfully performed in three human subjects [142]. The authors demonstrated the feasibility of using articulated instruments to improve triangulation, one of the main issues of LESS together with conflict of instruments and difficult tissues retraction (cfr. section 2.4). In parallel with urologists, who embraced LESS as an innovative advancement of minimally invasive surgery, general surgeons and other surgical specialists have adopted this techniques and principles for their respective fields of surgery. Cholecystecomy was chosen by many surgeons as the key procedure for comparing LESS with the multiport techniques.

An overview of the main historical milestones in the evolution of minimally invasive surgery is presented in fig. 2.21.

2.4 Instrumentation for no-scar surgery

As with any technological innovation, proponents of NOTES and LESS need to demonstrate how these techniques could be practically implemented, and whether their efficacy, risks and costs are comparable or better than the current standards of practice. However, new constraints introduced by no-scar surgery techniques require modified or specifically developed instrumentation. In the last years several endoscopic platforms have been proposed by research laboratories and manufacturers. They have been tailored to all the different potential points of entry access through natural orifices or skin incisions. In addition, some platforms have been designed for hybrid use, with potential usefulness for both NOTES and LESS.

2.4.1 NOTES instrumentation

There are four fundamental requirements for a NOTES platform [121]:

1. **Provide safe entry into the peritoneal cavity**: for most clinical applications such points of access include the proximal or distal gastrointestinal tract and the vagina; the most important complication to avoid during this phase is the damage to neighbouring organs.
2. **Provide a stable conduit for rapid passage of instrumentation, including imaging and therapeutic tools**: a trocar or, more generally, an overtube is necessary to give rigidity to the endoscope during the insertion phase; on the contrary, the endoscope itself should be as flexible as necessary to adapt its shape to anatomical constraints. While transvaginal access normally permits the use of completely rigid instruments, because the pelvic route allows a straight access to the lower abdominal cavity, flexible endoscopic platforms provide better access to more locations in the abdomen.

Fig. 2.21. Milestones in the evolution of minimally invasive surgery.

3. **Maintain safe peritoneal distention**: as in traditional laparoscopy, distention of the peritoneum has to be done using an inert absorbable gas (such as CO_2), but avoiding overinflations that can cause diaphagramatic and respiratory problems. Intraperitoneal pressure need to be monitored and regulated throughout the surgery.
4. **Provide quick, easy and robust closure of the visceral defect at the end of the procedure**: presently, multiple tools that allow safe closure of the peritoneal entry exist on the market (such as clips, full-thickness sutures, T-bars or the most recent OverStitch system by Apollo Endosurgery, see fig. 2.31), but none of these is integrated in a commercial NOTES platform.

The current trend in the development of NOTES platforms is toward the use of flexible systems rather than rigid, because their flexibility enables traversing tortuous trajectories and reaching many anatomical sites located far away from the insertion point. However, several problems can affect the functionality of a NOTES surgical system:

1. **Force limitations**: flexible tools cannot efficiently transmit forces that are not aligned with their axes, and they can be easily deformed when grabbing heavy organs or when pushing against other tools or rigid constraints (see fig. 2.22).

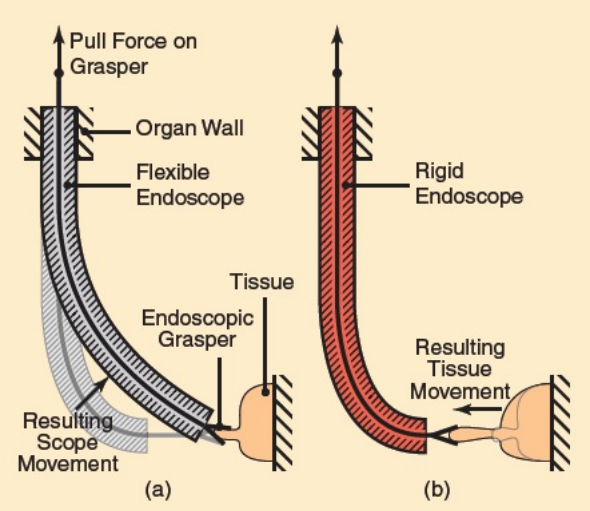

Fig. 2.22. Force limitation problem when using flexible systems (reprinted from [109]).

2. **Lack of triangulation**: triangulation is one of the fundamental concepts of laparoscopic surgery, because it permits traction on tissues to facilitate dissection along normal anatomical planes. When instruments are inserted close to each other and almost parallel, the "swordfighting" or "chopstick" effect [145] appears, so that instruments can easily collide together (see fig. 2.23).

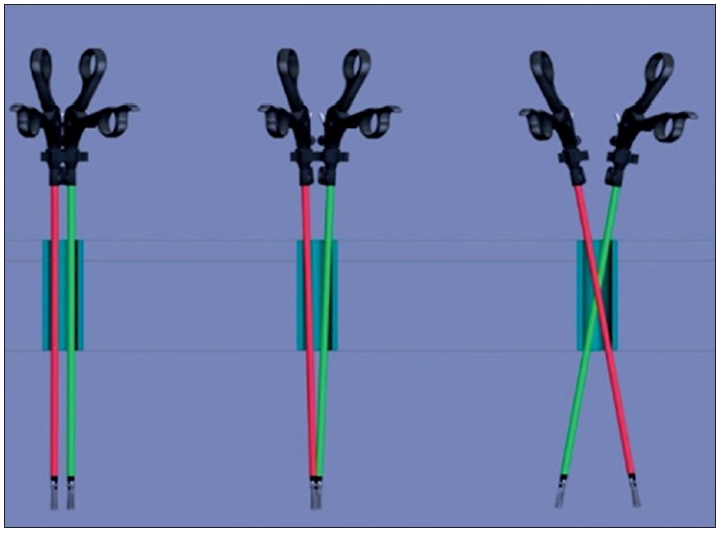

Fig. 2.23. When instruments are inserted from a narrow port, they enter almost parallel inside the body, and their triangulation is compromised. If the trocar is large enough to deviate their path, then the problem becomes the instruments inversion: the instrument that appears on the left in the image is controlled by the right handle and vice versa (reprinted from [40]).

3. **Size limitations**: there is a physical limit to the overall size of instruments determined by the natural orifice itself, and it cannot exceed a diameter that is comfortably and safely tolerated by humans.

Numerous endoscopic systems have been designed to overcome these limitations, but yet we are still far from a complete functional solution. One of the first systems utilized in NOTES animal tests was the Olympus R-Scope (XGIF-2TQ160R Olympus, Tokio, Japan), later modified into the NOTES scope. It was a modified dual-channel endoscope with two bending segments on the distal side, one of which is lockable. The two working channels (2.8 mm in diameter) have lifting gates that are orthogonally positioned, allowing for simultaneous lifting (vertical motion) and dissection (horizontal motion, see fig. 2.24) This permits dynamic retraction and cutting without moving the camera. This endoscope has standard flexible endoscopic optics embedded on its tip, and incorporates a separate channel for suction and irrigation. *In vivo* studies demonstrated the ability of this system to perform both intraluminal [125] and transluminal [120] procedures, but both studies highlighted the complications, introduced by the complexity in the system control, that make the surgical procedure technically demanding and time-consuming.

In 2009, Olympus developed a new prototype platform, named EndoSamurai (see fig. 2.25): it consists of a 15 mm flexible endoscope that integrates two hollow steerable instrument guide arms and one conventional operating channel. The hollow arms, which are cable actuated, permit to realize triangulation and give a total of five Degrees Of Freedom (DOFs) (deflection in two orthogonal directions, trans-

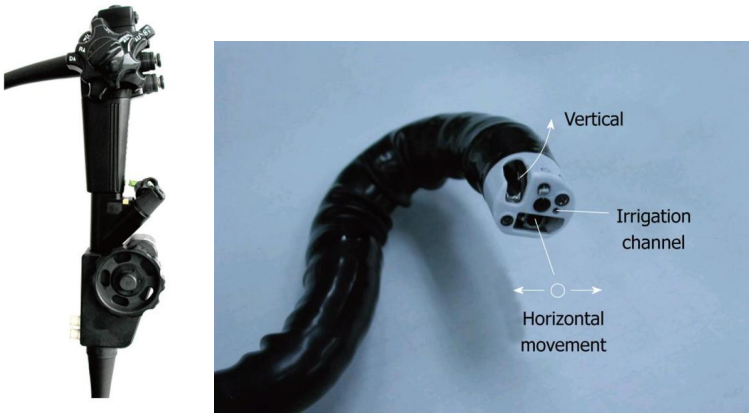

Fig. 2.24. Olympus R-Scope. Left: Endoscope handle. Right: Endoscope tip (reprinted from [165]).

lation, rotation and opening/closing of actuated tools) to each passive instrument inserted inside. In this manner, it is possible to interchange instruments during the operation without withdrawing the whole endoscope. As a drawback, the hollow arms attached on the endoscope head do not allow instruments movements independent from those of the camera, and they are not suitable for operating in narrow lumens such as in endoluminal procedures. In addition to the two conduits, EndoSamurai offers a third working channel that may be used for auxiliary equipment or for suction/irrigation. Stiffened by a locking overtube, the scope articulates in the same manner as a standard endoscope with identical visualization. The system workflow requires that the user navigates to the target with the endoscope, locks the overtube system in position and then proceeds to the user interface for moving the instruments. The control console simulates classical laparoscopic instrumentation handles, making the control of the platform intuitive. Recently, EndoSamurai has been used for *in vivo* transgastric small bowel resection [59].

Fig. 2.25. Olympus EndoSamurai with its control console (reprinted from [165]).

The Transport platform (USGI Medical, San Capistrano, CA, USA) is a 16 mm access device with four large working channels, one for a flexible 6 mm endoscope (N-scope from Olympus, Tokyo, Japan) and three others (one of 7 and two of 4 mm in diameter) for instruments (see fig. 2.26). In this manner, the endoscope becomes independent of the instrumentation, but optics and instrumentations still remain in a parallel axis, so triangulation is poor. The Transport platform adopts the stiffening overtube technology named ShapeLock® [180], which allows locking the system position and shape once the operation site is reached. The last improvement of the Transport platform is the Incisionless Operating Platform (IOP), which integrates an ergonomic user interface to improve bimanual coordination. Compared to the Transport platform, IOP can be mounted on the operating table and offers new tissue anchors and graspers.

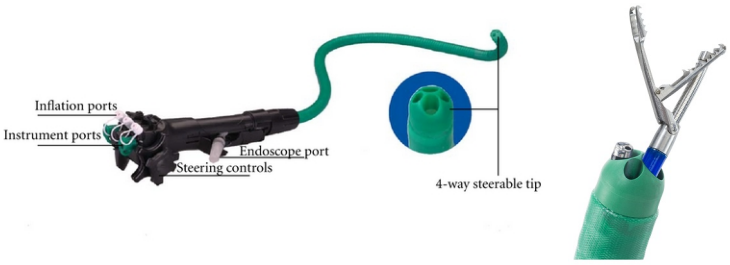

Fig. 2.26. Transport by USGI Medical. Left: Endoscope handle. Right: Endoscope tip (reprinted from [197] and `http://www.usgimedical.com`).

In an attempt to improve triangulation, a prototype device named Cobra was succesively developed by USGI. Cobra is based on the same ShapeLock® concept, but in this case three independent flexible arms are attached to the system tip (see fig. 2.27). These arms are cable-driven, but their design makes instruments interchange impossible without extracting the whole system from the operation site. This limitation, together with the inaccuracy when performing fine movements due to the tendon architecture, is probably responsible for the poor success of this platform (no further studies have been published since 2006 [12]).

Fig. 2.27. Cobra by USGI Medical (reprinted with permission from [197]).

The Direct Drive Endoscopic System (DDES) (Boston Scientific, Natick, MA, USA) is a prototype platform, suitable for both NOTES and LESS surgery, consisting of an articulated flexible guide with a 6 mm visualization channel and two 4 mm instrument channels (see fig. 2.28). A conventional neonatal endoscope is used for visualization, while two proprietary articulated flexible instruments are hosted inside the guide. On their proximal side, instruments are equipped with a special mechanical handle that controls 5 DOFs. The whole system is supported by a rail platform, which can be mounted on the operating table. The main guide adds two more DOFs for instruments positioning, and it can translate independently from the scope. As drawbacks, the thin size of instruments avoids a robust force transmission, and triangulation is poor, since instruments are in parallel axis with the camera.

Fig. 2.28. Direct Drive Endoscopic System (DDES) by Boston Scientific (reproduction from `http://www.bostonscientific.com`).

The ANUBISCOPE® system (Karl Storz GmbH, Tuttlingen, Germany) is another sophisticated endoscopic platform with an ergonomic user interface (see fig. 2.29). It consists of a multifunctional flexible endoscope that permits to introduce two flexible instruments inside the body. It embeds an endoscopic camera on its tip, and it offers a third operating channel for auxiliary instruments. ANUBISCOPE® has a particular head design that permits to realize triangulation: when it reaches its ideal target location, two flaps connected to the distal tip can be open, deviating the instruments channels from the camera axis. Instruments, specifically developed for this platform, are inserted from the endoscope proximal side. They have an ergonomic handle that permits to deflect their actuated section in one direction and to rotate and translate them inside theirs channels. The main endoscope is composed by a passive shaft and an articulated distal section, which can be bent in two orthogonal directions by means of lockable knobs located on the endoscope handle. An experimental version of ANUBISCOPE® was successfully used for the world first transvaginal cholecystectomy [113] (cfr. section 2.3), but also for transgastric hybrid NOTES procedures [30]. Though ANUBISCOPE® platform is one of the most advanced system for no-scar surgery, it still presents some limitations, such

as the complexity of its use: two or more surgeons are necessary to control all the possible movements, they have to share a restricted workspace (see fig. 2.19) and they must work in good coordination. Moreover, flaps are a good solution for the triangulation problem, but they could limit the system use in narrow or confined spaces, as in intraluminal interventions.

Fig. 2.29. ANUBISCOPE® by Karl Storz (reproduction from `http://www.karlstorz.de`).

Karl Storz also developed a rigid system for transanal surgery named TEO® (Transanal Endoscopic Operation): it consists in a large rectoscope that can accommodate an endoscope and rigid instrumentation (see fig. 2.30). This system provides an eyepiece for direct vision of the operating field. Instruments go straight through the rectoscope, so there is no triangulation on the system distal side. This system was employed for rectal excisions, but limitations in its design make its use technically demanding. Another system intended for transanal surgery is the Transanal Endoscopic Microsurgery (TEM) by Richard Wolf (Richard Wolf Medical Instruments Corporation, Vernon Hills, IL, USA). TEM is very similar in design to Karl Storz's TEO, but it additionally offers a binocular eyepiece for stereoscopic vision (see fig. 2.30).

Although it is only a complementary system designed specifically for suturing, it is worth citing the OverStitch^{TM} Endoscopic Suturing System (Apollo Endosurgery, Austin, TX, USA). It is a small platform that can be integrated on a standard dual-channel flexible endoscope: the suturing part is mounted on the endoscope tip, while on the proximal side a handle allows to control the needle movements (see fig. 2.31).

A summary of the main presented systems for NOTES, highlighting their advantages and limitations, is proposed in tab. 2.1.

Fig. 2.30. Left: TEO® (Transanal Endoscopic Operation) system by Karl Storz (reproduction from `http://www.karlstorz.de`). Right: TEM (Transanal Endoscopic Microsurgery) system by Richard Wolf (reproduction from `http://www.richardwolfusa.com`).

Fig. 2.31. OverStitch by Apollo Endosurgery (reproduction from `http://www.apolloendo.com`).

2.4.2 LESS instrumentation

Some of the previously presented systems can be easily adapted to LESS use, but because LESS is very close to traditional laparoscopy, many surgeons prefer to use classical rigid instrumentation eventually modified for this particular use. Instruments modifications for LESS mainly concern their sizes, which have to be reduced in order to permit their passage through a single common port. The single

System	Pros	Cons
Olympus R-Scope	independent motion of instruments and camera	complexity in control
Olympus EndoSamurai	triangulation, intuitive controls	fixed arms
USGI Transport	stiffening overtube	no triangulation
USGI Cobra	three flexible arms	fixed instruments, inaccuracy
Boston Scientific DDES	independent motion of instruments and camera	thin instruments, poor triangulation
Karl Storz Anubiscope	triangulation, instrument handles	complexity, head size

Table 2.1. Main commercial systems for NOTES.

access point introduces important constraints, such as very limited triangulation and instruments collisions (as explained in section 2.4.1), hence most of the manufacturers work consists in the development of new specific platforms or access trocars that try to overcome these limitations.

The SPIDER (Single-Port Instrument Delivery Extended Research) system (TransEnterix, Inc., Durham, NC, USA) is a disposable device that facilitates the movements of multiple instruments during LESS procedures. The first generation of this system was composed by a delivery tube (18 mm in diameter) with four working channels, two rigid and two flexible (see fig. 2.32). The rigid channels are in parallel axis with the main tube, and they are intended to accommodate a rigid endoscope and a standard rigid instrument. On the contrary, the flexible channels, intended for flexible instruments, are mechanically diverted in order to realize triangulation. Recently, TransEnterix developed a second generation of its system that uses articulated delivery tubes instead of the rigid ones, thus making the platform more flexible [67] (see fig 2.32).

Fig. 2.32. Left, middle: First generation of SPIDER platform by TransEnterix. Right: Second generation of SPIDER; (a) articulated delivery tubes using a vertebral design on the distal sides; (b) reduced length of the articulating portion (reproduction from `http://www.transenterix.com`, [67]).

Nowadays, most part of surgical instruments manufacturers have designed specific trocars for LESS (see fig. 2.33). The SILS^{TM} procedure kit (Covidien Inc., Norwalk, CT, USA) is a disposable packet containing an access device and the SILS^{TM} port (noted A, see fig. 2.33), both made from an elastic polymer. The port is slightly hourglass-shaped and can be deployed through a 2 cm fascial incision. It contains four openings: one for insufflation via a right-angled tube and

Fig. 2.33. Commercially available trocars for LESS: (A) SILS Port (Covidien); (B) Triport and Quadport (Advanced Surgical); (C) SSL Access System (Ethicon Endo-Surgery); (D) X-Cone (Storz); (E) GelPOINT (Applied Medical); (F) AirSeal (SurgiQuest) (reprinted from [102]).

three that can accommodate trocars 5-12 mm in size. The compressibility of the elastic polymer allows for the access ports to expand and form-fit the space in which it resides, as well as the ports passed through the working channels.

The ASC TriPort^{TM} (Advanced Surgical Concepts, Wicklow, Ireland), also known as the R-port, is a multi-instruments access port (noted B, see fig. 2.33) designed to be deployed through a single incision, typically at the umbilicus. It requires a fascial incision approximately 1-3 cm long. A sheath is placed through the fascial opening, and the peritoneal surface of this sheath has a self-expanding ring, allowing the TriPort to remain inside the peritoneum. The outer component of the TriPort has three ports: two 5 mm ports for instruments and one 12 mm port for the endoscope. In addition, the TriPort contains an insufflation port, allowing regulated gas insufflation without the additional need for a Veress needle. The QuadPort is a modified version of the TriPort: it is bigger (it could require an incision of 1.5-5 cm) and it has one 15 mm port for the scope (but also for the retrieval of specimen after a surgery), two 10 mm ports for instruments and one auxiliary 5 mm port.

SSL (Single Site Laparoscopy) system (Ethicon Endo-Surgery, Cincinnati, OH, USA) is an abdominal access system comprising a seal cap (noted C, see fig. 2.33) with some accessories: a retractor insertion tool, a reducer cap and a fixed-length retractor. The assembled device maintains peritoneal gas pressure while allowing

the insertion of multiple surgical instruments through a single incision into the abdominal cavity.

While all the previously presented systems are disposable, the X-Cone (Karl Storz GmbH, Tuttlingen, Germany) consists of two specially shaped metal hooks (which could be autoclaved together with standard instrumentation) and one rubber cap with 5 valves (noted D, see fig. 2.33). The two hooks are introduced separately in the incision, then theirs upper portions are folded together and kept attached by the rubber cap. Through the cap it is possible to introduce one optic and up to four instruments, and a valve for regulating the gas insufflation is provided.

The GelPoint system (Applied Medical, Rancho Santa Margarita, CA, USA) adopts a different design: it consists of a gel cap, three sleeves and an Alexis wound protector/retractor (noted E, see fig. 2.33). Once the retractor is in place, the gel cap is fixed externally to seal the incision. The sleeves can be placed freely on the cap and they can also be repositioned during surgeries, since the gel material is ductile enough to permits the sleeves passage while keeping its normal shape.

A new concept in trocar design, also usable in LESS, has been introduced with the AirSeal trocar (SurgiQuest, Orange, CT, USA) (noted F, see fig. 2.33). Typically, all traditional laparoscopic ports use a mechanical barrier to maintain pneumoperitoneum while allowing instrument passage and limited specimen extraction through their lumen. AirSeal rather uses a pressure barrier, created by gas pumped inside the port, that well exceeds the pneumoperitoneum. It uses a combination air pump and specialized tubing, with a filter serving to recirculate and filter the carbon dioxide used to create the pneumoperitoneum: in this manner, AirSeal is able to keep the induced pneumoperitoneum, but also to evacuate smoke. This 12 mm port permits to introduce two instruments and one scope without contact friction, since there are no valves inside the port lumen. On the contrary, instruments will not have fulcrum effect, so they will be less stable during operation.

To conclude this review, it is important to cite the efforts done by manufacturers (collaborating with surgeons partners in many cases) to improve triangulation and to enhance dexterity in LESS procedures. Karl Storz developed S-PORTAL instrumentation, a series of access ports and pre-bent instrument specifically developed for LESS cholecystectomy and appendectomy (see fig. 2.34). DAPRI is the name given to several set of instruments, which are intended to be directly inserted, together with the main scope, through the single trocar placed inside the umbilicus. Their design ensures that the handles do not collide with themselves and with the endoscope and, at the same time, it permits to obtain a good triangulation inside the patient body. DAPRI instrumentation includes:

- *Standard set*, consisting of one straight scissors and one curved grasper.
- *Cuschieri set*, consisting of two instruments (one scissors and one grasper) slightly bended on the proximal side, but with a double curvature on the distal side.
- *Carus set*, consisting of two instruments (one scissors and one grasper) straight on their proximal side, but curved on the distal side, with a relatively big radius starting at the middle of the shaft and ending exactly in the virtual line between instrument grip and tip.

- *Leroy set*, consisting of two instruments (one scissors and one grasper) with double bending.

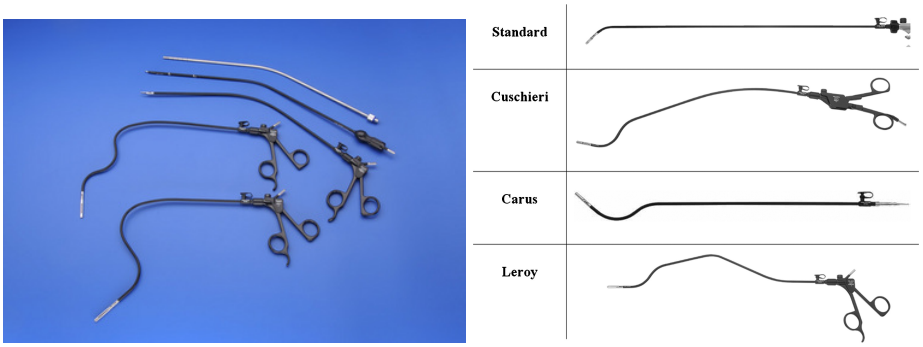

Fig. 2.34. DAPRI instrumentation by Karl Storz (reprinted from [8]).

Together with its SILS port, Covidien offers a complete set of articulated instruments designed for LESS (see fig. 2.35). These instruments have articulated distal tips that permit to gain a degree of freedom inside the body. A similar design was proposed by CambridgeEndo (Cambridge Endoscopic Device, Inc., Framingham, MA, USA) with the Autonomy^{TM} Laparo-Angle^{TM} Articulating Instruments, which provide a lockable rotating knob that deflects the instrument tip and block its position, if necessary (see fig. 2.36).

Fig. 2.35. Shears SILS grasper and SILS kit by Covidien (reproduction from `http://www.covidien.com`).

Since in LESS procedures instruments are inserted through trocars placed closely, collisions between instruments inside and outside the body can be frequent. Moreover, the instruments proximity compromises the triangulation, even if the various trocars designs try to compensate this problem. The proposed solutions are multiple, each with advantages and limitations, and it is up to the

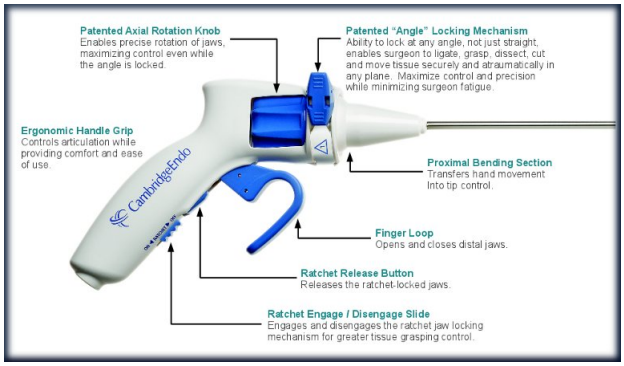

Fig. 2.36. Autonomy^{TM} Laparo-Angle^{TM} Articulating Instrument by CambridgeEndo (reproduction from `http://www.cambridgeendo.com`).

surgeon to find, test and adopt a specific one, according to his/her preferences and perceived easiness of use.

2.5 Conclusions

Although surgery is (almost) as old as men, in the last century an exponential improvement in both knowledge and technique made it a real lifesaving procedure for many cases. Fortunately, the high death rates after a surgery, so common at the beginning of the 20th Century and mostly related to infections and inappropriate methods, have been replaced by day-hospital procedures and, more generally, shorter recovery times. The minimization of the surgical invasiveness is one of the key-points behind these improvements, but no evolution is possible without good supporting tools. Nowadays, complex systems with high dexterity have been proposed, in order to overcome the limitations in movements of a minimally invasive surgical approach. These tools, potentially very effective, are in some cases difficult to be used in the medical routine, since they require multiple users and long training curves. Offering automatic interfaces in surgical instrumentation could be a valid solution, in order to simplify the use of systems with multiple degrees of freedom: the applications of robotics in surgery and the novel flexible robot object of this thesis work will be the main topics of the next chapter.

3

Robotics in Surgery

Contents

3.1 Introduction

As introduced in chapter 2 (cfr. section 2.4), several platforms have been recently proposed by the main instrumentation manufacturers, in an effort to overcome the new technical limitations and constraints of no-scar surgery techniques. The only common feature of the presented systems is that unlike in traditional laparoscopic surgery, where the surgeon has to choose the ports location for main scope and instruments according to the particular operation, now the whole instrumentation set follows a common path through a natural orifice or a single incision. Most part of these systems offers a specific solution for triangulating instruments. The mobility restriction imposed by the single port access drove manufacturers to use articulated sections in order to restore the lost degrees of freedom. This increased complexity in design is inevitably reflected on the control interfaces of these new tools: more mobile parts means more controls to be used during the operation. The result is that all these platforms require at least two surgeons to operate them: typically, the main surgeon takes control of instruments, while the second surgeon

adjusts the scope position according to the main surgeon's requests. This implies that the two surgeons should gather good communication and empathy between them, but also that the learning period for completely mastering these systems is quite long, since the controls are numerous and, sometimes, not intuitive at a first sight. In this scenario, robotics could represent a valid solution to improve control, precision and ergonomics. Moreover, a robotic interface could allow a single surgeon to completely telemanipulate a complex system by means of dedicated haptic interfaces.

In common meaning, a *robot* is a mechatronic machine equipped with sensors and actuators and pre-programmed to repeatedly execute the same tasks: its actions are deterministic and its workspace is well defined and limited. This definition could easily fit for industrial robots, which typically are automatically controlled anthropomorphic manipulators used in many industrial assembly lines. For these applications, a robot permits to realize a task faster and in a more precise way than a human operator, or to completely substitute him/her when the task could be dangerous (as the manipulation of radioactive elements in a nuclear plant [137] [39]) or physically not feasible (electronics micro-assembly [62] or big loads movements [61], for instance) [20]. Nowadays, robotics has moved further from this original vision, pervading many fields of the current society: it is not so uncommon today to hear about mobile, service, cognitive, assistive, rescue, biomimetic and humanoid (just to give some examples) as adjectives beside the word "robotics". Robotics researchers are trying to improve robots functionalities and behaviors, making them "smart" machines capable to interact with humans, to be controlled in real-time and, eventually, to take autonomous decisions based on previous learned experience.

Surgery is a field where robotics might have a high potential, but stricter technical and safety limitations than in other fields made its acceptance a slow process [13]: a surgical robot is continuously in contact with the human body, its workspace is easily occluded by physicians and legal complications about the responsibilities in case of harm during its use could be easily raised [84] [177] [35] [41]. These are some of the reasons why actually many prototypes of surgical robots exist in research, but few of them became (or are going to become) commercial products.

Since many different types of surgical robots exist, it could be useful to introduce a taxonomy: in section 3.2 the most common classifications in the robotic literature will be introduced. Afterwards, a brief historical review about the introduction of robotics in surgery is exposed in section 3.3. Current robotic systems for no-scar surgery, both from academy and industry, are the main subject of section 3.4, while section 3.5 will be consecrated to a general mechanical description of STRAS, the surgical robot object of this thesis.

3.2 Classification of surgical robots

Surgical robotics could be seen as a specific branch of the wider Medical robotics group, which also includes:

- **Assistive robotics**, *i.e.* mechatronic machines that help elderly and disabled people in their everyday life, such as active prostheses and motorized wheelchairs.
- **Rehabilitation robotics**, typically employed in neuromotor rehabilitation after strokes or accidents.
- **Non-surgical robotics**, such as diagnostic and imaging machines with a high level of automation.

The Surgical robotics family itself includes several types of robots, which differ according to the way they are controlled, how they interact with the patient, which place they take in the operating room and how much they are invasive.

Several taxonomies for Surgical robotics are unanimously accepted in the literature (see for instance [187], [170], [31]). The first was proposed in 1997 by R. H. Taylor, during the 6th Conference on Artificial Intelligence in Medicine Europe (AIME) [183]. This classification is based on the different role that robots could take during surgeries. Taylor's definition of "surgical robotics" regards the application of computation, sensing and manipulation to enhance the human's ability to perform surgical procedures. From this perspective, he identified five classes of robotic systems used in interventional applications:

1. **"Intern replacements"**: systems that perform all the tasks typically executed by the surgeon's assistants such as, for instance, retraction, camera holding and limb positioning. AESOP by Computer Motion, Inc. (cfr. section 3.3) was one of the first proposed systems that well represents this category.
2. **Telesurgical systems**: this category includes all the systems that have a master/slave configuration, where the robot (the slave system) is completely controlled by means of a remote interface (the master system) connected through a communication channel. In this case, the automation level of such systems is very low, since they are designed to reproduce the user requests as close as possible. A master/slave teleoperation scheme permits to treat the user input at the master level before sending it to the slave robot, thus allowing useful corrections such as hands tremor filtering, movements scaling and the possibility to control complex robotic architectures with dexterous and ergonomic interfaces. As drawback, the latency time in the communication between master and slave systems is a crucial aspect: a reasonable time delay in terms of surgeon's perception of safety was roughly established in 330 ms [114], therefore the communication medium must guarantee that limit, or the physical distance between master and slave system should be properly chosen in order to avoid delays in communication. The most typical example of teleoperated surgical robot is the da Vinci surgical system (Intuitive Surgical, Inc., Sunnyvale, CA, USA).
3. **Navigational aids**: often referred as Computer-Assisted Surgery (CAS) systems, they provide the surgeon with accurate positional information on selected instruments with respect to the patient anatomy. These systems are typically composed by a 3D localizing device (optic camera, electromagnetic tracker, etc.) and the corresponding active or passive markers. They are largely used in orthopaedics, since bones represent a trustworthy fixed reference. They would

be very useful in laparoscopic surgeries too, but, with the current technology, soft tissues and metallic instrumentation limit their practical use.

4. **Precise positioning systems**: after a registration process between the robot reference frame and the patient, the robot is used to precisely place an instrument at the desired position and orientation requested by the surgeon. Before the introduction of robotics, stereotactic frames represented (and, in some cases, represent still today) the most precise way to drill the head bone in neurosurgery, mechanically constraining the drill tip into a pre-formed guide. Stereotactic frames are very invasive (they are directly screwed on the patient head), while robotic positioning systems (such as Robodoc, cfr. section 3.3) can offer the same precision without invasiveness, as long as the registration process between the robot and the patient is performed correctly.
5. **Precise path systems**: robots that autonomously execute a pre-operative plan under the supervision of the surgeon who could, at any time, block their movements. The most common examples are orthopaedic surgery robots, such as Robodoc (cfr. section 3.3), and radiotherapy (such as the Cyberknife by Accuray, Inc., Sunnyvale, CA, USA) or Transcranial Magnetic Stimulation (TMS) robots (such as the TMS-Robot by Axilum Robotics, Strasbourg, France), which allow specific treatments by means of a radiation or field generator that can be automatically placed and moved all around the patient.

The system that we are going to present in the following (see section 3.5.2) can be collocated in the Telesurgical system category, since it has a master/slave structure and its movements are completely controlled by the user.

3.3 Historical evolution

The introduction of robotics in surgery dates back to 1983, when for the first time a robot named *Arthrobot* was developed and used in orthopaedic surgery. A team led by James McEwen and Geof Auchinlek, in collaboration with the orthopaedic surgeon Brian Day, used it in Vancouver (BC, Canada), but unfortunately any publications nor reports of their experiences are present in the literature.

In 1985 a modified PUMA 200 (Programmable Universal Machine for Assembly, Advanced Research & Robotics, Oxford, CT, USA) industrial robot was used to guide a needle for brain biopsy with 0.05 mm accuracy using CT guidance [103]. The surgeon, who had at his/her disposal a preoperative image of the intracranial lesion, could set the point for the biopsy, while the robotic system transformed it in stereotactic coordinates and find the appropriate drilling point. This system lacked safety features and did not take in consideration the brain shifting effect that occurs after a craniotomy, but the potential of this technology excited scientists all over the world. This first prototype was later developed and commercialized by Integrated Surgical Systems (Sacramento, CA, USA) under the name *Neuromate* (see fig. 3.1), the world first stereotactic robot for neurosurgical procedures approved in 1999 by the Food and Drug Administration (FDA, the agency of the United States Department of Health and Human Services responsible, among other things, for the regulation and supervision of medical devices). In 1992, Integrated

Surgical Systems, in collaboration with IBM, was also involved in the development of *Robodoc*, a milling robot designed for hip replacement procedures (see fig. 3.1).

In their first versions, Neuromate and Robodoc were basically industrial manipulators adapted as active instruments holders, since they could guarantee a precise positioning and a correct execution of pre-operative plans, better than any experienced surgeon's hand. Anyway, their industrial origin made them not so suitable for a sterile and relatively small environment such as the operating room.

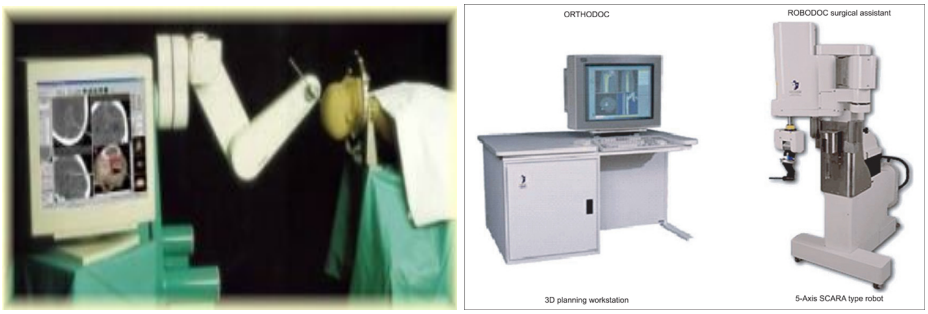

Fig. 3.1. Left: First version of the Neuromate robot (reproduction from `http://www.emsmedical.net`). Right: Robodoc (reprinted from [178]).

The real advancements in surgical robotics occurred in the early 1990s, when the Defense Advanced Research Projects Agency (DARPA), a government agency of the U.S. Department of Defense responsible for the development of new technologies for military use, envisioned the application of telecommunication and robotics technology to the battlefield. In the DARPA vision, a surgeon would be able to operate a wounded soldier from a remote location, with robotic arms duplicating the motion of the surgeon's hands: this technology was called *telepresence* [158]. With initial DARPA fundings, Yulan Wang founded Computer Motion, Inc. (Goleta, CA, USA) and developed the first voice activated robotic camera for laparoscopic surgery called *AESOP* (Automated Endoscopic System for Optimal Positioning) (see fig. 3.2). AESOP arose from a former robotic project carried on by the National Aeronautics and Space Administration (NASA) agency, and consisted of a robotic arm, modified to hold a laparoscopic camera, whose movements were controlled by the surgeon with feet and, later on, also with speech recognition, thanks to the *Hermes* voice activation system developed by Computer Motion, too. AESOP received the FDA approval in 1994 and, since then, it was successfully used in many different surgeries, providing steadier images than a human operator. However, the camera movements were slow and required continuously manual or verbal input from the main surgeon. In this case, the advantages of a robotic approach were partially limited by its drawbacks: an experienced assistant typically knows in advance the surgeon's requests according to the particular operation, and could prevent them or execute them promptly. Nevertheless, these drawbacks did not limit the spread of this new technological system and, principally, the idea of automatic surgical assistants.

The AESOP success paved the way for the following developments: so far, robotics manipulators were used just as steady holders but, to go toward the DARPA vision of surgical robotics arms, improvements in robot design and haptics were required. In 1997, Akhil Madhani, a PhD student from the MIT (Massachussets Institute of Technology, Cambridge, MA, USA) Artificial Intelligence lab directed by Kenneth Salisbury Jr., officially presented the *Black Falcon*, a new eight DOFs teleoperated surgical instrument with a distal dexterous wrist and force sensors (see fig. 3.2) [112]. The major improvement of the Black Falcon was the enhanced dexterity, exploited in the teleoperation scheme thanks to the first version of the PHANToM haptic interface, also developed in Salisbury's lab. This technology won several awards and became the standard structure for the upcoming multiarms surgical robots.

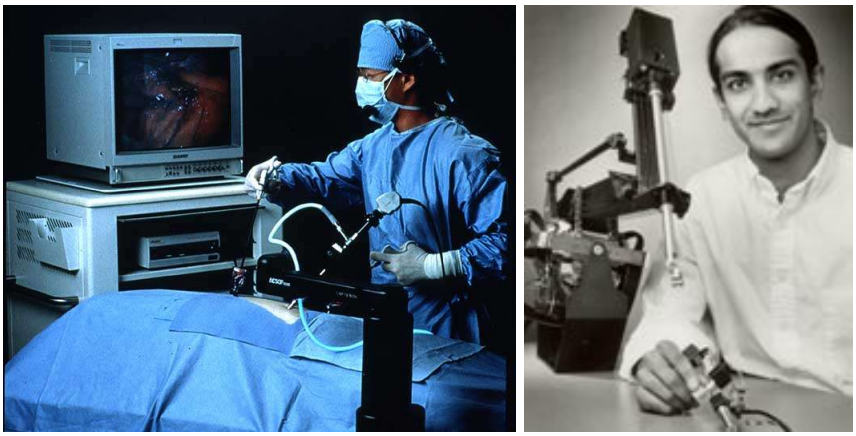

Fig. 3.2. Left: Surgeon performing laparoscopy with the support of AESOP (reproduction from `http://www.spineuniverse.com`). Right: Akhil Madhani and its Black Falcon (photo by Barry Hertherington, reproduction from `http://web.mit.edu`).

After the success of its AESOP, in mid 1990s Computer Motion started the development of a new surgical robot, named *Zeus*, composed by a patient cart, holding three robotic arms, and a workstation console, which implemented custom interfaces for its control and the visualization device. In the same period, Frederick Moll, Robert Younge and John Freund, researchers at the Stanford Research Institute (now SRI International, Menlo Park, CA, USA) who were working on a telesurgery robotic system with DARPA and NASA grants, founded Intuitive Surgical, Inc. (Sunnyvale, CA, USA) with the aim to develop robotically controlled instruments for minimally invasive surgery. Since the two companies were on similar markets at the same time, a strong rivalry between them inevitably started. Immediately after its development, Intuitive Surgical bought the Black Falcon patent from Madhani, and enrolled him and Salisbury as consultants. Together, they developed the *da Vinci* telerobotic surgical system (see fig. 3.3), which was used for the first time ever in 1997 in Brussels (Belgium) to perform a laparoscopic cholecystectomy on animal models [75]. The first version of the da Vinci robot had

three robotic arms (one for the endoscopic camera and two for instruments) and a surgeon console with a 3D vision system. A big effort in ergonomics and vision quality was done by Intuitive Surgical in order to improve the depth perception, normally lost because of 2D cameras employed in classical laparoscopes, and to regain eye-hand coordination with a natural posture.

Fig. 3.3. First generation of the da Vinci surgical system by Intuitive Surgical (©2013 Intuitive Surgical, Inc.).

The Zeus system from Computer Motion, introduced in 1999, had a different kinematic design compared to the da Vinci: it was a bed-mounted robot (cfr. section 3.2) composed by three arms with a SCARA architecture. These arms were similar to the AESOP, but they had two more passive DOFs for fine positioning of instruments. The Zeus workstation was designed so that the surgeon is seated in front of a video monitor and wears polarized 3D glasses to view the projected image (see fig. 3.4).

The da Vinci Surgical System was the first operative surgical robot that received the FDA approval in 2000, while Zeus was used in 2001 for the *Operation Lindbergh*, the world first transatlantic tele-surgical laparoscopic cholecystectomy performed with the surgeon located in New York, USA, and the patient in Strasbourg, France [114].

In 1999, Computer Motion sued Intuitive Surgical for infringement of nine patents, and in 2002 the District Court for the Central District of California has ruled that the da Vinci Surgical System infringed the US6244809 Computer Motion's patent [198]. In response, Intuitive Surgical and IBM filed the patent in-

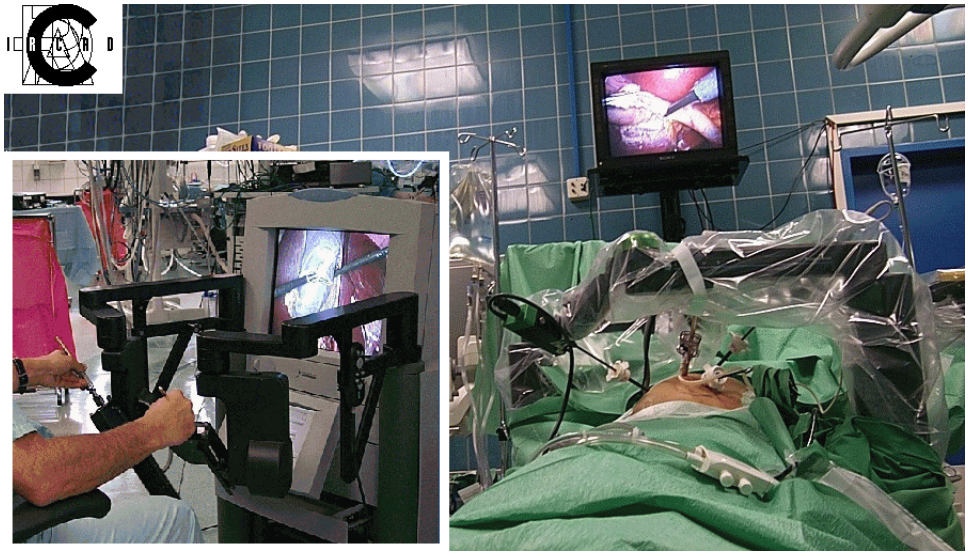

Fig. 3.4. Zeus surgical robot by Computer Motion (reprinted from [174]).

fringement suit against Computer Motion in reference to the Zeus voice-controlled technology [21]. In early 2003, a federal jury issued a ruling requiring Computer Motion to pay Intuitive and IBM $4.4 million for infringing a patent covering aspects of Intuitive's system [179]. After further complications, on March 7th, 2003 the two companies announced their merging: Intuitive Surgical paid $150 million for the property of Computer Motions, including all its patents and products [4]. At present, Intuitive Surgical stopped the sell of Computer Motion's products, while continuing to improve its da Vinci Surgical System arrived now to the fourth generation.

3.4 Robotics in no-scar surgery

Nowadays, the *da Vinci Surgical System* (Intuitive Surgical, Inc., Sunnyvale, CA, USA) is the main actor in laparoscopic surgical robotics: though at the beginning it was specifically designed for cardiac surgery, it is actually a multi-purpose teleoperated robot with applications in gynaecology, urology, gastroenterology and many other medical specialities. It offers all the advantages of a robotic system, such as motion scaling, tremor filtering, multi-arms control and, in its last generation, telementoring and virtual training. However, it still presents some limitations: its cumbersome slave system makes the preoperative installation laborious and time demanding, the four arms occupy a large part of the space around the operating bed, limiting the access of the assistant surgeon, and the slave robot design is barely suitable for no-scar surgery. In 2010, Intuitive Surgical introduced a new system, named *VeSPA*, to extend its robot applications to LESS. VeSPA is composed by two curved cannulae connected to standard da Vinci robotic arms. Cannulae can host semi-rigid instruments that are inserted inside the body through a special

silicon port (see fig. 3.5). The access port has an 8.5 mm gate for the scope (which goes straight through the port) and two 12 mm gates for instruments. Compared to standard da Vinci configuration, just three of the four available robotic arms are used, in an attempt to limit external collisions between them. Moreover, due to size limitation, VeSPA instruments do not have a wrist at their distal end, as in standard da Vinci instrumentation.

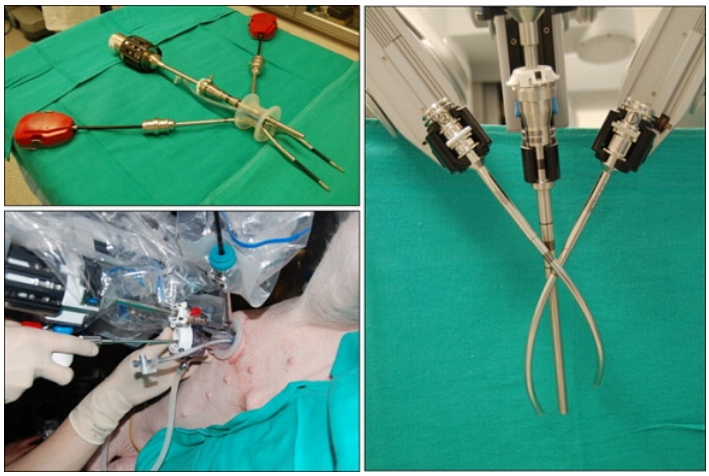

Fig. 3.5. VeSPA system by Intuitive Surgical (reprinted from [6]).

The da Vinci surgical system, who started to be sold in the early 2000s, represents the result of years spent in research and development during the 1990s with the aim to conceive a specifically designed robot for laparoscopic surgery, and not to adapt a generic industrial manipulator as done before (cfr. section 3.3). But when the da Vinci came out on the market, some surgeons had already begun to perform preliminary attempts in no-scar surgery with manual instrumentation (cfr. section 2.3). Articulated instruments (cfr. section 2.4.2) started to appear as an improvement of standard laparoscopic instrumentation, restoring inside the body the DOFs lost because of the trocar constraint. In an effort to enhance the easiness of use of such systems and to offer more ergonomics interfaces, some research groups started to produce robotized articulated instruments, controlled by joystick interfaces. A particular prototype was proposed in 2010 by Morel *et al.* (Université Pierre et Marie Curie, Paris, France) [72], which consists in an articulated instrument moved by an active trocar and controlled by a joystick handle (see fig. 3.6). This instrument has a total of 6 DOFs, three of which robotized: shaft rotation, tip bending and rotation. The active trocar is designed to fit inside a classical surgical trocars, and it contains the servoactuator for the shaft rotation: this choice allowed to reduce the instrument weight and, therefore, the fatigue in using it. The handle consists in a commercial joystick (Wii Nunchuck by Nintendo Company Ltd., Kyoto, Japan) connected to the proximal side of the instrument shaft by a passive knee joint: in this way it is possible to keep the handle orientation when the instrument rotates. The joystick provides a 2-DOFs

controller, which is associated to the tip movements, and two buttons, which controls the shaft rotation. The tip bending is performed thanks to Shape Memory Alloy (SMA) wires, which are pretensioned in the straight position and powered through the active trocar. This prototype has been recently tested *in vitro* and *in vivo* [71], but it still need improvements mainly on its control: when the handle orientation is not aligned with instrument's one, it could be difficult to keep the coordination between the joystick commands and the produced movements. Moreover, SMA wires typically present inner limitations, such as hysteresis in the actuation and heat management, that can compromise their practical use.

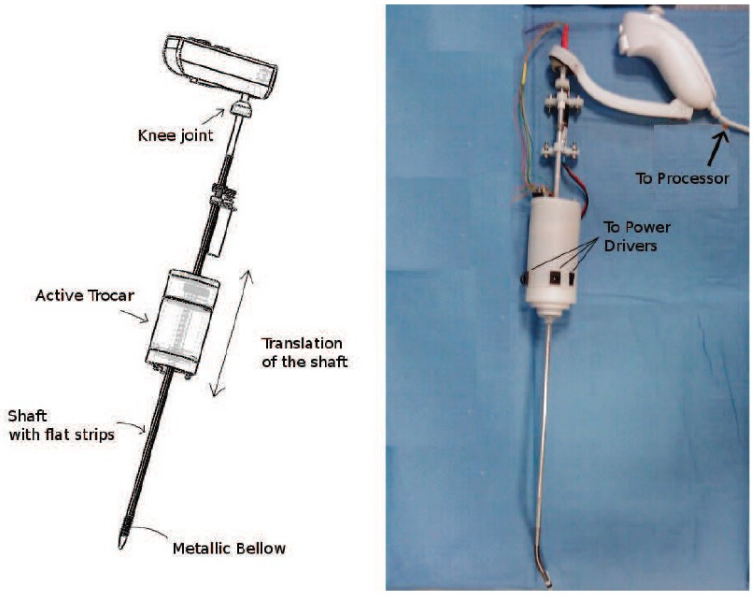

Fig. 3.6. Robotized surgical instrument by Université Pierre et Marie Curie, Paris (reprinted from [71]).

With the progressive adoption of MIS and, more recently, no-scar surgery techniques, many instruments manufacturers and research groups started to design dexterous robotic systems more suitable for a minimally invasive approach than a relatively big, multi-purpose robot as the da Vinci. The key-point in the early stage of development of these new robotic platforms (as for manual instrumentation, cfr. section 2.4) was the use of flexible sections, in order to increase dexterity and to enlarge the available workspace. In the medical practice, some flexible instruments were already used, such as gastroscopes and catheters, therefore they were taken as basis for the development of new robotic systems.

One of the first prototypes proposed in the early 2000s was the *ViaCath* by EndoVia Medical (now acquired by Hansen Medical, Norwood, MA, USA).ViaCath was a flexible system, evolution of the EndoVia Laprotek laparoscopic surgical

robot [57], intended for intraluminal transgastric operations. From the Laprotek, ViaCath borrowed the master interface, while the slave part was constituted by a standard flexible endoscope that carried two flexible instruments, which had two independent bending sections each and an articulated tip on their distal side (consisting in a total of 7 DOFs, see fig. 3.7) [1]. This prototype was tested on *ex vivo* tissue samples and *in vivo* animal trials, revealing some limitations in insertion and positioning of instruments and insufficient lateral force that the tool could exert during tissue manipulation. For these reasons, a second generation of the system was proposed, which included an overtube to rigidify the endoscope and a new actuated joint section design (which replicates the kinematic of the human arm) for instruments.

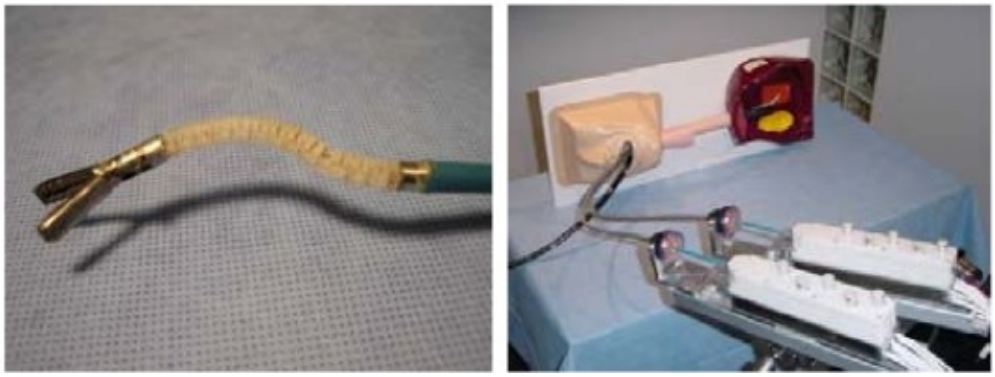

Fig. 3.7. First generation of ViaCath by EndoVia Medical (reprinted from [1]).

The ViaCath system never became a commercial product, but its technology served as basis to Hansen Medical, buyer of EndoVia Medical, to develop its *Sensei® X Robotic Catheter System*. Sensei® X consists of a master console equipped with a 3 DOFs haptic interface, a 3D screen for intraoperative stereoscopic visualization and several other screens for complementary informations (see fig. 3.8). The slave system is a robotized catheter that embeds both a force sensor and the CoHesion^{TM} 3D Visualization Module on its tip. This system obtained the FDA clearance in 2007, and since then it was used in many electrophysiology interventions.

The *NeoGuide Endoscopy System* (NES) (NeoGuide System, Inc., San Jose, CA, USA, acquired in 2010 by Intuitive Surgical, Inc.) is a multi-section flexible system intended for diagnostic and therapeutic colonoscopy [47]. It consists of a flexible shaft composed by 16 flexible segments (8 cm each long) electromechanically controlled that allow the system to follow the shape of the colon (see fig. 3.9). The scope embeds a position sensor on its tip, while on its proximal side an external sensor measures the insertion depth. The main body is advanced manually into the colon, while the navigation console records every tip movement and coordinates the shape of the flexible segments. Although the system was originally developed exclusively for colonoscopy procedures, recent trials on cadaveric mod-

Fig. 3.8. Sensei® X Robotic Catheter System by Hansen Medical (©2012 Hansen Medical).

els (performed by company's affiliated surgeons) demonstrated capabilities of NES for NOTES procedures, too [49].

Fig. 3.9. NeoGuide Endoscopy System (NES) by NeoGuide System, Inc. (reprinted from [47]).

In addition to the systems described above, which are so far the only ones commercially available, a number of robotic prototypes were proposed in the last years from several research groups worldwide. The *Master And Slave Transluminal Endoscopic Robot* (MASTER) by Phee *et al.* (Nanyang Technological University, Singapore, Republic of Singapore) is a two-armed manipulator that can be attached to the tip of a standard dual-channel endoscope [139]. Each arm, which is tendon-actuated, offers 4 DOFs but, since the instruments lengths are fixed, they cannot translate without a movement of the whole endoscope. The slave robot is controlled with a dedicated master interface, mounted on a metallic frame, that replicates the slave kinematics (see fig. 3.10). This robot was recently evaluated in both *ex vivo* and *in vivo* animal trials [80], showing a relatively short learning curve and capabilities for no-scar surgeries. However, it still presents limitations in sterilization and safety, since all the tendons and cables of the slave robot are exposed.

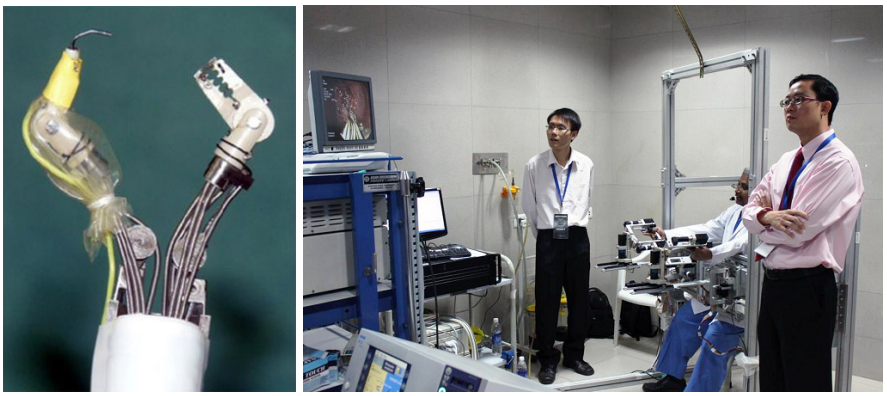

Fig. 3.10. Master And Slave Transluminal Endoscopic Robot (MASTER) by Nanyang Technological University, Singapore (reproduction from `http://research.ntu.edu.sg`).

The *Higly Versatile Single Port System* (HVSPS) proposed by Feussner *et al.* (TUM, Technological University of Munich, Germany) is a three-channels semi-rigid guide designed to host two flexible instruments and a scope for LESS surgeries [23]. The system is composed by a rigid overtube that contains three channels, which can independently translate and rotate (see fig. 3.11). The instrument channels are articulated at their distal side, and they end with a continuum section foldable in two orthogonal directions. Globally, each channel has 5 DOFs, plus 2 more DOFs from the instrument movements (translation inside the channel and grasper actuation). Only the instruments channels DOFs are actuated, and their control is achieved by means of two joysticks. The remaining DOFs (endoscope channel and overtube movements) are delegated to a second human operator. Instruments too are passive, so a third operator is necessary to move them. This system is still under development and, though some phantom tests were recently performed, it requires important improvements in control.

An experimental robotic prototype for LESS surgery was also developed in 2011 by Fujie *et al.* (Waseda University, Tokyo, Japan). Their system consists of

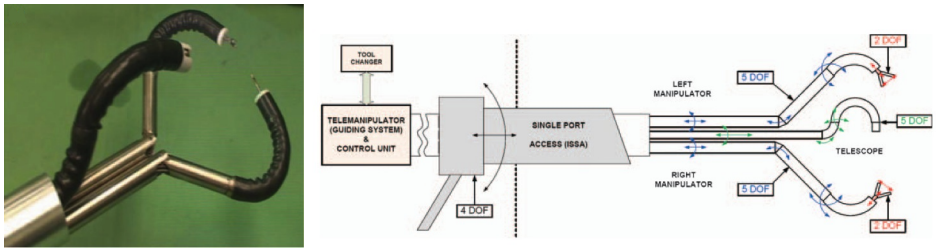

Fig. 3.11. Higly Versatile Single Port System (HVSPS) by Technological University of Munich (reprinted from [23]).

an external positioning manipulator that holds the slave robot and allow it to turn around a pivot point (see fig. 3.12) [99]. The slave robot is composed of a proximal rigid shaft linked to a distal snake-like continuum section. An endoscopic camera and two instruments come out from the distal tip in parallel directions, but a minimal triangulation can be achieved thanks to instruments design. After the pivot point, the system globally shows 11 DOFs: 3 for the continuum section, 5 for the forceps and 3 for the cautery tool. The slave system is controlled by two PHANToM Omni haptic interfaces (SensAble Technology, Woburn, MA, USA). This prototype system was tested in animal models for LESS resection of liver, but it still presents some issues concerning the limited workspace, difficult instruments interchangeability and cumulative error in the teleoperation control scheme that is not well compensated [163].

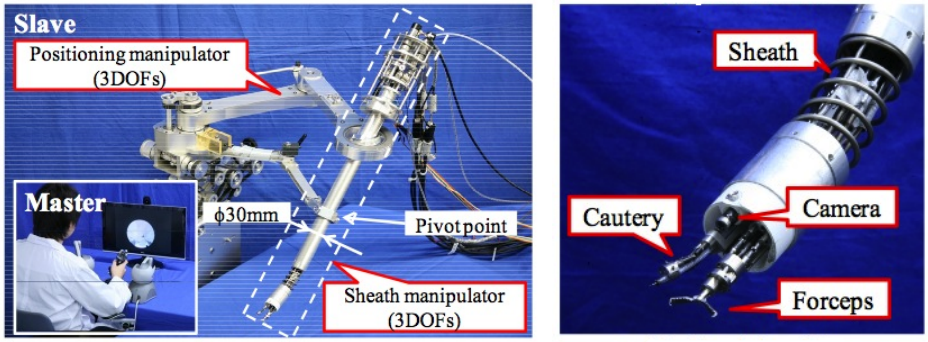

Fig. 3.12. Robotic prototype for LESS by Waseda University, Tokyo (reprinted from [163]).

Since the access into the human body from a single entry point constrains the instruments movements and largely limits their workspaces when using rigid instrumentation, flexible systems could represent a solution to restore the lost mobility inside the body. The prototype systems presented so far could be already considered as flexible robots, since they are provided with single bending sections on their distal side. Recently, in an effort to increase the dexterity of such systems, some research groups proposed novel solutions in which two or more

bending sections are coupled together. These systems, commonly called *snake-like robots* because of their biomimetic design, started to be developed in the 1970s mainly to study the snakes locomotion and replicate it on a robot [78]. In surgical applications, instead, a snake-like design allows to obtain dexterous instruments that have larger workspaces than the rigid ones in case of a single port access. The main challenge in this case is to miniaturize the actuation means of such systems and to find a good compromise between their flexibility and the rigidity needed for a proper force reflection during their use (cfr. section 2.4).

Simaan *et al.* from Vanderbilt University (Nashville, TN, USA) have developed the *Insertable Robotic Effectors Platform* (IREP), a compact foldable system for LESS surgery that can be inserted into the body through a 15 mm access port [9]. It consists of a rigid foldable shaft, which hosts two cameras in stereoscopic configuration, and two flexible instruments, arranged in order to obtain good triangulation (see fig. 3.13). The camera shaft allows pan, tilt and zoom movements, while each instrument has 6 DOFs: 4 for the continuum section, 1 for the distal wrist and another for gripper. Moreover, each arm can translate independently, which results in a total of 21 DOFs. For the time being, the system has never been tested *in vivo*. Some first lab experiments showed a limited wrist mobility that does not offer a good range of movements for complex tasks such as knot tying.

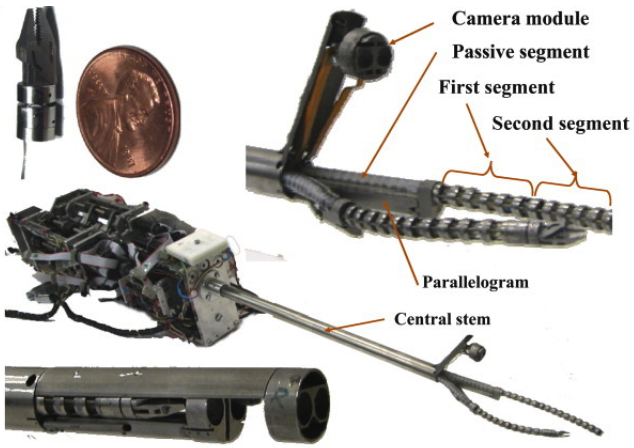

Fig. 3.13. Insertable Robotic Effectors Platform (IREP) by Vanderbilt University, Nashville (reprinted from [7]).

Yang *et al.* from Imperial College (London, UK) have recently developed the *i-Snake*®, a lightweight modular robotic prototype for transgastric surgeries based on universal joints with embedded micromotors [166]. This system features an articulated distal tip, mounted on the front of a rigid shaft, with 7 DOFs arranged as 2 universal joints (intersecting pitch and yaw) and 3 single DOF joints (yaw only) (see fig. 3.14). In the joints structure, two channels (3 mm in diameter) are reserved for the endoscopic camera and for an instrument. The system control is performed with a 2-axis thumbstick in a joint-per-joint way: the movements on the thumbstick control the pitch (only for universal joints) and the yaw of each single

joint, while a button permits to switch the thumbstick control to the following joint (as in a serial chain). This control system is not so intuitive and, together with the presence of just one instrument, represents a big limitation in its use. Recently, an evolution of the i-Snake®, which includes two tendon driven flexible arms and one foldable rigid arm for the camera, has been presented [167] (see fig. 3.14). In this new version, the thumbstick is still used to control the articulated section, but the two additional flexible arms, which come out from the main body when the system is placed in an S-shaped configuration, are controlled by two haptic interfaces (PHANToM Omni by SensAble Technology, Woburn, MA, USA).

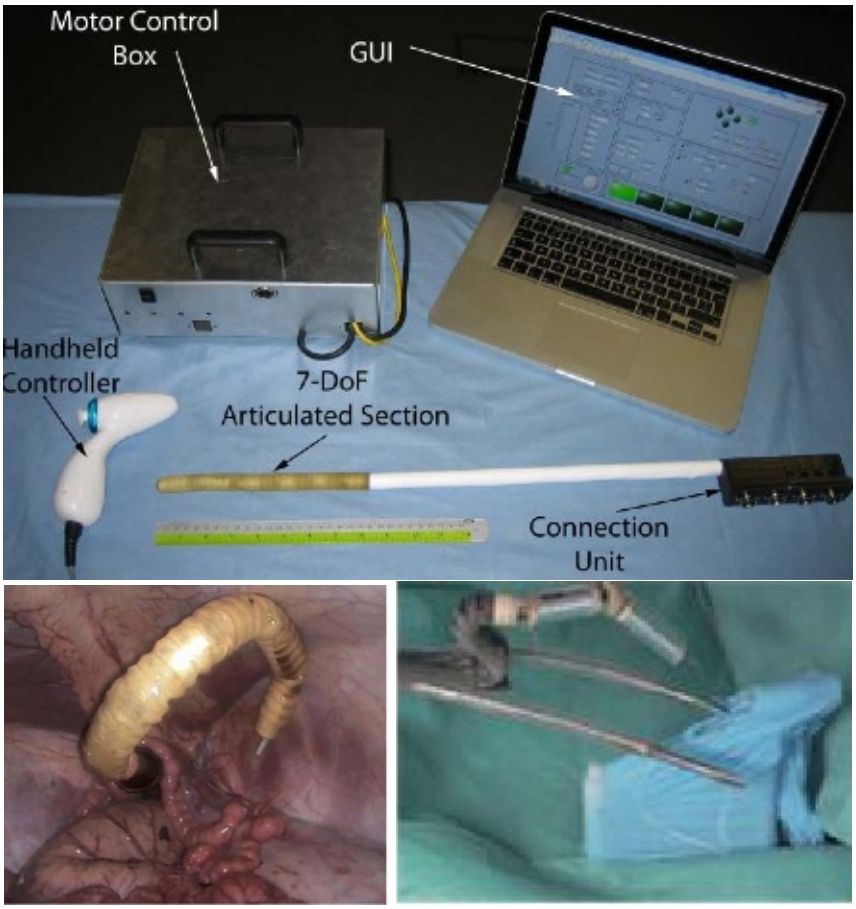

Fig. 3.14. Top: i-Snake® system and control box by Imperial College, London. Bottom left: i-Snake® in retroflexed configuration. Bottom right: second version of i-Snake® (reprinted from [166], [167]).

An example of robotic prototype become a commercial system is the *Highly Articulated Robotic Probe* (HARP), initially developed by Choset *et al.* (Carnegie Mellon University, Pittsburgh, PA, USA) and now commercialised as *Flex*^{TM} *Robotic System* by Medrobotics, Inc. (Raynham, MA, USA). HARP (formerly

named CardioARM) was designed with the aim to enable minimally invasive intrapericardial therapeutic delivery through a subxiphoid approach [133] (see fig. 3.15). It is composed by two concentric tubes, consisting of 50 cylindrical links serially connected through spherical joints. The overall actuation mean consists of three cables connected to the distal link: the moment exerted on that link is passively transmitted to the followings, which adapt their orientations according to the tubes rigidity. In a recent evolution of this system [150], two flexible articulated instruments (developed by Design Standards Corporation, Charlestown, NH, USA) are inserted from the proximal side, and a special cap mounted on the system tip, which embeds an endoscopic camera, achieves triangulation between them. This new version is primarily intended for transoral laryngeal surgery, in which the use of rigid instrumentation is not suitable.

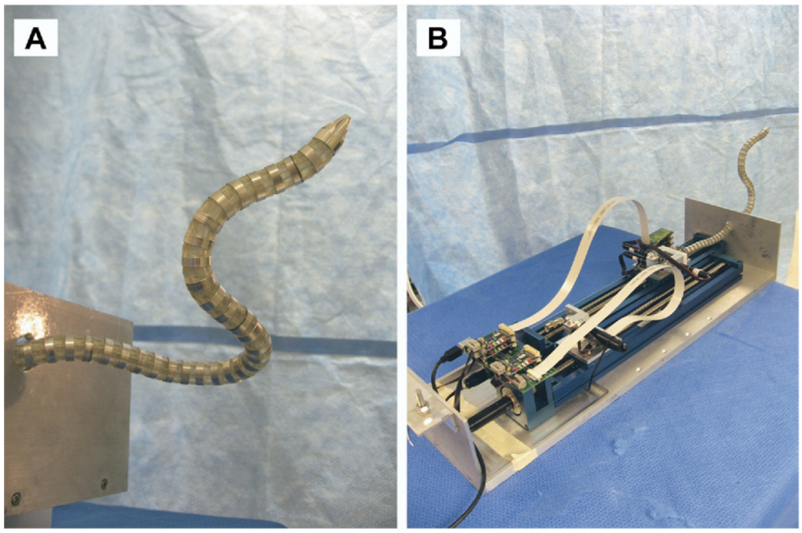

Fig. 3.15. Higly Articulated Robotic Probe (HARP) by Carnegie Mellon University, Pittsburgh. A: Distal flexible part; B: Feeder instrumentation box containing all the actuators (reprinted from [133]).

A different solution in the development of no-scar robotic instruments consists in using discrete articulated robots, in which small rigid links are connected in a way that mimics the human arm anatomy. With the support of the recent 7th Framework Program (2007-2013) coordinated by the European Community, a consortium named ARAKNES (Array of Robots Augmenting the KiNematics of Endoluminal Surgery) was established with the aim to develop a novel robotic platform for no-scar surgery. Eleven academic and industrial partners have collaborated for the whole project period, and several prototypes have been carried out. The *Single-Port lapaRoscopy bImaNual roboT* (SPRINT) is a robotic platform composed by two 6 DOFs arms that could be folded in order to pass through a 30 mm trocar [138]. Once the operation point is reached, the two arms take a configuration similar to the human arms (see fig. 3.17). A stereoscopic camera is

placed at the shoulder level, while the motors that actuate the distal segments of the system are directly embedded inside its structure. The slave robot is telemanipulated by means of two PHANToM Omni haptic devices (Sensable Technologies, Inc., Woburn, MA, USA), and a 3D screen allows stereoscopic vision with polarized glasses. Although recent *in vivo* trials have been performed on animal models, SPRINT is still too large for practical use in humans, requiring a platform miniaturization as future development.

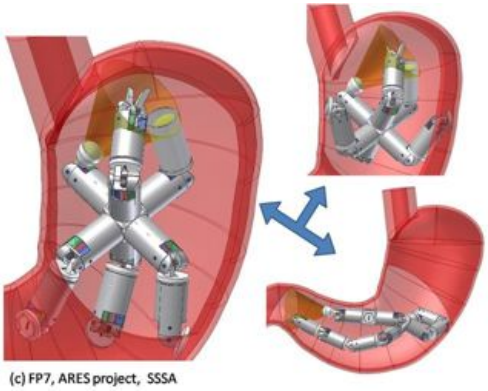

Fig. 3.16. Conceptual sketches of the ARES project, Scuola Superiore Sant'Anna, Pisa.

A previous project called Assembling Reconfigurable Endoluminal Surgical System (ARES) (supported by the 6th Framework Program, 2002-2006, European Community, and led by the Scuola Superiore Sant'Anna (SSSA), Pisa, Italy) aimed at developing a reconfigurable swallowable modular robot for intraluminal surgery [130]. In the conceptual design, several autonomous modules have to be swallowed by the patient and, once in the stomach, they rearrange themselves in order to form a two-arms robot with triangulated instruments and vision capabilities (see fig. 3.16). This project led to the development of a preliminary prototype with many limitations in practical use, from the large module size to the weak forces applicable by the instruments. But, starting from the idea of modular robotics, a new robotic prototype was designed by the ARAKNES consortium. It makes use of the Magnetic Anchoring and Guidance System (MAGS), originally developed by Park *et al.* [136], in order to control the system by means of external magnets placed on the skin. In this case, the system is not swallowable, but it is inserted through a skin incision. This prototype is composed by three main parts: a magnetic anchoring frame, the modular robotic units and a docking mechanism [184]. The anchoring frame, conceived to assure system stability inside the abdominal cavity during surgical tasks, is composed by three rigid sections serially connected. For its placement, it is inserted straight from the incision point, while once in place an internal actuation system (Shape Memory Alloy (SMA) wires) changes the sections orientations forming a triangular shape. The frame stabilization is then assured by external permanent magnets, placed on the skin, that anchor it to the abdominal wall. A miniaturized camera robot is coupled with the frame, and a dedicated

docking mechanism has been integrated in order to assure positioning and anchoring of robotic modules (see fig. 3.17). For the moment, this system was just tested *in vitro* in order to investigate the feasibility in reconfiguration. Since the size of the system is constrained by the access port, standard electric motors are not suitable to be embedded in such prototypes. MAGS actuation could represent a good solution in this case, but many advancements are still needed before arriving to a safe and effective clinical use. For this reason, many other research groups are studying the MAGS actuation system for their miniature robots [105] [143] [22].

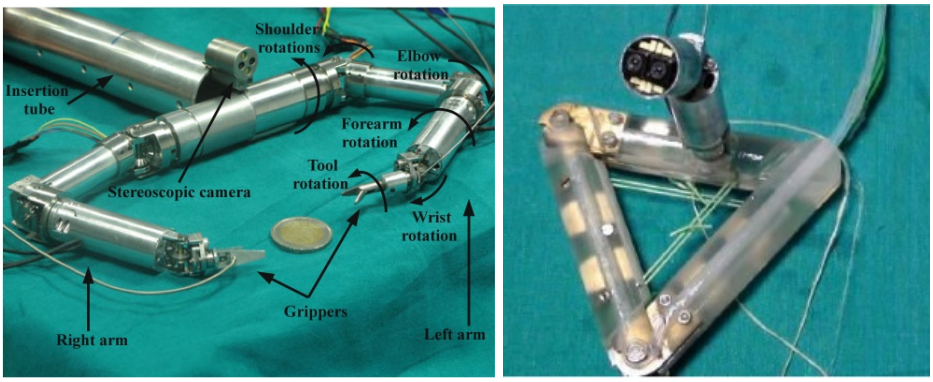

Fig. 3.17. Left: SPRINT prototype. Right: modular surgical robot, ARAKNES consortium (reprinted from [138], [184]).

3.5 STRAS: Single access and Transluminal Robotic Assistant for Surgeons

In 2009, a collaboration between the University of Strasbourg, IRCAD (Institut de Recherche contre les Cancers de l'Appareil Digestif, Strasbourg, France), Karl Storz GmbH (Tuttlingen, Germany) and with the financial support of the Alsace Biovalley Cluster (Illkirch, France), led to the establishment of a project called ISIS. The aim of this project was the development of a novel flexible surgical robot for no-scar surgery. The ISIS project (2009-2013) is the continuation of a former project, named ANUBIS (2005-2008), in which Karl Storz, with the collaboration of IRCAD surgeons, developed the ANUBISCOPE® platform (cfr. section 2.4). In the ISIS project, a shorter version of the ANUBISCOPE® is proposed to be robotized, since this novel system should be aimed for endoluminal or close transluminal operations.

3.5.1 ANUBISCOPE

As briefly described in section 2.4, ANUBISCOPE® consists of a flexible actuated endoscopic guide, which allows the insertion of two flexible instruments inside the body and the displaying of the surgical scene thanks to an endoscopic camera

embedded at its tip (see fig. 3.18). In this system, every actuated flexible part is composed by a passive vertebrae structure (noted B, see fig. 3.18) and a pair of antagonistic cables for each bending direction (noted A, see fig. 3.18). The main endoscope has a distal section that can be deflected in two orthogonal directions, thanks to a couple of lockable rotating knobs placed on its handle (noted A, see fig. 3.19). Each pair of deflecting cables ends on one knob that, if rotated, exerts a tension on one cable while releasing the other one. On their distal side, the cables are attached to the first top vertebra of the passive structure: in this way, the cables tension determines a flexional moment on the first vertebra that is passively transmitted to the following ones.

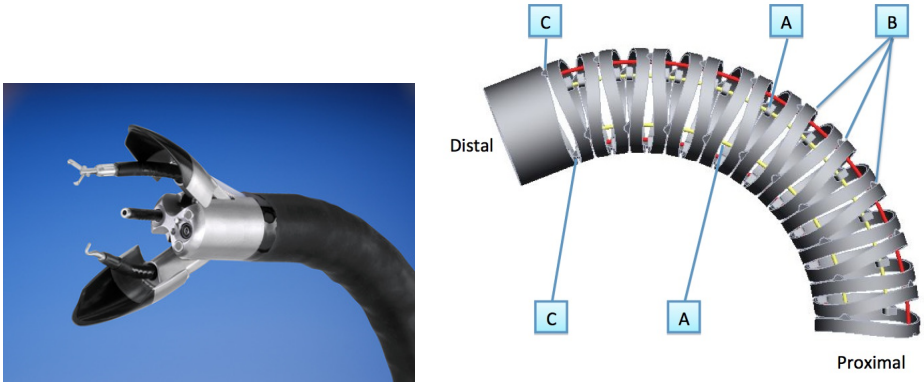

Fig. 3.18. Left: ANUBISCOPE® head detail. Right: vertebrae structure employed in ANUBISCOPE® flexible sections. A: Deflecting cables. B: Vertebrae. C: Cables attachment points.

A simplified and miniaturized vertebral structure is implemented inside each instrument, too: in this case, the deflection is allowed in just one direction, and the cables pair is linked to a sliding actuator placed on the instrument handle (noted C, see fig. 3.19). With this handle the main surgeon can mechanically rotate and translate the instrument inside its channel and vary the instrument deflection. In case of actuated instruments as grasper, a gripper on the handle (noted D, see fig. 3.19) allows its control thanks to a push-pull cable.

The overall manual control of the ANUBISCOPE® platform requires at least two operators: the main surgeon takes the control of the two instruments, while his/her assistant holds the endoscope handle and controls the deflections of the endoscope actuated section. Moreover, a third operator is typically placed near the endoscope access port, with the duty of manually insert or retrieve the main endoscope and exert slight rotations on it, according to the main surgeon requests (see fig. 2.19 for a typical physicians placement in the operating room during a no-scar surgery). It is evident that the coordination between all these operators must be optimal, since every change in the endoscope position affects both the endoscopic image and the instrument positions, thus representing a potential risk during a surgery if done without a common agreement.

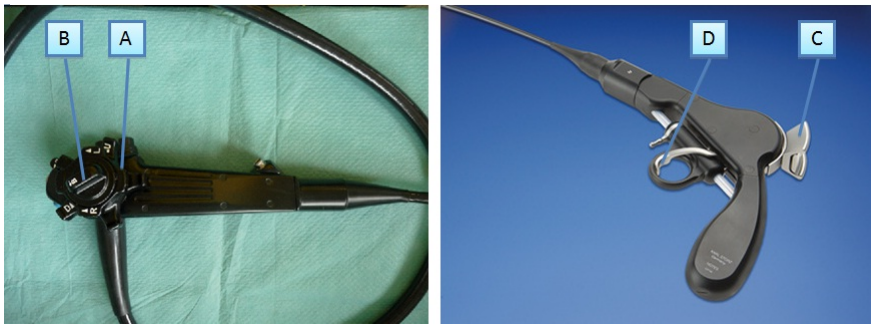

Fig. 3.19. Left: endoscope deflections actuators. A: Rotating knobs. B: Deflections lock control. Right: ANUBISCOPE® instrument handle. C: Deflection actuator. D: Gripper.

The main physical dimensions of ANUBISCOPE® are summarized in table 3.1.

Endoscope		
Part	Diameter (mm)	Length (mm)
Passive section	16	260
Actuated section	18	175
Rigid head	18	48
Instruments channels	4.2	648
Auxiliary channel	3.2	648

Instruments		
Part	Diameter (mm)	Length (mm)
Passive section	3.9	825
Actuated section	3.9	27
Rigid tool: grasper	3.9	13
Rigid tool: hook	3.9	12

Table 3.1. Main physical dimensions of ANUBISCOPE®.

3.5.2 Robotization

The first part of the ISIS project was aimed at the robotization of the short ANUBISCOPE® platform. At this stage, the choice was to preserve as much as possible the original mechanical structure of the ANUBISCOPE® system, in order to exploit its suitability for the clinical use. To achieve this objective, the robotization process concerned the proximal side of the manual system, where all the actuation controls are located.

For the main endoscope, the two rotating knobs were replaced by a set of spur and bevel gears (noted A, see fig. 3.20), driven by a pair of RSF-5A-50 servo actuators from Harmonic Drive (Harmonic Drive Systems, Inc., Tokyo, Japan)

(noted B, see fig. 3.20). To reproduce the manual translation, the endoscope is hosted on a mobile platform (noted C, see fig. 3.20), anchored to the operating table by means of a passive reconfigurable arm (noted F, see fig. 3.24), that can translate forward and backward. The instruments channels entrance (noted D, see fig. 3.20), as well as the buttons to control camera parameters, air/water feeding and suction (noted E, see fig. 3.20) are kept accessible and free of any mechanical part. Gears and motors parts are covered by plastic caps, in order to avoid any contact or injury during the use. Hitherto, this prototype version does not include an automatic system for rotating the whole platform, but a manual adjustment can be done by changing the configuration of the passive arm.

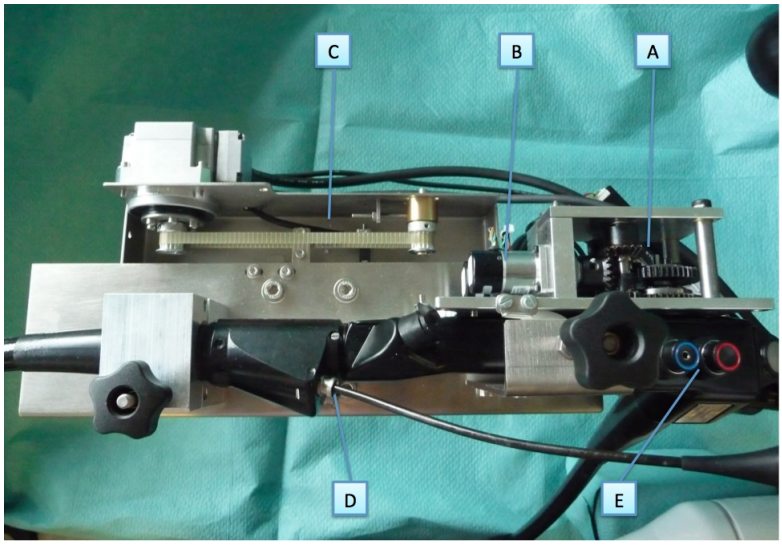

Fig. 3.20. Robotization of the endoscope. A: Gears. B: Harmonic Drive servo actuators. C: Mobile platform. D: Instruments channels entrance. E: Controls for camera parameters, air/water feeding and suction.

Regarding the instruments, each manual handle was totally replaced by a hollow casing (noted A, see fig. 3.21), made of polyamide and produced with the Selective Laser Sintering (SLS) prototyping method. This casing was designed to enclose the actuation mechanism for the instrument deflection: the deflection actuator (noted B, see fig. 3.21) with the two deflection cables attached (noted C1-C2, see fig. 3.21) is now connected, by means of a set of helicoidal and spurs gears (noted D, see fig. 3.21), to a Harmonic Drive RSF-3B-50 servo actuator (noted E, see fig. 3.21). The deflection actuator has a range of rotation of 56 degrees but, since the cables C1 and C2 follow two different paths, its movement affects the cable lengthening or shortening differently (see fig. 3.22):

$$\Delta C1\ (mm) \simeq 0.312\ \Delta\theta\ (degrees) \tag{3.1}$$

$$\Delta C2\ (mm) \simeq 0.275\ \Delta\theta\ (degrees) \tag{3.2}$$

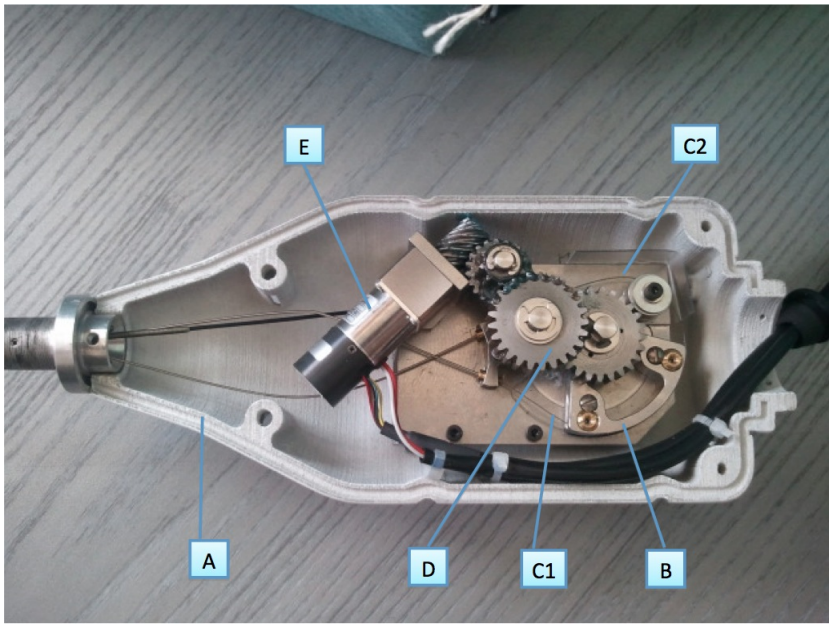

Fig. 3.21. Robotization of the instrument deflection mechanism. A: Casing. B: Semicircular element. C1-C2: Deflection cables. D: Gears. E: Deflection servo actuator.

where $\Delta\theta$ represents the variation of the actuator angular position, while ΔCx is the corresponding amount of cable pulled or released. In case of actuated instruments as graspers, the actuation mechanism for the opening and closing is embedded in the instrument casing, too: a pinion-rack system, actuated by a Harmonic Drive RSF-3B-30 servo actuator, controls the instrument push-pull cable (see fig. 3.23).

Each instrument casing is hosted inside a Translation/Rotation Module (T/RM) (see fig. 3.24), which produces the translational and rotational movements of the instrument. The cylindrical shape of the instrument casing is particularly designed to allow the instrument rotation around its axis, while the bull-nose shape of its distal part allows a good connection with the instrument sheath and saves space around the operating channels entry. When the casing is closed, a gear wheel is mounted on its proximal side (noted A, see fig. 3.24), which is connected to a servo actuator (Harmonic Drive RSF-3B-30) mounted inside the T/RM (noted B, see fig. 3.24). In this manner, the whole instrument could potentially rotate endlessly, but mechanical stops where placed in order to limit the rotation angle to 340 degrees, thus avoiding electrical cables twisting. A set of four pairs of ball bearings (noted C, see fig. 3.24), mounted inside the T/RM and located in correspondence of two grooves machined in the outer instrument casing (noted D, see fig. 3.24), serves as rotational guidance and axial stop for the instrument. The whole T/RM is mounted on a sliding guide, moved by a synchronous belt connected to a Harmonic Drive RSF-3B-50 servo actuator that controls the translational movement (noted E, see fig. 3.24). The choice to put rotation and translation actuators out of the instrument casing permits to reduce its size and weight, making instruments

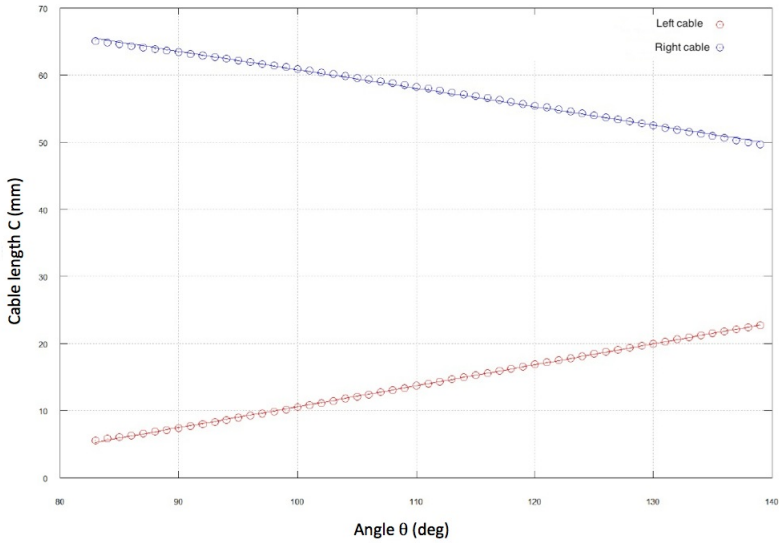

Fig. 3.22. Length variation of deflecting cables in function of the angular position of the deflection actuator.

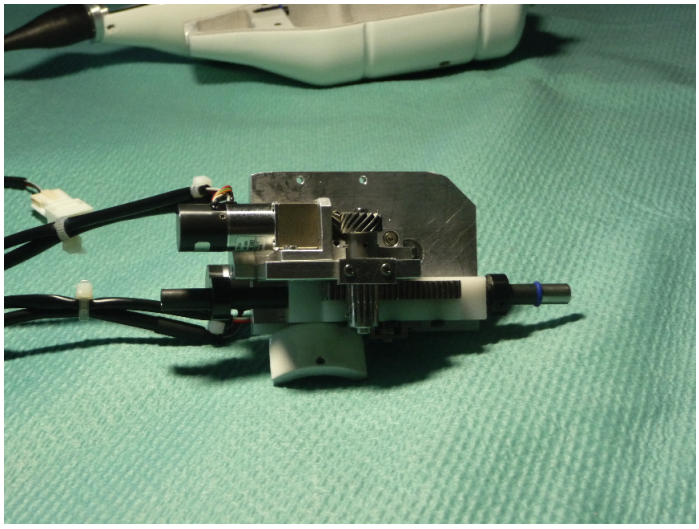

Fig. 3.23. Robotization of the instrument actuation mechanism.

interchange during the clinical use more practical. The two T/RMs are hosted on a stable platform, fixed to the operating table by means of a second passive arm (noted G, see fig. 3.24): this platform allows fine variations of the T/RMs position with respect to the instruments channels entries.

Servo actuators choice was motivated upon the system requirements in force / torque and velocity, but also for guaranteeing the smallest and lightest possible system. All the motors are from the RSF Supermini Series from Harmonic Drive,

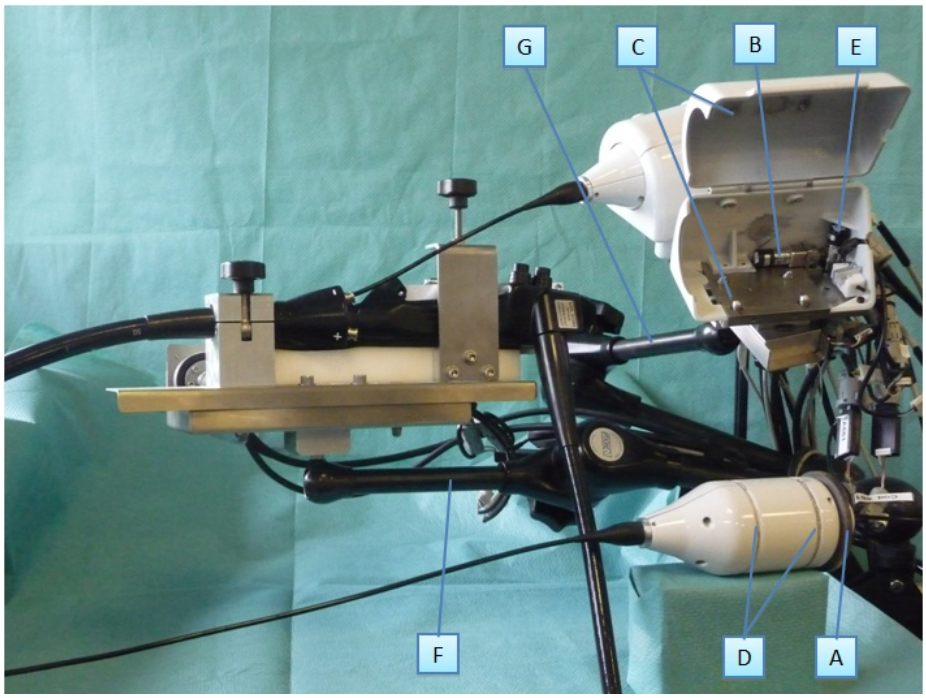

Fig. 3.24. Global view of the slave robot. A: Rotation gear wheel. B: Rotation servo actuator. C: Ball bearings. D: Instrument casing. E: Translation servo actuator. F: passive support arm for endoscope. G: passive support arm for instruments.

driven in velocity by means of servo drivers of the same manufacturer. The only exception is the servo actuator for the grasper actuation, which is controlled in current: in this way it is possible to evaluate the torque transmitted to the grasper claws, thus monitoring the force exerted on the grabbed tissue and avoiding potential damages.

3.5.3 Mechanical non-linearities

Because of its mechanical structure and cable actuation system, ANUBISCOPE®, and consequently STRAS, suffers of several mechanical non-linearities. They could be classified in three main groups:

- **Offset**: because of the mechanical design, when the instruments are inserted inside the channels, their handles are slightly deviated with respect to the tools axis. This expedient has been taken to guarantee a more natural hand posture for the surgeon, but inevitably this introduces a non-linearity in the control, which is more evident for the instruments rotation: the rotative movement applied on the instrument handle is not properly transmitted to the instrument tip, so a larger movement on the proximal side is needed. On STRAS, we tried to place the instruments as much as possible in line with their channels, so this effect is largely compensated on the robot.

- **Friction**: flexible instruments are constantly in contact with the instrument channels for almost all their lengths, and they must follow the endoscope shape when it is deflected. When the user tries to rotate the instrument, a rolling friction between the two large surfaces (instrument and channel) appears and, because of the instrument flexibility, it results in apparently no movements of the instrument distal tip when its proximal handle is rotated. On the other hand, the sliding friction is not relevant when the endoscope is straight, so that the instruments can translate in an almost straight channel slightly larger than them. When the endoscope is deflected, instead, its actuated part becomes a point of resistance for the instrument translation, and part of the instrument movement is lost for the instrument deformation inside the channel. A possible solution for the friction problem is the lubrication of the instrument channels with water: inside them a special substance was applied, which becomes slick in contact with water and facilitate the tool sliding.
- **Motion backlash**: the cable actuation system is a common choice in many different types of systems, because it is cost-effective and permits to displace any other mechanical or electrical actuator away from the system. As drawback, cables dynamics is hard to be modelized, because it depends on several factors: cables extensibility and compliance, shape of the cable conduit, frictions and loss of tension are the main ones [2]. As stated in section 3.5.1, flexible sections on ANUBISCOPE® are actuated by means of two antagonistic cables. For the instruments, these two cables are attached on the proximal side to a sliding actuator that, when rotated, applies a tension on one of them producing the desired deflection. The relationship between the actuator movement and the cable tension is almost linear in the pulling phase (cfr. eq. (3.1) and (3.2)). On the contrary, when a change of deflection is requested it will be necessary to first recover the tension on the unstrained cable before seeing any movement of the instrument tip. Since there are no cable pretension systems, this results in a hysteresis-like characteristic of the instrument deflection, with a large dead zone in the middle that is manifested each time the deflection direction is changed (see fig. 3.25). This non-linearity is the most influential cause of control issues, its behavior depends on several factors (included the endoscope shape), therefore it is very difficult to obtain a deterministic model that could compensate its effect.

3.5.4 Electrical Scheme

When designing STRAS, one of the main requirements was modularity: the idea is to have a surgical robot, completely controllable by a single user, that allows an easy interchange of instruments during the operation and that could work with a variety of different instruments, all with the same mechanical and electrical interfaces. Our current prototype is actually composed by three sub-systems (see fig. 3.26): the main endoscope, driven by three motors (two deflections and one translation), the electric knife tool, driven by three motors (rotation, translation and deflection) and the grasper, driven by four motors (same as the electric tool plus the grasper opening/closing). The sub-systems are electrically independent, each providing its own electrical box that contains servo drivers and power supply. Each electrical box is connected to a low-level controller, constituted by two

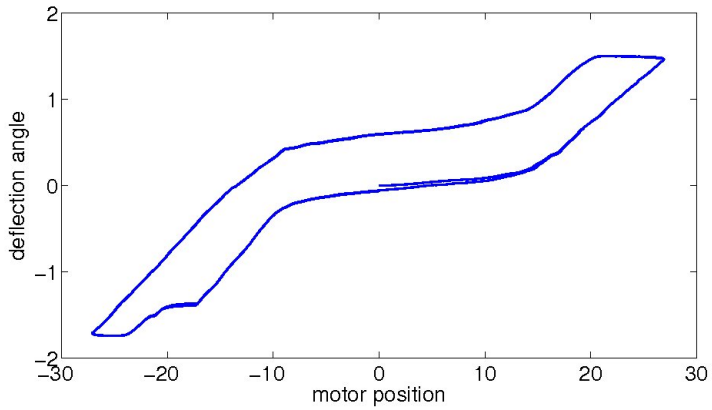

Fig. 3.25. Motion backlash for the instrument deflection.

SmartMotion^{TM} sMI6 from Adept Technology, Inc. (Pleasanton, CA, USA) serially connected. SmartMotion^{TM} is a motion controller designed for the real-time control of robotic actuators. Built on the IEEE 1394 (FireWire) standard, it allows to simultaneously control up to six motors and to report about servo drivers status and faults. It is possible to serially connect up to 4 SmartMotion^{TM} controllers, in order to drive a maximum of 24 axes. In our case, since STRAS has a total of 10 actuated DOFs, two controllers are enough for the whole system. Besides the standard low-level control, the SmartMotion^{TM} controller offers some motion planning routines that create customizable acceleration or velocity profiles according to the received motors references. It also disposes of an embedded programmable flash memory in which it is possible to upload the middleware code for interfacing the low-lever layer with the high-level controller (see section 3.5.5).

An emergency switch is available, in order to immediately shutdown the system if needed.

3.5.5 Master console

STRAS is a teleoperated system in which the slave part is composed by the robotized endoscope and instruments. The master part, *i.e.* the interface between the user and the robot that allows its control, consists of two omega.7 haptic interfaces from Force Dimension (Nyon, Switzerland), a pedal board and a high-level controller, which manages the user input and transforms it in proper references for the low-level controller (see fig. 3.30).

Haptic interfaces

Omega.7 (see fig. 3.27) is a 7 DOFs haptic interface that offers three active translations, three passive rotations and one active gripper (active and passive refer to the possibility to apply or not a force feedback effect). Its kinematic design completely decouples translations and rotations, making possible a versatile use for several different applications. It has an hemispheric workspace with a maximum

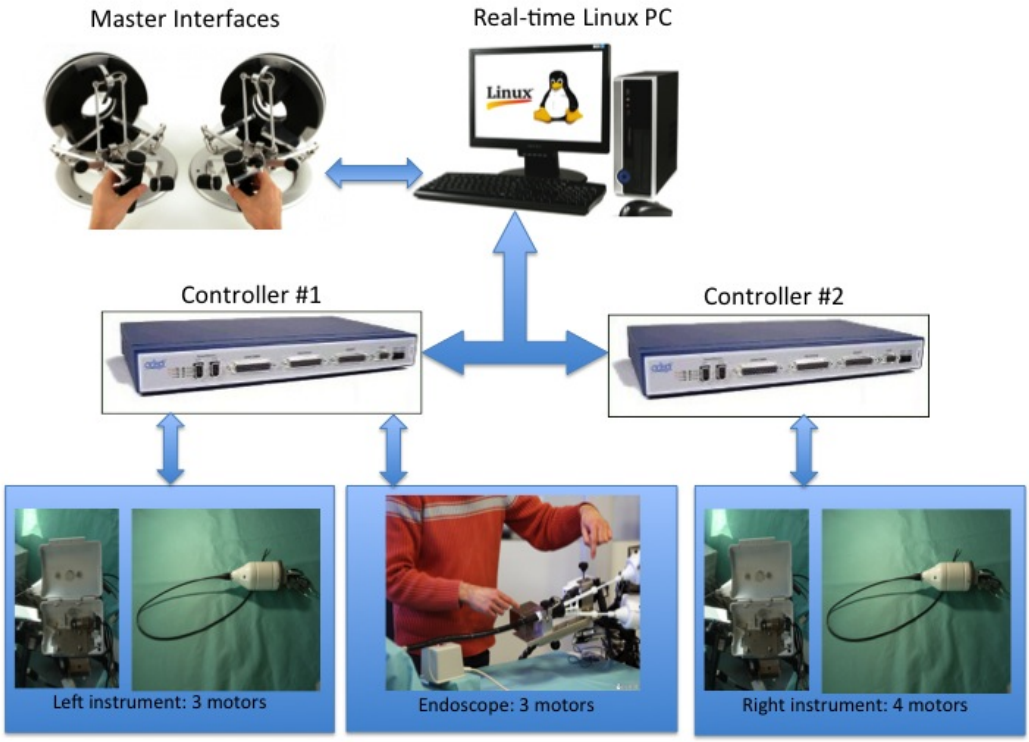

Fig. 3.26. Block scheme of the main robot hardware components.

excursion of 220 mm on the X and Y directions and 160 mm on the Z direction, and a translational resolution of 0.01 mm.

The translational base has a Delta kinematics structure, with three independent kinematics chains fixed to the device base on one side and linked together by the interface end-effector on the other side. Thanks to its parallelogram structure, the Delta chain allows to translate the end-effector in the space while keeping its orientation fixed. As a drawback, this structure is in singular position when a kinematic chain is completely extended or folded: in that cases, the end-effector mobility in at least one direction is limited. The interface base embeds three motors, capable to reproduce a force feedback effect up to 12 N on each active axis. However, the real reproduced effort largely depends on the end-effector position, with a minimum in correspondence of singular positions: in these cases, the interface could show instability due to an erroneous force reproduction.

The rotational wrist extension is mounted on the end-effector, forming the user handle: it has a serial kinematics structure with an arrangement of three pivot joints intersecting their axes in the interface workspace central position. Its maximum excursion is 240 x 140 x 180 degrees, with a resolution of 0.09 degrees.

The handle layout has been optimized in order to be as much as possible statically balanced with respect to its center of gravity, but this does not guarantee

a steady position of the handle when not held by the user. A Universal Serial Bus (USB) 2.0 interface connects the interface to a PC, and a proprietary Software Development Kit (SDK) allows to detect the interface status, read the encoders position and apply the force feedback effect with a refresh rate up to 8 kHz.

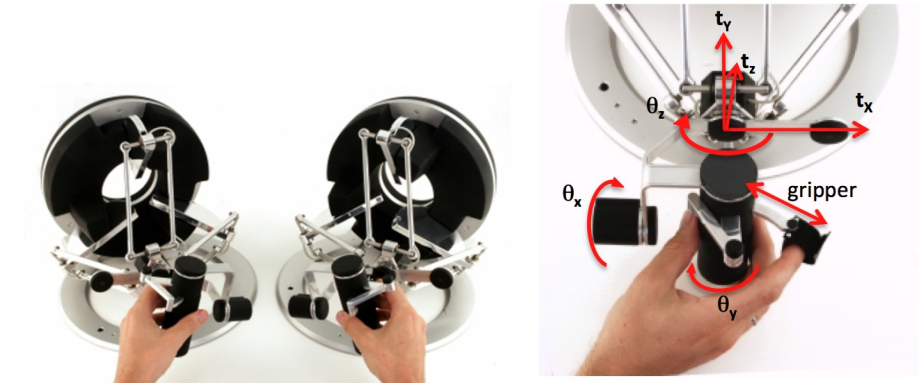

Fig. 3.27. Left: omega.7 haptic interfaces by Force Dimension. Right: Interface degrees of freedom, which include three translations (t_X, t_Y and t_Z), three rotations (θ_X, θ_Y and θ_Z) and an analogic gripper.

Pedal board

Since the user's hands are continuously in contact with the haptic interfaces during the robot teleoperation, a pedal board represents a good and common solution to send commands and to have more control options by using feet. In the STRAS master system a programmable pedal board with three monostable pedals was integrated (see fig. 3.28). The behavior of the first two pedals changes according to the chosen control strategy, while the third pedal is reserved for the emergency stop of the slave system (cfr. section 4.4.9).

High-level controller

The two haptic interfaces and the pedal board are connected to a PC running the Linux Slackware 13.37 distribution, patched with the Xenomai extension [131] in order to obtain a hard real-time environment. This PC serves as high-level controller, since it gathers the user input from the master interfaces, transforms it in joint speed references according to the chosen control strategy (see par. 4.4.5), sends these references to the low-level controller (connected via a FireWire 800 interface) and receives back the slave system status. The PC is equipped with an Intel® Core™ i7 2600 @ 3.4 GHz, 8 GB of DDR3-1333 RAM, an ATI Radeon™ HD 5800 graphic card with 1 GB of embedded GDDR5 RAM and two monitors.

The high-level controller executes an application specifically developed for STRAS (see fig. 3.29). The application is written in C/C++ with the support of several external libraries:

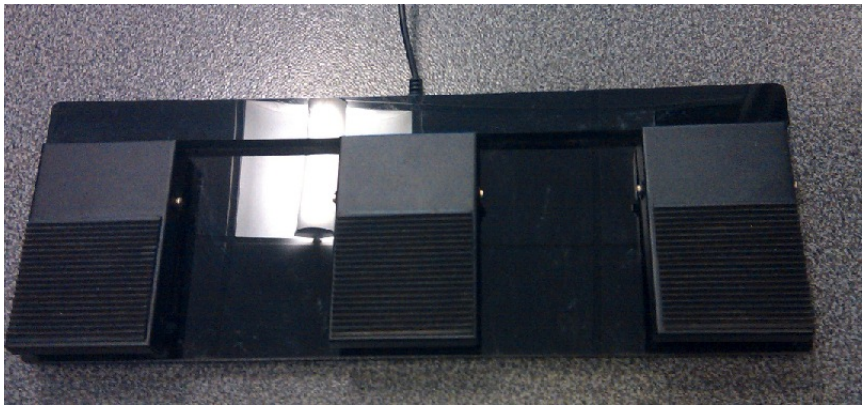

Fig. 3.28. Pedal board.

- Qt Framework 4.7.1 [42] for the Graphical User Interface (GUI);
- Armadillo 3.8 [128], a C++ linear algebra library for matrices computations;
- Force Dimension Haptic and Robotic SDKs 3.3 [54] for communicating with the haptic interfaces
- Adept CALinux API, as FireWire 1394 driver between the low-level controller and the PC.

From the user point of view, the control application offers a user-friendly interface that allows to explore the different control strategies implemented for STRAS. It is also possible to control each slave DOF separately, imposing the desired position or applying a reference speed, by means of specific graphical controls (sliders, dials and buttons). The application core is constituted by the real-time loop, which runs at a refresh rate of 2 kHz and executes the main tasks (reads the haptic interface status, computes motor references, communicates with the low-level controller), while an asynchronous loop manages the GUI refresh and the application complementary functions.

3.5.6 Installation and workflow

While the ANUBISCOPE® is designed to be an hand-held system (as standard gastroscopes), we have chosen to develop STRAS as a bed-mounted robot that can be easily clamped to the operating bed in a suitable position according to the surgical insertion point. As schematically depicted in fig. 3.31, the endoscope platform (noted A) and the instruments support (noted C) are held by two 6 DOFs passive arms (noted respectively B and D).

The installation procedure requires that the endoscope must be mounted first: the arm clamp is fixed to the operating bed and the endoscope is manually inserted inside the patient body by the surgeon. During the insertion, the support passive arm is unlocked and the endoscope head flaps are kept closed, in order to facilitate the passage and to avoid tissue damages. The flaps will be open only when the endoscope placement is concluded, deviating the instruments channels orientation and realizing triangulation between instruments. The insertion phase has been

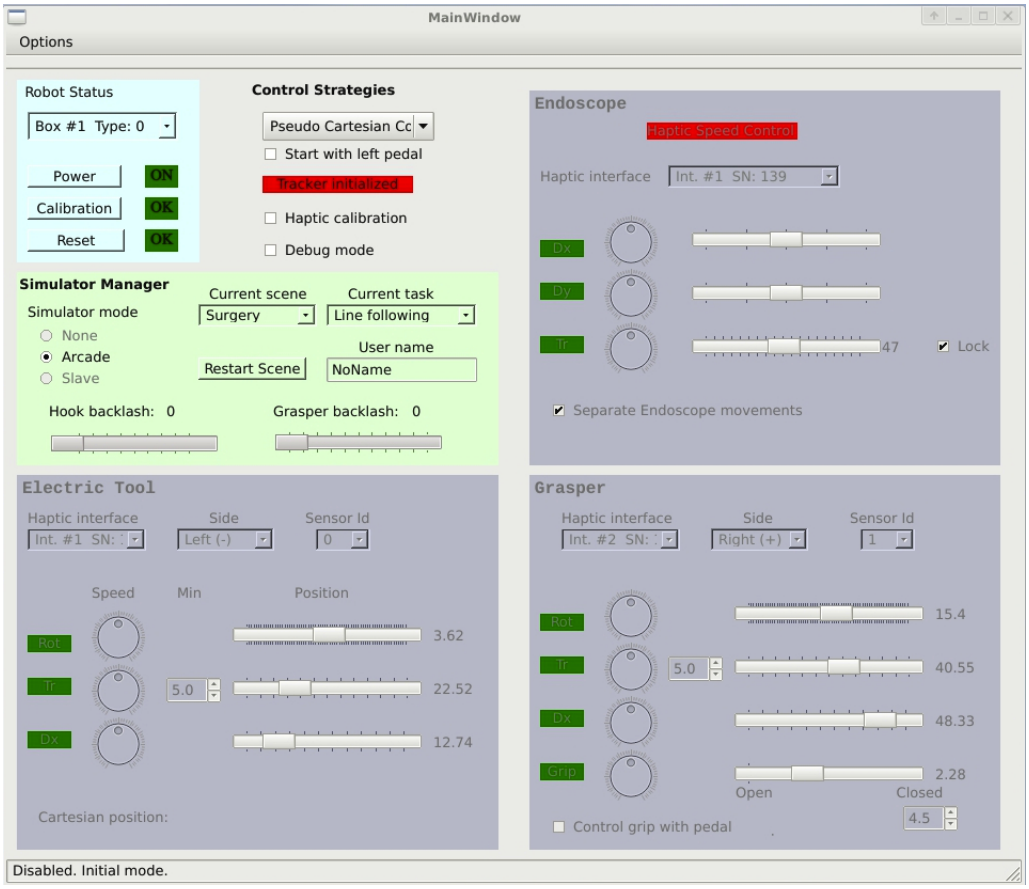

Fig. 3.29. High-level application for the control of STRAS.

kept manual for safety reasons: according to the size of the access point, frictions could appear during the passage of the endoscope inside the trocar. Therefore, we have chosen to leave the control of the needed effort to the surgeon judgement. Moreover, in this phase the surgeon can precisely adjust the endoscope orientation, in order to have a correct rotation of the endoscopic image. Once the endoscope is in place, its passive arm is locked and the position is stored. Successively, the second passive arm holding the instruments is placed beside, in a way that permits an easy insertion of the instruments inside the endoscope channels. As for the endoscope, the instruments passive arm is fully adjustable, allowing to find the proper position and orientation of the T/RMs with respect to the instruments channels.

Before starting the clinical use of the robot, a calibration procedure for both master and slave system is needed, because position encoders are relative and they reset when turned off. For the master system, the calibration consists in simply placing the haptic interfaces end-effectors in a particular position marked on the interfaces frames: this position corresponds to a known encoders configuration,

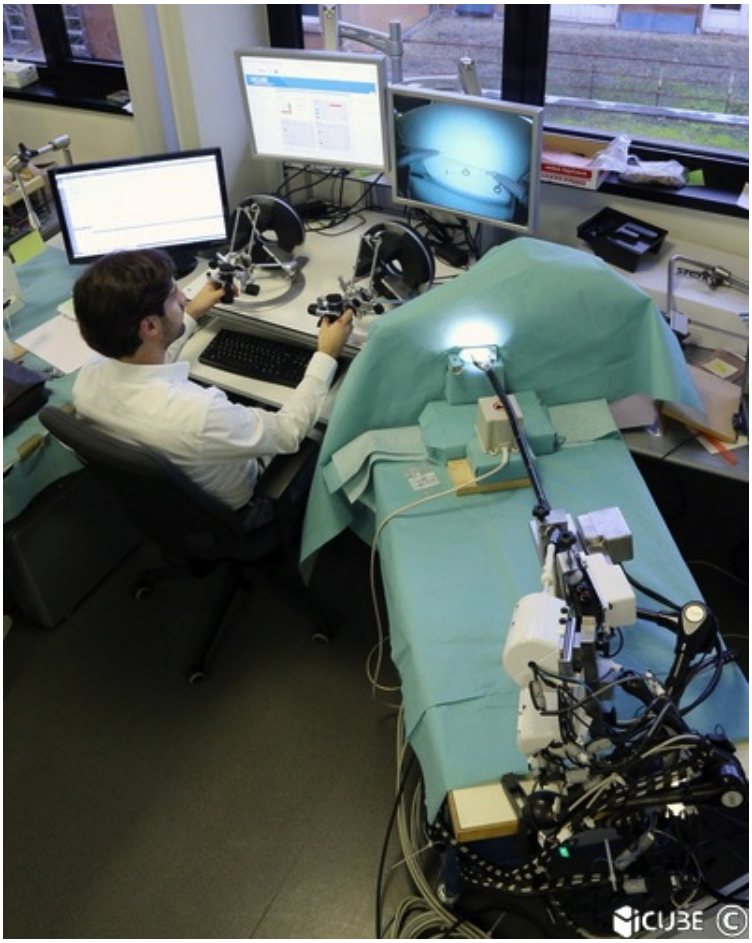

Fig. 3.30. Global view of the STRAS robot: on the top-left corner the user workstation, with displays and haptic interfaces, is visible, while the slave system is mounted on a mobile table.

which is automatically setted by the interfaces internal controller. The slave system calibration, instead, is an automated procedure in which every motor spans its own motion range. Since the motors could rotate infinitely, their motion is physically limited by mechanical stops: during the calibration, each motor searches its two limits, then sets the intermediate position as zero. For safety reasons, the low-level controller applies narrower logical limits, with the aim to avoid motor gears stress and limit the possibility of crossing the mechanical stops due to backlash. When the calibration procedure is concluded, the low-level controller enables the teleoperation, waiting the references from the high-level controller.

During a surgical operation, there could be the need to substitute an instrument: the modularity of STRAS allows to perform this operation without stopping the whole system or compromising its functionality. When an interchange of instrument is needed, the user has to indicate it by pushing a button: in this case,

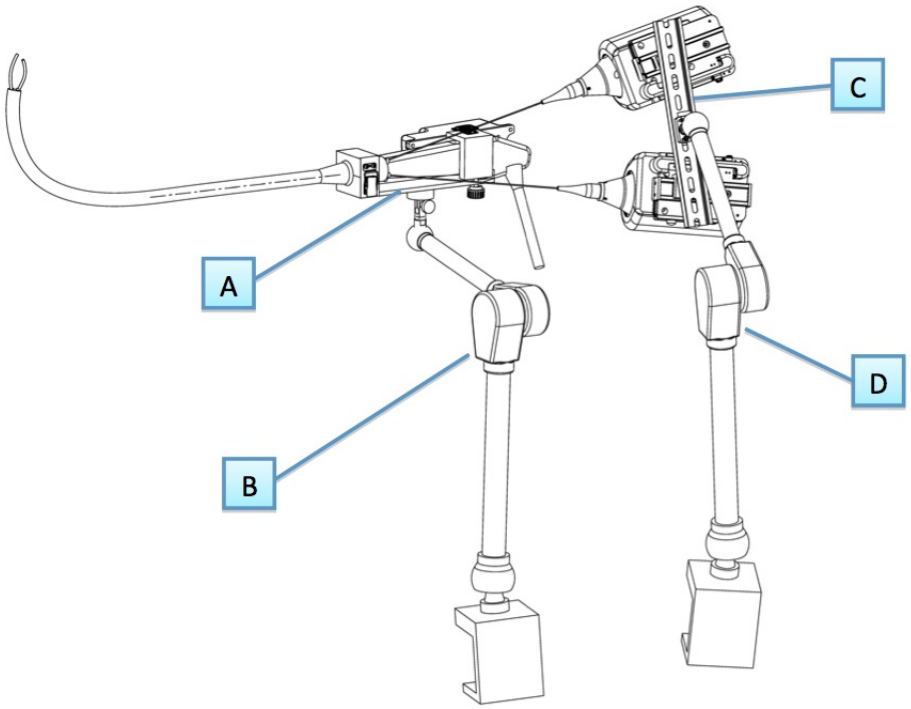

Fig. 3.31. CAD sketch of the STRAS support system. A: Endoscope mobile platform. B: Endoscope support passive arm. C: Instruments platform. D: Instruments support passive arm.

the instrument that has to be changed is led in a straight position, in order to facilitate its discharge from the channel, and the endoscope movements are forbidden. Afterwards, the user has to open the corresponding T/RM, extract the instrument module and insert the new one. Each instrument has the same mechanical interface, therefore the T/RMs can host different types of instruments. After closing the T/RM, the type of instrument (electrical or mechanical) is detected by the number of its actuators, then a calibration procedure for the new instrument is launched. Once this procedure is performed, the instrument body can be inserted in the endoscope channel and the normal teleoperation loop is restored.

A schematic description of the presented workflow is depicted in fig. 3.32.

3.5.7 Clinical applications

Because of its size, STRAS is mainly intended for LESS surgeries or for close NOTES operations. In the first case, the most common accesses are two:

- the *transumbilical*, which allows a complete access to the abdominal cavity for mainly general and digestive surgery [141], gynaecology [203] or bariatric surgery [85];

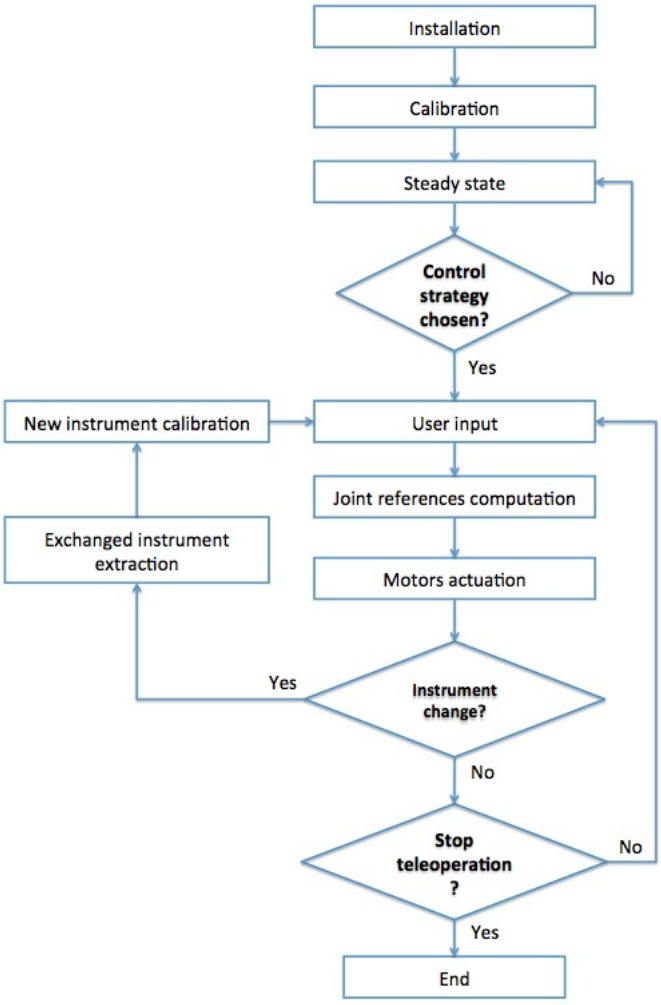

Fig. 3.32. STRAS workflow.

- the *transaxillary*, in case of thyroid surgeries [52] or cardio-thoracic sympathectomy [63].

A transluminal approach, suitable with STRAS dimensions, could be envisaged for ENT surgery [181] with a mouth access, gynaecology [68] or colorectal surgery [50]. In the latter case, a particular technique that is mostly performed transluminally is the *Endoscopic Submucosal Dissection* (ESD), a procedure that aims at the total removal of flat tumoral lesions of the gastrointestinal tract [182]: when these lesions are located in the sigmoid colon, they could be reached through the rectum and dissected. The main difficulty in ESD with standard instrumentation is the absence of triangulation, due to the limited size of the lumen: in this case, the particular design of STRAS is well adapted for guaranteeing the correct triangulation between instruments, thus facilitating the operation.

3.6 Conclusions

The panorama of surgical robots for no-scar surgery is wide and crowded of many different solutions, mainly proposed by academic research groups. Compared to manual instrumentation, these systems have the aim to offer more precision, dexterity and more intuitive user interfaces. However, the difficulty to obtain a clearance for human use, together with the own technological limitations of each presented system, represents a big impediment for their clinical routine use. In the last part of this chapter, our new robotic system, named STRAS, was presented in its mechanical and robotic structures. STRAS might represent a valid solution in the field of no-scar surgery instrumentation: it is mainly intended for LESS and close transluminal surgeries, offers a simplified master interface and several customizable control strategies. The availability of multiple control strategies derives from the high number of DOFs of both master and slave systems and from their different kinematic structures, allowing a number of possible mappings that relate them. In the next chapter, a kinematics study of STRAS and the proposed control strategies will be presented.

4

STRAS Kinematics and Control

Contents

4.1 Introduction

As stated in chapter 3, a robot typically consists of mechanical and electrical/electronics parts (the *hardware*) linked together in order to constitute a machine capable to perform, under the control of a *software* embedded application, one or more pre-programmed tasks. In Surgical robotics, more than in Industrial robotics, the link between hardware and software is very strict and unique, since surgical robots architectures are very different, requiring custom-made solutions for their control.

In par. 3.5, the mechanical description of STRAS (Single access and Transluminal Robotic Assistant for Surgeons) and the robotization process were discussed. In the first part of this chapter, a detailed dissertation about the STRAS kinematics, its workspace and its singularities will be presented. Afterwards, the adopted teleoperation structure will be explained, together with the control strategies proposed for the slave robot control.

4.2 From Discrete to Continuum robots

The design of discrete manipulators commonly took inspiration from the human arm: they have a shoulder, an elbow and a wrist joint, offering five to seven Degrees Of Freedom (DOFs), and they typically have a grasping tool as end-effector, mimicking the human hand. For this reason, they are often called *anthropomorphic manipulators* (see fig. 4.1). This design, largely used in industrial applications, has

Fig. 4.1. The Kuka KR 30-3, an anthropomorphic manipulator for medium payloads (courtesy of Kuka Roboter GmbH, Augsburg, Germany).

been proved to be effective in open space environments, where 6 DOFs are required to guarantee a desired pose (position and orientation) of an object, but it might not be suitable in constrained environments, where potential obstacles could limit the reachable workspace, thus the set of allowed robot joints configurations. In this case, redundancy could be a solution: if the manipulator has more DOFs than those requested by the task, a single point in the task space could be reached with more than one joints configuration. A particular type of redundant robots, called *Hyper-redundant* or *Serpentine robots* [151], combine short rigid links with a high number of actuated joints, creating a structure that can produce smooth shapes and, thus, can be adapted to overtake obstacles (see fig. 4.2).

The main drawback of serpentine robots is that their design increases costs and complexity because of the numerous parts needed. To overcome these issues, researchers tried to find alternative solutions to the redundancy problem by taking inspiration from the nature: there are many animals such as snakes, worms, elephants and octopus, just to give few examples, with flexible bodies (or

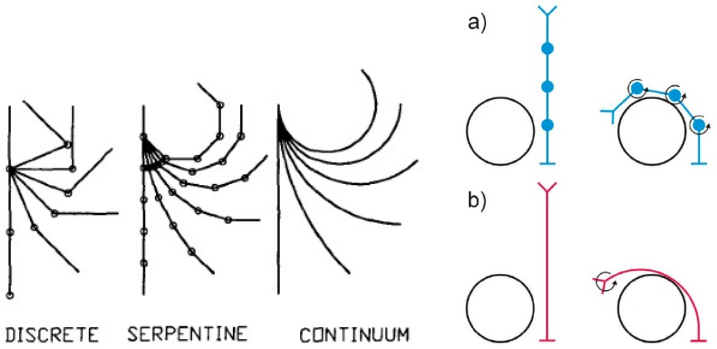

Fig. 4.2. Left: schematic comparison between discrete, serpentine and continuum manipulators (reprinted from [151]). Right: obstacle avoidance in case of (a) serpentine or (b) continuum manipulators (reprinted from [70]).

parts of them) used for locomotion, feeding or as grabbing and defense tools [77]. *Biomimetic robotics* is nowadays a large field of research that tries to understand the most impressive biological and physiological mechanisms of animals and plants and to reproduce them on robotic systems. From this research field a type of robots, called *Continuum robots* (see fig. 4.2), arose more than forty years ago (cfr. section 3.4): their particularity is that they do not contain rigid links and standard joints, but their structures, typically cylindrical, can bend continuously along their length thanks to an elastic deformation obtained by intrinsic (embedded in the structure, typically pneumatic), extrinsic (cables) or hybrid actuators (a combination of the previous two), producing smooth curves. Continuum robots offer a high number of kinematic DOFs (theoretically infinite) and, if arranged in multiple sections, they could be employed in tortuous environments. The big difference with hyper-redundant robot is that their DOFs are not directly actuated, but they are virtually coupled and their movement is the result of the overall actuation system.

4.2.1 Discrete robots kinematics

Formally, Kinematics is the branch of Mechanics that deals with the phenomenon of bodies motion without taking care of its causes: there is no reference to body masses or applied forces, the only concern is about relative positions of the involved bodies and their changes during time [16]. A typical robot is formed by several rigid parts, called **links**, connected together by means of **joints** in order to form a discrete multi-Degrees-Of-Freedom chain (serial or parallel). In classical Robotics kinematics, the links are modeled as rigid bodies, while joints are assumed to provide pure revolute or translational relative movements: the aim of Kinematics is therefore to compute a mathematical model that allows to express the pose of the last link of the robot chain (typically called *end effector*) in the robot base frame.

The frames choice on a robotic manipulator is a fundamental task, because it influences the complexity of the kinematic model. Though this choice is not unique, a commonly used convention for selecting frames of reference in robotics

applications is the Denavit-Hartenberg (DH) convention, which was introduced in 1955 by Jacques Denavit and Richard S. Hartenberg [38]. If one considers a serial chain composed by n rigid links, this convention makes use of four parameters to describe the relative position and orientation of two consecutive links, i_{-1} and i, connected by a joint (see fig. 4.3):

- **link length** $\boldsymbol{a_i}$: distance between the origins of the two consecutive frames i_{-1} and i measured along the X axis, it corresponds to the physical length of link i;
- **link offset** $\boldsymbol{d_i}$: distance between the origins of the two consecutive frames i_{-1} and i measured along the Z axis, variable if the joint i is prismatic;
- **link twist** $\boldsymbol{\alpha_i}$: angle between Z_{i-1} and Z_i measured along X_i, it is a constant value that depends on the link shape and on joints arrangement;
- **joint angle** $\boldsymbol{\theta_i}$: angle between X_{i-1} and X_i measured along Z_i, variable if the joint i is rotational.

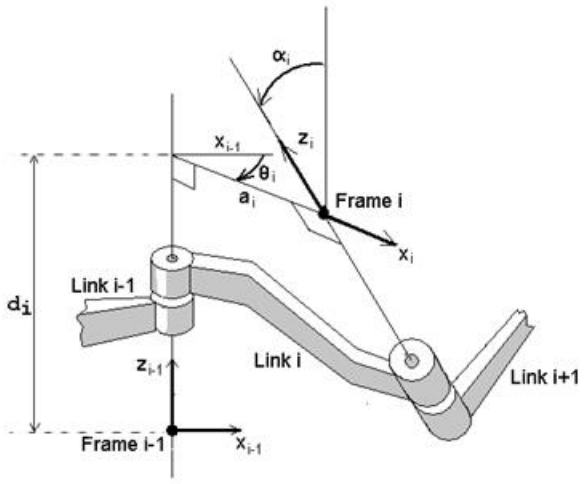

Fig. 4.3. Kinematic parameters of the Denavit-Hartenberg convention (courtesy of Rachid Manseur, Electrical and Computer Engineering Dept., University of West Florida, Pensacola, FL, USA).

The general transformation matrix ${}_{i-1}\mathscr{T}^i$ for a single link can be obtained as a product of four basic transformations, one for each parameter:

$$
\begin{aligned}
{}_{i-1}\mathscr{T}^{i} &= R_{\theta_i|Z} \quad T_{d_i|Z} \quad T_{a_i|X} \quad R_{\alpha_i|X} = \\
&= \begin{bmatrix} \cos(\theta_i) & -\sin(\theta_i) & 0 & 0 \\ \sin(\theta_i) & \cos(\theta_i) & 0 & 0 \\ 0 & 0 & 1 & 0 \\ 0 & 0 & 0 & 1 \end{bmatrix} \begin{bmatrix} 1 & 0 & 0 & 0 \\ 0 & 1 & 0 & 0 \\ 0 & 0 & 1 & d_i \\ 0 & 0 & 0 & 1 \end{bmatrix} \begin{bmatrix} 1 & 0 & 0 & a_i \\ 0 & 1 & 0 & 0 \\ 0 & 0 & 1 & 0 \\ 0 & 0 & 0 & 1 \end{bmatrix} \begin{bmatrix} 1 & 0 & 0 & 0 \\ 0 & \cos(\alpha_i) & -\sin(\alpha_i) & 0 \\ 0 & \sin(\alpha_i) & \cos(\alpha_i) & 0 \\ 0 & 0 & 0 & 1 \end{bmatrix} = \\
&= \begin{bmatrix} \cos(\theta_i) & -\sin(\theta_i)\cos(\alpha_i) & \sin(\theta_i)\sin(\alpha_i) & a_i\cos(\theta_i) \\ \sin(\theta_i) & \cos(\theta_i)\cos(\alpha_i) & -\cos(\theta_i)\sin(\alpha_i) & a_i\sin(\theta_i) \\ 0 & \sin(\alpha_i) & \cos(\alpha_i) & d_i \\ 0 & 0 & 0 & 1 \end{bmatrix}
\end{aligned} \tag{4.1}
$$

To compute the global transformation matrix for the serial chain it is necessary to repeat this procedure for each couple of links.

4.2.2 Continuum robots kinematics

As introduced in section 4.2.1, the DH convention makes the assumption that a robotic manipulator is composed of rigid links and standard joints, hence it does not offer a valid representation for continuum robots. The problem of the kinematic description of continuum robots is not trivial: a kinematic model can define the theoretical pose of a point of interest on a continuum section based on a geometrical model, but it does not take account of the actuation method and of the internal and external forces and moments applied on the robotic structure. A dynamical model, therefore, should be computed in order to obtain better results, but the general complexity of such systems makes difficult to express this model in closed form. Indeed, the most common models are computed numerically, and the computational load is directly proportional to the length of the continuum section and the delta assumed as discrete integration step (see [26] for an example of a parallelized numerical algorithm for hyper-redundant and continuum robots). Such models could compute very accurate results, but they are often unsuitable for real-time control due to their high computational request. Therefore, some approximations should be taken in order to obtain a closed-form solution for the kinematic problem. Among others, a simplifying approach that led to valid results is to approximate the continuum section as a series of arcs with constant curvature. This method, called *piecewise constant curvature kinematics* [199], considers the continuum section as composed by a finite number of curved links, each described by a finite set of arc parameters: the curvature κ, the orientation ϕ of the plane containing the arc and the arc length ℓ (see fig. 4.4).

Although the constant curvature is a desirable but unattainable feature in continuum robots, mainly because of mechanical imperfections in their structure and actuation, it was demonstrated that this assumption allows to obtain a closed-form kinematic model with a good level of accuracy in control [199]. One of the firsts formulations of the piecewise constant curvature method was proposed in 1999 by Hannan and Walker [196] [70] for the control of their "Elephant Trunk" manipulator (see fig. 4.5). At Clemson University (Clemson, SC, USA) they developed a continuum robot consisting of four flexible sections, where each section has two actuatable DOFs, *i.e.* the two orthogonal deflections, controlled by cables. Analyzing more in detail a single section (see fig. 4.5), one could see that the rigid

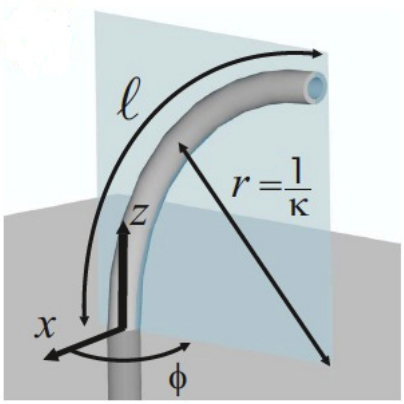

Fig. 4.4. Frame convention and main parameters of a flexible arc (reprinted from [199]).

parts of two consecutive sections are connected by means of four 2 DOFs springs (each spring can bend in two directions), coupling the movements of the consecutive sections. Therefore, each section has 8 kinematic DOFs and 2 actuatable ones, yielding to a total of 32 coupled kinematic DOFs, but 8 directly actuatable for the whole manipulator.

Fig. 4.5. Elephant Trunk manipulator by Clemson University. Left: global view. Right: detail of a section (reprinted from [70]).

To describe the motion of their manipulator, Hannan and Walker first analyzed the planar motion case, demonstrating that both differential geometry and classical geometry methods led to the same results. Notably, they assumed the pla-

nar motion of a constant curvature flexible section as composed by three coupled movements (see fig. 4.6):

1. rotation by an angle θ
2. translation by an amount of $||\boldsymbol{X}||$
3. rotation by the angle θ again

where $\mathbf{X}$ is the position vector of the end-point of the curve with respect to its initial point, and θ is the angle between $\mathbf{X}$ and the tangent vector $\mathbf{T(0)}$ to the curve at the initial point. In this case, the torsional moment on the flexible section is neglected. To extend this formulation to the spatial case, it is sufficient to consider the rotation angle ϕ of the planar curve out of its plane (as shown in fig. 4.4): this rotation, done before the three coupled movements described before, will affect the tangent vector $\mathbf{T(0)}$. With such kinematic description, it is possible to set up the kinematic frames as in a standard serial manipulator: each movement is a virtual joint with a frame centered on it. A possible frames choice for a flexible section is shown in fig. 4.6, which led to the DH parameter table 4.1.

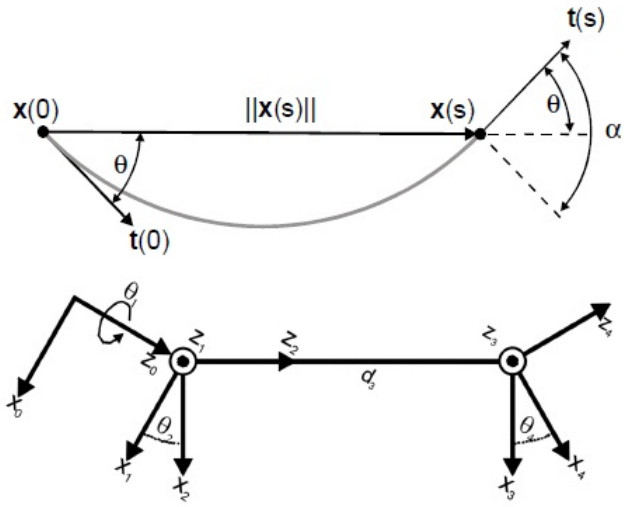

Fig. 4.6. Top: planar section of a flexible arc described in terms of magnitude and angle. Bottom: DH parameters for a spatial flexible section (reprinted from [70]).

Joint	θ	d	α	a
1	θ_1	0	$\pi/2$	0
2	θ_2	0	$-\pi/2$	0
3	0	d_3	$\pi/2$	0
4	θ_4	0	$-\pi/2$	0

Table 4.1. Denavit-Hartenberg parameters for the spatial motion of the constant curvature flexible section.

Putting:

$$\theta_1 = \phi, \quad \theta_2 = \theta_4 = \theta = \frac{\kappa\ell}{2}, \quad d_3 = \frac{\ell}{\theta}\sin(\theta) \tag{4.2}$$

the homogeneous transformation matrix for a flexible section can be computed in terms of the curvature κ, the rotation angle ϕ and the total arc length $\boldsymbol{\ell}$:

$$\mathscr{T}_{FS} = {}_0\mathscr{T}^4 = \begin{bmatrix} \cos(\phi)\cos(\kappa\ell) & -\sin(\phi) & \cos(\phi)\sin(\kappa\ell) & \frac{\cos(\phi)(1-\cos(\kappa\ell))}{\kappa} \\ \sin(\phi)\cos(\kappa\ell) & \cos(\phi) & \sin(\phi)\sin(\kappa\ell) & \frac{\sin(\phi)(1-\cos(\kappa\ell))}{\kappa} \\ -\sin(\kappa\ell) & 0 & \cos(\kappa\ell) & \frac{\sin(\kappa\ell)}{\kappa} \\ 0 & 0 & 0 & 1 \end{bmatrix} \tag{4.3}$$

This matrix represents the Forward Kinematic (FK) model for a continuum flexible section (FS) under the assumptions of uniform curvature and no torsional moments. If a continuum robot is composed by multiple sections linked together, it is possible to obtain the global FK model by multiplying the matrices relative to each section.

This model allows to correctly compute the position of the continuum section tip with respect to its base frame, but it fixes the tip orientation in a way that its X axis always points toward the virtual center of the circle, if the continuum section is assumed as an arc. Jones and Walker proposed a corrected version of this model, which orients the tip frame such that it aligns with the base frame by post-multiplying the rotation $R_{-\phi|Z}$, providing this new model [90]:

$\mathscr{T}_{FS} = {}_0\mathscr{T}^4 =$

$$= \begin{bmatrix} c^2(\phi)c(\kappa\ell-1)+1 & s(\phi)c(\phi)(c(\kappa\ell)-1) & c(\phi)s(\kappa\ell) & \frac{c(\phi)(1-c(\kappa\ell))}{\kappa} \\ s(\phi)c(\phi)c(\kappa\ell-1) & c^2(\phi)(1-c(\kappa\ell))+c(\kappa\ell) & s(\phi)s(\kappa\ell) & \frac{s(\phi)(1-c(\kappa\ell))}{\kappa} \\ -c(\phi)s(\kappa\ell) & -s(\phi)s(\kappa\ell) & c(\kappa\ell) & \frac{s(\kappa\ell))}{\kappa} \\ 0 & 0 & 0 & 1 \end{bmatrix} \tag{4.4}$$

In a recent review on continuum robots [199] it was demonstrated that the model (4.4) could be derived in several other ways than the modified DH convention, but always obtaining the same result if the piecewise constant curvature simplification is assumed. This model, called *robot-independent mapping* by the review's authors, is applicable to any flexible section regardless its internal structure or actuation method, because it is expressed in the configuration space $(\kappa, \phi, \boldsymbol{\ell})$. The link between the configuration space and the joint space is given by the *robot-specific arc parameter mapping* (see fig. 4.7), which requires a geometrical or dynamical modeling of the robot actuation and transmission structure in order to compute the equivalence between physical joints and robot-independent mapping variables (as it was done in the equalities (4.2)).

4.3 STRAS Kinematics

STRAS is not a typical robot: it does not have rigid links, but flexible actuated parts arranged in a *tree-like* structure, with the main endoscope that bounds

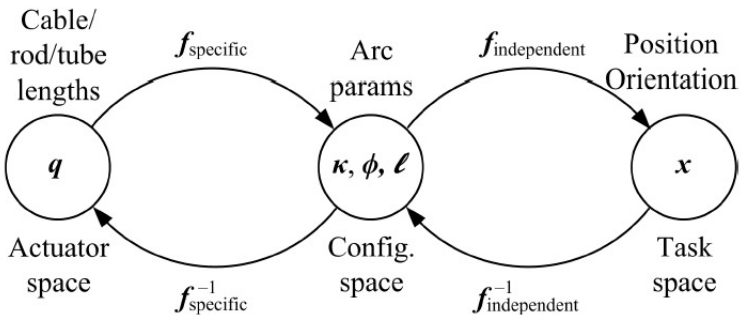

Fig. 4.7. The kinematics of a flexible section with the piecewise constant curvature assumption could be decomposed in two mappings: the first is from the actuator space $\mathbf{q}$, specific of the considered robot, to the configuration space (κ, ϕ, ℓ), robot-independent; the second is from the configuration space to the Cartesian task space in which the robot end-effector moves (reprinted from [199]).

the instruments and influences their positions. Since the instruments channels are embedded in the main endoscope body, every endoscope deflection modifies the instruments poses.

4.3.1 Forward Kinematics

What is of interest for the kinematic control of STRAS is the possibility to compute the Cartesian positions of the instruments, expressed in a common base frame, in function of the current robot joints configuration. Five kinematic frames have been identified for the endoscope:

1. Endoscope Base (noted F_{EB}, see fig. 4.8), located at the base of the endoscope actuated section;
2. Endoscope Head (noted F_{EH}, see fig. 4.8), located at the top of the endoscope actuated section;
3. Camera (noted F_{C}, see fig. 4.8), located in correspondence of the endoscopic camera, on the endoscope rigid tip;
4. Left and Right Jaws Heads (for reasons of clarity, on fig. 4.8 only the Right Jaw Head frame is reported, noted F_{JH}), located on the exit points of the instruments channels.

Three frames, instead, are identified for each instrument:

1. Instrument Base (noted F_{IB}, see fig. 4.8), located at the base of the instrument actuated section;
2. Instrument Head (noted F_{IH}, see fig. 4.8), located at the top of the instrument actuated section;
3. Instrument Tip (noted F_{IT}, see fig. 4.8), located at the top of the tool.

For the transformations ${}_{EB}\mathscr{T}^{EH}$ and ${}_{IB}\mathscr{T}^{IH}$ the model (4.4) was used, while the other transformations depend on geometrical parameters of the system (see appendix A). Particularly, transformation ${}_{IH}\mathscr{T}^{IT}$ is constant and takes account of the length d_{HT} of the rigid tool attached on the instrument flexible section.

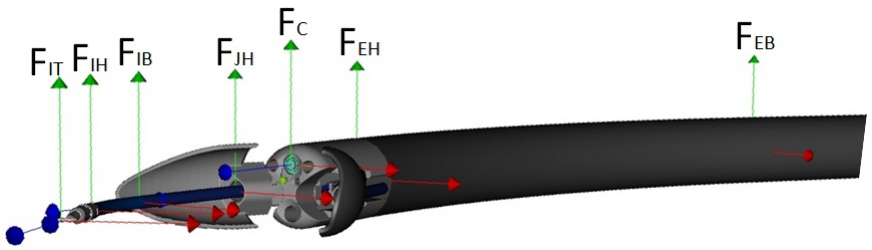

Fig. 4.8. Main kinematic frames of the slave robot. EB: Endoscope Base. EH: Endoscope Head. C: Camera. JH: Jaw Head. IB: Instrument Base. IH: Instrument Head. IT: Instrument Tip.

In our case, we have considered two base frames, according to the specific application:

- the base of the endoscope actuated part (noted F_{EB}, see fig. 4.8), since it represents a fixed point for the whole system. In this case, the FK model will be computed with the following series of transformations:

$$FK_{EB} = {}_{EB}\mathscr{T}^{IT} = {}_{EB}\mathscr{T}^{EH}\ {}_{EH}\mathscr{T}^{JH}\ {}_{JH}\mathscr{T}^{IB}\ {}_{IB}\mathscr{T}^{IH}\ {}_{IH}\mathscr{T}^{IT} \tag{4.5}$$

- the endoscopic camera (noted F_C, see fig. 4.8), useful when the control is limited to instruments only or for visual servoing applications. The corresponding FK model will be:

$$FK_C = {}_{C}\mathscr{T}^{IT} = {}_{C}\mathscr{T}^{JH}\ {}_{JH}\mathscr{T}^{IB}\ {}_{IB}\mathscr{T}^{IH}\ {}_{IH}\mathscr{T}^{IT} \tag{4.6}$$

Globally, STRAS has 10 DOFs (see fig. 4.9):

- 3 DOFs from the main endoscope: longitudinal translation t_E (noted 1, see fig. 4.9) and two orthogonal deflections dx and dy (noted 2, 3, see fig. 4.9);
- 3 DOFs for each instrument: longitudinal translation t_I (noted 4, see fig. 4.9), rotation θ_I (noted 5, see fig. 4.9) and deflection β (noted 6, see fig. 4.9);
- an additional DOF for the opening and closing of actuated instruments such as the grasper (noted 7, see fig. 4.9).

In order to use the model (4.4) for the flexible sections of STRAS, it is necessary to determine the robot-specific arc parameter mapping, *i.e.* the relationship between the generic arc parameters (κ, ϕ, ℓ) and the slave robot DOFs. As explained in section 3.5.1, the flexible sections on the ANUBISCOPE® platform, and therefore on STRAS, are actuated by means of two antagonistic cables, supposed inextensible, that are simultaneously moved in opposite directions. Considering one

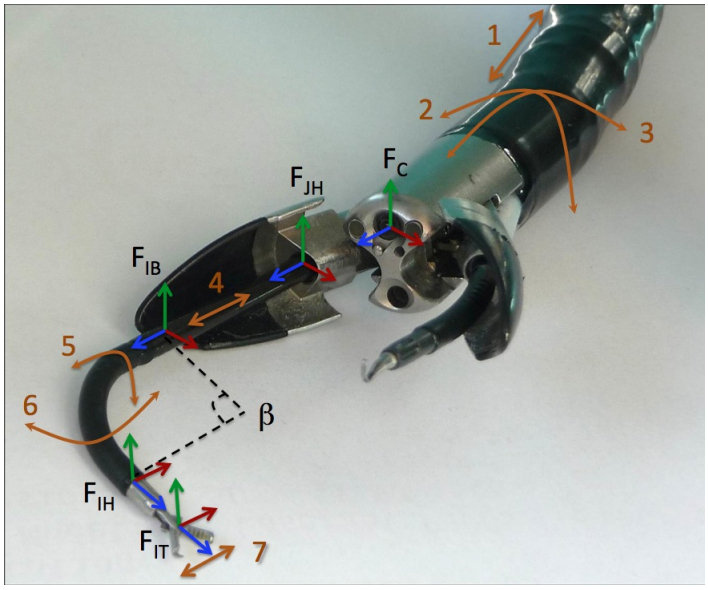

Fig. 4.9. Degrees of freedom of the slave system.

flexible section bent with a curvature κ, under the assumption of constant curvature and inextensible arc length, it describes a circular sector of radius $r = 1/\kappa$ and inner angle $\beta = \kappa\ell$. While the central arc length is assumed constant, the lengths of the circular arcs formed by the two cables at the boundaries of the flexible section vary according to the cables lengthening or shortening (see fig. 4.10). Indicating with dx the displacement in mm of the actuation cables (with respect to the central straight position) needed to produce a bending with curvature κ in the XY plane, the following relationship can be written:

$$r = \frac{dx}{\beta} = \frac{dx}{\kappa\ell} \qquad \rightarrow \qquad dx = \beta\, r = \kappa\, \ell\, r. \tag{4.7}$$

Equation (4.7) is valid for instruments because they deflect in one plane only, thus κ depends on one parameter, dx. This parameter refers to the cable displacement measured at the base of the flexible part (see fig. 4.10): since actuation cables go through the instrument passive body, the measured displacement at the deflection motor level will be different because of frictions.

Regarding the instrument rotation, it is performed by directly rotating the instrument base, so it corresponds to the parameter ϕ of the robot independent mapping:

$$\theta_I = \phi. \tag{4.8}$$

The mapping for the endoscope is slightly different, because in this case κ and ϕ are determined by both parameters dx and dy. It will be necessary, therefore, to consider the component of κ in the two orthogonal planes XY and YZ:

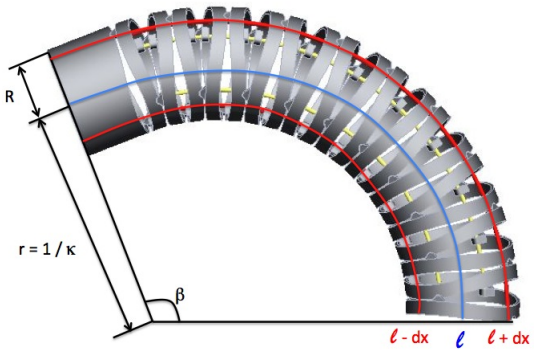

Fig. 4.10. Kinematic parameters for a flexible section bending in one direction.

$$dx = \ell R\kappa\cos(\phi),\ dy = \ell R\kappa\sin(\phi) \rightarrow \begin{cases} \kappa = \frac{\sqrt{dx^2+dy^2}}{\ell R} \\ \phi = \arctan 2(dy, dx) \end{cases} . \tag{4.9}$$

4.3.2 Workspace

In a surgical robot, instruments are the surgeon's hands inside the patient body. Therefore, it is very important to know which are the positions attainable by instruments, the common workspace in which they could cooperate and the mobility of the base platform that carries them. In this paragraph a study of the STRAS workspace will be proposed, starting by analyzing that of a single instrument. For this purpose, it is convenient to adopt the FK_C model (see eq. (4.6)), which does not take account of the endoscope DOFs: we will see hereinafter that they do not influence the workspace shape, but just move it rigidly in the space.

With the aid of the virtual simulator (see section 5.4.2), we first tried to numerically evaluate the instrument workspace by spanning the range of motion of deflection and rotation actuators (without varying the translation) and storing the instrument tip positions. The result, visible in fig. 4.11, looks similar to an ellipsoid, truncated at the base because of the deflection limit: it represents the **local workspace**, *i.e.* the surface reachable by the instrument tip when all joints but the translation are moved. Assuming the hypothesis of the ellipsoidal shape, we could express this surface as an analytical function:

$$\frac{(x-x_0)^2}{r_x^2} + \frac{(y-y_0)^2}{r_y^2} + \frac{(z-z_0)^2}{r_z^2} = 1 \qquad (z > z_{min} = -4.106) \tag{4.10}$$

where $(x_0, y_0, z_0) = (0, 0, 3.253)\ mm$ are the coordinates of the ellipsoid center with respect to the F_{IB} frame, $r_x = r_y = 30.243\ mm$ and $r_z = 29.257\ mm$ are the ellipsoid radii in the X, Y and Z directions. These parameters are obtained with the numerical evaluation of the instrument workspace, depicted in red on fig. 4.11: expressing all the discrete positions of the instrument tip in the frame F_{IB}, the maximum values on X and Y directions allow to determine r_x, r_y and

the ellipsoid center (x_0, y_0, z_0), while r_z is the difference between the maximum Z value and z_0. If the instrument translation is varied, the local workspace is rigidly translated along the instrument Z direction, forming the **global workspace**: it consists of a cylinder with a convex ellipsoidal cap on top and a concave one on bottom (depicted in cyan, see fig. 4.11). The global workspace represents the area

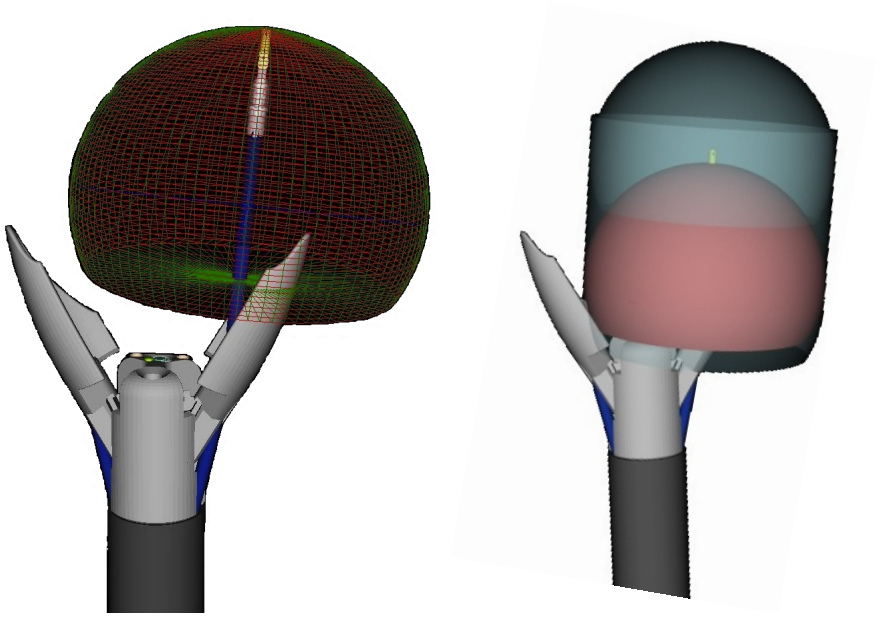

Fig. 4.11. Instrument workspace. Left: numerical evaluation. Right: analytical workspace (red: local, cyan: global).

attainable by the instrument with all its DOFs. The cylinder has a radius equal to r_x and r_y, while its height is 65 mm (excluding the top cap), which corresponds to the instrument translation range.

Since the instrument can deflect with both positive and negative curvature values, hypothetically each point of the workspace could be reached with two different instrument configurations: given a specific value of t_I, the joint configurations $(\beta,\ \phi)$ and $(-\beta,\ \phi + \pi)$ will conduct the instrument tip to the same Cartesian point. Practically, when considering the instrument deflections in one direction only, the mechanical stops imposed on the instrument rotation (cfr. section 3.5.2) inhibit a sector of the workspace located in the interval $\phi \in [-20°, 20°]$ (on red in fig. 4.12) when the deflections are positive ($\beta > 0$) and in $\phi \in [160°, 200°]$ (on yellow in fig. 4.12) when they are negative ($\beta < 0$).

Considering both instruments, the respective global workspaces will overlap in a common central zone (depicted in green on fig. 4.13), located in front of the endoscopic camera, that could be considered as a truncated cone. This cone has its center located about 90 mm away from the camera in the Z direction, while its maximum cross-section is at 25 mm from the camera: this area corresponds to the

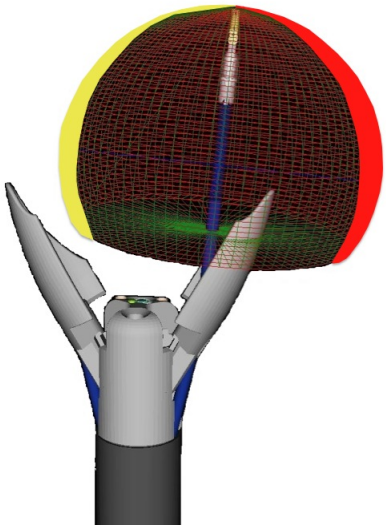

Fig. 4.12. The imposed limits on the instrument rotation restrict the available workspace when the deflection is performed in the positive (restricted area coloured in red) or the negative (yellow) direction.

optimal operation position, since the instruments are close to each other, so they can easily cooperate. Moreover, in that configuration instruments are largely inside their channels, which results in more rigidity and strength that they could apply at their tips (one of the common problem of flexible systems is force transmission, cfr. section 2.4). The cooperation workspace has a surface of about 1800 mm^2 and a volume of about 3500 mm^3.

4.3.3 Differential Kinematics

A useful tool for both the control and the kinematic analysis of a robot is its Jacobian matrix, which expresses the link between joints velocities $\dot{\boldsymbol{q}}$ and the corresponding linear $\dot{\boldsymbol{V}}$ and angular $\dot{\boldsymbol{\omega}}$ velocities of the end-effector:

$$\begin{bmatrix} \dot{\boldsymbol{V}} \\ \dot{\boldsymbol{\omega}} \end{bmatrix} = J\,\dot{\boldsymbol{q}} \tag{4.11}$$

where:

$$\dot{\boldsymbol{V}} = \begin{bmatrix} \dot{x}_{EE} \\ \dot{y}_{EE} \\ \dot{z}_{EE} \end{bmatrix} \quad \dot{\boldsymbol{\omega}} = \begin{bmatrix} \dot{\omega}_{xEE} \\ \dot{\omega}_{yEE} \\ \dot{\omega}_{zEE} \end{bmatrix} \quad \dot{\boldsymbol{q}} = \begin{bmatrix} \dot{q}_1 \\ \dot{q}_2 \\ \vdots \\ \dot{q}_n \end{bmatrix} \quad J = \frac{\partial f(\boldsymbol{q})}{\partial \boldsymbol{q}} = \begin{bmatrix} \frac{\partial x_{EE}}{\partial q_1} & \frac{\partial x_{EE}}{\partial q_2} & \dots & \frac{\partial x_{EE}}{\partial q_n} \\ \frac{\partial y_{EE}}{\partial q_1} & \frac{\partial y_{EE}}{\partial q_2} & \dots & \frac{\partial y_{EE}}{\partial q_n} \\ \vdots & & & \vdots \\ \frac{\partial \omega_{zEE}}{\partial q_1} & \frac{\partial \omega_{zEE}}{\partial q_2} & \dots & \frac{\partial \omega_{zEE}}{\partial q_n} \end{bmatrix} \tag{4.12}$$

where $f(\boldsymbol{q})$ is the forward kinematic model of the system. The derivation of the models (4.5) or (4.6) allows to compute the Jacobian matrix of STRAS, but in this

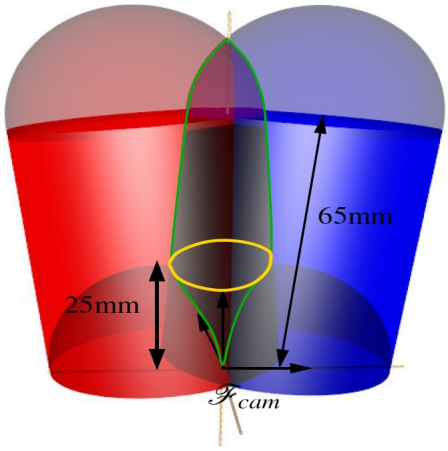

Fig. 4.13. Workspaces of the two instruments expressed in the frame attached to the endoscopic camera. Blue: left instrument workspace. Red: right instrument workspace. Green: common intersecting area.

manner each flexible section will be described by the independent variables (κ, ϕ, ℓ): in order to express the Jacobian in terms of the robot-specific joint variables (dx_E and dy_E for the endoscope deflections, β for the instrument deflection) it will be necessary to post-multiply the transformation:

$$\begin{bmatrix} \dot{\kappa_E} \\ \dot{\phi_E} \\ \dot{\kappa_I} \\ \dot{\phi_I} \end{bmatrix} = \begin{bmatrix} \frac{dx_E}{\ell_E R_E \sqrt{dx_E^2+dy_E^2}} & \frac{dy_E}{\ell_E R_E \sqrt{dx_E^2+dy_E^2}} & 0 & 0 \\ -\frac{dy_E}{dx_E^2+dy_E^2} & \frac{dx_E}{dx_E^2+dy_E^2} & 0 & 0 \\ 0 & 0 & \frac{1}{\ell_I} & 0 \\ 0 & 0 & 0 & 1 \end{bmatrix} \begin{bmatrix} \dot{dx}_E \\ \dot{dy}_E \\ \dot{\beta} \\ \dot{\theta}_I \end{bmatrix} \tag{4.13}$$

where the subscripts E and I refer to Endoscope and Instrument, ℓ represents the length of the considered flexible section and R its radius (see fig. 4.10). The complete Jacobian for our system is a matrix with twelve rows, *i.e.* six Cartesian components for each instrument, and eight columns, *i.e.* the number of joints (the endoscope translation and the opening/closing of the grasper are not considered in the model, cfr. eq. (4.34) and (4.35)).

Considering STRAS in its entirety, its DOFs can be redundant for many of the potential tasks that could be performed. But the DOFs relative to the endoscope are not always practically usable, because an endoscope movement forces the camera to move in the same way, thus changing the surgical point of view. When the endoscopic image has to remain still, the endoscope DOFs are therefore constrained and the system mobility is limited to the instruments movements only. In this case, it could be useful to simplify the Jacobian computation by choosing an appropriate subset of $\dot{\boldsymbol{q}}$, thus restricting it to a part of the system, *e.g.* a single instrument. If considering just the linear velocity $\dot{\boldsymbol{V}}$ of the end-effector, the instrument Jacobian will be a 3 x 3 square matrix, and the corresponding joint vector is $\boldsymbol{q}_I = [\beta\ \phi\ t_I]^T$:

$$J_I(\boldsymbol{q}_I) = \begin{bmatrix} \frac{\partial X}{\partial \beta} & -Y & 0 \\ \frac{\partial Y}{\partial \beta} & X & 0 \\ \frac{\partial Z}{\partial \beta} & 0 & 1 \end{bmatrix} \tag{4.14}$$

where:

$$\begin{bmatrix} X \\ Y \\ Z \end{bmatrix} = {}_{JH}T^{IT} = \begin{bmatrix} d_{HT}\cos(\phi)\sin(\beta) + \frac{\ell\cos(\phi)(1-\cos(\beta))}{\beta} \\ d_{HT}\sin(\phi)\sin(\beta) + \frac{\ell\sin(\phi)(1-\cos(\beta))}{\beta} \\ d_{HT}\cos(\beta) + t_I + \frac{\ell\sin(\beta)}{\beta} \end{bmatrix}. \tag{4.15}$$

When the instrument is in straight position, $\beta = 0$ and the Jacobian can be computed with a second-order development of (4.14):

$$J_I(0, \phi, t_I) = \begin{bmatrix} \cos(\phi)(\ell/2 + d_{HT}) & 0 & 0 \\ \sin(\phi)(\ell/2 + d_{HT}) & 0 & 0 \\ 0 & 0 & 1 \end{bmatrix} \tag{4.16}$$

4.3.4 Inverse Kinematics

As stated in section 4.3.1, the FK model allows to compute the current Cartesian position of the robot end-effector, expressed in the robot base frame, corresponding to the actual joints configuration. What is useful for the system control is to solve the inverse kinematics (IK) problem, computing a joints configuration that brings the robot end-effector to a desired Cartesian position. Theoretically, the problem consists in inverting the direct model (4.4) and in expressing the kinematic functions in terms of the joints vector $\boldsymbol{q}$. But while the direct kinematic problem allows to immediately determine a unique solution given a joints configuration, the resolution of the inverse kinematic problem presents more complications:

- the equations that relate the robot pose in the operative space with the joints variables are generally non-linear, and often it is not possible to find a closed-form solution;
- the IK problem could not admit any solution when the desired pose is outside the robot workspace, or when the robot kinematic structure limits the set of admissible solutions;
- the IK problem could have multiple or infinite solutions when the dimension of the joint space is bigger than that of the task space (for instance, in the case of redundant manipulators).

When an analytical solution for the IK problem does not exist, or it is hard to compute because of the high number of variables, it is necessary to resort to numerical solution techniques. These techniques have the advantage of being applicable to any robotic structure, and they do not require geometrical computation efforts. One of the most common numerical technique, proposed for the first time in 1969 by Whitney [200], consists in inverting the differential kinematics (4.11), which represents a linear transformation between the joints velocities and the Cartesian velocity of the end-effector. In this case, given a Cartesian motion trajectory $v_e(t)$, the joint trajectory $\dot{q}(t)$ that would reproduce it is given by:

$$\dot{q} = J^{-1} v_e \ . \tag{4.17}$$

If the initial configuration q(0) of the robot is known, the solutions can be computed by integrating the velocities in the time domain:

$$q(t) = \int_0^t \dot{q}(\tau)\, d\tau + q(0) \ . \tag{4.18}$$

The integration could be easily computed numerically with the Euler method, by choosing an integration time step Δt and computing the joints positions at each time step:

$$q(t_{k+1}) = q(t_k) + \dot{q}(t_k)\Delta t \ . \tag{4.19}$$

However, this method does not guarantee that the computed solution will be coherent with the robot kinematic structure, as well as the convergence time of the solution is not known *a priori*. Moreover, just one solution is computed, thus ignoring any redundancy or alternative joints configuration.

For STRAS, we were able to obtain an approximate IK model by discretizing the instrument local workspace. Considering the translational vector of the transformation ${}_{IB}\mathcal{T}^{IT}$ between the instrument base and the instrument tip and plotting the evolution of the Z component when $\beta = \kappa\ell$ varies (see fig. 4.14), one obtains:

$${}_{IB}T^{IT} = \begin{bmatrix} d_{HT}\cos(\phi)\sin(\kappa\ell) + \frac{\cos(\phi)(1-\cos(\kappa\ell))}{\kappa} \\ d_{HT}\sin(\phi)\sin(\kappa\ell) + \frac{\sin(\phi)(1-\cos(\kappa\ell))}{\kappa} \\ d_{HT}\cos(\kappa\ell) + \frac{\sin(\kappa\ell)}{\kappa} \end{bmatrix} \tag{4.20}$$

where d_{HT} is the length of the rigid tool attached at the top of the instrument flexible section (cfr. table 3.1 and section 4.3.1).

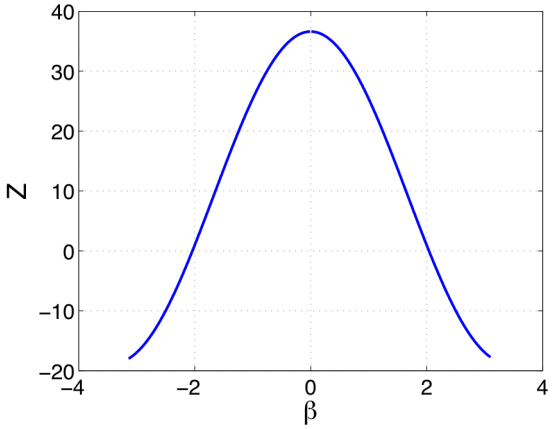

Fig. 4.14. Evolution of the instrument tip Z coordinate expressed in frame F_{EB} when the instrument curvature varies.

Due to the cylindrical symmetry, the Z component depends on the joint variable β only. Being an even function, it provides a mutual relationship between the instrument curvature and the local Z coordinate of its tip. Starting from this relation, it is possible to express an algorithm for solving the inverse kinematics problem:

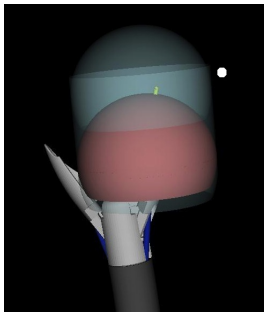

1. Let's consider a generic point P = (x, y, z) expressed in a frame F. The first thing to do is to transform the point coordinates in frame F_{JH}, *i.e.* the frame in which we will express the instrument workspace, and check if the computed point (x', y', z') is inside the instrument global workspace. This can be done by computing its distance from the instrument axis and comparing it with the XY ellipsoid radius.

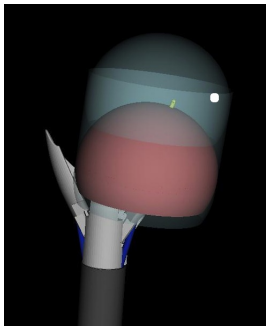

2. If the point (x', y', z') is outside the global workspace, it is necessary to compute the endoscope deflections needed to translate the workspace so as to include the desired point. At this stage, there could be no solution to the inverse kinematic problem if the endoscope deflections are not sufficient to enclose the desired point inside the global workspace: in this case the algorithm stops.

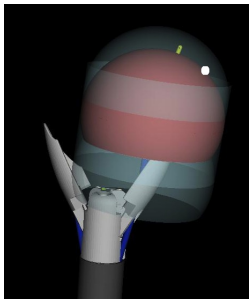

3. Once the desired point lies in the global workspace, it is necessary to find the corresponding local workspace that encompasses the point on its surface. This can be done by imposing the point coordinates (x', y', z') in equation (4.10) and finding out the corresponding ellipsoid center coordinates (x_0, y_0, z_0). Since the ellipsoid is centered on the instrument axis, $x_0 = y_0 = 0$. With its second-order equation (4.10) is possible to compute the two solutions for z_0, one relative to the ellipsoid that contains the point on its upper-half side and the other for the ellipsoid that contains it on the lower-half side. Since the local workspace is modeled as a truncated ellipsoid because of instrument deflection limits, the second solution should be discarded if $(z' - z_0) < z_{min}$. The computed local workspace center permits to determine the needed translations for both instrument and endoscope (a translational movement of the endoscope is mandatory if the computed local workspace is outside the global workspace).

4. Using the $\beta - z$ relationship (see fig. 4.14) it is possible to compute the two curvature values (positive and negative, identical in absolute value) that correspond to the desired z' coordinate. The instrument rotation is immediately computed with:

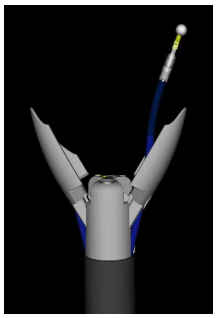

$$\phi = \begin{cases} \arctan 2(y', x') & \text{if } \beta > 0 \\ \arctan 2(y', x') + \pi & \text{if } \beta < 0 \end{cases} \tag{4.21}$$

There are two solutions physically identical, because a deflection β with a rotation ϕ will bring the instrument tip to the same point as a deflection $-\beta$ and a rotation $\phi + \pi$. This means that every point inside the local workspace is reachable at least by two complementary solutions.

As stated in point 3, the second-order formula of the ellipsoid gives two possible solutions for the workspace center relative to the desired Cartesian position. Most of the time, the second solution is discarded because of the deflection limitation, *i.e.* when the desired Cartesian point is below the truncated part of the local workspace. However, when it does not happen, the IK algorithm provides four solutions: the first couple is relative to an instrument deflection in the upper side of the workspace ($\beta < \beta_{sing}$), while the second corresponds to a retroflected configuration ($\beta > \beta_{sing}$). These two couples of solutions, of course, refers to two different values for the instrument translation, since belonging to two different workspaces. There will be, therefore, an area of the workspace (depicted in red, see fig. 4.15) in which multiple solutions can be computed. The particular choice of the employed solution among the computed ones will depend on the selected control strategy and on the current instrument configuration.

An evaluation of the correctness of the proposed IK algorithm will be given in par. 4.3.5.

4.3.5 Validation of the Inverse Kinematics algorithm

The most immediate way to verify the correctness of the proposed IK algorithm (cfr. section 4.3.4) is to span the instrument joints motions and compute the corresponding Cartesian positions of the instrument tip with the kinematic model. Successively, the Cartesian positions are fed to the IK algorithm, which will give the corresponding joints configurations and, again with the direct model, the reached Cartesian positions are computed. The comparison between the desired Cartesian positions and the obtained ones makes possible to verify if the assumption of ellipsoidal shape for the local workspace is correct. Moreover, the gap between analytical and numerical workspaces can be computed. As one can see in fig. 4.16, a rough comparison shows a good similarity between them. Analyzing more in detail the workspaces shapes, a slight gap can be seen in the middle of the upper part (marked in blue, see fig. 4.16), and a more important gap is present on the lower part (marked in green, see fig. 4.16). Numerically, the mean gap between the two workspaces is:

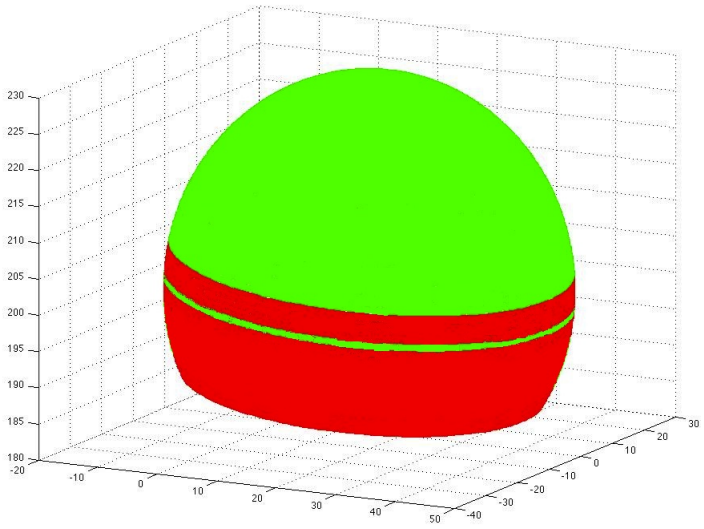

Fig. 4.15. Instrument local workspace. In red, the Cartesian positions reachable by four different configurations are highlighted. Note that the workspace diameter corresponds to a singular position.

$$(\bar{e}_X, \bar{e}_Y, \bar{e}_Z) = (0.34, -6.24 \cdot 10^{-5}, 1.04)\, mm. \tag{4.22}$$

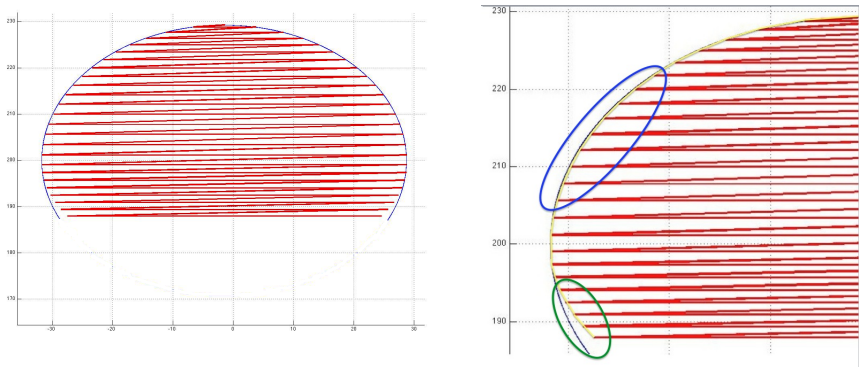

Fig. 4.16. Left: comparison between the analytical (in blue) and the numerical (in red) workspaces. Right: a closer detail shows slight differences in the upper part (marked in blue) and a more consistent deviation at the limit of the instrument deflection (marked in green).

The maximum errors correspond to a deflection value $\beta \approx 128°$, *i.e.* at the limit of the deflection range:

$$(e_X, e_Y, e_Z) = (1.264, 1.223, 3.68)\ mm. \tag{4.23}$$

This results show that the IK algorithm has a good theoretical accuracy in the upper part of the workspace, while a tracking error should be expected if employed on the lower part.

4.3.6 Kinematic singularities

A singularity is a joints configuration that brings the end-effector to lose mobility in one or more directions, which are called *singular directions*. From the mathematical point of view, singularities can be detected by analyzing the Jacobian, because they decrease the matrix rank by making its columns dependent. If the Jacobian is a square matrix, it is possible to simply analyze where the determinant is null. Otherwise, in the general case of a non-square matrix, the Singular Value Decomposition (SVD) method can be used. For a generic mxn matrix M, the SVD is a factorization of the form:

$$M = U\Sigma V^* = U \begin{bmatrix} \sigma_1 & 0 & \cdots & 0 \\ 0 & \sigma_2 & \cdots & 0 \\ \vdots & \vdots & \ddots & \vdots \\ 0 & 0 & \cdots & \sigma_r \end{bmatrix} V^* \tag{4.24}$$

where $r = \min(m, n)$. The number of non-null singular values σ_i in Σ corresponds to the rank of M:

$$rnk(M) = N(\sigma_i \neq 0) \tag{4.25}$$

In our case, if we consider the Jacobian associated to a single instrument (4.14), its determinant is:

$$\Delta = \frac{\partial X}{\partial \beta} X + \frac{\partial Y}{\partial \beta} Y = \frac{\partial (X^2 + Y^2)}{\partial \beta} \tag{4.26}$$

where X and Y are the first two elements of transformation (4.15). This formulation is valid when $\beta \neq 0$, and it is independent of ϕ and t_I. Hence, a graphical analysis of the Jacobian determinant variation in function of the instrument deflection only can immediately shows the singular positions (see fig. 4.17).

Two singularities have been identified in the instrument workspace (see fig. 4.18):

1. Straight position ($\beta \to 0$): in this situation the rotational joint loses its effect, because the instrument rotation does not change the instrument position.
2. $\beta = \beta_{sing} = 101.77°$: this singularity corresponds to the ellipsoid diameter, which represents the maximum distance from the instrument axis reachable by the instrument tip.

Close to a kinematic singularity, the classical inverse kinematics solution based on Jacobian inverse (see eq. 4.17) becomes ill-conditioned, leading to very high joint

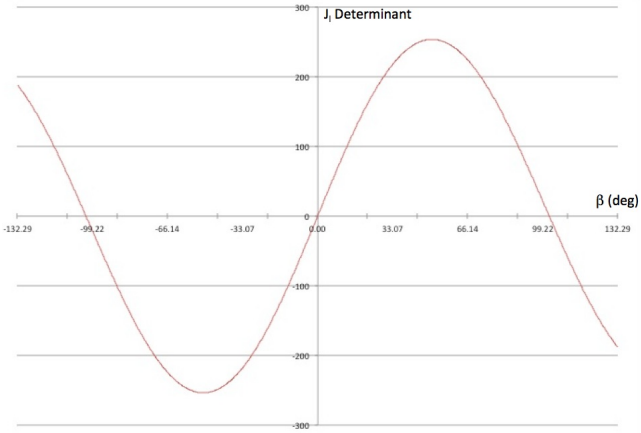

Fig. 4.17. Evolution of the instrument Jacobian determinant when the instrument deflection varies.

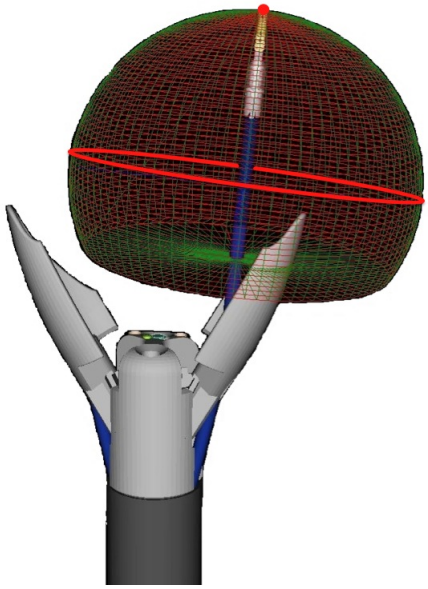

Fig. 4.18. Kinematic singularities of an instrument.

velocities and large control deviations against small Cartesian references. A possible solution could be to translate the desired Cartesian path in joint coordinates, in order to avoid the singular positions, but this could not be easily done in real-time control, since the user movements are unpredictable and a post-processing filter is unsuitable because it would introduce important time delays.

Although a common and universal method for singularity avoidance does not exist, several approaches have been proposed. One of the most known and used methods to overcome the singularity avoidance problem is the Damped Least-Square (DLS) method, originally proposed by Nakamura and Hanafusa in 1986

[123]. It is based on the Moore-Penrose pseudo-inversion method for rectangular matrices:

$$M^{\#} = M^T(MM^T)^{-1}. \tag{4.27}$$

The DLS method modifies the Moore-Penrose pseudo-inverse by introducing a variable damping factor λ:

$$M^{\#} = M^T(MM^T + \lambda^2 I)^{-1}. \tag{4.28}$$

Large values of λ permit to reduce the overshoot in joints velocity references due to the magnitude of the Jacobian inverse elements, but at the same time the robotic system is largely slowed down and the tracking accuracy of the control scheme is degraded. Therefore, it is necessary to accurately tune the damping factor λ according to the particular robot. Also, it could be convenient to put an activation threshold in order to enable the DLS method in the neighborhood of a singularity only, while keeping the normal differential kinematics control in the remaining part of the workspace. Since close to a singularity the Jacobian determinant tends to zero, it is possible to identify a value that discriminates between the singularity neighborhood and the non-singular part of the workspace:

$$\lambda = \lambda_0 \left(1 - \frac{|Det(J)|}{Det(J)_{Threshold}}\right). \tag{4.29}$$

In our case, since the singularities could be easily located in the joints space by means of the deflection value, we could use β as discriminant for the DLS method activation.

Here we are proposing another singularity avoidance method especially thought for the Straight position singularity. As stated before, when the instrument approaches that position, its curvature parameter $\kappa \to 0$ and the kinematic model (4.4) is no longer consistent. In this singular situation, the instrument rotational joint receives high speed references, resulting in uncontrolled rotations of the instrument tip. This singularity avoidance method is employed when the instrument enters inside the central conical zone depicted in red in fig. 4.19, *i.e.* when it is approaching the straight position and its curvature $\kappa \to 0$. To avoid the drift of the curvature value, inside the conical zone the kinematic model is computed as the instrument would keep the same curvature value κ_T relative to the zone threshold: this value is used thorough the conical zone and its sign is changed when passing the central position. Once the instrument exits from the central zone, its curvature value is updated and the model computation is performed with the right joints values. Although this method introduces a tracking error because of the wrong configuration used for the model computation, it allows to avoid the straight singular condition, thus the undesired and uncontrollable movements of the instrument.

4.4 Teleoperation

4.4.1 Introduction

Teleoperation is a composite word that makes use of the Greek prefix *tele*, which means "at a distance", to indicate the extension of the human capabilities to

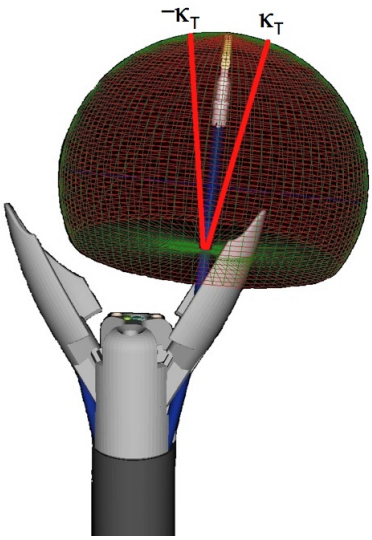

Fig. 4.19. Neighborhood of the straight position singularity.

manipulate remote objects with similar conditions as those at the remote location [81]: this situation is typically called *telepresence* [158]. A teleoperator is a mechatronic machine consisting of a master interface, in contact with the user, and a slave manipulator, in contact with the remote environment, connected via a communication channel (see fig. 4.20).

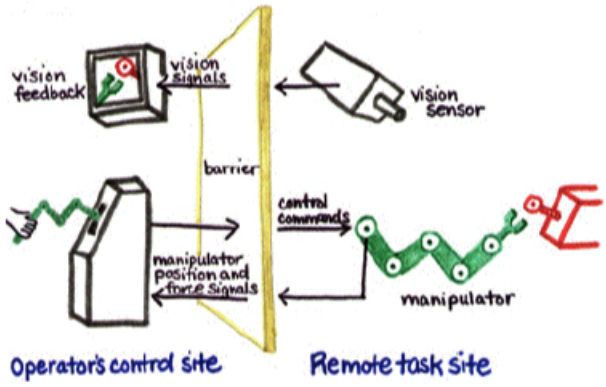

Fig. 4.20. Simplified sketch of a teleoperated system.

Raymond C. Goertz, a former researcher of the Atomic Energy Commission at Argonne National Laboratory (Lemont, IL, USA), is credited for the development of the first modern master-slave teleoperator in 1945 [168]. He designed a teleoperated system for the remote manipulation of radioactive materials [64] (see fig. 4.21). Indeed, teleoperation arose with the first aim of substituting humans in

hazardous and dangerous environments, where a human could not be physically present, but where a standard pre-programmed robot was unable to cope with unknown conditions.

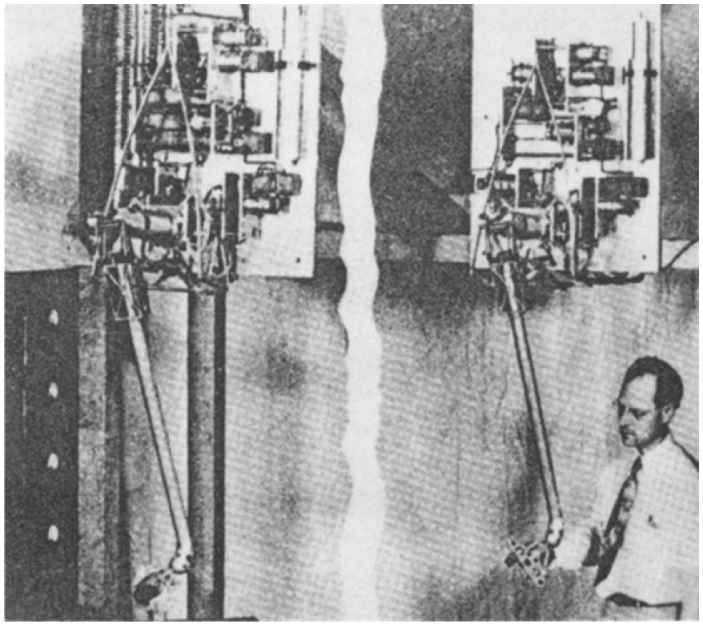

Fig. 4.21. R. Goertz and his E1 telemanipulator (reprinted from [168]).

The original concept of teleoperated system was a master robot that moved its remote kinematic replica. During the following years, evolutions in haptic interfaces, sensors and robotic technologies allowed to use teleoperation methods in several different fields, from assistive robotics for disabled people to teleoperated vehicles.

The most common robot architecture employed in surgery is the teleoperation scheme. The slave system is the part in contact with the patient, containing the surgical tools and the actuator means for their movements. The master manipulator is the user console, controlled by the main surgeon in order to perform the surgical operation. Master and slave systems could be placed in two separate places, and their communication is assured by a connection cable. The interest to apply teleoperation in surgical applications came with the advent of laparoscopy, where surgeons did not have anymore a direct access into the abdominal cavity. There are several advantages when using a teleoperated system in surgery:

- the user input can be properly filtered before being sent to the slave part, *e.g.* to reduce natural hands tremor or to scale their movements in order to gain dexterity;
- different mappings between master and slave systems can be used;
- surgeon and patient could be located in two different places (cfr. Operation Lindbergh, see section 3.3).

4.4.2 Bilateral teleoperation scheme

In a teleoperation system there is a continuous exchange of informations between master and slave parts, particularly positions and forces references. Typically, the human operator moves the master manipulator, which detects and transmits the movement to the slave manipulator. The movement produces a change in the slave manipulator configuration and, potentially, an interaction with the environment, which could be sent back to the human operator by means of the master manipulator in order to reflect the remote conditions to the user. This scheme is usually called *bilateral teleoperation*, since it involves a two-way transmission inside the teleoperator (see fig. 4.22). This particular feature is what differences teleoperation from *remote control*. Remote control could be seen as *unilateral teleoperation*, since there is no transmission of the slave references back to the master manipulator.

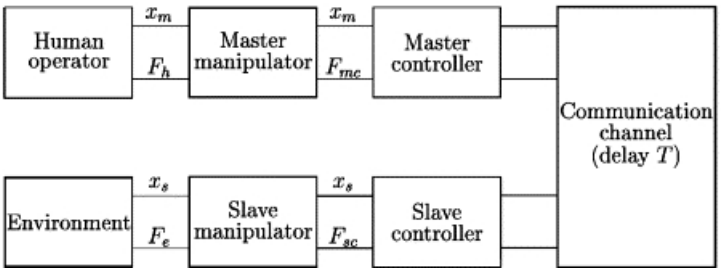

Fig. 4.22. Bilateral teleoperation scheme (reprinted from [3]).

In order to be safe, effective and accurate, a teleoperated system should guarantee two main aspects that are generally conflicting [104]:

1. **Stability**: the two-ways communication between master and slave part corresponds to a closed-loop control scheme, which should be able to compensate the error, i.e. the difference between the user references and the slave responses. This process must guarantee that, at steady state, the error tends to zero and the system is capable to compensate any external disturbance or sensor error.
2. **Transparency**: the teleoperated system should not introduce any modification between the user and the environment, it should replicate the desired user references on the slave manipulator and reproduce the environment conditions and reactions on the master manipulator. The user references, as for the haptic feedback, should be reproduced with a reasonable latency: in this case the delay introduced by the communication channel plays an important role.

In a system affected by time delays and external disturbances, a transparent transmission of position and force references between master and slave systems could easily lead to the system instability, because of the difficulty to keep master and slave states synchronized. On the other hand, a robust stability scheme presupposes damping and modifications to master and slave dynamics, thus affecting transparency.

A bilateral teleoperation system could be modeled as a two-port block that, as stated before, exchanges two types of informations between its master and slave parts: positions/speeds and forces/torques. This led to four different possibilities to couple master and slave systems [204]:

- position/speed on both master and slave;
- position/speed on master, force/torque on slave;
- force/torque on master, position/speed on slave;
- force/torque on both master and slave.

4.4.3 STRAS slave control schemes

Since STRAS is a flexible system, a force control scheme could lead to erroneous references computations without a feedback from exteroceptive force sensors. We chosen, therefore, to use a position/speed teleoperation scheme. Particularly, the slave robot is controlled in joints velocity, receiving the velocities references $\dot{\boldsymbol{q}}_{ref}$ in input and producing the Cartesian movements $\mathbf{X}$ in output (see fig. 4.23). We can assume the slave robot as an integrator that introduces a time delay, mainly due to the system actuation dynamics affected by cables friction and mechanical non-linearities (cfr. section 3.5.3). This delay is difficult to estimate, it is not deterministic and it depends on several parameters, primarily system shape, friction between cables and sheaths, elasticity and pretension of cables (see [2] for an analytical description of cables actuated systems). For this reason, in the following sections the time delay will be not taken into account.

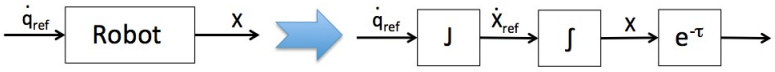

Fig. 4.23. Modelization of the slave robot.

Generally speaking, three common control schemes could be envisaged for the kinematic control of the slave robot:

1. **Open Loop**: the user input is expressed as a desired Cartesian speed $\boldsymbol{\Omega}_{ref}$, which is directly multiplied by the Jacobian inverse J^{-1} in order to obtain the corresponding speed references $\dot{\boldsymbol{q}}_{ref}$ for the motors (see fig. 4.24). There is no feedback on the robot position at the control scheme level: in this case the user is left to close the loop by visualizing the system reactions, captured by the endoscopic camera, and properly rectifying his/her input.
2. **Closed Loop Joint Control**: using the IK algorithm described in section 4.3.4, it is possible to control the position of the instrument tip in the Cartesian space. The position (t_x, t_y, t_z) of the master handle will represent the desired Cartesian reference $\mathbf{X}_{ref}$ for the instrument tip position, expressed in a frame coherent with the considered model (FK_{EB} or FK_C, see section 4.3.1). The interface gripper controls the grasper actuation, while the interface rotations are not used. No force feedback effect but the interface gravity

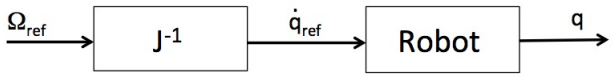

Fig. 4.24. Open loop control scheme.

compensation is applied in this case. The IK algorithm is responsible to compute the joints reference $\mathbf{q}_{ref}$ corresponding to the desired Cartesian reference $\mathbf{X}_{ref}$ (cfr. section 4.3.4). The computed reference $\mathbf{q}_{ref}$ is then compared with the actual robot configuration $\mathbf{q}$ in order to compute an error vector $\mathbf{e}$ (see fig. 4.25). A proportional control law K_P is applied to the error vector, obtaining the joints speed references $\dot{\boldsymbol{q}}_{ref}$ that will be sent to the slave robot.

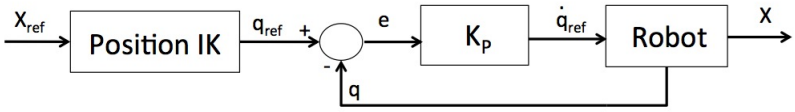

Fig. 4.25. Closed loop joint control strategy.

3. **Closed Loop Position Control**: the user input, expressed as a desired Cartesian position $\mathbf{X}_{ref}$, is compared with the estimated robot Cartesian position $\tilde{\mathrm{X}}$ in order to compute an error vector $\mathbf{e}$. A feedback controller K_P, together with an additional feedforward term, will provide the Cartesian velocity input, which is then fed to the Jacobian inverse J^{-1} (see fig. 4.26). The controller can be as simple as a proportional controller because of the integrator in the robot.

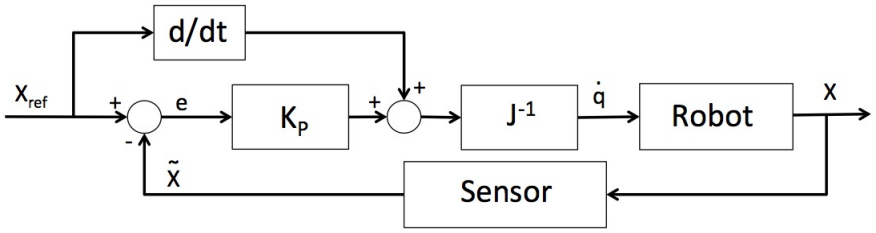

Fig. 4.26. Closed loop control scheme.

The estimate of the robot Cartesian position $\tilde{\mathrm{X}}$ can be obtained in several ways, each with its own strengths and weaknesses:

- **Direct kinematic model**: the robot state vector $\mathbf{q}$ is fed to the direct kinematic model, in order to obtain the corresponding end-effector Cartesian po-

sition. This method has the advantage of being fast, since no external devices are needed, but its precision relies on the accuracy of the kinematic model.

- **External sensors**: in this case, an external device is used to measure the robot Cartesian position. This device, typically called *tracker*, consists of a source that is able to localize a number of sensors on the basis of optical, electromagnetic or radio-waves changes. The sensors poses are given as vectors expressed in the source frame, so a registration procedure with the robot base frame is mandatory to obtain consistent measures. Practically, the use and precision of the tracker is limited by the tracker source physics principle: optical trackers require free lines-of-sight between the source and the sensors, electromagnetic trackers suffer from field distortions caused by metallic objects and radio-waves are not suitable for precise localisation. Moreover, their acquisition speed is often much slower than the robot control loop in real-time applications, and the measure acquisition and elaboration introduce a delay in the control scheme that must be taken into account. Finally, the integration of a tracking system inside the robot for a standard routine use is not straightforward, because it would require a mechanical redesign of the tools and a specific choice of compatible materials (*e.g.* non-metallic parts if an electromagnetic tracker is used).
- **Endoscopic camera**: when using manual instrumentation in the surgical routine, the endoscopic camera is the only sensor used by the surgeon to establish the instruments positions and, thus, decide the type of movements that he/she should perform. In some robotics systems, as well as in STRAS, the endoscopic camera represents the only sensor embedded on the slave system. Automatic routines for the instruments detection inside the image could be envisaged, with the aim to obtain an estimation of the position and, eventually, the shape of instruments. The inner limitations of such technique lie in the difficulty to correctly modeling flexible sections and estimate depth in the 2D endoscopic image. Moreover, during a surgical operation smoke and fluids could deteriorate the quality of the image, hide some system parts or create light reflections: these issues could lead to an erroneous estimation and be potentially dangerous during the clinical use.
- **Inertial sensors**: subdivided in motion (*accelerometers*) and rotational (*gyroscopes*) sensors, they permit to detect a change of a system state of inertia. To achieve this, they are pre-calibrated and mounted on the system to be measured in a known position, in a way that any pose change can be correctly measured. The main issue with such sensors is the *integration drift*, *i.e.* the progressively increasing error due to the accumulation by integration of small inner errors in the measurement of acceleration and angular velocity. Therefore, the position must be periodically corrected by comparing it with other types of sensors [206].
- **Fiber optic sensors**: they are particular sensors, shaped as cables, that use optical fiber to detect their shape change according to the light wavelength shift, or by sensing the time delay as light passes along the fiber through each sensor inserted inside the bundle. They could be used, therefore, to estimate the shape of a flexible section and detect its movements. They have the advantage of not requiring electrical power at the remote location, thus simplifying the

integration. As drawback, light is not anymore transmitted when the optical fiber is bended over a critical angle, which depends on the fiber quality, length and radius [188]. Moreover, their cost makes their use sometime prohibitive.

4.4.4 Master output

The control strategies presented in par. 4.4.5 basically require two types of input: positions ($\mathbf{X}_{ref}$) or velocities ($\boldsymbol{\Omega}_{ref}$) references expressed in the Cartesian space. The user can send these references by means of the master interfaces, which can provide a position output $\mathbf{X}_M$, based on their encoder positions, or a velocity output $\mathbf{V}_M$, computed internally on the interfaces or derived numerically as the position variation over time. Therefore, several ways to correlate the master output with the slave input could be envisaged, and we can classify them in two main categories:

- **Position control**: the master output is used as a position reference input for the slave system (see fig. 4.27). In this case, the absolute interface position (scheme 1, see fig. 4.27), the variation with respect to the last position (scheme 2, see fig. 4.27) or the interface velocity (scheme 3, see fig. 4.27) can be considered.

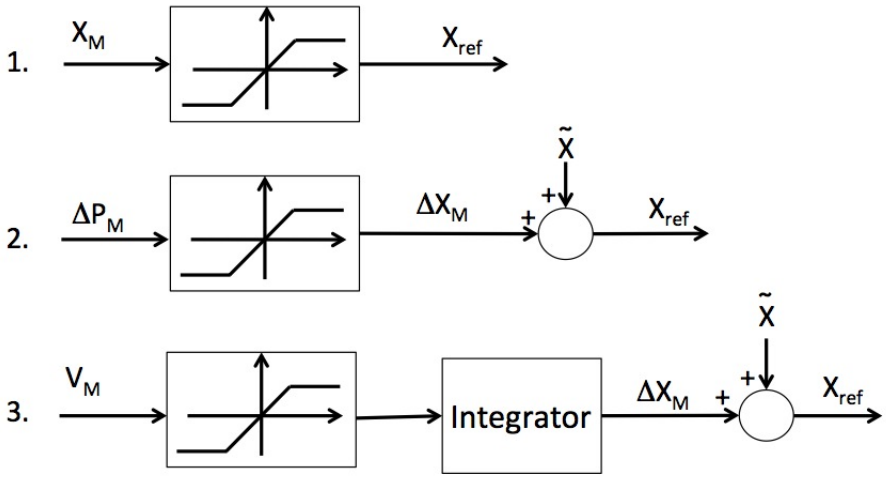

Fig. 4.27. Master position control.

- **Speed control**: the master output is used as velocity reference for the slave system (see fig. 4.28). If the master position is used as velocity reference (scheme 2, see fig. 4.28), a force feedback effect acting as a spring is applied on the interface (cfr. section 4.4.8), with the aim is to drive the interface toward its rest central position in which the master output is null. In this manner, if the user wants to stop the system, he/she has to accommodate the force effect and gradually conduct the interface on its center.

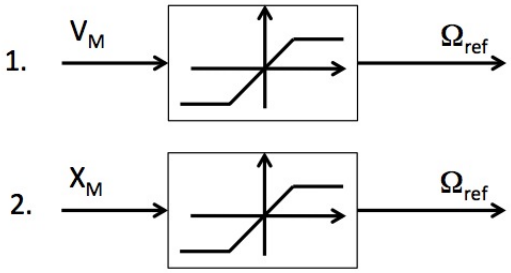

Fig. 4.28. Master speed control.

4.4.5 Master / Slave mappings

As introduced in section 3.5, STRAS is a teleoperated system composed by a master interface, consisting in two omega.7 haptic interfaces from Force Dimension (Nyon, Switzerland), and a slave robot, consisting in three robotized subsystems structured in a tree-like architecture (cfr. fig. 3.26). Master and slave systems have completely different kinematic structures: on the master side 14 DOFs are available, while the slave robot offers 10 DOFs globally, so an adequate mapping between them should be established. Furthermore, the two master interfaces have to control the three slave subsystems for allowing a single user to operate the whole robot alone.

Although the omega.7 interface is redundant with respect to the task of controlling a single instrument, its mechanical architecture gives enough flexibility to exploit different mappings. The choice to use a commercial interface in this stage of development is motivated by the fact that it can allow to test the user reactions to different operation modalities: once a first evaluation will be performed, the development of a dedicated interface, tailored on a specific preferred mapping, could be envisaged.

For our robot we are proposing four different mappings, which will be detailed in the following:

1. Direct Joint Control
2. Orientation guidance
3. Cartesian control
4. Pseudo-Cartesian control

In all the proposed control strategies, the mapping between master and slave systems is established in a way that the left (resp. right) haptic interface is connected to the left (resp. right) instrument (see fig. 4.29). The endoscope control is achieved with the left interface, after pressing a pedal on a pedal board that locks the position of the left instrument and enable the endoscope movement (cfr. section 4.4.9 for a detailed list of pedal board functionalities). During the passage from instrument control to endoscope control, the interface position is stored and a force feedback effect, acting as a spring that drives the interface toward the stored position (cfr. section 4.4.8), is applied: in this way, the endoscope does not move

if the user leaves the interface, while when switching back to the normal control of left instrument the haptic interface is already in place, avoiding unwanted and sudden instrument movements because of a discrepancy between the left instrument and the master positions. This enforces to control the endoscope velocity by small displacements around the switch position.

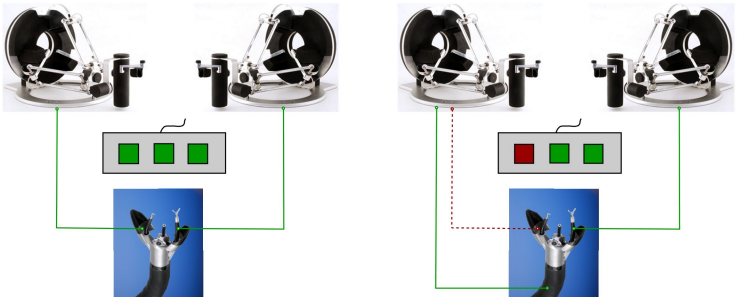

Fig. 4.29. Left: in the normal control, left and right interfaces control respectively left and right instruments. Right: when the left pedal is pressed, the left interface control passes to the endoscope.

A summary of the proposed mappings, which will be detailed hereinafter, is presented in table 4.2.

	Instruments				**Endoscope**	
Mapping	**Rotation** $\boldsymbol{\phi}$	**Translation** $\mathbf{t}_I$	**Deflection** $\boldsymbol{\beta}$	**Grip**	**Deflection dx**	**Deflection dy**
Direct Joint Control	θ_Z	t_Z	Gripper	Pedal	t_X (vel)	t_Y (vel)
Orientation guidance	θ_Z	Δz_M (vel)	$\propto \sqrt{x_M^2 + y_M^2}$	Gripper	t_X (vel)	t_Y (vel)
Cartesian Control	IK model/Jacobian			Gripper	t_X (vel)	t_Y (vel)
Pseudo-Cartesian	eq. (4.30)	eq. (4.31)	eq. (4.32)	Gripper	t_X (vel)	t_Y (vel)

Table 4.2. Summary table of the proposed mappings ((vel) indicates a control in velocity).

Direct Joint Control

In this modality, each joint of the slave system is directly controlled by an elementary motion of the master interface. The aim is to reproduce a manipulation feeling close to the ANUBISCOPE® system, but avoiding side effects as actuation frictions and poor ergonomics. For this mapping a subset of the master DOFs (depicted in fig. 4.30) is used, in which the interface gripper, the translation t_z along Z and the rotation θ_z around Z on the haptic interface control respectively the deflection β, the translation t_I and the rotation ϕ of the instrument. A force feedback effect is applied in order to lock the unused translational DOFs: the interface handle is free to move in the Z_M direction only, while every attempt to move it in the $\mathrm{X}_M\mathrm{Y}_M$ plane is contrasted by an opposite force.

In case of an actuated instrument, such as the grasper, the opening and closing is performed with the middle pedal of the pedal board in a two-way modality (the grasper can be completely closed or completely open).

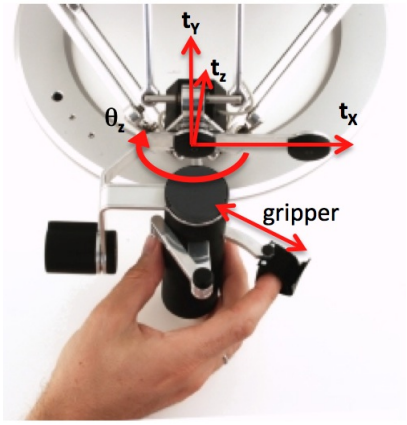

Fig. 4.30. Master interface's degrees of freedom employed in the Direct Joint Control strategy.

Orientation Guidance

The underlying idea of this modality is to offer a kind of joint control where the master interface movements are constrained to those the instrument could do from the current configuration: in this manner, the user movements mimic the instrument tip movements and the user's hands orientation follows the tool orientation, giving the feeling of direct control over the instrument tip. As for the Direct joint control, in this modality θ_z still directly controls the rotation ϕ of the instrument. For the deflection control, the reference is given by the haptic handle, which is constrained on a straight line on the $X_M Y_M$ plane that passes through the haptic central position (see fig. 4.31). Since the handle orientation is aligned with that of instrument, the straight line represents the trajectory, projected on a plane, that the instrument covers when its deflection varies. In this modality, the gripper controls the grasper actuation analogically, while the instrument translation is controlled in velocity, with the haptic interface movements constrained in the plane $Z_M = 0$ by a force feedback effect. This choice is due to the particular interface workspace shape, which is hemispheric: to guarantee the maximum excursion of the handle in the $X_M Y_M$ plane it is necessary to keep it in the middle of its workspace. In this case, the user has to gently push or pull the handle if he/she wants to move the instrument forward or backward.

Cartesian Control

As described in section 4.4.3, a Cartesian control of STRAS can be achieved either using the IK model or its Jacobian. In both cases, the user references consist in

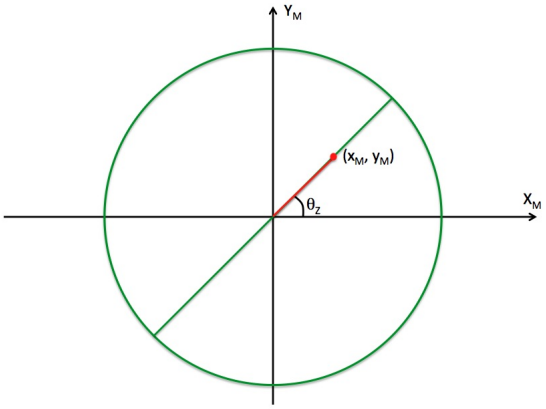

Fig. 4.31. Schematic representation of the Orientation Guidance mappings. The interface workspace is depicted as a green circle, the master handle is free to move on a straight line with slope identical to the current orientation θ_Z. The position (x_M, y_M) of the master handle determines the instrument deflection reference.

desired Cartesian positions of instruments, described by translations of the master interfaces. If the IK model is used, the corresponding joints position references are directly computed, compared with the actual robot state and sent to the slave robot (see fig. 4.25). With the differential kinematics, instead, the estimation of the current robot Cartesian position is mandatory in order to compute the discrepancy with the input position reference (see fig. 4.26). This aspect limits the practical use of such control method because, as explained in section 4.4.3, the kinematic model does not provide reliable position references and external sensors are difficult to integrate for a clinical use.

Pseudo-Cartesian Control

Named "Pseudo" because it gives almost the same control feelings as a Cartesian control strategy, this modality does not use a kinematic model to control the system. In this strategy, the master interface movements in the $X_M Y_M$ plane control both instrument deflection and rotation, while t_z directly controls the instrument translation:

$$\phi = \arctan 2(y_M,\ x_M) \tag{4.30}$$

$$t_I = z_M \tag{4.31}$$

$$\beta = \lambda \sqrt{x_M^2 + y_M^2} \tag{4.32}$$

where (x_M, y_M, z_M) is the current haptic handle position, while λ is a scaling factor that adapt the interface workspace to the instrument one. The interface gripper is available for the control of actuated instruments (such as the grasper) and the master interface rotations are not used for the control.

The mapping between (x_M, y_M) and (β, ϕ) takes inspiration from the instrument workspace shape: if seen in the XY plane, the instrument local workspace appears as a series of concentric circles with radii dependent of the instrument deflection. Therefore, one can consider the distance of the haptic handle from the interface center, computed in the $X_M Y_M$ plane, as a deflection reference for the instrument: when the handle is in the center, the instrument should be in the straight position, while at the boundaries of the haptic workspace the instrument should be at the maximum deflection. Because of the limited instrument DOFs, the orientation is a consequence of its position, and it is computed as in eq. (4.30). To take account of the instruments rotational limits (cfr. sections 3.5.2 and 4.3.2), a triangular zone is identified and inhibited on the $X_M Y_M$ plane, according to the current sign of deflection. To make the user aware of such limitation, a force feedback effect is applied on the interfaces when their current positions (depicted as a small red circle, see fig. 4.32) are close to the forbidden zone of the workspace (depicted as a red triangle with a vertex pointing on the workspace center, see fig. 4.32): the feedback effect will apply a repulsive force all along the forbidden zone boundaries in order to avoid that the interface could enter in it. Despite this effect, one can still apply a higher force and overpass the forbidden zone: in that case, the force feedback effect is deactivated and the teleoperation is freezed until the interface is brought back in the allowed workspace. To help the user to understand the relative positions of the interfaces projected on the instruments workspaces, two radars (one for each instrument) are showed on the user screen during the teleoperation (see fig. 4.32).

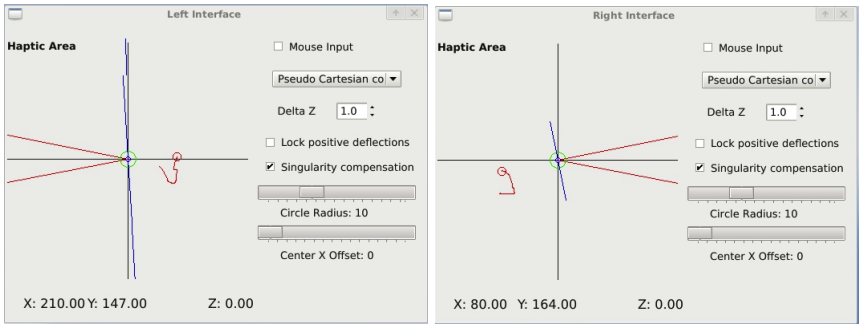

Fig. 4.32. Graphical radars showing the position of the haptic interfaces in their workspaces and the location of the workspace restricted zone.

4.4.6 Workspace restrictions

As already introduced in sections 3.5.2 and 4.3.2, the mechanical stops setted on the instruments rotation motors limit their attainable workspaces. This is true when the instrument deflections are limited to positive values only: in this case, the forbidden zones are located on the outer sides of the instruments workspaces, keeping the central cooperation area completely reachable.

Since the instrument could deflect in both positive and negative directions, the obtained redundancy (cfr. section 4.3.2) can be exploited to recover the full workspace. But the only way to switch the deflection sign without discontinuous position references is to pass through the central straight position. As seen in section 4.3.6, the central position is singular, leading to an indeterminate rotation of the instrument. To avoid this singular configuration, a circular zone at the workspace center (depicted as a green circle, see fig. 4.32) is indicated: in this zone, the instrument rotation variation is no longer permitted, and the deflection sign is changed when the interface passes to the complementary workspace half-plane (the boundary between the two half-planes is depicted as a blue line, see fig. 4.32). In this way, a small tracking error on the rotation is compensated when exiting from the central circular zone, because the user trajectory typically does not follow straight lines, so the instrument rotation value stored at the approach of the central zone does not correspond to that of leaving. A compromise about the size of the central circular zone is therefore needed: if it is chosen large, the deflection switch will be easier for the user, but the rotational tracking error will be larger; if it is small, a better rotational tracking error is achieved, but the deflection switch will be more complicated to do without looking at the instrument radars and choosing the right trajectory. The advantage of the deflection switch is that the workspace is completely restored, since the forbidden zone changes its position according to the current instrument deflection sign.

4.4.7 Automatic endoscope control

The mappings proposed so far do not provide any form of automatic movements on the slave system, since all the DOFs are directly controlled or activated only when the user wants. Moreover, each slave subsystem is controlled separately, and the computed references for one instrument do not take account of the other instrument position. In order to exploit the entire mobility of STRAS in a coordinate way, a model of the whole system is necessary. As briefly introduced in section 4.3.4, the Jacobian is a common solution in robotics to solve the IK problem in terms of velocities. In case of rectangular matrix, and when the system is not in singular position, the Jacobian inverse $J^{\#}$ can be computed with the Moore-Penrose pseudo-inverse formula (4.27).

Despite the classical case in which a robotic manipulator has a single end-effector, in STRAS the two instruments represent two end-effectors that have to be controlled at the same time. Moreover, the tree-like architecture implies that the use of the endoscope DOFs modifies the poses of both instruments. The main control problem in this case is how to manage potential conflicts between the tasks assigned to the two instruments: some constraints cannot be satisfied at the same time, especially when an endoscope movement is requested.

We have tried to explore different solutions:

- **Automatic endoscope repositioning**: from a robotic point of view, it could be interesting to introduce automatic movements in the STRAS teleoperation, with the aim to facilitate the manipulation by anticipating the surgeon's requests. One of the most common movements during a surgical operation is the camera repositioning: the assistant surgeon is typically responsible for the

correct location and zoom of the endoscopic image, in order to center the operation field and visualize the instruments. Unlike traditional laparoscopy, in which the endoscope is independent from the instruments, STRAS has the camera embedded on the endoscope head and, consequently, its position is fixed with respect to the instruments channels. Since the camera field of view does not completely contain the instruments workspaces, an endoscope movement is mandatory when one or both instruments are outside it (see fig. 4.33). But when just moving the endoscope, the absolute Cartesian positions of instruments are not kept. The robotic assistance in this case should allow a camera repositioning, while calculating a new joints configuration that preserves the actual target.

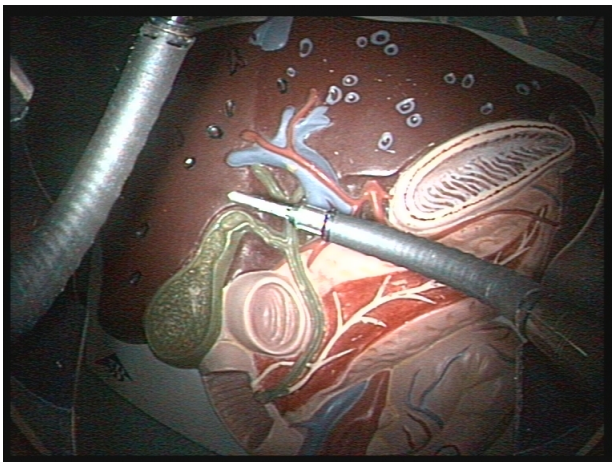

Fig. 4.33. Instrument outside the camera field of view.

To explain how this modality works, let's consider the XY plane aligned with the camera frame and located at a certain Z coordinate from the camera itself. On this plane, the X axis corresponds to the dx endoscope deflection direction, while the Y axis corresponds to dy. From this point of view, the instruments workspaces appear as two ellipses, because the instrument channels are deviated with respect to the camera axis, but for simplicity we will assume them as circles. We could represent the actual instrument position as a complex vector, with the magnitude corresponding to the deflection and the phase to the rotation. This vector will have X and Y components, with directions that depend on the quadrant in which the vector lies. We can identify three possible situations:

1. Instruments movements are toward the same X and Y directions (see fig. 4.34): this is the ideal case for an automatic movement of the endoscope, since it will allow to rearrange the instruments in a position close to the straight one, while keeping their targets.

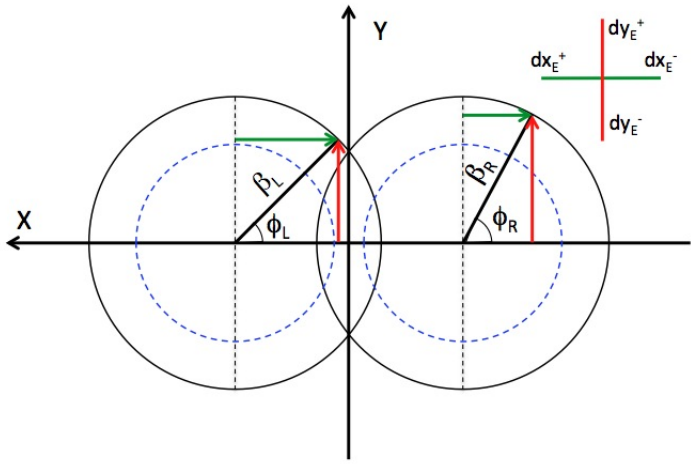

Fig. 4.34. Instruments pointing toward the same X and Y directions.

2. Instruments movements have one common direction (see fig. 4.35): in this situation, only the endoscope deflection relative to the common direction will be involved.

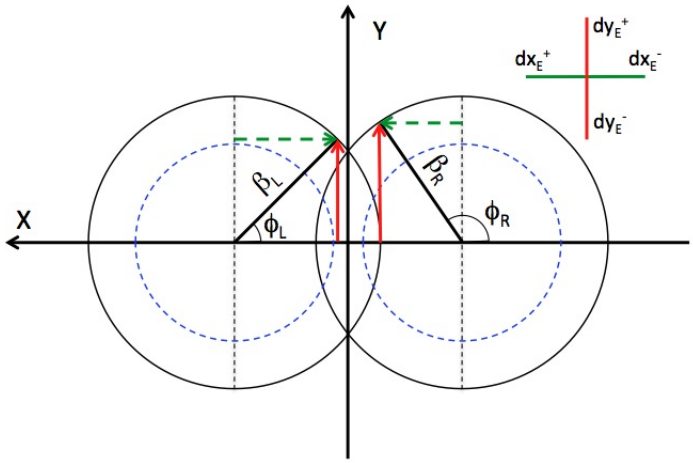

Fig. 4.35. Instruments pointing toward one common direction.

3. Instruments movements are toward opposite directions (see fig. 4.36): in this case no endoscope movements are possible, because they will not guarantee the current instruments positions.

In this modality, the endoscope movement is automatically activated when one instrument is close to its workspace limit, while the other is inside the central part of its workspace. The endoscope repositioning is arrested when the first

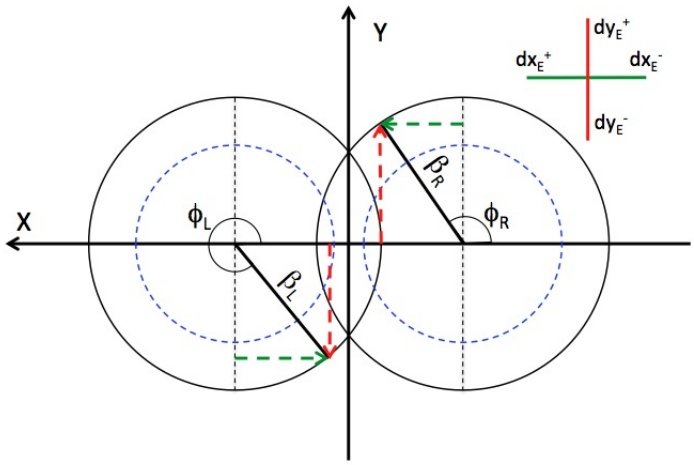

Fig. 4.36. Instruments pointing toward opposite directions.

instrument results centered in the image, while for the second instrument a new configuration that guarantees the same position is computed. The automatic activation and deactivation can be tuned with two thresholds, which are based on instruments deflection values: when an instrument is bended over the activation threshold values, the endoscope repositioning is executed and the instrument is led to an almost straight position, defined by the deactivation threshold. The final aim is to provide an auto-centering camera mode that is able to change the camera view according to the instruments positions.

- **Weighting matrix**: a single Jacobian for the whole robot is considered

$$J = \begin{bmatrix} \lambda_E J_{EL} & \lambda_L J_L & \emptyset \\ \lambda_E J_{ER} & \emptyset & \lambda_R J_R \end{bmatrix} \Rightarrow \dot{\boldsymbol{q}} = J^{-1}\dot{\boldsymbol{X}} \tag{4.33}$$

where:

$$\dot{\boldsymbol{q}} = [\dot{dx}_E,\ \dot{dy}_E,\ \dot{\phi}_L,\ \dot{tr}_L,\ \dot{\beta}_L,\ \dot{\phi}_R,\ \dot{tr}_R,\ \dot{\beta}_R]^T \tag{4.34}$$

$$\dot{\boldsymbol{X}} = [\dot{x}_L,\ \dot{y}_L,\ \dot{z}_L,\ \dot{\omega}_{XL},\ \dot{\omega}_{YL},\ \dot{\omega}_{ZL},\ \dot{x}_R,\ \dot{y}_R,\ \dot{z}_R,\ \dot{\omega}_{XR},\ \dot{\omega}_{YR},\ \dot{\omega}_{ZR}]^T \tag{4.35}$$

and the subscripts E, L and R refer respectively to Endoscope, Left and Right instruments. With this modality, all the slave DOFs are involved in order to execute the desired task. λ_E, λ_L and λ_R are weight factors that could be assigned in order to define the relative importance of the robot subsystems: one could decide to privilege one instrument movement with respect to the other, or to emphasize or limit the endoscope movements for the task completion. In case of conflictual tasks between the two instruments, this strategy does not satisfy any of them exactly, but the solution will be a compromise based on the weight factors.

- **Task priority strategy**: rather than a compromise, as in the Weighting matrix strategy, in this case the two conflictual tasks are managed by assigning a priority to one of them, executing the primary task and try to accomplish as

close as possible the secondary task without influencing the primary one. The task priority strategies make use of the concept of *null space* of the Jacobian matrix, *i.e.* the set of joints configurations that do not vary the end-effector pose. This concept is extremely important for hyper-redundant robots that, having more DOFs than those needed for their task, could exploit their redundancy to accomplish a secondary task (as obstacle avoiding, for instance) while reaching their target. This strategy was originally proposed in 1981 by Hanafusa *et al.* [69], and later developed in two different formulations by Chiaverini [25] (see eq. (4.36)) and Maciejewski [111] (see eq. (4.37)):

$$\dot{q} = J_1^{-1} v_1 + (I - J_1^{-1} J_1) J_2^{-1} v_2 \tag{4.36}$$

$$\dot{q} = J_1^{-1} v_1 + (J_2 (I - J_1^{-1} J_1))^{-1} (v_2 - J_2 J_1^{-1} v_1) \; . \tag{4.37}$$

In both cases, the subscript 1 indicates the primary task, executed with the classical kinematic inversion method. The difference between the two proposed formulations lies in the secondary task execution: in eq. (4.36) the secondary task is computed with the kinematic inversion method as it if were a single task, but its solution is then projected in the null space of J_1, in order to guarantee the primary task position; in eq. (4.37) the secondary Jacobian is projected and reversed in the null space of the primary Jacobian, with a compensation term for the eventual movements of the secondary task that are already realized by the first one.

Although STRAS is not a hyper-redundant robot, the idea of tasks with different priorities could be useful in a surgical scenario where there are two instruments: a grasper, which holds a tissue, and an electric knife that cuts it (see fig. 4.37). In this case, the electric knife will be the primary task, because its movements must be executed as much accurately as possible, while the grasper, once positioned, does not need too much precision or a large movements range.

4.4.8 Force feedback effect

As briefly explained in section 3.5.5, the haptic interfaces employed for STRAS are capable to reproduce a force feedback effect on their active axis, *i.e.* the translations and the gripper. Since STRAS does not embed any force sensor on its instruments, the force feedback effect applied on the haptic interfaces cannot reflect the real interactions of the robot with the environment. Anyway, this capability of the interfaces can be useful to guide the user gesture during the teleoperation: since in all the proposed mappings the interfaces DOFs are redundant compared to the task, the force feedback effect could block the unused DOFs (if they are active) and create active constraints on the interfaces workspaces in order to limit their movements in specific allowed areas.

We implemented several force feedback effects according to the different mappings:

- **Spring**: the force feedback acts as a spring that, at any times, drives the haptic interface toward a rest position (which could be different from the interface

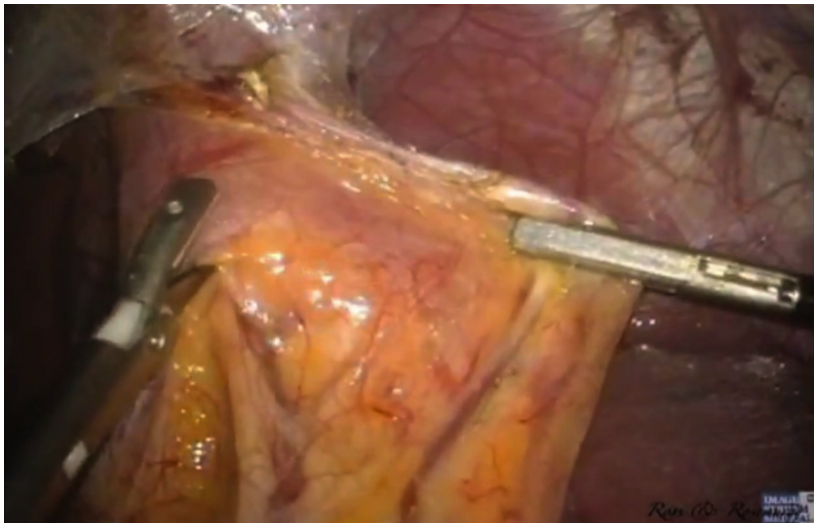

Fig. 4.37. Typical surgical dissection: the grasper (on the right) stretches the tissue, while the electric knife (on the left) cuts it.

center). This effect is useful with slave schemes that require a velocity input, since it allows to send the user reference as small Cartesian variation with respect to a neutral position.

- **Error**: the force applied on the interface is proportional to the error vector between the instrument position and the interface position. This force feedback effect can be effective with position control schemes, creating a direct mapping between the interface and the instrument workspaces and avoiding large interface movements that could not be followed by the instrument because of the implemented motors speed limitations.
- **Gravity compensation**: a zero resultant force is applied on the interface, in order to compensate its weight.
- **Line**: this force effect constrains the interface end-effector movement on a straight line, being its slope determined by the Z rotation θ_Z of the master handle. This is the force feedback effect used for the Orientation guidance mapping.
- **Triangle**: as explained in section 4.4.6, the instrument rotation limits restrict a part of the instrument workspace. While with a direct control of the instrument rotation it is possible to take account of such limitation, in a Cartesian control scheme the user reference may lead to an unattainable joints configuration if it lies in the restricted part of the instrument workspace. Therefore, it is important to avoid the user movement in that zone by limiting the haptic interface displacements: to achieve this, a repulsive force along the border of the forbidden zone is produced.

In table 4.3 a summary of the different force feedback effects applied on the proposed control strategies is presented.

Control modality	Instruments	Endoscope
Open Loop	Spring	Spring
CL Joint	Gravity comp, Triangle	Spring
CL Position	Error	Spring
Direct joint control	Lock t_X, t_Y	Spring
Orientation guidance	Line	Spring
Pseudo-Cartesian control	Gravity comp, Triangle	Spring

Table 4.3. Summary of the force feedback effects according to the chosen control modality.

4.4.9 Pedal board input

In table 4.4 a summary of the different pedals mapping is proposed.

Modality	Left Pedal	Middle Pedal	Right Pedal
Cursor control	Launch Strategy	Not used	Close application
Direct joint control	Activate endoscope	Activate grasper	Stop teleoperation
Orientation guidance Cartesian control Pseudo-Cartesian control	Activate endoscope with left interface	Activate endoscope with right interface	Stop teleoperation

Table 4.4. Summary of the pedals behaviors according to the chosen control modality.

4.5 Conclusions

In a teleoperated robot the possible implementable control strategies are not limited to a single one, especially when master and slave systems have different kinematics, or when a redundancy in one or both systems is present. In this chapter we went more in detail about the kinematics of STRAS, its teleoperation structure and the different control strategies that could be envisaged. The proposed strategies are multiple and the choice of one of them depends on several factors, such as the specific task that should be performed or the user preferences. Moreover, as all the robotic surgical system, STRAS could not be immediately used without a preliminary training phase, which should permit to familiarize with the different available options and understand how the system behavior is influenced by a particular control law. For all these reasons, a virtual simulator of STRAS, which will be presented in the next chapter, was specifically developed.

5

Virtual simulation

Contents

5.1 Introduction

With the term *simulation* is common to indicate the imitation of the operation of a real-world process or system over the time [10]. Before simulating something, it is necessary to have a proper model that could describe the system that has to be simulated, highlight its most important features and provide a good compromise between realism and complexity. This model could be obtained in several different ways, according to the characteristics of the system: generally, it could be *deterministic*, if a complete knowledge of the system transfer function between input and output is available, or *stochastic*, if some randomness, such as noise, affect the future evolution of the system. In every case, in the simulation environment the model will substitute the system itself, and the simulation will provide the system behavior over time.

Historically, humans started to realize the *physical simulation*, *i.e.* the simulation in which physical objects substitute real things: the advantage was that the chosen objects were smaller or cheaper than the real systems, so they could provide a scale model usable for studies or tests. With the advent of informatics and computers in the second half of the 20th Century, the physical simulation started to be gradually substituted by the *virtual simulation*, which represents a specific category of simulation that uses hardware and software equipment to create synthetic worlds. Virtual simulation allows users to interact with these worlds

and the virtual objects that populate them: the interaction is realized by means of input interfaces, which capture user movements and send them to the virtual environment, and output devices, to visualize the simulation results in a graphical way.

Four main key elements contribute in having a realistic experience when using a virtual simulator [169]:

1. **Virtual world**: it should graphically reproduce the environment in which the simulation takes place, but it also has to manage all the physical constraints of a real world, such as interactions between objects, gravity and illumination.
2. **Immersion**: the user should not only be mentally, but also physically involved in the simulation, in order to reduce as much as possible the barrier between the real and the synthetic worlds and to give the sensation of being inside the virtual environment.
3. **Sensory feedback**: a complete immersion in a virtual world is possible when the user main senses are stimulated as in the real life. Vision and hearing are commonly involved in virtual simulation, but tactile feedback, as well as motion capturing systems and specifically designed interfaces for particular simulations (*e.g.* the cockpits reproductions in car or flight simulators) go a step further to the virtual immersion.
4. **Interactivity**: a simulation could be carried in an autonomous way, with a pre-programmed input sent to the system model, or in a real-time interaction with the user. In the latter case, the virtual simulator should be able to respond to the user input and to adapt the virtual environment accordingly.

Nowadays, virtual simulation is used in many different contexts, from the chemistry and biological research to the flight training for pilots. The advantages are multiple: it is possible to set up a test environment in which perform experiments quickly and cheaply, without risks for the user and without the need to dispose of the real system. On the contrary, several drawbacks could limit the simulation validity: the virtual simulator is based on a simplified model of the real system, so its results are approximated and do not exactly represent the real system behavior. The model complexity should be chosen according to the level of detail needed, but also to the computational capabilities of the equipment used for simulation. Finally, a bad user immersion, due to graphical glitches or inappropriate user interfaces, could severely limit the user performance in interactive simulations.

5.2 Surgical simulators

From the advent of Minimally Invasive Surgery (MIS), one of the main doubts raised by a large part of surgeons was how could they practice this new exciting, but problematic technique continuously and without risks for the patients. Compared to open surgery, MIS introduced new severe problems to surgeons, such as loss of hand-eye coordination, no haptic feedback and wrong depth perception. At the beginning, the only way to gain experience in MIS was to practice on animals or on real patients: the instructor shows the procedure and the trainees tries to repeat it without hurting the patient. Before the introduction of simulation in

surgery, the common paradigm in surgical training was *"See one, do one, teach one"*, coined by William Halsted at the beginning of the 20th Century: it assumes that a trainee, after observing a particular procedure once, should be capable of performing that procedure and, successively, teaching another trainee. It has been demonstrated that this paradigm represents a real safety risk for the patient, while not being really educative for a large percentage of trainees [101]. Moreover, Halsted's paradigm results outdated now that many more young students begin a medicine school, all needing a continuous and repetitive training. These reasons led to the introduction of simulation as a training tool in the surgical practice, as well as aviation pilots did with their flight simulators from the early 1900s already.

Actually, we can classify surgical simulators in five main categories [45] [95]:

1. **Mechanical simulators**: they are the oldest type of simulator, initially developed in 1960s for the simulation of internal vessels and gastrointestinal tract. In the current technology, they typically are mannequins equipped with internal organs, reproduced by elastic materials (such as latex) and that could incorporate pathological alterations to be treated. Despite their high level of details and the reproduction of soft tissues, these simulators are commonly inanimate, so they do not take account of breathing movements, blood circulation and tissues alterations. With the evolution of electronics, now more complex electro-mechanical simulators exist, which are capable of simulate breathing motions and vital signals (see fig. 5.1). As drawback, these new simulators are expensive, and they need parts replacement after each simulated procedure.

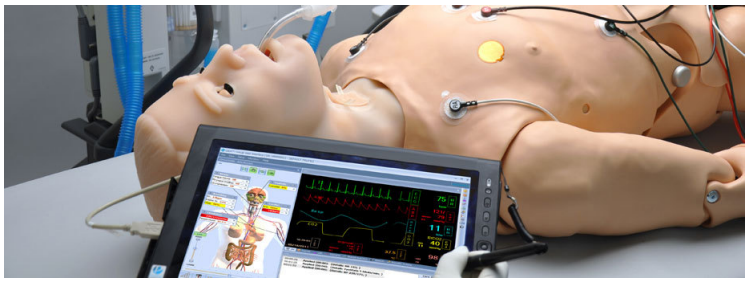

Fig. 5.1. The HAL® S3201 Tetherless Patient simulator by Gaumard (Gaumard Scientific, Miami, FL, USA. Reproduction from `http://www.gaumard.com`).

2. **Animal models**: the use of animals is common in research, and sometimes their anatomy could be similar to the human one, so justifying their use for surgery training (see fig. 5.2). The main advantage is that they offer a living model, with tissue reactions very close to those of humans. As counterpart, the ethical question of whether or not it is worth and correct to use a live being for tests is still open. Moreover, animals anatomy is similar, but not identical to those of humans. Finally, animal tests require a proper housing, veterinary support and general anaesthesia during the operation, which represent important costs to be considered.

Fig. 5.2. Typical training session on animal models at IRCAD, Strasbourg (reproduction from `http://www.visualphotos.com`).

3. **Hybrid simulators**: they consists in mechanical simulators that make use of biological specimens in order to increase the simulator realism. They represent a compromise between a pure mechanical model and an animal model, being also cost-effective because the specimens are typically collected from past experiments, from veterinarians or slaughters. A commercial hybrid simulator is produced by EndoSim, LLC (Marlborough, MA, USA), which consists of a box, with several silicone access ports, containing *ex vivo* tissues (see fig. 5.3). This simulator, named EASIE, is provided with different optional training set for both laparoscopy and transluminal surgery.

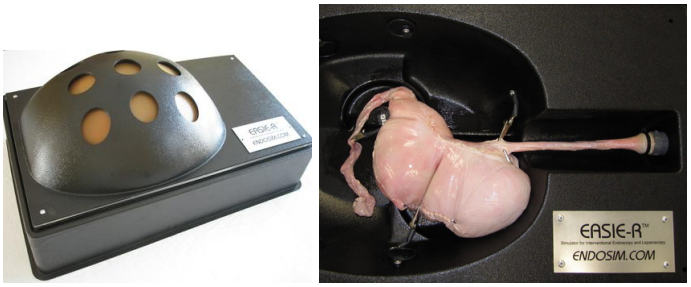

Fig. 5.3. EASIE surgical simulator by EndoSim, LLC (reproduction from `http://www.endosim.com`).

4. **Virtual Reality (VR) simulators**: they create a complete virtual environment in which the user can perform the gesture by means of haptic interfaces (specifically designed for the task, in most cases). They are typically provided with optional modules that simulate specific surgical operations, and they define an internal metrics to evaluate surgical skills. The firsts VR simulator were proposed in the early 1990s, with the leg simulator, presented by Delp *et al.* [37], for the practice of Achille's tendons repair, and the first VR simulator

for general surgery, presented by Satava [157], which used a head-mounted display for the visualization and a CyberGlove (a glove equipped with sensors and capable of tactile feedback), produced by CyberGlove Systems LLC (San Jose, CA, USA), to interact with the image (see fig. 5.4).

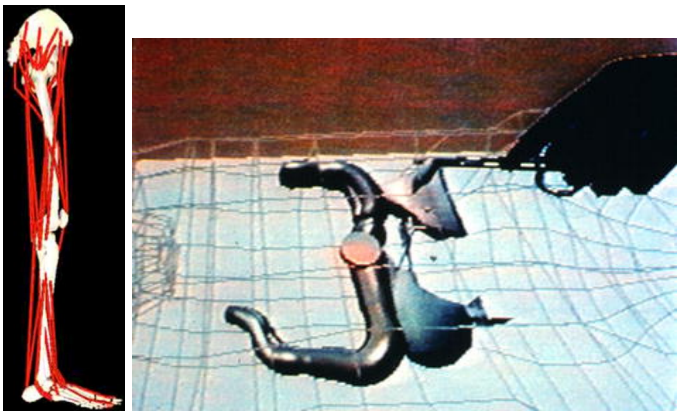

Fig. 5.4. First proposed VR simulators. Left: leg simulator for the practice of tendons repair. Right: VR simulator for general surgery (reprinted from [159]).

One of the first commercial VR simulators was the MIST-VR, introduced in 1997 by Mentice AB (Göteborg, Sweden) [202], which consisted of two haptic interfaces with handles similar to laparoscopic instruments (later the MIST-VR was proposed with the Virtual Laparoscopic Interface produced by Immersion Medical (Gaithersburg, MD, USA), see fig. 5.5) and a PC running the virtual simulator. A recent commercial product, widely used in laparoscopy training, is LapSim by Surgical Science Sweden AB (Göteborg, Sweden, see fig. 5.5): it can be combined with different haptic interfaces, it offers several optional surgical modules and it permits to train (as well as all new laparoscopic simulators) for the standardized FLS (Fundamental of Laparoscopic Surgery) exercises: peg transfer, precision cutting, ligating loop, extracorporeal and intracorporeal knots (see [53] for more details about the program).
Another VR simulator that deserves to be mentioned is the dV-Trainer developed by Mimic Technologies, Inc. (Seattle, WA, USA): it is a former Mimic simulator specifically modified to be used with the da Vinci master console (see section 3.3). The simulator hardware is enclosed in a plastic case (also known as "backpack") that is mounted on the back side of the da Vinci master console (see fig. 5.6): in this way the surgeon can perform exercises and surgical tasks, using the same master interface he/she will use in the real operation and taking advantage of the 3D vision.

5. **Computer-Enhanced (CE) videoscopic trainers**: they can be seen as a combination of a mechanical and a VR simulator, because they are composed of physical objects (as mannequins, training boxes, operating tables), that try to mimic the real surgical environment outside the human body as close as

Fig. 5.5. Top: The MIST-VR simulator by Mentice AB (reprinted from [95], [159]). Bottom: LapSim simulator by Surgical Science Sweden AB (reproduction from `http://www.surgical-science.com`).

Fig. 5.6. The dV-Trainer by Mimic Technologies, mounted on a da Vinci surgical system (reproduction from `http://www.mimicsimulation.com`).

possible, while the specific operation is virtually simulated and displayed on a screen.
A well-known example of this category is the ProMIS simulator by Haptica Ltd. (Dublin, Ireland, acquired in 2011 by CAE Healtcare, Saratosa, FL, USA): it consists of a torso plastic model that contains optical motion sensors to detect instrument movements (see fig. 5.7). ProMIS was the first simulator that allowed the use of real instruments, inserted through standard trocars into the torso model, and combined physical models with virtual reality. According to the specific simulated procedure, the surgeon could perform it either on a physical model, with the aid of "virtual" informations added on the screen (as in augmented reality), or in a complete virtual environment.
Another CE trainer is the VIST-Lab (Vascular Interventional System Trainer) by Mentice AB (Göteborg, Sweden), which reproduces the OR environment with a full body mannequin, equipped with several access options (femoral, radial and jugular) and hosted on an adjustable table (see fig. 5.7).

Fig. 5.7. Left: ProMIS by Haptica Ltd. (reprinted from [95]). Right: VIST-Lab by Mentice AB (reproduction from `http://www.mentice.com`).

VR and CE simulators potentially represent a solution to all the issues of mechanical simulators and animal models, such as costs, repeatability and ethical limitations, but, as it could be easily realized, it is not straightforward to correctly simulate a complex environment as the human body and the totality of interactions it could have with other entities. However, improvements in the computational power of modern PC and better management of the huge amount of data involved in a virtual simulation (with the parallelization method, for instance) led nowadays to realistic virtual simulators for specific operations.

5.2.1 Simulators metrics

One of the main problem in surgical training is the objective evaluation of a gesture: since manual instruments typically do not have any type of sensor, the only measurable means of evaluation is the execution time, but no informations are available on how the surgery was performed. A solution was proposed in 1997 with the introduction of the Objective Structured Assessment of Technical Skill

(OSATS) method [115], which consists in a checklist, specifically prepared for the surgical operation that has to be evaluated, containing the main passages that must be performed in order to correctly accomplish the gesture. The evaluation is executed under the supervision of an experienced surgeon, who has to indicate if the passages are correctly executed or not (or wrongly) executed.

Although the OSATS method has been proven to be valid and reliable [32], it cannot offer a quantitative analysis of the surgical gesture in terms of dexterity, motion size and ergonomics. The introduction of robotic systems in surgery paved the way to the use of external sensors on both instruments and surgeon, with the aim to collect informations about their positions and their movements. One of the first proposed measurement system was the Imperial College Surgical Assessment Device (ICSAD), which consists in a series of sensors, placed inside the surgeon's gloves, that can be detected by an electromagnetic tracker, thus giving a measure of the surgeon's hands movements. Afterwards, a gesture analysis is performed, and some objective parameters as the instruments path length and the economy of movement are computed [33].

A more complex assessment system was proposed in 2002, with the aim to measure the movements of both laparoscopic instruments and camera. The Advanced Dundee Endoscopic Psychomotor Tester (ADEPT) consists of a training box capable to hold two standard endoscopic instruments and an endoscope (see fig. 5.8) [56]. Internally, a dual-gimbal mechanism records the instruments movements and transmits them to a PC, which performs a gesture analysis according to the specific task proposed.

Fig. 5.8. ADEPT assessment system (reprinted from [56]).

With the introduction of virtual simulation in the surgical training, the skills evaluation became simpler because of the immediate availability of several simulated parameters. In addition to execution time and number of errors, and according to its level of detail, a virtual simulator could be capable to quantitatively measure the amount of instruments collisions, the misapplied energy time, the quantity of insufflated air, the eventual blood loss and a global economy of motion in the gesture [97]. All these parameters can contribute to formulate a score

function that should represent a synthetic judgement of the performed gesture, allowing a direct comparison with other users.

5.3 Virtual simulators for no-scar surgery

In section 5.2, the most known commercial surgical simulators were presented, but many others products, developed by private companies or research groups worldwide, exist. The common aspect of these simulators is that they are specifically conceived for laparoscopy, hence for the simulation of rigid instruments inserted through independent trocars.

Actually, very few solutions are conceived for the virtual training of no-scar procedures, and this represents one of the barriers to the widespread use of transluminal procedures as highlighted by the NOSCAR (Natural Orifice Surgery Consortium for Assessment and Research) white paper [124]. There are several difficulties introduced by no-scar surgery techniques, compared to laparoscopic MIS, that are not as straightforward as it may seem to be simulated in a virtual environment:

- **Flexibility**: no-scar surgery instrumentation is typically flexible, which means that the virtual simulator should take account of the force exchange between instruments and tissues in both senses, since a flexible instrument could be deformed by an excessive load or by a contact with something harder than itself. In general, one of the most computational demanding situation is the collision between two flexible bodies, because multiple point of contacts are detected and an online topology change of both bodies meshes should be performed. This is not the case of laparoscopy simulators, where instruments are supposed rigid, non-deformable and modelized as a bounding box for the collision detection.
- **Kinematic specificity**: laparoscopic instruments are generally very similar, because they all consist of a rigid shaft, a scissors-like handle and a specific tool mounted on the tip. Their kinematics, therefore, is very simple, having the only constraint of the fulcrum (*i.e.* the instrument access point that blocks the instrument translations on the XY plane), and a similar distribution of DOFs for the most part of them. On the contrary, no-scar surgery instruments are very different and unique (cfr. section 3.4), requiring specific kinematics models (sometimes complex to compute, if all the mechanical and dynamic features are taken into account) to be correctely described in a virtual environment. This means that while in laparoscopy a single simulator is valid for training multiple techniques, in no-scar surgery each instrument manufacturer should propose its own simulator (or, at least, the system model usable in a common framework) in order to train its future users.
- **Skill assessment**: a typical no-scar surgery procedure is composed by a navigation part, in which the flexible system is introduced in the body and controlled in order to reach the operation point, and a therapeutic part, *i.e.* the surgery itself. These two parts are very different, requiring abilities from two different medical specialities: endoscopy for the former, surgery for the latter. A complete simulator should be able to train both these skills, and it should also take account of the multiple different access that could be envisaged for no-scar surgery.

All these issues are the main reasons behind the poor availability of commercial simulators for no-scar surgery. Simbionix (Simbionix Ltd., Lod, Israel) is the main company involved from 1998 in flexible endoscopy simulation: its GI Mentor was the first commercial CE trainer for gastrointestinal endoscopy [11]. The first version consisted in a mannequin, positioned on its left side over a table, a modified Pentax endoscope and the virtual simulator (see fig. 5.9). The mannequin provides force feedback effect on the endoscope by means of pneumatic brakes placed inside the simulated gastrointestinal (GI) tract, and the endoscope embeds a position sensor that transmits the scope position to the simulator. The visual output consists in a reproduction of the GI tract, properly modified according to the endoscope interactions with the mannequin.

Fig. 5.9. Top: GI Mentor by Simbionix Ltd. Bottom: 2013 Simbionix simulators family (reproduction from `http://www.simbionix.com`).

Further developments of the GI Mentor led to a wide family of CE simulators for specific medical specialities, such as urology, orthopaedics, pneumology, angiology and gynaecology (see fig. 5.9).

Another company involved in flexible endoscopy simulation was HT Medical Systems Inc. (Gaithersburg, MD, USA), a private company founded in 1987 with the aim to design and develop new medical virtual trainers. In 1999, they introduced the PreOp Flexible Sigmoidoscopy Trainer [34], a CE trainer, similar to the GI Mentor, that consisted of a mannequin, an endoscope and a computer running the virtual simulator. The difference with the GI Mentor was that this simulator could be used for both gastrointestinal endoscopy or bronchoscopy simulations, by choosing the corresponding option. Moreover, the provided endoscope was not a real one, but a reproduced model with a custom-made tool capable of force feedback. In 2000, HT Medical Systems Inc. was acquired by Immersion Corporation (San Jose, CA, USA), who continues to sell the simulator under the name AccuTouch Endoscopy Simulator [110] (see fig. 5.10).

Fig. 5.10. AccuTouch Endoscopy Simulator by Immersion Corporation (reproduction from `http://www.laparoscopytoday.com`).

In our best knowledge, no VR simulators for no-scar procedures are currently available, neither from industries nor research groups. We can just cite a past project, called ULIS (Unlimited Laparoscopic Immersive Simulator), carried on by IRCAD (Institut de Recherche contre les Cancers de l'Appareil Digestif, Strasbourg, France), Karl Storz GmbH (Tuttlingen, Germany), Digital Trainers (Strasbourg, France) and the SOFA (Simulation Open Framework Architecture) development team with the aim to develop a patient-specific simulator that uses the patient pre-operative images (CT or MRI exams) to build the 3D models of his/her internal organs and simulate the procedure [175]. This simulator was recently enhanced in order to simulate a flexible endoscope in transgastric procedures (see fig. 5.11), but no official publications are present in the literature.

Fig. 5.11. ULIS simulator for transgastric procedures (courtesy of Digital Trainers).

5.4 STRAS Virtual simulator

5.4.1 Motivations

The idea to develop a virtual simulator of STRAS was already proposed at the beginning of the ISIS project: the aim was to have a close kinematic replica of the real system on which start to propose control strategies while the robot was under development. Indeed, the robotization process was quite long, because of the specificity of some parts and the complexity in the assembly and wiring. The initial specifications did not include the use of the simulator as training tool for the users, leaving this feature for a future development. In fact, over time we became aware of the potential usefulness of a complete virtual environment for preparing users to the telemanipulation of STRAS: the proposed control strategies began to increase, and the mechanical non-linearities present on the system appeared as difficulties for users in correctly understanding the system behavior changes according to the chosen strategy in realistic tasks. This led to the development of a second simulator.

In both simulator versions, the development started from scratch, given the lack of adaptable existing environment for surgical simulation (cfr. section 5.3). For the first version, we took advantage of a series of libraries, developed in our lab, specifically conceived for the basic simulation of robot parts and for the algebraic computations. For the second version, instead, we focused on the choice of a game engine, as those used in the video-games factories: such choice is motivated by the fact that modern video-games require physical computations for the object interactions, and offer a reasonable compromise between the realism sensation and the computational complexity. Moreover, in the last years many well-known commercial game engines started to be distributed freely for non-commercial purposes:

their big advantage is that they offer some pre-implemented object primitives, as cameras, lights, physics and environment, immediately usable to set-up a game scene. We exploited this opportunity and, after a comparison between the main available game engines as Unreal UDK [51], Microsoft XNA Game Studio [116], Unity 3D [190] and Blender [15] we chose the latter: the main motivations behind this choice are the open-source nature and multiplatform capabilities of Blender.

5.4.2 First Version

The first version of the STRAS virtual simulator is a Windows stand-alone application, written in C# with the use of the VtkDotNet library [43] (an unofficial wrapper of the Kitware Visualization Toolkit (VTK) [98] for the Microsoft .NET environment) for the 3D graphic rendering. At startup, the main application form is presented, together with a graphic window in which a 3D model of STRAS is depicted (see fig. 5.12). The main form permits to access to all the simulator features: it contains the graphical controls for interacting with the robot DOFs, tuning the main simulation parameters and accessing to some specific test environments implemented to assess the simulator features.

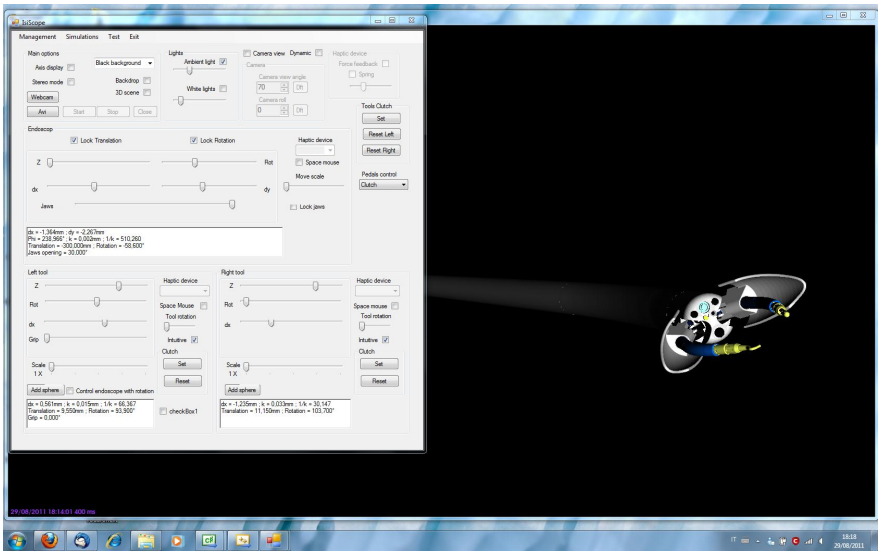

Fig. 5.12. First version of the STRAS virtual simulator.

Visual modalities

This simulator offers two possible visual modalities (see fig. 5.13):

1. An **external view**, which permits to see the whole 3D model of the robot from an outside perspective. The 3D camera can be moved and rotated freely with the mouse. This view is useful for analyzing the robot movements consequent to a user input, as one would do when observing the real system.

2. A **camera view**, that simulates the point of view of the endoscopic camera. In this case, the 3D camera is locked in a fixed position, the mouse navigation is no longer permitted and some camera parameters, such as Field Of View (FOV) and distortion, are properly setted.

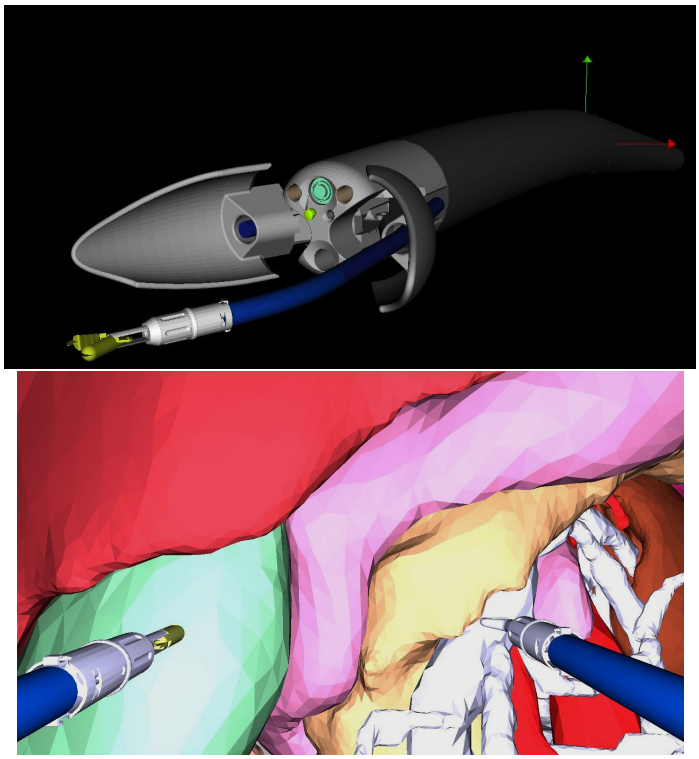

Fig. 5.13. External view (top) and camera view (bottom) on the STRAS virtual simulator.

In an attempt to improve the depth perception, a stereoscopic 3D options is offered, which changes the visual output to anaglyph: in this case, it will be necessary to wear polarized glasses to have a basic 3D effect.

An effort was done to keep the graphical refresh separated and asynchronous from the kinematics computations: the refresh rate at which the kinematic model should be computed could be too fast for the 3D rendering, leading to potential bottlenecks for the whole system because of the amount of data to process.

3D Modeling

For the realization of the robot 3D model, some meshes provided by our industrial partner Karl Storz GmbH (Tuttlingen, Germany) were used, especially those of the endoscope head, jaws and the tools. The flexible sections, instead, are obtained starting from the VTK cylinder primitive, modified with a Spline filter in order to

produce the bending effect. Each 3D model has its own frame, which determines the model position expressed in the world coordinates and which is in relationship with the robot kinematic frames (cfr. section 4.3.1). In this way, it is possible to correctly define the relative positions of each mesh and properly update the global 3D model when a kinematic change is performed.

External libraries

As it happens on the STRAS high-level controller, the simulator communicates with the haptic interfaces and receives the input from the pedal board (cfr. par. 3.5.5). The specific programming environment chosen for the first version of the simulator imposed some workarounds to assure compatibility with libraries written in C++, as those for interacting with the haptic interfaces or for mathematical computations. The advent of the .NET Framework marked a radical change in the Microsoft vision of programming languages: there was a passage from *compiled languages*, in which the high-level code is translated in machine language code that is immediately executable on a specific machine, to *interpreted language*, in which the source code is translated in a meta-language that will be executed by a virtual machine. The compiled languages, as C++, have the big advantages of speed and optimization, since the compilation process is specific for the type of machine in which the final applications will run, so the executables will use the native code of the specific processor. However, this feature represents also the main limitation of compiled languages: since the executable is platform-dependent (with the term *platform* we intend the combination of hardware architecture and operating system), it will be necessary to re-compile the source code on each different machine in which it must run. The interpreted languages instead, as Java or .NET indeed, produce an intermediate code, called *bytecode*, that remains the same for all the platforms: what varies is the virtual machine that has to execute it, which will be specific for the particular platform. This virtual machine, called *Java Runtime Environment* (JRE) in the Java SDK or *Common Language Runtime* (CLR) in .NET, should guarantee the multi-platform execution of the application. In this case, however, the application performances will be lower compared to a compiled application because of the interpretation process done at runtime.

To guarantee interoperability between interpreted and compiled code (called respectively *managed* and *unmanaged* in .NET), it is necessary to use a specific function, called Platform Invoke (PInvoke), that enables calling any function contained in an unmanaged library (such as DLL libraries, COM and ActiveX components) in managed code (see fig. 5.14).

As stated before, this operation, called *wrapping*, was performed for all the external libraries used in the simulator, implementing a middleware layer inside the simulator.

Internal refresh timer

The .NET Framework provides an inner Timer class that allows to execute a specific function every desired time interval, expressed in milliseconds. There are

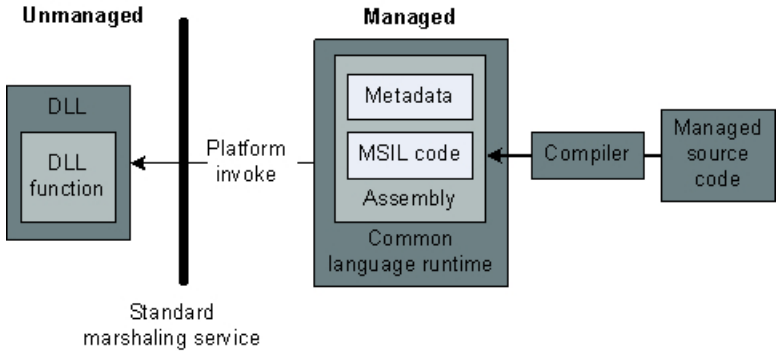

Fig. 5.14. Interoperability between managed and unmanaged code in the .NET framework (reproduction from `http://technet.microsoft.com`).

three variants of the standard Timer class: *System.Windows.Forms.Timer*, *System.Timers.Timer* and *System.Threading.Timer*. The first two classes appear as controls in the Visual Studio toolbox window, so they can be easily dragged into the main form, while the third must be instantiated directly in the source code. The main difference within the three classes lies in the way the timer is invoked: the first timer works in the application main thread, so it raises an event synchronously with the rest of the application code; the second timer resides in a worker thread obtained from the CLR thread pool, so it is independent of the main application, but it is managed by the virtual machine that executes it; the third timer has an architecture similar to the second one, but it is better managed in a multi-threaded environment. While the first timer is purely for simple applications that do not need a precise timing, the other two are much more accurate. However, since they are instantiated at the CRL level, they do not guarantee an absolute precision when low-level interrupts (as those of the operating system) could request more resources and, thus, the application is delayed for some processor cycles.

In the virtual simulator a correct timing is fundamental, since it affects the kinematics computation and the precision of the robot simulation. Although Microsoft Windows 7 does not offer hard real-time capabilities, a good solution comes from the *Multimedia timer*, a particular service based on the hardware platform that allows applications to schedule timer events with the greatest possible resolution. This timer is widely employed in multimedia applications (from which comes its name), such as MIDI sequencer, where a high-resolution timing of the order of 1 ms is needed to correctly communicate with the external MIDI device.

In our case, the kinematics loop is executed periodically every 20 ms thanks to a Multimedia timer, while the graphical refresh is performed under the control of a *System.Threading.Timer* every 100 ms (see fig. 5.15).

A specific form is implemented in the simulator in order to compare the different timer classes and test the accuracy of each of them (see fig. 5.16).

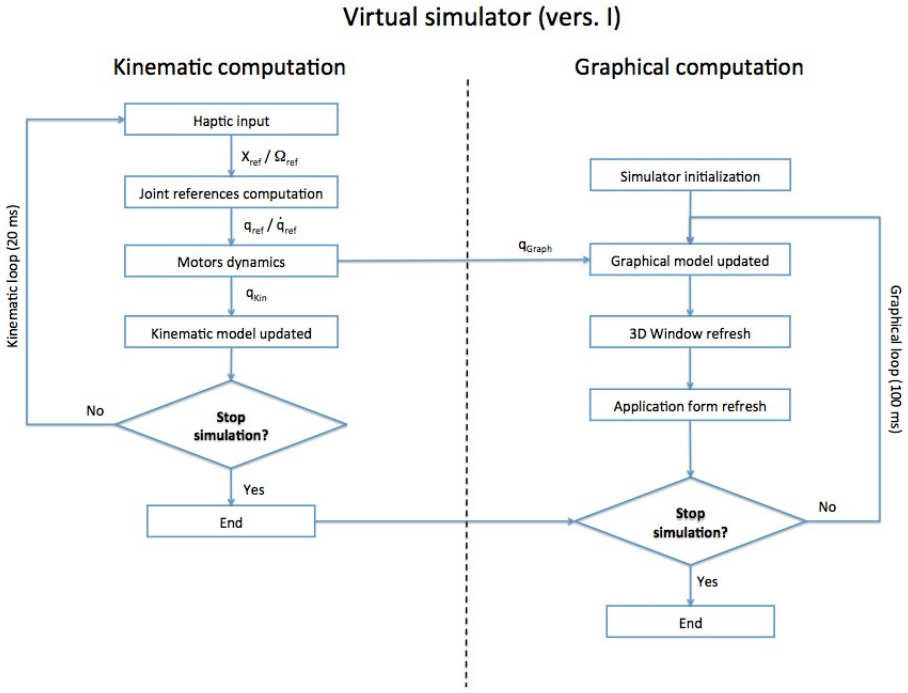

Fig. 5.15. Workflow of the virtual simulator (first version).

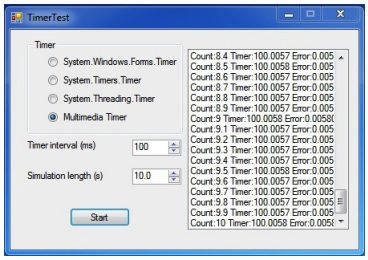

Fig. 5.16. Application form for the comparison of the different timer classes.

Motors simulation

A specific class was written in order to simulate the motors behaviors. In STRAS three types of motor are used (cfr. par. 3.5.2), each with different maximum speed and acceleration. A trapezoidal velocity profile with linear accelerations and decelerations was chosen as model, because it provides a smooth motion that well simulates the real behavior without being computationally demanding. The trapezoidal velocity profile has three regions (see fig. 5.17): acceleration, constant velocity and deceleration.

In the implemented motor class it is possible to set a velocity or a position reference. In the first case, the maximum acceleration (or deceleration) will be applied to pass from the current velocity to the desired one in the minimum time:

once the desired speed is reached, the acceleration becomes null and the motor keeps its speed until a new reference is sent. When a position reference is sent, it is necessary to compute the time needed to pass from the current position to the desired one based on the current velocity. When using a trapezoidal velocity profile, the distance θ that the motor travels is expressed as the integral of its instantaneous velocity over time (see fig. 5.17):

$$\theta = \frac{1}{2}\, t_{acc}\, \omega_{max} + t_{max}\, \omega_{max} + \frac{1}{2}\, t_{dec}\, \omega_{max} = \omega_{max} \left(\frac{t_{acc}}{2} + t_{max} + \frac{t_{dec}}{2} \right) \quad (5.1)$$

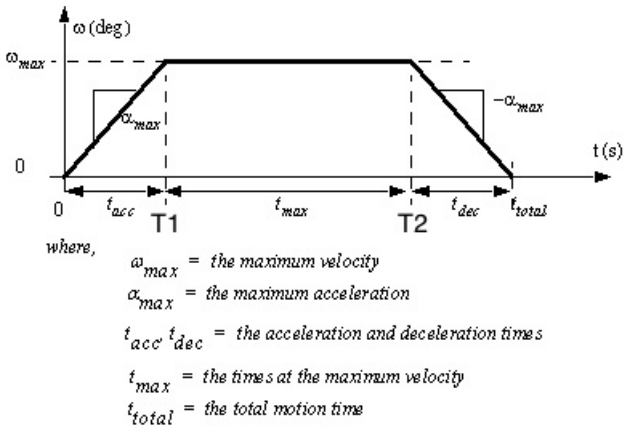

Fig. 5.17. Typical trapezoidal velocity profile with the main parameters (reproduction from [86]).

When θ is imposed, the problem consists in computing t_{acc}, t_{max} and t_{dec} according to the current motor velocity and acceleration. The computation is performed numerically inside the simulator using the kinematic refresh rate as time step: at each computational cycle, the current motors positions are updated and any new references are eventually taken into account. Dynamic parameters, such as inertia or friction, are not considered for the simulation, because of the small size of real motors and because their introduction would not improve significantly the simulation results, while slowing down the general performances. A specific form allows to test the motor class: it is possible to give a fixed reference, or to impose a position profile over the time, and compare the user input with the produced movement (see fig. 5.18).

In order to increase the realism of the simulator from the kinematic point of view, some non-linearities were implemented:

- **Delay**: it is possible to introduce a time delay between the instant in which the desired references are sent to the motors and the actual moment in which they are practically executed. This delay could happen in teleoperated systems, and is mainly due to potential limits in the communication channel between master and slave systems or to filters and external devices, included in the control

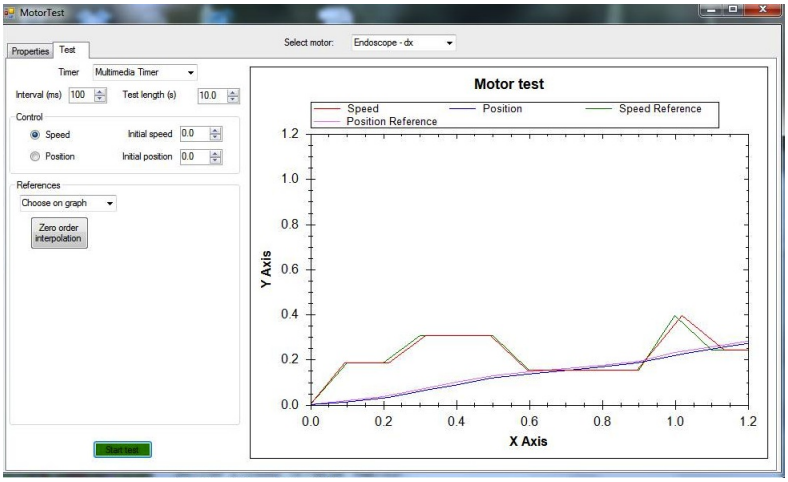

Fig. 5.18. Application form for the assessment of the Motor class.

loop, that could work at slower frequencies. Although STRAS is not affected by communication delay, it could be interesting to analyse the system behavior in such conditions. Inside the simulator, this is reproduced by instantiating a FIFO (First In First Out) queue that starts to collect the references after the selected number of delay time steps.

- **Encoders offset**: since the three subsystems that compose STRAS are not constrained in their relative movements, the system position assumed as neutral is fixed manually by changing the configuration of the passive arms (cfr. section 3.5.2). During the calibration procedure, this position is assumed as zero by the motor encoders, but the manual regulation does not guarantee uniformity of values at each change of the passive arms position. Since the encoders values are taken as references for the computation of the kinematic model, an offset on them leads to tracking errors of the slave robot. It is possible to simulate this error by using two different references: the ideal one for the kinematic model, the real one (which takes account of the offset) for the graphical model.
- **Backlash**: when the instrument deflection is changed, the relative encoder is properly updated by the motor movement, but nothing apparently happens on the instrument until the corresponding deflecting cable is put in tension (cfr. section 3.5.3). This effect is realized at the motor level by detecting the change of deflection direction and adding a mean dead zone on the movement. As for the encoder offset, two different references will be considered, one for the kinematic model and one for the graphical model. This means that when crossing a backlash zone, the kinematics computation is done on a wrong configuration that does not reflect the actual one and that gives bad velocity references as result. The kinematic and the graphical references are realigned only when the dead zone is crossed in the opposite direction, because the new applied dead zone compensates the previous one.

Control strategies

In the first version of the simulator all the Jacobian and Cartesian strategies were implemented. The simulator represents a good way to assess the closed-loop strategies, since it can provide at any time the Cartesian position of the robot without dealing with the technical limitations of an external tracker (cfr. section 4.4.3). For this purpose, several test environments have been conceived to evaluate every possible combination of movements: it is possible to control just a single instrument, one instrument and the endoscope or the whole slave system.

Every simulation can be recorded on disk: all the useful informations (motors positions and speeds, instrument Cartesian positions, haptic interfaces input) are stored in specific files, together with a summary of the particular task executed, the simulator parameters and the user name. The simulator offers the possibility to analyze the recorded gesture and reproduce it graphically: as in a video recorder, a specific form permits to load the simulation data and to re-apply them on the virtual system in order to see all the slave robot movements, possibly from a different point of view. An embedded chart allows to display the data numerically, and eventually to evaluate them with a reference or with another user (see fig. 5.19).

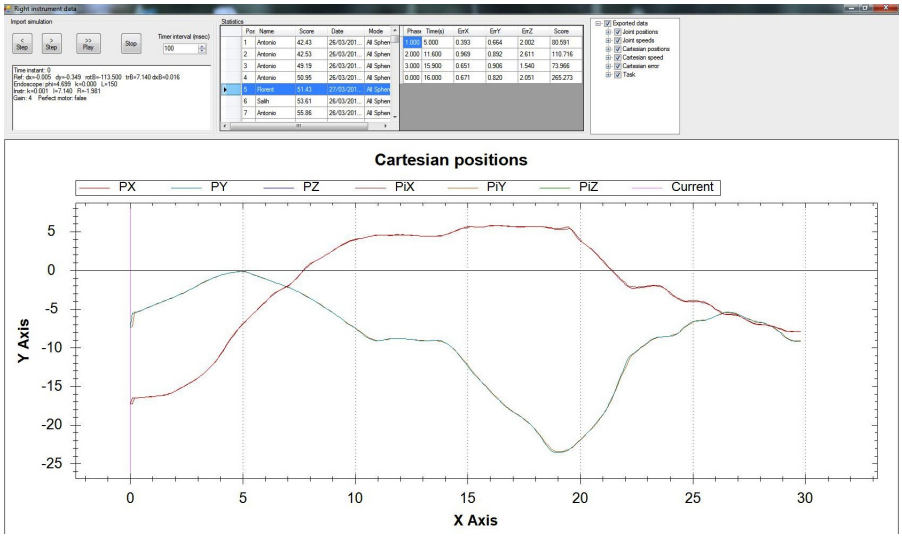

Fig. 5.19. After a simulation, it is possible to analyze the performed gesture and leave the simulator to re-execute it.

Virtual scenes

Since physical interactions are not taken into account inside the first version of the simulator, the tests that can be performed with it are limited to positioning and path following tasks, in which instruments have to follow a particular path

shown on the 3D window. These types of tasks are not particularly intended for the user training, but they could represent a good method to assess the changes in the system behavior when different control strategies are used.

For the Cartesian control strategies comparison, two test environments were implemented in the simulator: the aim is to evaluate the accuracy of the gesture and the response speed of one instrument in both ideal and realistic cases, in order to understand how much the non-linearities influence the system control. A good way to do this could be to define a path that the user has to follow with one instrument. In our simulator, a path is defined as the cubic interpolation of a number of key points placed in the virtual space. In the simulator, it is possible to load a previously stored path, or to define a brand new one by directly clicking with the mouse on the virtual scene and putting some key points. To obtain a realistic effect, the key points are attached over a 3D model of a human organ, in order to obtain a path drawn over the organ surface (see fig. 5.20). This also helps to improve depth perception in the virtual scene.

During the task, the instrument position is sampled at a constant rate and stored in memory, and the execution time is recorded. When the task is accomplished, an offline routine performs a warping, based on the key points, between the user and the interpolated paths, thus providing an error vector. Thus, a score function can be defined as a weighting of the execution time (weight ϕ_T) and the error between the desired and the user paths (weight ϕ_e):

$$Score = \phi_T T + \phi_e \sqrt{e_X^2 + e_Y^2 + e_Z^2}. \tag{5.2}$$

The function (5.2) gives a reference to evaluate and compare different gestures according to the type of task executed. In order to evaluate accuracy and response speed, two tasks have been implemented in the simulator (see fig. 5.20):

- **Precision task**: the path has 4 key points and mimics a motion during a suturing task. The precision in the gesture represents the most part of the final score ($\phi_T = 1$, $\phi_e = 10$).
- **Simple task**: the path is a large, simple motion. An error, shown as a cylinder around the desired path, is tolerated, and the aim is to accomplish the task as fast as possible ($\phi_T = 10$, $\phi_e = 5$).

5.4.3 Second version

As explained in section 5.4.1, the first version of the simulator was conceived as just a kinematic replica of the real system, which should allow to conduct some tests and compare the different control strategies. Compared to a classical numerical simulation (such as in Matlab, for instance), the advantage in the use of a virtual simulator is the realistic graphical results of the movements, which aid to better understand the system behavior as if one is watching the real system. But when the implementation of the proposed control strategies was complete, very soon the limits of this simulator became evident:

- the absence of a **physical engine** did not allow to simulate the interactions of the robot model with other virtual objects, thus preventing the reproduction

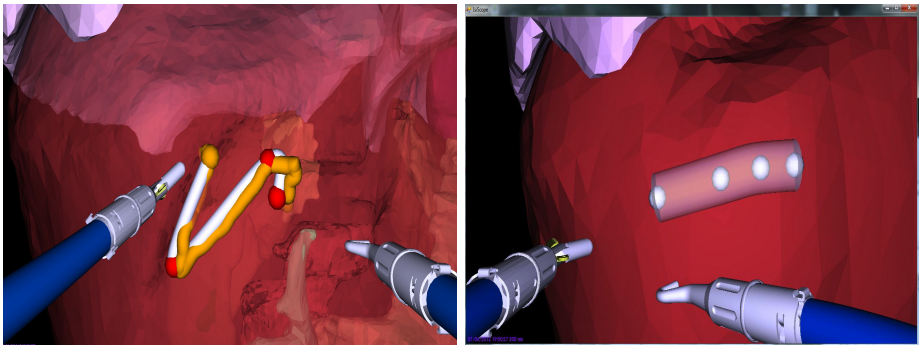

Fig. 5.20. Precision task (left) and Simple task (right)

of any type of realistic task that should require collision detection and force reflection between objects;

- the chosen development environment did not allowed compiling **multiplatform** application, limiting the execution of the virtual simulator to the Microsoft Windows platforms;
- the **code duplication** between the virtual simulator, who is a stand-alone application, and the high-level controller application for the slave robot (cfr. section 3.5.5), became evident when all the kinematic model implemented in the first was re-coded for the latter.

All these reasons led us to a complete refactoring of the virtual simulator application, with the aim to overcome the highlighted limitations and extend the simulator capabilities: with the introduction of a physical engine, the simulator could also become a training environment for the future users, as well as a tool for the kinematic study of the system. The solution to avoid the code duplication consists in developing the virtual simulator as a plugin of the high-level controller, rather than a stand-alone application: in this manner, the kinematic model is coded only one time, the simulator becomes just a graphic viewer and the references that it receives are the same sent to the low-level controller, thus allowing a reproduction of the realistic conditions. Blender [15] (Blender Foundation, Amsterdam, The Netherlands) has been chosen as development environment.

Blender

Blender was born in 1995 as an internal project of the Dutch company NeoGeo, co-founded by Tim Roosendaal. The big change happened in 2002, when Roosendaal created the Blender Foundation with the aim of making Blender an open source 3D rendering environment supported by a community of artists, animators and programmers. Very soon the community contributions started to improve the capabilities of Blender, making it a complete multi-platform development tool for the realization of 3D rendering and animations. From 2004, the Bullet Physics Library [60], an open source physics engine specifically conceived for games, was integrated into Blender, offering the possibility to detect collisions within 3D objects and simulate force fields (wind, magnetism and several others). In the last ten

years, one of the major improvements was the introduction of the Blender Game Engine (BGE), a series of functions and tools for the game development such as the already cited physical engine, soft bodies simulations and complete lights and textures management. The BGE also implements the Sensor-Controller-Actuator (SCA) logick bricks (see fig. 5.21), which represent the basic architecture of the game control and execution:

- the sensor detects the activation of an input device, such as a key pressed or a mouse movement, or creates an exteroceptive sensor, as ray detectors or radars, that is capable to detect a specific situation and trigger an event;
- the controller collects the event triggered by the sensors and, according to an implemented Boolean function, transmits it to the actuator; a controller can also consist of a Python script, which is executed when the sensor is active, performing an event-based execution;
- the actuator changes the current state of the 3D objects by applying position or speed references, changing the application parameters and executing pre-programmed routines.

The BGE establishes an iterative routine, called Game Loop (see fig. 5.21), that represents one logical frame, *i.e.* the actions executed at each logic tick. The first operation in the Game Loop is the scene processing, in which the SCA bricks are evaluated, the physics engine is updated and an eventual sound is played. Afterwards, the new references from the input devices are collected, and finally the rendering of the updated scene is performed. Typically, the standard refresh rate of the render process is 60 fps (frames per second), but this value is related to the computational capacities of the PC and the complexity of the scene.

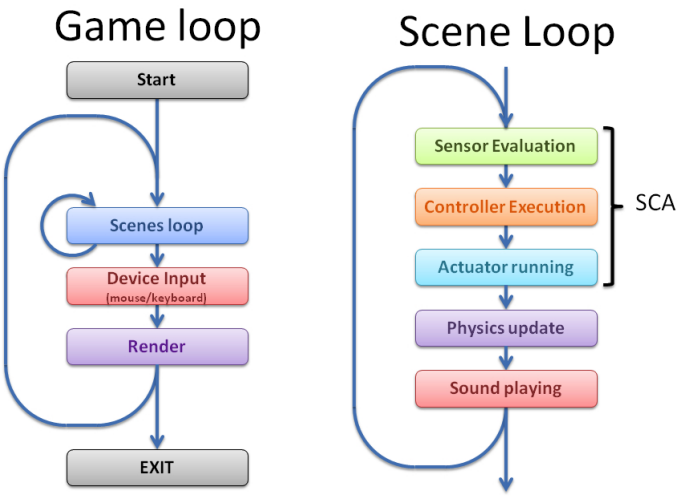

Fig. 5.21. Game loop and scene loop in Blender (reproduction from `http://wiki.gameblender.org`).

In Blender it is possible to create a graphical application by simply using the controls on its user interface, but in order to exploit the most powerful features offered by the Blender API an internal Python interpret is available, allowing the execution of advanced source code.

Since the control of robotic systems and the animation of virtual characters have many aspects in common, the interest to apply Blender potentialities in robotics has grown in the last years. Blender's developers are already going in this direction implementing particular features such as an inverse kinematics method for redundant serial chains (as those of humanoid robots) and specific proprioceptive and exteroceptive sensors, largely used in robotics. Moreover, an initiative called *Blender for Robotics*, led by the Katholieke Universiteit of Leuven, Belgium, and the LAAS-CNRS (Laboratoire d'Analyse et d'Architecture des Systèmes) of Toulouse, France, was recently proposed to put together all the research groups interested in such applications. Actually, the main contributions come from the group leaders:

- the LAAS-CNRS group started the development of MORSE (Modular Open Robots Simulator Engine) [46], a Blender-based application mainly focused on the simulation of mobile robots in various environments;
- the Department of Mechanical Engineering at KU Leuven, directed by Herman Bruyninckx, is involved in the integration of the Orocos' Kinematics and Dynamics Library (KDL) in Blender for exploiting the implemented algorithms directly in the Blender environment.

Simulator structure

Blender allows to immediately execute the developed application with an internal player, or to compile it and execute it as a stand-alone application. It is possible (but not so straightforward) to create a GUI via Python, but in our case the simulator receives the commands from the high-level control application and takes advantage of its GUI. The communication between the simulator and the control application is guaranteed by an UDP (User Datagram Protocol) socket (see fig. 5.22), which is instantiated at the application startup and kept opened during the whole simulation.The UDP socket is typically less reliable than the most known TCP (Transmission Control Protocol) socket, because it does not manage the rearrangement of packets and the retransmission of those lost, but it is much more faster in communication and lighter in resources. Since the kinematic computations are executed on the real-time loop at a higher speed than the graphical refresh, a loss of one packet does not represent a critical event: it does not compromise the correctness of computations, and the corresponding graphical glitch could even be imperceptible.

Considering the classical structure of a network application, the virtual simulator acts as a server that continuously listens a specified port, waiting for the packets sent by the client, *i.e.* the high-level control application. To ensure the proper interpretation of the exchanged informations, a specific packet structure was chosen:

- every packet starts with a numerical code, which identifies the type of informations it contains: position references, speed references, control commands, key pressed or scene selector;
- in case of position or speed references, the data order is: electric tool (rotation, translation, deflection), mechanical tool (rotation, translation, deflection, grip), endoscope (X deflection, Y deflection, translation), haptic interfaces positions (left and right), strategy-specific parameters;
- every unit of information inside the packet is separated by a Tab ('\t') character;
- the global packet size cannot exceed 256 bytes.

A Python script is executed at the simulator launch: it sets the standard simulator options, creates the server socket and runs the endless server loop, waiting for the data packets from the control application. When something is received on the specified port, the packet is recovered and analyzed, in order to detect the header code and properly process the received data. When a position or speed reference vector is received, the various joints values are extracted and the corresponding graphical models are updated.

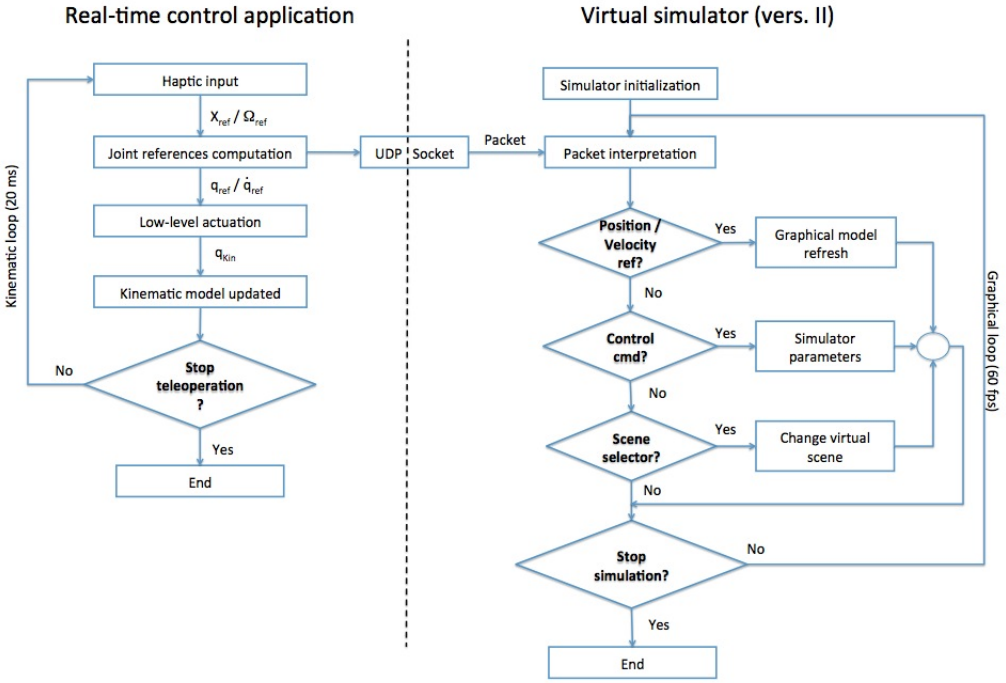

Fig. 5.22. Workflow of the virtual simulator (second version).

There are two main operation modes for the simulator:

1. **Slave mode**: during the normal teleoperation of STRAS, the virtual simulator receives the same references as the real robot and follows its movements. This modality could be useful to have a visual representation of the theoretical position of the system and compare it with the real one.
2. **Arcade mode**: in this modality the high-level application controls exclusively the virtual simulator, without sending the references to the real robot.

With the aim to help the user during Cartesian strategies, two radars are depicted on the top-left and top-right corners of the screen (see for instance fig. 5.25): they show the actual interface position in the workspace and the forbidden area of the instrument workspace.

3D Modeling

As in the first version, the original meshes of the ANUBISCOPE® system were used in order to recreate the virtual model of STRAS. What is completely different in the second version is the way the meshes are kept together, moved and, in case of flexible sections, modified. Each mesh in Blender is a separate object, and its physical properties (such as position, orientation and speed) can be changed autonomously. However, in presence of complex 3D models composed by different meshes joined together, a one-by-one control of them would be difficult to be performed. Since Blender is also thought for characters animation, a useful feature it proposes for the meshes modification is the **armature**, which represents a skeleton that, if applied to one or more meshes, could modifiy their aspects by moving, rotating or scaling them. Indeed, as in the human skeleton, an armature is composed by a series of **bones**, basic control objects that are related ("rigged", in the Blender jargon) to a group of vertices and influence their behaviors (see fig. 5.23). The armature is invisible during the rendering, but every change in its bones position or shape is visualized as a mesh movement or deformation.

Fig. 5.23. An example of character mesh modified by an armature in Blender (reprinted from [191]).

In our simulator, a global armature for the whole system has been implemented. It reflects the tree-like structure of STRAS: it is composed by a base bone (noted A, see fig. 5.24), fixed at the endoscope base, a set of eight rotating bones (noted B, see fig. 5.24), which reproduce the endoscope deflections, and two bones sub-chains for the instruments (noted C, see fig. 5.24). In turn, each instrument armature is composed by a base bone (noted D, see fig. 5.24), which controls the instrument translation and rotation, eight rotating bones (noted E, see fig. 5.24), which permit the instrument deflection, and a fixed bone (noted F, see fig. 5.24) corresponding to the tool. The bones positions and orientations can be modified only with a Python script, and after every change a refresh must be performed in order to render the updated scene.

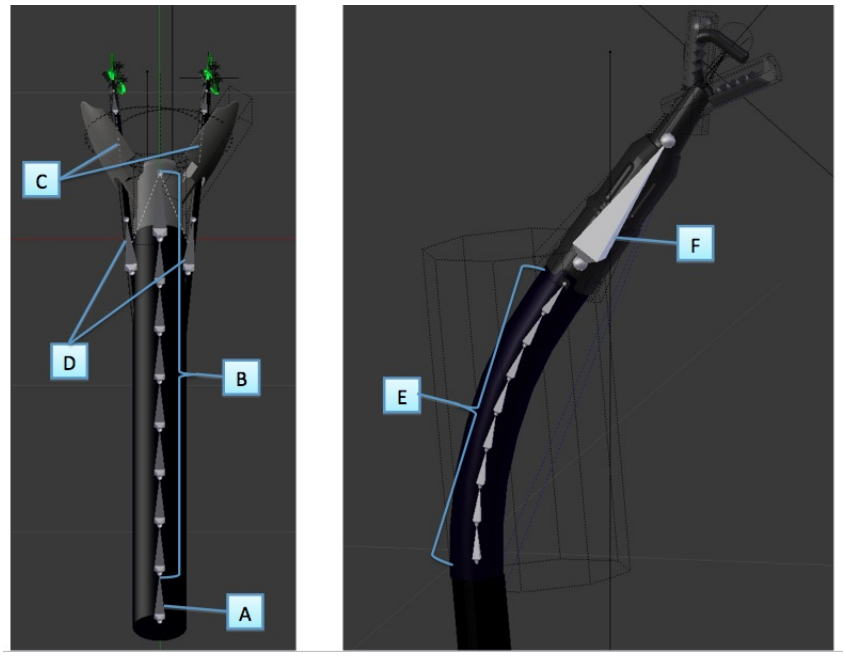

Fig. 5.24. Endoscope and instruments armatures. A: endoscope base bone. B: endoscope deflecting bones. C: instruments sub-chains. D: instruments base bones. E: instrument deflecting bones. F: tool fixed bone.

Virtual scenes

Several virtual scenarios have been implemented inside the simulator, with the aim to train the user on realistic tasks:

- **Rings**: three rings, which lie on some nails, must be taken one by one with the right instrument, passed to the left one and then posed on the stick that becomes coloured in red in a 3x3 sticks stand (see fig. 5.25). The red stick is chosen randomly, and the endoscope deflections are required to reach the

different objects in the scene. During the task, several parameters are collected, in order to give an assessment of the gesture at the end of the simulation:

- time of execution: the timer starts when the endoscopic camera points at the nails stand and ends when the last ring is correctly put around the selected stick;
- number of fallen rings: this can happen if the ring is not grabbed properly, if it remains entangled in a scene object or if the passage from one instrument to the other is not executed correctly;
- number of missed grabs: when the depth is not correctly perceived in the image, the user could close the grasper without grabbing the ring.

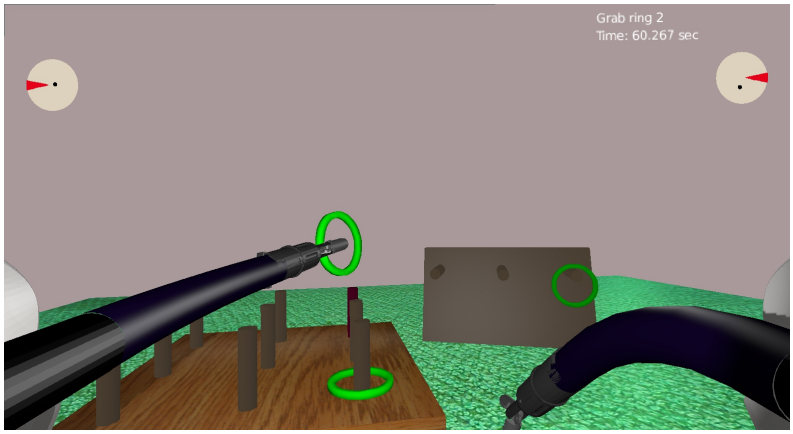

Fig. 5.25. Screenshot during the Rings task.

- **Rings 2**: three rings are hidden inside a box covered by a hinged cap, which can be raised by its spherical handle. The user has to pull up the cap, grab the three rings one by one and leave them on a nail placed on the right (see fig. 5.26). The same parameters as in the Rings scene are collected during the simulation, and the task ends when the third ring is correctly put around the nail.
- **Surgery**: the aim of this task is to perform a simplified cholecystectomy. A 3D model of a liver is shown, and the user has to raise the fifth segment of the liver in order to expose the gallbladder: to facilitate this procedure, the correct grabbing point is shown as a red sphere. The gallbladder resection is performed by cauterizing the cystic duct with the electrical tool. Once the cauterization is complete, the gallbladder can be taken with the grasper and put inside a retrieval box, located on the right side of the scene. Together with the execution time, the misapplied energy time, *i.e.* the time in which the electric hook is active without being at the correct resection point, is evaluated. The task timer starts when the endoscopic camera points at the liver grabbing point and ends when the gallbladder is inside the box.

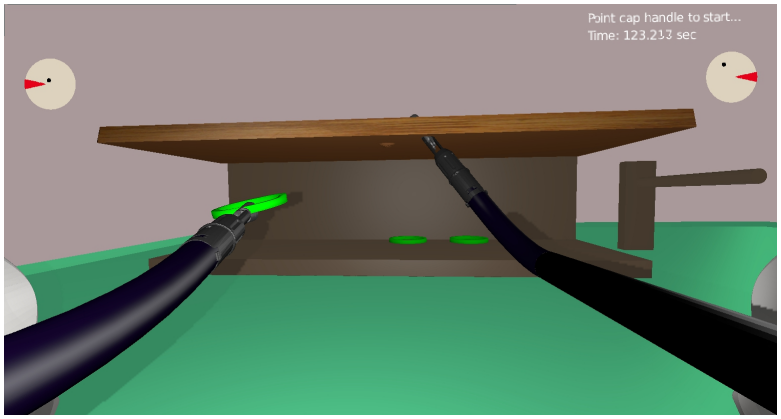

Fig. 5.26. Screenshot during the Rings 2 task.

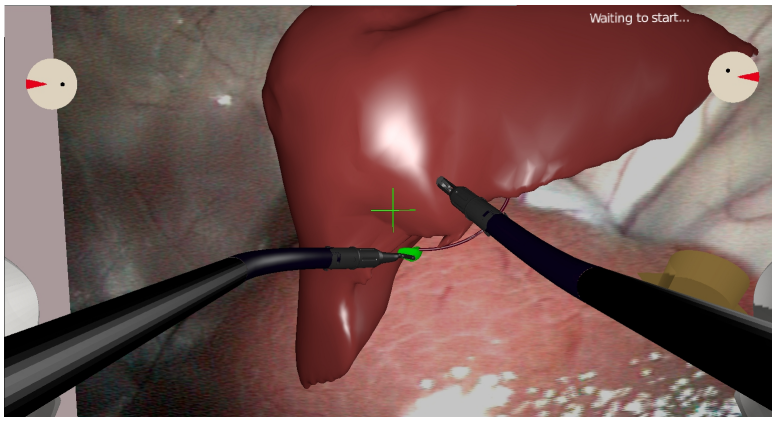

Fig. 5.27. Screenshot during the Surgery task.

5.5 Conclusions

One of the main open questions in surgery is how to train inexperienced surgeons in new techniques without involving live beings: from one side there is the need to test new instruments and procedures in conditions as much as possible similar to those of a surgical operation; on the other hand, ethical and safety aspects limit the number of feasible *in vivo* tests. Simulation might be a solution to this problem, offering virtual test environments that can be repeated endlessly and safely, not requiring an expensive operating room and trained staff. But to be effective, simulation should offer realistic operation conditions to the surgeon, trying to replicate the surgical scenario, the interaction with the tissues and their reactions to external solicitations. This result has been almost completely achieved in laparoscopy simulation, with a number of commercial simulators employed every year to train thousands of surgeons. The same thing cannot be said for no-scar surgery, which lacks of virtual simulators for training for multiple reasons, as we discussed before.

In this context, we are proposing a new virtual simulator for STRAS. This simulator, initially created for the kinematic study of the real robot, was recently improved and enhanced to be capable of training, too. Since STRAS can be teleoperated in several different ways, its simulator could represent a good way to familiarize with the system, understand its behavior and choose the preferred control modes. This can be done by performing simple but effective tasks, which propose the typical gestures that will be performed in the real clinical use.

6

Results

Contents

6.1 Introduction

The success of a new system is the result of its potential capabilities and its acceptance inside the community that should use it. Surgery is not the easiest field in which big changes can be introduced frequently: surgical procedures tend to be standardized for obvious reasons, so new technologies must pass long experimental and regulatory phases before being potentially adopted. However, as showed in chapters 2 and 3, no-scar surgery techniques are rapidly emerging as new frontier in minimally invasive surgery, but they require proper instrumentation to be performed. Because of the complexity of the manual systems proposed so far for this kind of surgeries (cfr. section 2.4), robotics could represent a valid aid offering simpler and more precise interfaces, increasing precision and improving the general ergonomics of such systems.

The aim of this chapter is to present the results of our experiments with STRAS, obtained both on the virtual simulators and with the real system. The conducted tests aim to show the system capabilities, the differences between the proposed control strategies and if STRAS improve the easiness of use and the gesture precision compared to the manual ANUBISCOPE® platform.

6.2 Virtual simulators

6.2.1 Single instrument tests

When STRAS was still under development, we conducted some experiments with the first version of its virtual simulator, in order to compare the Cartesian control strategies we are proposing. To doing this, we implemented two test environments in the simulator (cfr. section 5.4.2), with the aim to test how much the accuracy in the gesture and the system response speed are affected by a particular control strategy. The two tasks consisted in a path that the user had to follow with one instrument: in the first case (the *Precision task*), the path is tortuous, mimicking the motion during a suture, and it has to be followed as close as possible by the instrument tip; in the second case (the *Simple task*), the instrument tip must go along a linear path as fast as possible. The user has to perform these tasks with the control schemes presented in section 4.4.3, first with an ideal model of the system, and then introducing non-linearities. The advantages of such study were multiple: with the ideal model of the system we could evaluate the system behavior without the need to deal with known practical problems such as mechanical non-linearities or the lack of exteroceptive sensors; afterwards, we gradually introduced perturbations in the simulation with the aim to evaluate their effect on the system behavior and, eventually, try to correct the system kinematic model in order to compensate them.

Task Protocol

Two groups of ten persons were involved in this test. None of the participants had previous experience with the simulator. The first group tested the encoder offset error for the instrument rotation, while the second group tested the backlash non-linearity in the instrument deflection (cfr. section 3.5.3). We have chosen the values of 20 degrees for the rotation encoder offset and 2 mm of cable attached to the motor at the proximal side for the deflection backlash: both values come from a direct evaluation on the real system.

Each user starts with an initial apprenticeship phase, in order to familiarize with the control laws and the force feedback applied on the haptic interface. In this phase, that lasts three minutes, the user is guided to perform simple movements and to understand the differences among the proposed control laws. After this initial phase, the Precision task (cfr. section 5.4.2) is proposed: the user has to complete it with the different combinations of slave control laws and master interface inputs chosen at random, first without simulated non-linearities and then adding the error. When the Precision task is completed, the Simple task (cfr. section 5.4.2) is proposed with the same rules.

Results

The final results of these test sessions are summarized in Table 6.1. Each task must be evaluated separately, because the scores are computed with different weights. The two groups obtained similar scores in ideal conditions, so we report a mean

Precision task						
Slave Control	**Master Output**	**Slave Input**	**Force Feedback**	**Mean Score (no error)**	**Mean Score (rot error)**	**Mean Score (backlash)**
Open Loop	Position	Velocity	Spring	75.268	143.265	151.029
	Velocity	Velocity	Gravity comp	77.056	117.600	507.05
CL Joint	Position	Position	Error	87.317	89.141	184.342
CL Cartesian	Position	Position	Error	83.345	104.262	110.255
	Velocity	Position	Gravity comp	84.110	88.683	199.71

Simple task						
Slave Control	**Master Output**	**Slave Input**	**Force Feedback**	**Mean Score (no error)**	**Mean Score (rot error)**	**Mean Score (backlash)**
Open Loop	Position	Velocity	Spring	80.451	81.726	92.577
	Velocity	Velocity	Gravity comp	91.879	149.493	101.64
CL Joint	Position	Position	Error	77.131	92.958	153.863
CL Cartesian	Position	Position	Error	72.268	99.290	88.591
	Velocity	Position	Gravity comp	78.754	129.780	143.820

Table 6.1. Path following results for both considered tasks.

global score for both. This denotes the same starting level of both groups and allows us to make a direct comparison of errors effects in a specific task.

In ideal conditions, a velocity control strategy with a position master input permits to obtain better results for the Precision task. After an initial adaptation to the control method, the most common user feedback is that this modality permits to perform precise gestures, because the user input is given as small Cartesian velocity variations with respect to the actual instrument Cartesian position. The counterpart is a lower instrument reactivity for large requested movements, and this is the reason why position control strategies provide better results in the Simple task.

The observations change significantly when an error is introduced inside the simulation. In Table 6.2 we reported the results of the second group with the strategies for which the position of the master interface is used as the reference.

	Precision task			**Simple Task**		
Slave Input	Open Loop	CL Cartesian	CL Joint	Open Loop	CL Cartesian	CL Joint
Master Output	Position	Position	Position	Position	Position	Position
Mean	81.637	82.321	88.138	79.01	68.196	78.57
(with error)	151.029	110.255	184.342	92.577	88.591	153.863
Median	69.626	67.705	78.08	73.225	52.93	46.94
(with error)	106.465	83.72	128.57	78.622	63.195	105.105
Min / Max	54.08/124.69	50.59/152.29	51.77/123.35	36.34/142.54	32.365/173.89	31.82/176.37
(with error)	84.15/324.94	63.99/290.53	63.17/564.24	50.134/175.23	46.205/203.515	46.09/455.485
Best results (# users)	3	3	4	2	4	4
(with error)	2	5	3	3	5	2

Table 6.2. Comparison between the results of the second group (the error added is the backlash).

The backlash introduction gives the impression that nothing happens when one requests a direction change, so the user spontaneously moves the interface further. This situation could lead to the system instability because:

- in a velocity control law, a large Cartesian speed reference is sent to the slave system, that reacts abruptly when it comes out from the backlash zone;
- in a position control law, the error vector computed by the feedback loop increases rapidly during the backlash effect; the control loop tries to reduce this error, but this can cause large velocities when exiting from the backlash dead zone.

For both situations, these behaviors are definitively unacceptable in a surgical scenario and, from a robotic point of view, they apply an important stress to the mechanical parts of the system. This points out the need to correctly take into account the major mechanical non-linearities. From these first tests one can see that a Cartesian control with a position master output gives the best results for the majority of people involved in the simulations. The direct mapping between the instrument and the haptic interface workspaces, provided in this control strategy, gives a good sense of control for almost all users, because the position of the haptic interface directly represents the position of the instrument in the virtual scene, so the movement coordination is simpler. Also, the force feedback applied in the position input (cfr. section 4.4.8) helps to keep track between the interface and the instrument, especially when the instrument does not follow exactly the user requests because of a simulated error. On the real system, this means that an external tracking system is mandatory to correctly reproduce the force feedback effect, because the estimated instrument Cartesian position, computed with the theoretical kinematic model and based on the encoders positions, does not represent the actual instrument position. Finally, a direct mapping decreases the resolution of the movement because of the different sizes of instrument and interface workspaces. This problem could be resolved by scaling the interface movements with a filter on the user input: in this case it is necessary to implement a repositioning system (declutching) for the interfaces.

6.2.2 Tests with the second simulator

With the second version of the virtual simulator it was possible to test the STRAS behavior with three realistic tasks (cfr. section 5.4.3), implemented with the aim to evaluate the system capabilities in complex comanipulation tasks. In these tasks the whole system is involved, and the cooperation between instruments is mandatory for the correct accomplishment.

Task protocol

Eight users were involved, divided in three groups:

- Experts (Users 1-3): three users with previous experience on both the real system and the simulator;
- Intermediates (Users 4-6): three users with previous knowledge of the real system, but without experience on the simulator;

- Beginners (Users 7-8): two users without any previous experience on neither the real system nor the simulator.

Each user had to execute the proposed tasks with four different control modalities: Direct axis, Orientation guidance, Pseudo-Cartesian and Cartesian (cfr. section 4.4.5). The simulations were performed using the ideal model of the system, without introducing any perturbation.

A maximum time slot of ten minutes was given to the user before starting the tasks, in order to familiarize with the proposed strategies, test the different mappings and try to interact with the virtual objects. During the task execution, all the most important parameters are recorded: Cartesian and articular positions of the robot, haptic interfaces positions and execution times. Moreover, several possible user mistakes are detected:

- Missed grab: it happens when a grasper is closed, but nothing is grasped; it is typically related to the difficulties in depth perception.
- Number of fallen rings (Rings tasks only): an error is counted when a ring falls on the floor because the grasping is not performed correctly, the ring is not well positioned or a collision with an instrument causes an unwanted fall.
- Misapplied energy (Surgery task only): number of times the electric hook is activated, but it is not in the right cutting point.

During the simulations, it could happen that a virtual object falls outside the system reachable workspace because of a collision or a wrong movement. Since in that case the scene completion is compromised, there is the possibility to reset the scene and start again the task. A maximum of three resets are allowed for each scene and each modality, otherwise the experiment will be marked as failure.

Results

In figs. 6.1, 6.2 and 6.3 the execution times of the proposed tasks are presented. What it can be immediately noticed for the majority of users is that a Cartesian modality (either the Pseudo-Cartesian and the Cartesian control) gives the best results in average. This probably derives from the user input modality, more natural in the gesture than a non-Cartesian one. In the Rings task, User 5 collected four resets with the Orientation Guidance strategy, therefore the task was considered as failed.

The haptic interfaces architecture is flexible enough to permit several different mappings, but the unused DOFs disturbed users during the tasks executions. During Cartesian strategies, most part of users spontaneously tended to rotate the interface handle with the aim to rotate the instrument, also if the correct mapping (which includes the translational DOFs only) has been mentioned several times during the execution. The rotational DOFs of the haptic interfaces are passive, and it is impossible to lock them with force feedback. Therefore, in Cartesian strategies a simpler interface with the three translational DOFs and the gripper could represent a better solution.

The Orientation Guidance strategy is a particular mapping in which the force feedback effect is largely employed on the master interfaces, with the aim to constrain theirs movements to those the instruments tips can do from theirs actual

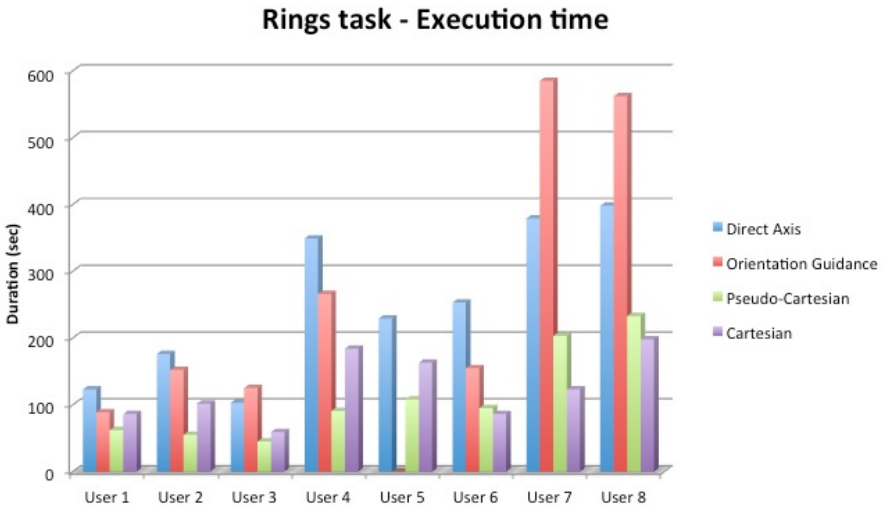

Fig. 6.1. Execution times for the Rings task.

Rings task					
Group	Parameters	Direct Axis Control	Orientation Guidance	Pseudo-Cartesian Control	Cartesian Control
Experts	Left Grabs (min/Max)	6 / 9	1 / 4	1 / 7	1 / 4
	Right Grabs (min/Max)	3 / 5	1 / 3	0 / 3	0 / 4
	Fallen rings (min/Max)	0 / 9	0 / 11	0 / 0	0 / 2
	Reset (min/Max)	0 / 0	0 / 0	0 / 0	0 / 0
	Fastest modality (# times)	0	0	3	0
	Slowest modality (# times)	2	1	0	0
Intermediates	Left Grabs (min/Max)	9 / 12	0 / 4	2 / 5	0 / 3
	Right Grabs (min/Max)	3 / 15	0 / 2	0 / 2	2 / 2
	Fallen rings (min/Max)	3 / 19	2 / 5	0 / 3	0 / 0
	Reset (min/Max)	0 / 2	3 / 4	0 / 2	1 / 3
	Fastest modality (# times)	0	0	2	1
	Slowest modality (# times)	2	1	0	0
Beginners	Left Grabs (min/Max)	6 / 21	4 / 12	3 / 9	3 / 4
	Right Grabs (min/Max)	4 / 11	4 / 6	3 / 5	3 / 4
	Fallen rings (min/Max)	15 / 43	8 / 24	2 / 7	3 / 6
	Reset (min/Max)	0 / 2	0 / 1	1 / 2	3 / 3
	Fastest modality (# times)	0	0	0	2
	Slowest modality (# times)	0	2	0	0

Table 6.3. Parameters collected during the executions of the Rings task, divided by group of users.

configurations. The idea is to create a direct mapping between the instrument and the interface motions, in order to give the impression of directly controlling the instrument tip. During the tests, this mapping resulted one of the worst, but we believe that this is mostly due to the limitations in the force feedback reproduction on the haptic interfaces. When the force effect was implemented, we searched a compromise between the interface rigidity and its stability. In case of two high repulsive forces fixed closely (as it happens for the Line force effect, cfr. section 4.4.8), the interface end-effector could be induced to instability because of the feedback effect. On the contrary, choosing a lower interface stiffness results in a lighter effect that does not completely constrain the interface movements and, thus, decreases the desired haptic sensation. Moreover, the hemispheric shape of the interface workspace obliged us to block the handle movements on the plane $Z_M = 0$ and to use a velocity control for the instrument translation, in order to keep the maximum XY excursion needed to correctly control the instrument deflection. These facts represent an added difficulty for the user, who has to learn the interface mapping, but also cope with wrong behaviors in that particular conditions. We are convinced that a brand new haptic interface specifically designed for this modality can offer a better feeling to the user, making the Orientation Guidance strategy a valid alternative to Cartesian strategies.

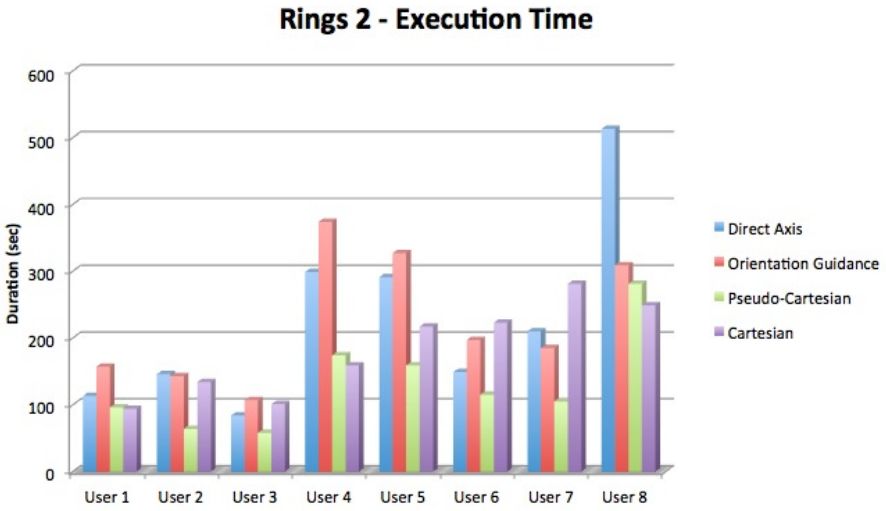

Fig. 6.2. Execution times for the Rings 2 task.

Since the number of users involved in this experiment is limited, the parameters collected during the tasks (cfr. tables 6.3, 6.4 and 6.5) are not sufficient to conduct a solid statistical analysis in order to correlate them to the gestures. On the average, and as one might easily expect, the performed errors increase when the group level decreases. The depth perception largely influences the number of missed grabs, but this reflects the actual conditions on the real system. Several users spent some time at the beginning of their tasks to exactly understand the depth of the 3D scene,

Rings 2 task					
Group	Parameters	Direct Axis Control	Orientation Guidance	Pseudo-Cartesian Control	Cartesian Control
Experts	Left Grabs (min/Max)	2 / 6	2 / 4	1 / 3	0 / 1
	Right Grabs (min/Max)	6 / 14	3 / 4	0 / 4	0 / 5
	Reset (min/Max)	0 / 0	0 / 0	0 / 0	0 / 0
	Fastest modality (# times)	0	0	2	1
	Slowest modality (# times)	1	2	0	0
Intermediates	Left Grabs (min/Max)	3 / 6	2 / 16	0 / 10	0 / 6
	Right Grabs (min/Max)	8 / 14	2 / 5	3 / 7	3 / 9
	Reset (min/Max)	0 / 0	0 / 2	0 / 0	0 / 2
	Fastest modality (# times)	0	0	2	1
	Slowest modality (# times)	0	2	0	1
Beginners	Left Grabs (min/Max)	6 / 12	2 / 3	2 / 3	3 / 11
	Right Grabs (min/Max)	6 / 8	3 / 8	7 / 7	11 / 13
	Reset (min/Max)	0 / 0	1 / 2	0 / 1	0 / 3
	Fastest modality (# times)	0	0	1	1
	Slowest modality (# times)	2	0	0	0

Table 6.4. Parameters collected during the executions of the Rings 2 task, divided by group of users.

trying to reach objects with instruments. This, of course, influenced the execution time and has to be taken into account.

To avoid to get used to a sequence of control modalities, the strategies order was chosen at random for each user. In some users, especially the beginners, this has caused confusion and difficulties in using the correct mapping: some movements related to a previous strategy were repeated in the next one, also if the users were made aware of the variations at each change of modality.

In the Direct Axis control, the choice to control the opening and closing of the graspers with pedals resulted disturbing for many users: the action was judged not natural, and many times users had to look at their feet in order to search the right pedal. This partially justifies the higher number of missed grabs obtained with this modality compared to the other strategies. The choice to use pedals for the graspers actuation was the only possible solution with our setup, since the haptic interface gripper is used to control the instrument deflections, and the other available master DOFs are not suitable for such use. To solve this issue, an additional control on the master handle should be introduced (such as, for instance, a thumbstick) in order to control the mechanical instruments actuation with fingers and avoid the feet actuation.

6.3 Robotic system

We have tried to assess the behavior of STRAS through several analyses and experiments.

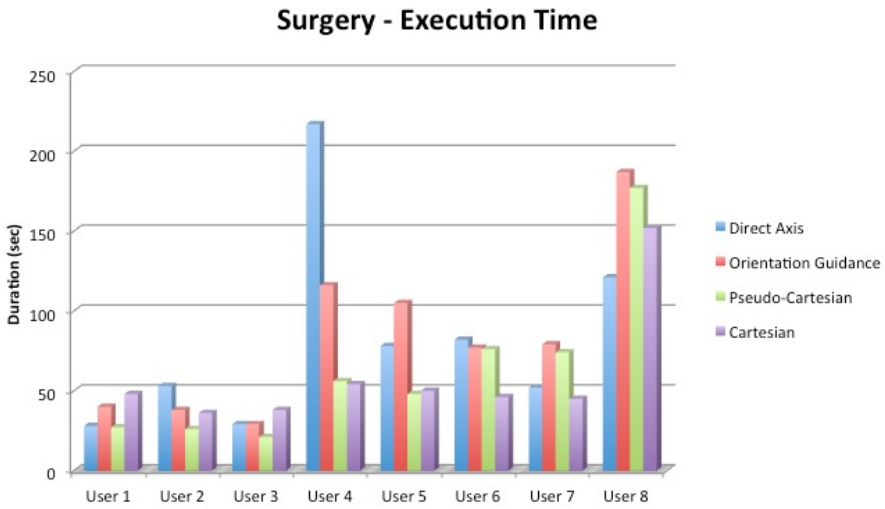

Fig. 6.3. Execution times for the Surgery task.

Surgery task					
Group	Parameters	Direct Axis Control	Orientation Guidance	Pseudo-Cartesian Control	Cartesian Control
Experts	Right Grabs (min/Max)	2 / 4	0 / 2	0 / 0	0 / 1
	Misapplied energy (min/Max)	1 / 4	2 / 4	3 / 3	2 / 6
	Reset (min/Max)	0 / 0	0 / 0	0 / 0	0 / 0
	Fastest modality (# times)	0	0	3	0
	Slowest modality (# times)	1	0	0	2
Intermediates	Right Grabs (min/Max)	3 / 11	0 / 3	2 / 8	0 / 8
	Misapplied energy (min/Max)	3 / 5	6 / 10	2 / 7	2 / 4
	Reset (min/Max)	0 / 2	0 / 0	0 / 1	0 / 2
	Fastest modality (# times)	0	0	1	2
	Slowest modality (# times)	2	1	0	0
Beginners	Right Grabs (min/Max)	4 / 5	2 / 3	2 / 5	0 / 3
	Misapplied energy (min/Max)	1 / 3	7 / 13	3 / 9	4 / 8
	Reset (min/Max)	0 / 0	0 / 1	0 / 0	0 / 0
	Fastest modality (# times)	1	0	0	1
	Slowest modality (# times)	0	2	0	0

Table 6.5. Parameters collected during the executions of the Surgery task, divided by group of users.

6.3.1 Validation of the continuum section model

The assumptions given in section 4.2.2 allowed us to describe the flexible sections of STRAS with the standard Denavit-Hartenberg parameters, thus computing a kinematic model in the same manner as discrete robots. In order to see if the piecewise constant curvature model gives a proper representation for our system, we conducted a test in which we compared the instrument positions over an imposed path and the corresponding computed positions given by the kinematic model.

Using the model (4.4) for representing the flexible section, the Cartesian position of the instrument tip, expressed in the jaw head frame F_{JH}, is computed with eq. (4.15).

The instrument positions were captured by an external camera, placed perpendicularly to the instrument deflection plane at a fixed distance of 20 cm. Two visual markers were placed on the instrument, one at the flexible section base and the other at the tip (see fig. 6.4). The instrument movements were performed in its deflection plane, therefore the rotational joint was not involved: they consisted in a complete span of deflection and translation joints, realized separately. The camera

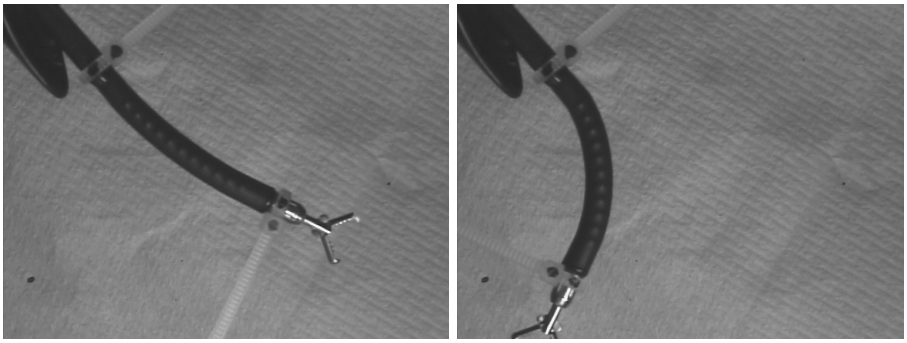

Fig. 6.4. Screenshots of the continuum section model validation: the instrument, which performs a complete deflection, has two markers placed respectively at the base and at the tip of its flexible section.

was connected to a PC via a graphic acquisition card, which sent the images to an application developed in our lab. This application detects the markers on each image and compute their positions, expressed in the camera axis center. The results are visible in fig. 6.5, where the blue lines refer to the measured positions, while the red lines come from the model computations: on the left image, the circular path represents the deflection movement, while the straight path refers to the instrument translation. It could be seen that the theoretical and the measured paths are very similar, with small deviations visible only at the joints range limits. These deviations could be caused by several factors: uncertainties on geometrical parameters in the robot model, registration errors between the robot and the camera and mechanical non-linearities. The translation deviation, more evident when the instrument is completely outside its channel, is largely caused by the gravity effect and the system flexibility. Moreover, the not accurate perpendicularity between the camera and the plane affected the measures.

Although the comparison between the model and the measured position of the system gives close results, the direct comparison between the instrument deflection angles and the corresponding motor positions clearly shows backlash when changing direction and slope around the straight position, as already explained in section 3.5.3 (see fig. 6.5). This behavior, difficult to be compensated analytically because dependent on several factors, prevents the direct use of the kinematic model as feedback sensor in the Cartesian closed-loop strategies (cfr. section 4.4.3): the Cartesian position computed by the model would not represent the real instrument position, thus leading to a wrong error vector computation in the scheme loop. Moreover, during a motion backlash the user has the sensation that nothing happens, thus increasing its input reference and, potentially, causing the system instability. This is the reason why the Cartesian strategies were assessed with the virtual simulator only. In order to correctly employ the closed-loop Cartesian control scheme on STRAS, a proper feedback sensor will be needed.

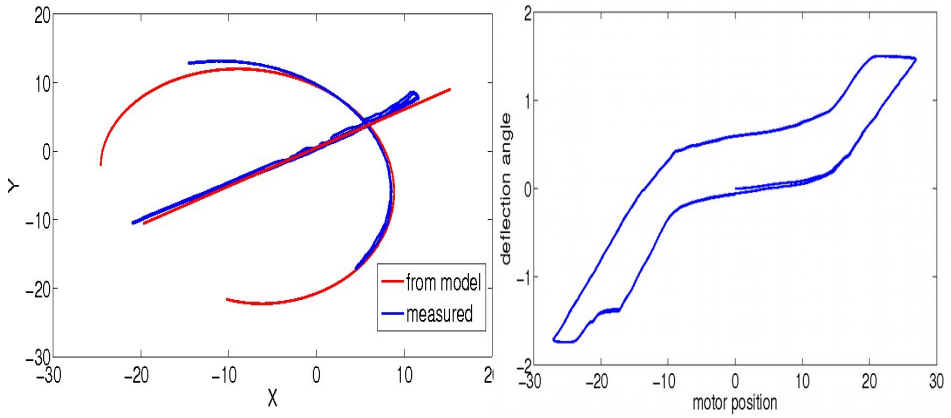

Fig. 6.5. Left: comparison of the model-based and measured positions of one instrument for translation and deflection. Right: motor position / measured deflection quasi-static characteristic.

6.3.2 Pick-and-place task

With this experiment we want to demonstrate the ease of use of STRAS, compared to the ANUBISCOPE® system, in the execution of a complex task involving grasping and cooperation between instruments. For this preliminary experiment, conducted just after completing the system robotization, we have chosen to use the Direct Joint Control strategy (cfr. section 4.4.5), because it requires user inputs that are very close to those typically performed on the ANUBISCOPE®, so allowing an immediate direct comparison between the two systems.

The task consisted in seizing a ring, placed on a stand on the left, with the left instrument (electrical hook), exchanging it with the right instrument (grasper) and bringing it on a nail, placed in front of the camera. The task is done two times,

with the only feedback provided by the embedded endoscopic camera. In this experiment, all the slave system DOFs are involved, since an endoscope movement is mandatory to correctly reach every part of the task workspace. Fig. 6.6 shows snapshots of a performed task: after the hook seizes the ring (a), it is grabbed by the grasper (b); during this passage the ring dropped (c), but the user was able to regrasp it (d), adjust its orientation with the aid of the left instrument (e) and finally put it around the nail (f). The whole task was completed by a single user in less than three minutes, despite the limited depth perception due to the use of a monocular camera.

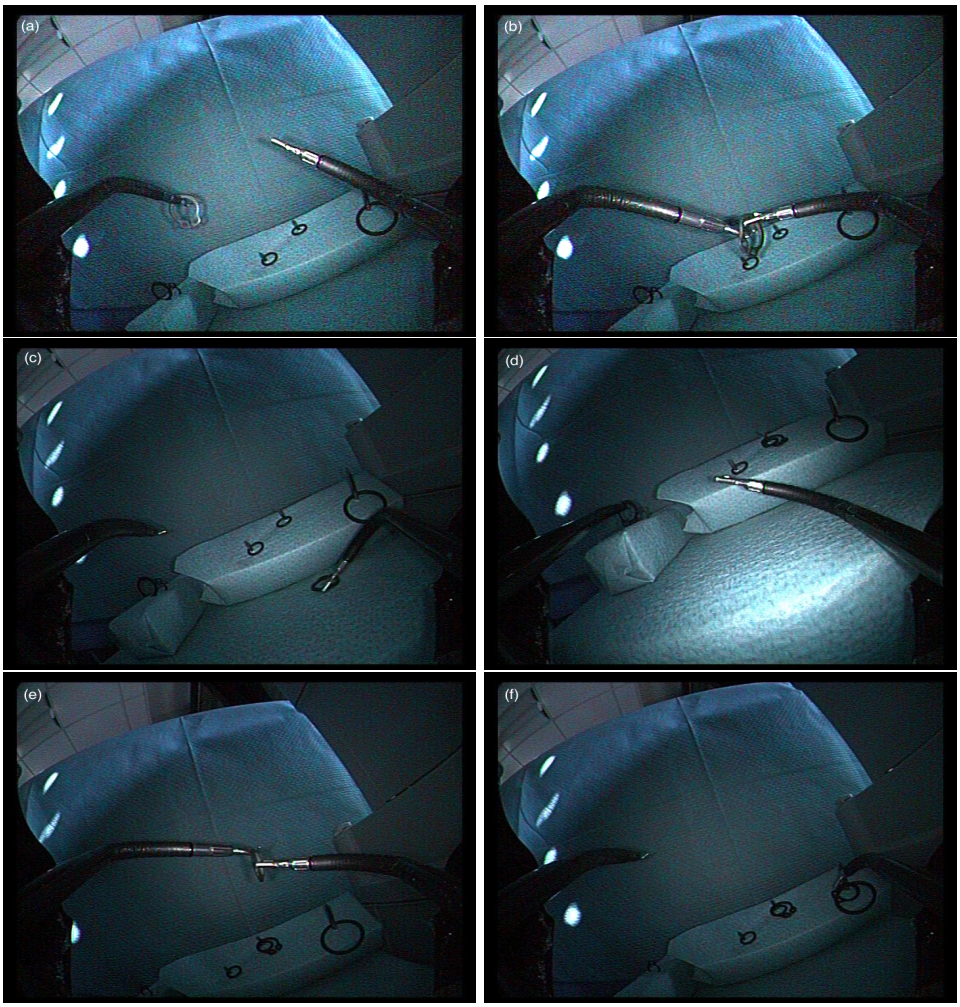

Fig. 6.6. Snapshots of the pick-and-place task.

The evident advantage of STRAS compared to ANUBISCOPE® is that such type of task is impossible to be executed with the manual system by a single user:

it would require a continuous switch of the user's hands between the instruments handles and the endoscope control knobs, compromising the gesture effectiveness and requiring much more time. In STRAS the control of either the left instrument or the endoscope is setted with the pedal board, leaving the user's hands always in contact with the haptic interfaces. Another big advantage, highlighted by the surgeons (especially those who had experience with the ANUBISCOPE®) that executed this task, is the complete absence of sense of friction and the improved ergonomics: the same movements performed on manual instruments would require much more efforts, in order to overcome instruments friction, and could lead the surgeon to uncomfortable postures.

6.3.3 Path following and pointing

When STRAS was under development, we started to test Cartesian strategies with the virtual simulator (cfr. section 6.2.1). When the robotization was concluded, we performed a similar experiment with the real robot, in order to compare the non-Jacobian strategies in tasks which required to follow a path, showed on the image, and reach some points. The experiment was conducted with a single instrument, without the assistance of the endoscope movements: this choice was done with the aim to assess the effects of non-linearities and singularities, which were voluntarily included in the requested movement, in the instrument motion. Moreover, some intraluminal operations could limit the endoscope movements because of the lumen size or the presence of other anatomical structures: in these conditions, it is important to evaluate the system capabilities with a reduced number of DOFs.

A testbed proposing three tasks was developed, each of which should be replicated with five different control strategies: Direct Joint Control, Orientation guidance, Pseudo-Cartesian Control and Cartesian Control (cfr. section 4.4.5). The last two modalities give the possibility to choose among only positive or positive and negative instrument deflections: in the first case the workspace has a forbidden area on its outer part (cfr. section 4.3.2), in the latter the workspace is complete and redundant, but the user should be prevented about the deflection switching modalities (see section 4.4.6). Therefore, if considering the switching possibility, a total of six modalities were tested, with the aim to compare them in terms of accuracy, reactivity and singularities management.

The first task consists in following a path in the image with the left instrument tip (see Fig. 6.7): the user has to do a counterclockwise tour passing from the first two vertical lines depicted on a grid. The instrument tip must be kept inside the thickness of the black line, otherwise an error is counted.

The second task consists in pointing four points drawn on a testbed, without any constraint about the order. For this task it is sufficient to reach the points in the image plane, without taking care if the instrument tip is physically in contact with the testbed.

The third task is similar to the second, but in this case it is necessary to touch the points with the instrument tip and reach the cavity behind each of them.

For every task, the execution time is recorded. In the first two tasks the depth perception does not represent a real limit, since the instrument movements are evaluated in the image. Tasks 2 and 3 are aimed at assessing the ease of pointing

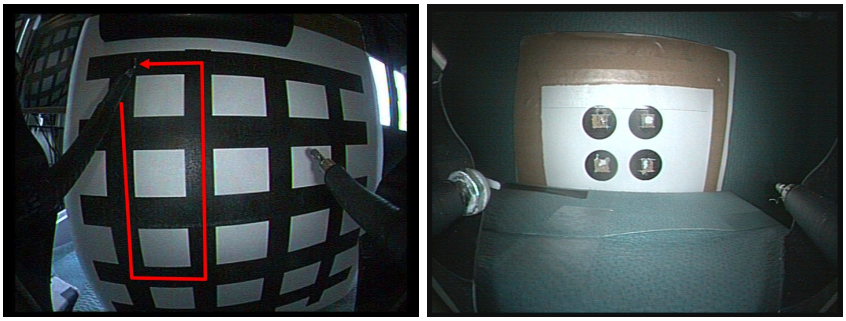

Fig. 6.7. Snapshot from the endoscopic images, as seen by the user during task 1. Left: the path (indicated in red) has to be followed using the left instrument only. The path goes through the straight configuration and reach the limit of the instrument workspace (top and bottom). Right: task 2 consists in reaching four points in the image, while in task 3 the instrument tip must physically reach the point on the testbed.

by switching from large and fast motions, performed between the points, to accurate and fine movements for the final positioning. The initial endoscope position guaranteed that the task area was inside the instrument workspace. The proposed tasks include challenging motions or positions, located at the extremity of the instrument workspace, near the straight configuration and near the mechanical limits of the rotation. Although they are not directly representative of surgical procedures, pointing and trajectory following are necessary in most clinical procedures, such as for instance in Endoscopic Submucosal Dissection (ESD, cfr. section 3.5.7).

Three users, familiar with the manipulation of the robotic system, have been requested to successively perform the tasks with all modalities. For each modality the users could train on a neutral environment.

Results for task durations are reported on Table 6.6 and showed graphically on fig. 6.8.

In task 1, the number of detected errors for all users and all modalities is important (between 4 and 8), with two main types of errors:

- Slight deviations: drifts of a few millimeters with respect to the fixed path. When using a Cartesian or Pseudo-Cartesian strategy, they are mainly caused by kinematic singularities, which produce uncontrolled rotations of the instrument when crossing its straight configuration. In case of non-Cartesian strategy, singularities do not influence anymore the instrument motion, but the user has to mentally inverse the robot kinematic in order to figure out which joints configurations allow to reach the desired Cartesian points.
- Large motions: deviations of more than one centimeter from the fixed path. They typically happen when the limit of the workspace has been reached, so a joints reconfiguration is required to continue the task (note that the endoscope DOFs are not used in these tasks). Excessive references on the master system, applied by the user because of the apparent slave system immobility caused by motion backlash, or a high sensitivity of master DOFs, especially the gripper

Fig. 6.8. Durations of path following (task 1) and pointing (tasks 2 and 3) tasks.

Task 1						
User	Direct Joint Control	Orientation Guidance	Pseudo-Cartesian	Pseudo-Cartesian with switching	Cartesian	Cartesian with switching
1	39.55	38.36	24.52	26.10	48.25	43.11
2	21.25	33.79	13.39	18.49	14.45	32.30
3	62.85	86.10	72.91	61.59	98.05	113.76

Task 2						
User	Direct Joint Control	Orientation Guidance	Pseudo-Cartesian	Pseudo-Cartesian with switching	Cartesian	Cartesian with switching
1	12.50	14.50	10.13	8.88	12,88	11.75
2	13.95	38.78	12.69	24.97	22.60	32.78
3	14.70	19.40	18.67	10.58	22.05	16.46

Task 3						
User	Direct Joint Control	Orientation Guidance	Pseudo-Cartesian	Pseudo-Cartesian with switching	Cartesian	Cartesian with switching
1	10.90	13.84	10.57	16.90	10.25	14.61
2	18.10	24.25	17.56	13.58	14.30	16.47
3	30.30	36.06	31.21	40.91	35.45	43.33

Table 6.6. Results of the Path following and pointing tasks (duration in seconds).

when controlling the deflection in the Direct Joint Control, are the two others main reasons of this type of error.

Tasks 2 and 3 were accomplished more easily than task 1 because there was no fixed path between the points, therefore users could avoid workspace limits and singularities by choosing alternative movements.

During these tasks, we found similar drawbacks related to the use of the Orientation Guidance modality as those revealed during the tests with the virtual simulator (cfr. section 6.2.2). We confirm, therefore, our impression that a brand new interface specifically designed for this mapping would give better results for the slave robot control, but also more stability and transparency at the master side level.

Comparisons between Cartesian and Pseudo-Cartesian modalities (with and without negative deflections) show that the latter allows better control, mainly because the singularity at the workspace boundaries is largely compensated by the separate control of instrument deflection and translation. As explained in section 4.3.4, the lower part of the instrument local workspace represents a redundancy in control, because all the points below the workspace diameter could be reached keeping the current translation value and putting the instrument in retroflected position ($\beta > \beta_{sing}$, cfr. section 4.3.6), or searching the corresponding lower workspace that contains the same point, with $\beta < \beta_{sing}$ and a different translation value. When using the Cartesian modality, a small movement of the instrument tip in the X or Y direction near the workspace boundaries results in a large variation of the z coordinate due to the elliptical shape of the workspace. But

while the instrument translation is immediately applied, the backlash that affects deflection does not allow a correct instrument tip positioning. The result is that the user sees the instrument in a wrong configuration and pull back the interface, the deflection remains in the backlash dead-zone and the instrument translation is solicited in a continuous forward and backward movement. The Pseudo-Cartesian modality, instead, allows to avoid these unwanted motions because the instrument translation is controlled separately, thus a linear movement of the haptic interface in the X or Y direction does not affect it.

Always speaking about the Cartesian strategies, the possibility to use both positive and negative deflections does not seem to represent a real advantage in this case: since the tasks did not require specific orientations and the targets were in the instrument workspace, on the average the switch possibility represented an increase in execution times because of the management of the straight configuration singularity, which requires specific movements when crossing the workspace apex (cfr. section 4.4.5).

6.3.4 ANUBISCOPE-STRAS Comparison

After performing the preliminary assessment tests on the proposed control strategies, we started to focus on the comparison between the manual ANUBISCOPE® system and our robotic prototype STRAS. The aim was to assess how much the robotization process represented an advantage, the real improvements that STRAS offers and the limits at the actual stage of development.

Before describing the experience, it is important to say that an objective assessment of such complex systems is really hard to figure out, because of the number of variables that determine the results: beside the mechanical system limits, an experiment is largely influenced by the user, who could have different preferences in terms of control strategies, could be used or not to the manipulation, could be tired or frustrated by a difficult mapping. Moreover, the depth perception is different among users, leading them to different performances just because the objects are not correctly localized in the 2D image and time is spent to evaluate the right depth.

For comparing the two systems we developed, with the cooperation of our surgeons partners, a testbed with three elementary tasks (see fig. 6.9):

- **Task 1**: a wall with three nails in line is presented, the first nail on the right holds two rings. The task consists in transferring the rings from the rightmost nail to the middle one. The task must be performed with the grasper only, without moving the endoscope. The nails position is such that they are inside the grasper workspace.
- **Task 2**: in this task, similar to the first one, the rings must be transferred from the rightmost to the leftmost nail. To perform this movement it is necessary to exploit the endoscope DOFs, because the grasper alone does not permit to reach both nails. Since the endoscope is controlled with the left interface and the grasper with the right interface, for this task the user will have both hands occupied.
- **Task 3**: it consists in retrieving a ring covered by a gauze and bringing it on a rack placed on the left side of the testbed. The gauze must be raised using

the grasper, and the ring should be pulled out with the hook. Once the ring is outside the gauze cover, it has to be taken with the grasper and laid around the left rack. Endoscope movements are allowed and necessary, so in this case the whole slave system has to be controlled.

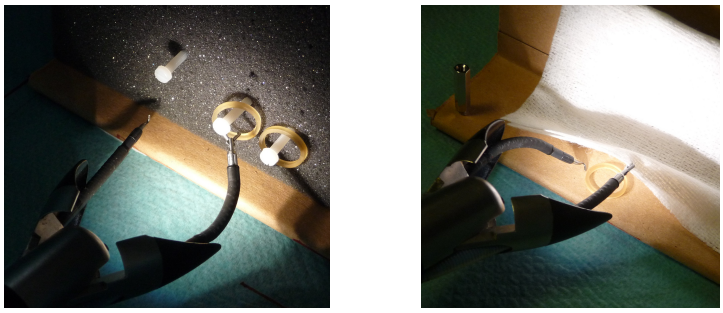

Fig. 6.9. Testbeds for task 1 and 2 (left) and for task 3 (right)

For each task the electric hook is in the left channel and the grasper in the right channel, and the only user feedback is the monoscopic camera embedded on the endoscope head. The maximum time allowed for each task is four minutes.

The tests have been carried out with ten users:

- one digestive surgeon, experienced in the use of the ANUBISCOPE® system;
- one digestive surgeon and one gastroenterologist, with no experience neither with the manual nor the robotic systems;
- two roboticists, experienced in the STRAS teleoperation;
- five engineers, with no previous experience on STRAS.

Each user was requested to perform the three tasks successively with the ANUBISCOPE® and with STRAS, the order being selected at random. For STRAS, all the control strategies but the Jacobian-based was proposed in a random order for the tasks execution. Each user had five minutes before starting the task in which he/she could read the task directions, practice on a training pad and find the most appropriate postural position on the master console. In the directions there are no technical details about the robot functioning or limits, but the user can gain more informations by asking during the training time.

The ANUBISCOPE® system was fixed with a passive arm on a table, in order to avoid the presence of another person just for holding it (as it happens during its clinical use): in this manner, the user was responsible for the movement of both endoscope and instruments. There are no means to measure the ANUBISCOPE® motions, so the execution time was the only basis for comparison. On the contrary, all the motions at the master and slave levels performed with STRAS were recorded for subsequent analysis. Overall, the common objective features used for assessing the modalities are the success or the failure of the task, the execution time and the number of errors committed (missed grasping, missed ring release, unwanted collisions with the environment).

The user was asked to fill a questionnaire after each sequence of tasks and a general questionnaire at the end of the tests. The subjective elements used for assessing the modalities are their intuitiveness, the difficulty of manipulation, the tiredness and the frustration provoked by the manipulation and the overall preferences.

Unfortunately, before starting the tests one of the master interfaces has broken, so it has been replaced by an omega.3 by Force Dimension (Nyon, Switzerland): compared to the omega.7, the omega.3 has just the three active translational DOFs, and it does not dispose of a gripper control. Hence, it could not be used for those strategies in which rotations and gripper are employed, such as Direct Joint Control or Orientation guidance. For this reason, task 3, which requires both instrument control, has been performed on STRAS with the Pseudo-Cartesian strategy only.

Almost all users were able to complete all tasks in the allotted time for both manual and robotic system without any particular assistance: they have notably been able to re-grasp a dropped ring, except two cases in which the rings fell too far (these cases, concerning the robotic system, were marked as task failures). However, in some accomplished tasks, users had difficulties in correctly positioning the rings on their final destinations because of the impossibility to change the instrument rotation while keeping the position: this limitation, own of both systems because of their instruments mechanical architecture, resulted in longer tasks durations. Another reason of failure was the misperception of the depth in the image, which led to difficulties in grasping and leaving the rings.

On the ANUBISCOPE®, no significant differences in completion times between users have been observed for tasks 1 and 2: this was partly expected because these tasks are artificially constrained and surgeons being used to manipulate with both instruments. On the contrary, the experienced surgeon outperformed other users in task 3. In their questionnaires, users pointed out some issues relative to this system: they mainly complained the important efforts, due to friction, when moving the instrument (which results also in unwanted endoscope movements), the impossibility to control the endoscope without leaving the instruments control and the limited workspace compared to tasks sizes. On the contrary, manual actuation gave them a better feeling of direct control compared to the robot.

On STRAS, we observed that the number of errors (missed grasping, fallen rings, collision with the environment) is not influenced by the chosen control strategies, but it is mainly linked to the depth perception. All modalities allow fine enough control of the instrument, and the limited movements and efforts requested for the task did not highlight any preferred mode (cfr. fig. 6.10). The main disturbance during the system control is due to the unused DOFs on the master interfaces, as already noticed during the experiments with the virtual simulator (cfr. section 6.2.2): because of the impossibility to block the passive rotational movements, often not employed in the strategies mappings, users tended to use them spontaneously without producing any movement of the slave robot. Moreover, some users were disturbed by the grasper actuation in the Direct Joint Control, which is done by pedal: especially surgeons, who are used to press a pedal just when they want to cut or coagulate, asked for a different actuation method. Since the used haptic interfaces are generic commercial products, these remarks

confirm that a specifically developed interface, tailored on one or more particular mappings, should improve consistently the user experience in the telemanipulation. However, already with the omega.7 interfaces, the fluidity of motions and the absence of sense of friction were two of the most common positive comments, together with the possibility of controlling the whole system without discontinuities. These positive comments represent an important advantage of STRAS compared to the ANUBISCOPE®, especially thinking to a real clinical case, which is surely longer and more tiring than the proposed *in vitro* tasks: with STRAS it is possible to perform a surgical operation while sitting comfortably, without an excessive effort required and with the complete control of the system.

These preliminary tests showed also that the preference about a specific control strategy is a subjective aspect, related at this first stage to the extemporaneous feelings of users: the short experiment time, the limited number of people involved and their common inexperience do not permit to draw objective conclusions about that. But, from another point of view, the availability of multiple control strategies could allow more different users to find their preferred one and to have several choices on which do training. Moreover, a personalized tuning of some system parameters, such as force amplitudes, velocity gains and motion scaling, could improve the user experience and result in a shorter learning curve.

6.3.5 *Ex vivo* test

In order to test STRAS in realistic conditions, we performed some *ex vivo* tests in collaboration with our surgeons partners with the aim to reproduce an Endoscopic Submucosal Dissection (ESD, cfr. section 3.5.7). We used a pig stomach, sutured to keep the insufflation and attached around the endoscope head, in order to simulate a transgastric approach (see fig. 6.11). Although STRAS is too short for a real transgastric access, this particular test setup is similar to an ESD performed into the colon, where the endoscope head would be constrained by the colon lumen. Using a grasper and an electric hook as instruments, we tried to dissect a part of the gastric submucosa by cutting the stomach external mucosa layer.

We found several system limitations in performing this procedure, mainly regarding the inappropriate size of instruments. The grasper claws were too thin to correctly grab the viscous tissue, and the electric hook was small compared to the size of the needed cut, thus requiring much time to cut the mucosa layer. Indeed, the manual instruments employed in this kind of surgery are wider than those at our disposal, and therefore they guarantee a stiffer grasping and a more efficient tissue ablation.

Another detected drawback is the impossibility to control the insufflation and evacuate the smoke from the user console: the corresponding controls are on the endoscope body, but they have not been robotically actuated on the current prototype version.

On the other hand, the system mobility was adequate, allowing a complete exploration of the stomach. We were also able to extract the electric hook for cleaning without compromising the system functionality. We and the surgeons deemed the general robot architecture as satisfactory: the system installation and setup were performed in a relative short time (less than 15 minutes), and no

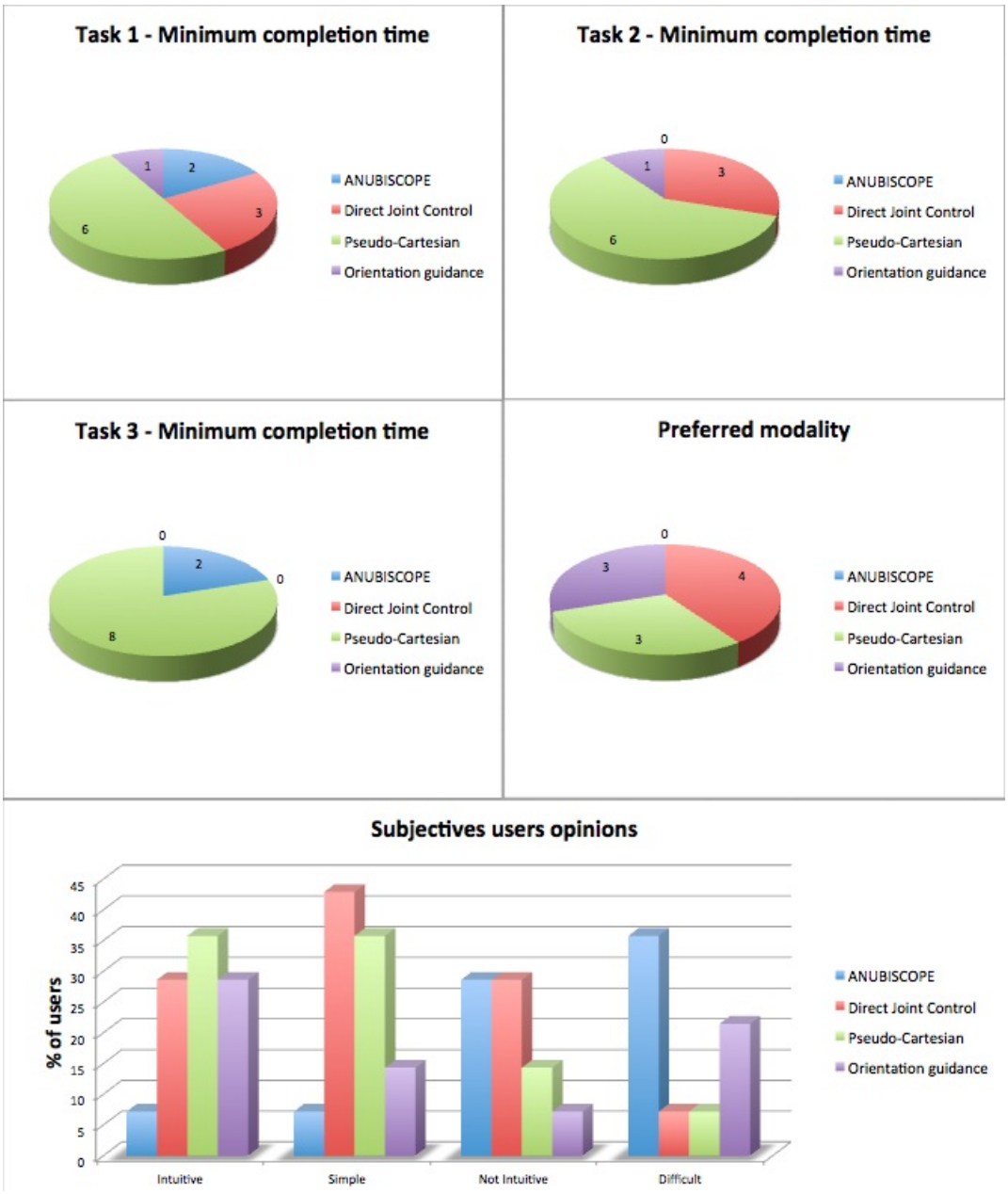

Fig. 6.10. Main results of the ANUBISCOPE-STRAS comparison. The Pseudo-Cartesian strategy gives the best execution times in all the proposed tasks, although it is not the preferred modality indicated by users. Actually, theirs preferences are almost equally shared, without a real predominant choice. Subjective users opinions show, instead, a general preference for STRAS because of the more intuitiveness and simplicity in use.

Fig. 6.11. Ex-vivo tests performed with STRAS. Top: surgical setup, with STRAS mounted on a operating bed and inserted inside a pig stomach. Bottom: user workstation during the tests; the left screen shows the endoscopic images, while the right screen displays the high-level control application and the robot informations.

particular problems were found in integrating our robot in the operating room environment. The robot supporting platform can be easily mounted at every side of the operating bed, thus being adaptable to different access ports. The compact size of the robotized instruments permitted a simple access to the endoscope control (insufflation and camera parameters), and their movements during the use do not represent a potential risk for the personnel who might be next to the robot. We are convinced that, with proper instrumentation, STRAS could be easily employed for a complete surgical operation.

6.4 Conclusions

In this chapter we presented the preliminary results we obtained with STRAS, both using its virtual simulator, in order to compare the proposed control strategies, and the real robot, to understand its real capabilities and to compare it to the ANUBISCOPE®, its manual counterpart. These first results did not highlight any unanimously preferred modality, pointing out the subjective preferences when choosing a control strategy. This could be considered as a first advantage of STRAS compared to the manual system: our robot can be adapted to different type of users, which could train more on the modalities they prefer. Another big achievement of STRAS consists in the possibility for a single user to control the whole slave robot: we demonstrated that a complex comanipulation task that involves all the slave subsystems can be performed without any additional assistance, in relatively short time and comfortably seated at the user workstation. We have experienced, therefore, that in our case robotics represented a real improvement in the use of a complex surgical platform, enhancing its capabilities and offering a better user experience.

7

Conclusions and perspectives

Conclusions

The next frontier in Minimally Invasive Surgery (MIS) is represented by *no-scar surgery*, which has the ambitious aim to avoid any visible scar on the patient skin after the operation. The increasing constraints introduced by this new approach require proper instruments, which must be able to pass from a narrow port, adaptable to the body anatomy but strong enough for reflecting forces on the tissues. Although in the last years several prototypes specifically developed for no-scar surgery have been introduced, their manual use is still laborious because of the complexity of their interfaces.

In this thesis we have introduced STRAS (Single access and Transluminal Robotic Assistant for Surgeons), the novel flexible robot for no-scar surgery developed in our laboratory. STRAS derives from the ANUBISCOPE® platform by Karl Storz GmbH (Tuttlingen, Germany). A shorter version of the ANUBISCOPE® was robotized, and in this process all its manual handles were substituted by servo actuators. The robotic architecture given to STRAS was the teleoperation scheme, and a master console consisting of two haptic interfaces, a pedal board and a high-level controller was designed in order to teleoperate the system.

Being flexible in its structure, STRAS cannot be kinematically described with the classical methods of robot kinematics: we used a specific formulation developed for continuum robots in order to compute its kinematic model. An effort was done in order to obtain the inverse kinematic model of the robot, which permits to compute all the joints configurations relative to a desired Cartesian position of the instruments.

We performed a fist numerical evaluation of the robot workspace, finding that the local instrument workspace can be approximated to an ellipsoid, which represents the surface that the instrument tip attains when using the deflection and the rotation articular movements (the ellipsoid is truncated at the base because of the deflection limits). When the instrument translation is involved, the local workspace is translated along the instrument axis, describing a cylinder with ellipsoidal caps. The cylinder represents the instrument global workspace, *i.e.* the area reachable by the instrument with its degrees of freedom. The two instruments

global workspaces intersect in a common central area, the cooperation workspace, in which comanipulation tasks involving both instruments are possible.

The singularity analysis showed the presence of two main singular positions: one located in correspondence of the instrument straight configuration, in which the instrument rotation does not involve a change in the tip position, while the other being located at the maximum extension of the workspace, which represent the farthest area reachable by the instrument on the XY plane. In both cases, the inverse differential kinematics becomes ill-conditioned, leading to the computation of high joints references. We have proposed two solutions for the singularity avoidance problem: the first consists in the Damped Least Square methods, which introduces a damping factor in the matrix inversion computation that takes account of the low magnitude of Jacobian inverse elements; the second method, more specific for the straight configuration singularity, consists in identifying a conical neighborhood of the singular position and, in that zone, computing the kinematic model with the configuration correspondent to the zone boundary. In this manner, a tracking error is introduced, but the uncontrolled movements of the instrument will be avoided.

The kinematics of master and slave systems are very different, therefore multiple mappings are possible to relate them. Concerning the slave robot, three main conceptual control schemes can be envisaged:

- an open-loop scheme, in which a Cartesian velocity reference is directly transformed in joints velocity reference with the inverse differential kinematic model;
- a closed-loop scheme with a joint control, in which the discrete inverse kinematic algorithm is exploited to compute the joints position references corresponding to the desired Cartesian positions;
- a closed-loop position scheme, in which the desired Cartesian position is compared with the actual robot position, and the computed error vector is then fed to the inverse differential kinematic model.

Beside these control schemes, which make use of the robot kinematic model, we have proposed three additional mappings that relate the slave robot DOFs with the motion of the haptic interfaces:

- Direct Axis control: each joint of the slave robot is directly controlled by a specific DOF of the master interfaces.
- Orientation guidance: the haptic interface movements are constrained to those the instrument can perform starting from the actual configuration, thus offering the sensation of controlling the instrument tip.
- Pseudo-Cartesian control: the master movements in the $X_M Y_M$ plane of the haptic interface determine the references for the instrument deflection and rotation, while the instrument translation is directly controlled by the interface movements in the Z_M direction.

The master interfaces architecture offers a good flexibility in use, but it results often redundant with respect to the task. For this reason, we used the force feedback effect provided by the interfaces to block (when possible) the unused DOFs and to guide the user gesture according to the chosen mapping.

We have also proposed to automate the movements of the endoscope, with the aim to auto-center the endoscopic image with respect to instruments, or to automatically expand the instruments workspaces with the endoscope motions. Moreover, the tree-like architecture of STRAS can lead to conflicting tasks between instruments when the user references diverge in opposite directions. In this case, a compromise solution could consist in assigning relative weights to instruments, thus computing an approximate solutions for both instruments, otherwise it is necessary to decide which instrument has the highest priority in case of conflicts.

In order to have a safe test environment in which assess the proposed mappings and control strategies, we developed a virtual simulator of STRAS. In its first version, the simulator was meant to be a kinematic replica of the real robot, including its main non-linearities and imperfections. With this simulator we performed some experiments in which we compared the behavior of STRAS against the different proposed strategies and we analyzed the effects of non-linearities. These experiments have shown that, with an ideal model, speed control permits to obtain better accuracy, while position control assures a faster system response. On the contrary, when the mechanical non-linearities are introduced inside the simulation, a position control strategy on the slave side, together with a direct mapping between the haptic interfaces and the instruments workspaces on the master side, permits to better compensate the non-linearities effects for the majority of people involved in the simulations. The force feedback effect applied on the haptic interfaces seems to play an important role in this case, because it allows to keep track between the interface and the instrument positions, thus avoiding large errors in the control scheme. Transferring these conclusions on the real system, this points out the need to estimate the instruments Cartesian positions with a proper sensor, rather than rely on the encoders position references, and to compute a kinematic model that takes account of the non-linearities effects.

The main limitation of the first version of the virtual simulator was the absence of a physical engine to manage the interactions between virtual objects, thus avoiding the possibility to perform standard exercises as peg transfers or simulated surgeries. We chosen, therefore, to develop a new version of the simulator that was capable of physical interactions. Three tasks that require complex instruments cooperation were implemented inside the simulator. We organized a test session with eight users, chosen according their previous experience with STRAS and with the virtual simulator. In this test session, we asked to execute the three proposed tasks with four different mappings (Direct Axis control, Orientation Guidance, Pseudo-Cartesian and Cartesian control) using an ideal model of the system. At the end of the test session, we found that a Cartesian modality gives better execution times for the majority of users, regardless of their previous experience. Anyway, the choice of a preferred modality largely depends on subjective preferences, and after a training period the outcomes with the different modalities tend to equalize, as it can be seen on the average with the most experienced users. Haptic interfaces largely influenced this evaluation: we found that the unused master DOFs can cause confusions in understanding the correct mapping, pointing out that a specific interface tailored for a particular mapping can improve the user experience and give better results.

Similar results were found during the experiments conducted with STRAS: a Cartesian control strategy is more natural for the most part of users and permits to obtain better results in terms of execution times. Moreover, the master interfaces architecture is too generic for every mapping, avoiding an immediate understanding of the requested movements. These common results give us a preliminary validation of our virtual simulator, showing that it represents a useful tool for assessment and training.

Finally, the direct comparison between STRAS and ANUBISCOPE® showed a users preference for the first, judged simpler and more intuitive than its manual counterpart. The big advantage of STRAS is that the whole system can be controlled by a single user, in an ergonomic way and with the possibility to choose among several control solutions.

Perspectives

At its current development phase, STRAS is a preliminary prototype created with the ambition of developing a flexible robotic platform for no-scar surgery. For the first prototype, the main choice during the robotization phase was to preserve as much as possible the original system components of the ANUBISCOPE®, in order to exploit its suitability for clinical use. After our tests and simulations, we found that several improvements can be proposed for both master and slave systems.

On the slave robot, the main mechanical issue is represented by the backlash, which compromises the deflection motion of the flexible sections. This effect is mainly due to the absence of pretension on the deflection cables: the deflection sliding actuator is common for both cables, but a change in the deflection sense would require a preliminary cable tensioning to be immediately transmitted to the distal flexible section. A solution to this issue could consist in controlling separately the two deflections cable by means of two different servo actuators that always keep the right tensions on cables. Such solution could largely compensate the backlash non-linearity that exists on our system, requiring less efforts on the kinematic modeling of mechanical imperfections.

As we noticed during *ex vivo* tests, new and better robotized instruments are necessary to extend the system capabilities. On our current prototype we dispose of one grasper and one electric hook only, but the availability of different graspers, scissors and dissectors will be an important factor when clinical *in vivo* tests will be performed. Moreover, specific needle-holders have to be developed to really figure out a complete clinical use of STRAS: with the current grasper is impossible to correctly manipulate a surgical needle, thus performing sutures.

Regarding the master system, several different tests have shown that a specific haptic interface designed for STRAS can largely improve the user experience, especially in the non-Cartesian modalities (Direct Axis control and Orientation guidance) where the interface movements reflect the instruments motions. For those who already had experience with the ANUBISCOPE® platform, it could be advantageous to propose a master interface which reproduces the instruments

handle. In this case, they could find the same control modality as with real instruments, but without deal with motion frictions and uncomfortable postures. Indeed, ergonomics would be greatly increased by the possibility, unlike manual instrumentation, to perform an interface repositioning when desired.

An important improvement could be also done on the slave robot support. Actually, endoscope and instruments are hosted on two different platforms that do not move together: this means that an endoscope translation, which is robotized in the actual prototype, is not followed by the instruments platform, which is statically fixed to its passive arm. This constrains the feasible motion of the endoscope because of the presence of instruments overtubes placed to avoid the folding of the instruments passive bodies. Arranging the whole slave robot on a single platform will permit to avoid this limitation. Moreover, it could be useful to provide a rotational movement to the whole platform, in order to robotically control the system orientation.

From the control point of view, a real advancement could be represented by the possibility to have a reliable sensor that could estimate the real robot position or the actual shapes of flexible sections. Our first tests with an electromagnetic tracker showed a poor measurements quality due to the presence of metallic parts. An alternative solution could be to use the endoscopic image in order to estimate the instruments positions. This solution is not feasible in some conditions, *e.g.* when instruments are out of the camera view or when reflections or smoke alter the image, but it could be a worthy track to be explored.

Finally, the dynamics of the second version of the virtual simulator has to be improved, in order to implement the mechanical imperfections of the real system. This will permit to obtain more valuable results and to subject users to cope with the real system reactions in a safe and replicable environment.

Waiting for a valid and universal *Gene therapy*, which has the ambitious aim to biologically heal pathologies from the inside of the body, *no-scar surgery* is the next frontier, partly reached but still not consolidated, in the minimization of the surgical invasiveness. What is still missing is mostly on the technological side: surgeons know how to perform operations, but they need the proper instrumentation. New materials, sensors and actuators need to be developed, or properly adapted for being implemented in surgical instrumentation, which has to be effective, but simple in use. Both requirements could be fulfilled thanks to robotics, which can offer, beside precision and accuracy, simpler and intuitive interfaces. It is opinion of the author that the LESS approach is actually the more feasible for the development of functional robotic instrumentation: compared to NOTES, the shorter lengths needed for instruments and the possibility to mix rigid and flexible parts can lead to more effective tools. STRAS is going toward this direction and, once the highlighted limitations will be solved, it could represent a valid surgical robot for abdominal and gastrointestinal LESS surgery.

Part II

Appendix and References

A

Kinematic models

A.1 Kinematic model $\mathbf{FK_{EB}}$

$$FK_{EB} = {}_{EB}\mathscr{T}^{IT} = {}_{EB}\mathscr{T}^{EH}\ {}_{EH}\mathscr{T}^{JH}\ {}_{JH}\mathscr{T}^{IB}\ {}_{IB}\mathscr{T}^{IH}\ {}_{IH}\mathscr{T}^{IT} \tag{A.1}$$

Transformation Endoscope Base → Endoscope Head ($\kappa_E \neq 0$)

${}_{EB}\mathscr{T}^{EH} =$

$$\begin{bmatrix} c^2(\phi_E)c(\kappa_E\ell_E - 1) + 1 & s(\phi_E)c(\phi_E)(c(\kappa_E\ell_E) - 1) & c(\phi_E)s(\kappa_E\ell_E) & \frac{c(\phi_E)(1-c(\kappa_E\ell_E))}{\kappa_E} \\ s(\phi_E)c(\phi_E)c(\kappa_E\ell_E - 1) & c^2(\phi_E)(1 - c(\kappa_E\ell_E)) + c(\kappa_E\ell_E) & s(\phi_E)s(\kappa_E\ell_E) & \frac{s(\phi_E)(1-c(\kappa_E\ell_E))}{\kappa_E} \\ -c(\phi_E)s(\kappa_E\ell_E) & -s(\phi_E)s(\kappa_E\ell_E) & c(\kappa_E\ell_E) & \frac{s(\kappa_E\ell_E))}{\kappa_E} \\ 0 & 0 & 0 & 1 \end{bmatrix} \tag{A.2}$$

Parameters:

- κ_E: curvature of the endoscope actuated section;
- ϕ_E: rotation of the endoscope actuated section;
- ℓ_E: length of the endoscope actuated section.

Transformation Endoscope Base → Endoscope Head ($\kappa_E = 0$)

$$ {}_{EB}\mathscr{T}^{EH} = \begin{bmatrix} 1 & 0 & 0 & 0 \\ 0 & 1 & 0 & 0 \\ 0 & 0 & 1 & \ell_E \\ 0 & 0 & 0 & 1 \end{bmatrix} \tag{A.3}$$

Parameters:

- ℓ_E: length of the endoscope actuated section.

Transformation Endoscope Head → Jaw Head

$$
{}_{EH}\mathscr{T}^{JH} =
$$

$$
\begin{bmatrix}
c(\psi)c(\gamma) - s(\psi)s(\gamma) & 0 & c(\psi)s(\gamma) + s(\psi)c(\gamma) & -2.69\, c(\psi)c(\alpha) + 17.56\, s(\psi) + 6.80\, c(\alpha) \\
0 & 1 & 0 & -1.42 \\
-s(\psi)c(\gamma) - c(\psi)s(\gamma) & 0 & c(\psi)c(\gamma) - s(\psi)s(\gamma) & 2.69\, s(\psi)c(\alpha) + 11.39 + 17.56\, c(\psi) \\
0 & 0 & 0 & 1
\end{bmatrix}
\tag{A.4}
$$

Parameters:

- α: 0 for left instrument, π for right instrument;
- γ: -25° = -04361 rad for left instrument, +25° = 0.4361 rad for right instrument;
- ψ: jaws angle, positive for left instrument, negative for right instrument.

Transformation Jaw Head → Instrument Base

$$
{}_{JH}\mathscr{T}^{IB} = \begin{bmatrix}
\cos(\phi_I) & -\sin(\phi_I) & 0 & 0 \\
\sin(\phi_I) & \cos(\phi_I) & 0 & 0 \\
0 & 0 & 1 & t_I \\
0 & 0 & 0 & 1
\end{bmatrix}
\tag{A.5}
$$

Parameters:

- ϕ_I: instrument rotation;
- t_I: instrument translation.

Transformation Instrument Base → Instrument Head ($\kappa_I \neq 0$)

$$
{}_{IB}\mathscr{T}^{IH} = \begin{bmatrix}
\cos(\kappa_I \ell_I) & 0 & \sin(\kappa_I \ell_I) & \frac{1-\cos(\kappa_I \ell_I)}{\kappa_I} \\
0 & 1 & 0 & 0 \\
-\sin(\kappa_I \ell_I) & 0 & \cos(\kappa_I \ell_I) & \frac{\sin(\kappa_I \ell_I)}{\kappa_I} \\
0 & 0 & 0 & 1
\end{bmatrix}
\tag{A.6}
$$

Parameters:

- κ_I: curvature of the instrument flexible section;
- ℓ_I: length of the instrument flexible section.

Transformation Instrument Base → Instrument Head ($\kappa_I = 0$)

$$
{}_{IB}\mathscr{T}^{IH} = \begin{bmatrix}
1 & 0 & 0 & 0 \\
0 & 1 & 0 & 0 \\
0 & 0 & 1 & \ell_I \\
0 & 0 & 0 & 1
\end{bmatrix}
\tag{A.7}
$$

Parameters:

- ℓ_I: length of the instrument flexible section.

Transformation Instrument Head → Instrument Tip

$$ {}_{IB}\mathscr{T}^{IH} = \begin{bmatrix} 1 & 0 & 0 & 0 \\ 0 & 1 & 0 & 0 \\ 0 & 0 & 1 & d_{HT} \\ 0 & 0 & 0 & 1 \end{bmatrix} \tag{A.8} $$

Parameters:

- d_{HT}: length of the rigid tool.

A.2 Kinematic model FK$_C$

$$ FK_C = {}_{C}\mathscr{T}^{IT} = {}_{C}\mathscr{T}^{JH}\ {}_{JH}\mathscr{T}^{IB}\ {}_{IB}\mathscr{T}^{IH}\ {}_{IH}\mathscr{T}^{IT} \tag{A.9} $$

Transformation Camera → Jaw Head

$$ {}_{C}\mathscr{T}^{JH} = $$

$$ \begin{bmatrix} -c(\psi)c(\gamma) + s(\psi)s(\gamma) & 0 & -s(\psi)c(\gamma) - c(\psi)s(\gamma) & 2.69\, c(\psi)c(\alpha) - 17.56\, s(\psi) - 6.80\, c(\alpha) \\ 0 & -1 & 0 & 6.22 \\ -s(\psi)c(\gamma) - c(\psi)s(\gamma) & 0 & c(\psi)c(\gamma) - s(\psi)sin(\gamma) & 2.69\, s(\psi)c(\alpha) - 15.44 + 17.56\, c(\psi) \\ 0 & 0 & 0 & 1 \end{bmatrix} \tag{A.10} $$

Parameters:

- α: 0 for left instrument, π for right instrument;
- γ: -25° = -04361 rad for left instrument, +25° = 0.4361 rad for right instrument;
- ψ: jaws angle, positive for left instrument, negative for right instrument.

B

Abstract in French

Développement et contrôle d'un systeme robotique pour la chirurgie sans cicatrice

Contents

B.1 Contexte médical

Après une longue période d'expérimentations et de scepticisme entre la fin des années 1980 et le début des années 1990, la chirurgie mini-invasive (CMI) est aujourd'hui le standard *de facto* pour les procédures chirurgicales. Les avantages d'une approche mini-invasive sont nombreux, principalement axés sur le patient. A la différence de la chirurgie dite « ouverte » (ou *laparotomie*), les interventions équivalentes laparoscopiques réduisent le traumatisme causé par les cicatrices, diminuent le volume de sang perdu pendant l'opération, réduisent la douleur post-opératoire liée à la cicatrisation et permettent une hospitalisation plus courte, ainsi qu'une réhabilitation plus rapide. En revanche, les procédures de CMI forcent les chirurgiens à faire face à de nouvelles contraintes. Le contact direct entre chirurgien et patient disparaît, et la palpation manuelle des organes et des tissus est remplacée par leur manipulation à l'aide d'instruments. De plus, la vision des structures anatomiques est réalisée avec des images bidimensionnelles, capturées

par une caméra miniaturisée insérée à l'intérieur du corps et retransmises sur un écran.

Aujourd'hui la chirurgie sans cicatrice (*no-scar surgery* en anglais) représente l'avant-garde dans le domaine de la CMI. Elle a pour but de permettre aux chirurgiens d'opérer sans laisser de cicatrices visibles. Cette nouvelle technique inclut deux approches (voir fig. B.1) :

- NOTES (Natural Orifice Transluminal Endoscopic Surgery), dans laquelle les orifices naturels sont exploités comme des portes d'accès du corps humain ; dans ce cas, il n'y a pas d'incisions externes sur la peau du patient, et la seule cicatrice est à l'intérieur du corps.
- LESS (Laparo-Endoscopic Single-site Surgery), dans laquelle les instruments chirurgicaux sont insérés dans le corps du patient par une porte d'accès commune, choisie dans une zone cachée du corps (typiquement le nombril) de telle manière que la cicatrice n'est pas visible après l'opération.

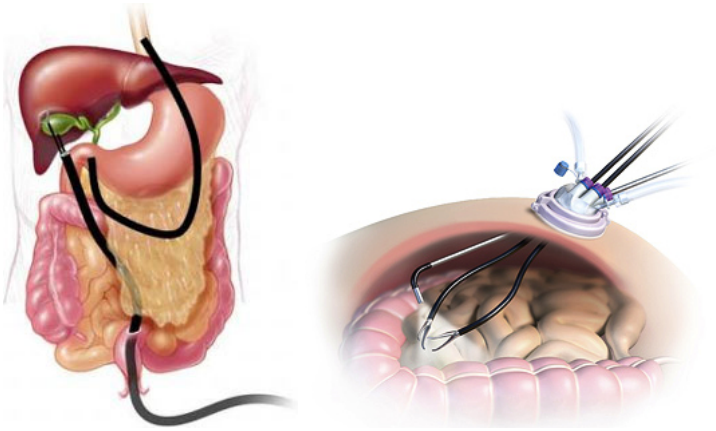

Fig. B.1. Approches NOTES (gauche) et LESS (droite) dans la chirurgie sans cicatrice.

Par rapport à la laparoscopie standard, ces deux approches impliquent un avantage supplémentaire pour le patient, qui consiste en un meilleur résultat esthétique après l'opération. Par contre, les nouvelles contraintes imposées afin de minimiser le caractère invasif de l'opération chirurgicale rendent son exécution plus difficile. La triangulation, la dextérité et la taille des instruments sont en grande partie limitées par la seule porte d'accès, qu'elle soit transluminale ou non. Une nouvelle instrumentation est donc nécessaire afin de surmonter, en partie ou intégralement, les contraintes d'accès liées à cette technique particulière. Idéalement, les instruments parfaits pour la chirurgie sans cicatrice devraient être en mesure de passer par une porte étroite, atteindre le point cible (qui pourrait être situé à des dizaines de centimètres de l'orifice d'accès), puis se reconfigurer pour exécuter l'opération. Cela implique des compromis : tout d'abord, les instruments doivent être aussi flexibles que nécessaire pour adapter leur forme aux contraintes anatomiques, mais

suffisamment rigides pour transmettre correctement les forces. De plus, en fonction de la porte d'accès choisie, les longueurs des instruments pourraient varier et être plus longues que celles des instruments de laparoscopie (en particulier dans les opérations transluminales). Il est donc necessaire d'utiliser un actionnement approprié, capable de transférer de manière transparente les mouvements de l'utilisateur aux instruments. La dextérité pourrait être améliorée en utilisant des sections flexibles pour les instruments. Le but étant d'obtenir des outils adaptables à des environnements tortueux.

La robotique peut apporter de nombreux avantages en chirurgie : par rapport à une procédure manuelle, la même tâche effectuée grâce à l'assistance d'un système robotique peut être réalisée avec de meilleures précision, répétitivité et ergonomie. Un robot chirurgical pourrait intervenir de multiples façons pendant une intervention. Tout d'abord, il peut guider les mains du chirurgien afin d'éviter les mouvements des outils dans les zones considérées comme dangereuses. L'interface entre le chirurgien et les instruments peut permettre de filtrer les mouvements des mains du chirurgien, en compensant leurs tremblement naturel et en réduisant ou en amplifiant le geste pour une meilleure dextérité. En revanche, un système robotique chirurgical doit être de taille convenable afin d'être adapté à l'environnement de la salle opératoire, il ne doit pas constituer un risque pour les physiciens et pour le patient et il doit toujours pouvoir être retiré en toute sécurité en cas d'urgence.

B.2 STRAS : Single access and Transluminal Robotic Assistant for Surgeons

Dans ce contexte, nous proposons un nouveau robot flexible, appelé STRAS (Single access and Transluminal Robotic Assistant for Surgeons), spécifiquement développé pour la chirurgie LESS et pour les opérations transluminales proches (voir fig. B.2). STRAS est un guide endoscopique, basée sur le système Anubiscope produit par Karl Storz GmbH (Tüttlingen, Allemagne), qui permet d'introduire deux instruments flexibles (une pince et un crochet électrique) à l'intérieur du corps en passant par une porte d'accès unique.

L'endoscope et les deux instruments sont équipés de parties articulées distales qui permettent leur déflexion, augmentant ainsi l'espace de travail du système et obtenant une meilleure dextérité. Les instruments sont insérés à l'intérieur de l'endoscope principal de son côté proximal et, grâces à deux volets pliables mises en oeuvre au niveau de la tête de l'endoscope, leurs canaux sont déviés côté distal afin d'obtenir une triangulation. STRAS dispose d'un total de 10 Degrés De Liberté (DDL) actionnés, organisés comme suit :

- 3 DDL de l'endoscope principal, qui peut avancer et reculer, et sa section distale peut être pliée dans deux directions orthogonales ;
- 3 DDL pour chaque instrument, qui peut translater, tourner et plier dans une direction ;
- 1 DDL supplémentaire pour l'ouverture et la fermeture de la pince.

Étant donné que STRAS a une architecture arborescente, la position des instruments dépend également des mouvements de l'endoscope. La présence de

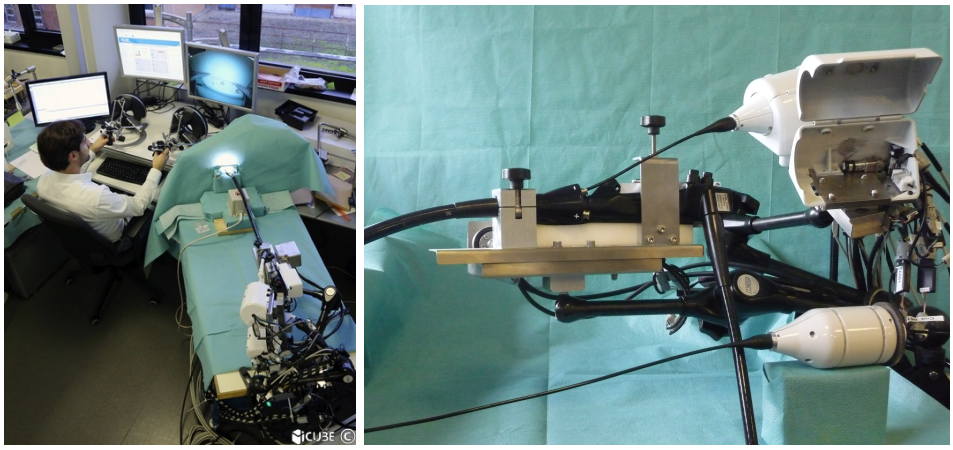

Fig. B.2. Vue d'ensemble de STRAS (gauche) et détails du robot esclave (droite).

sections flexibles dans la structure du robot ne permet pas une description de sa cinématique avec des méthodes classiques de la robotique. Une modélisation spécifique devrait donc être adoptée. Nous avons développé STRAS comme un robot téléopéré, dans lequel l'endoscope et les instruments robotisés sont le système esclave (voir fig. B.2). L'interface-maître est composée de deux interfaces haptiques avec 7 DDL chacune. Par conséquent, la première problématique consiste à trouver un mappage approprié entre les systèmes maître et esclave, car ils ont des cinématiques différentes. Cette problématique est étroitement liée au choix d'une stratégie de contrôle pour le robot esclave, c'est-à-dire la loi de commande qui permet de transformer les références souhaitées, données par l'utilisateur au moyen des interfaces maîtres, dans les références de bas niveau pour les actionneurs du robot. Plusieurs choix de mappages et stratégies de contrôle sont possibles, elles dépendent de l'application spécifique et de la préférence personnelle de l'utilisateur.

B.3 Cinématique

La convention de Denavit-Hartenberg, utilisée en robotique pour décrire cinématiquement un manipulateur série, fait l'hypothèse de liaisons rigides et d'articulations standards. Elle n'offre donc pas une représentation valide pour les robots flexibles. Une approche simplificatrice qui conduit à des résultats valides consiste à approcher la section continue par une série d'arcs à courbure constante. Cette méthode, appelée « piecewise constant curvature kinematics » (cinématique de courbure constante par morceaux), considère que la section continue est composée d'un nombre fini de liens courbés, chacun décrit par un ensemble fini de paramètres : la courbure κ, l'orientation ϕ du plan contenant l'arc et la longueur de l'arc ℓ (voir fig. B.3).

De cette manière, il est possible de représenter la partie flexible au moyen d'une transformation rigide entre un repère situé à la base de la section continue et le correspondant situé au sommet :

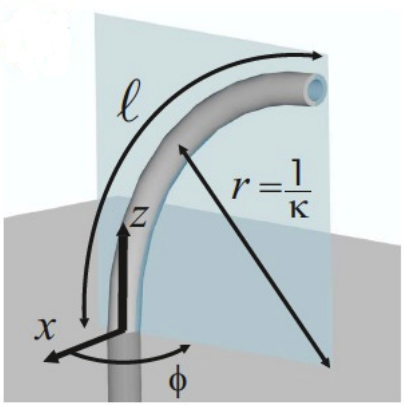

Fig. B.3. Notations pour la description cinématique d'un arc flexible.

$$\mathscr{T}_{FS} = \begin{bmatrix} \cos(\phi)\cos(\kappa\ell) & -\sin(\phi) & \cos(\phi)\sin(\kappa\ell) & \frac{\cos(\phi)(1-\cos(\kappa\ell))}{\kappa} \\ \sin(\phi)\cos(\kappa\ell) & \cos(\phi) & \sin(\phi)\sin(\kappa\ell) & \frac{\sin(\phi)(1-\cos(\kappa\ell))}{\kappa} \\ -\sin(\kappa\ell) & 0 & \cos(\kappa\ell) & \frac{\sin(\kappa\ell)}{\kappa} \\ 0 & 0 & 0 & 1 \end{bmatrix} \tag{B.1}$$

Pour obtenir le modèle cinématique direct du robot, qui permet de calculer la position Cartésienne des instruments par rapport à un repère fixe de base, il faut calculer la transformation globale entre les repères internes identifiés sur le système. Nous avons défini cinq repères principaux pour l'endoscope :

1. « Endoscope Base » (noté F_{EB}, voir fig. B.4), situé à la base de la partie flexible actionnée de l'endoscope.
2. « Endoscope Head » (noté F_{EH}, voir fig. B.4), situé au sommet de la partie flexible actionnée de l'endoscope.
3. « Camera » (noté F_{C}, voir fig. B.4), situé en correspondance de la camera endoscopique.
4. « Left and Right Jaws Heads » (pour des raisons de clarté, dans la fig. B.4 uniquement le repère de droite est reporté, noté F_{JH}), situés en correspondance des sorties des canaux qui contiennent les instruments.

Par ailleurs, trois repères sont identifiés pour chaque instrument :

1. « Instrument Base » (noté F_{IB}, voir fig. B.4), situé à la base de la partie flexible actionnée de l'instrument.
2. « Instrument Head » (noté F_{IH}, voir fig. B.4), situé au sommet de la partie flexible actionnée de l'instrument.
3. « Instrument Tip » (noté F_{IT}, voir fig. B.4), situé au sommet de l'outil.

Comme anticipé dans la partie B.2, globalement STRAS a 10 DDL (voir fig. B.5) :

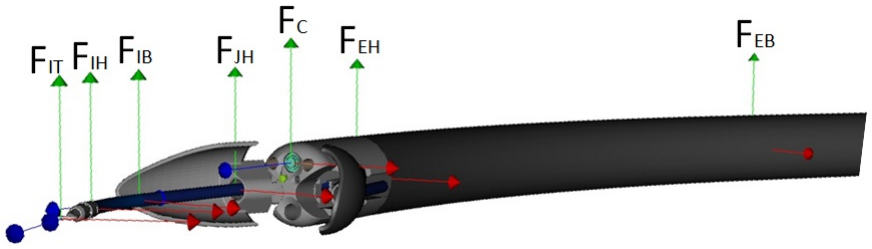

Fig. B.4. Repères principaux de STRAS.

- 3 DDL de l'endoscope : translation longitudinale t_E (notée 1, voir fig. B.5) et deux déflexions orthogonales dx et dy (notées 2 et 3, voir fig. B.5) ;
- 3 DDL pour chaque instrument : translation longitudinale t_I (notée 4, voir fig. B.5), rotation θ_I (notée 5, voir fig. B.5) et déflexion β (notée 6, voir fig. B.5) ;
- un DDL supplémentaire pour l'ouverture et la fermeture des instruments actionnés comme la pince (noté 7, voir fig. B.5).

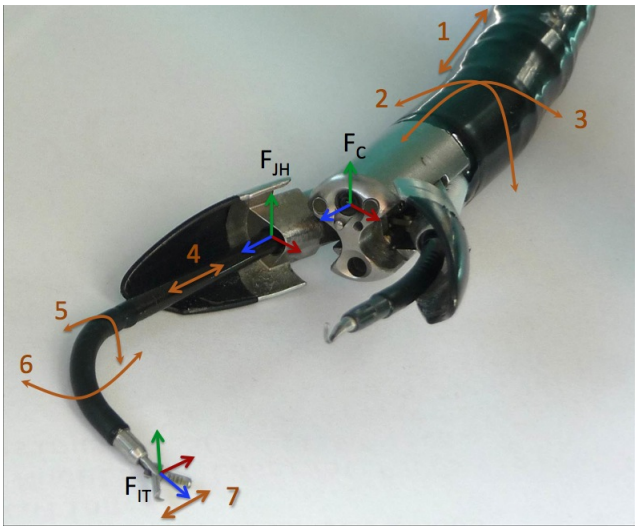

Fig. B.5. Degrés de liberté de STRAS.

Une étude numérique de l'espace de travail du robot a montré que chaque instrument couvre une surface ellipsoïdale en utilisant uniquement les mouvements de déflexion et rotation. Quand l'instrument est translaté, la surface ellipsoïdale est déplacée d'une façon rigide dans l'espace pour former un cylindre (voir fig. B.6). Les espaces de travail des deux instruments se croisent dans une zone centrale commune qui a une forme conique. Cette zone a une extension maximale située 25 mm devant la caméra endoscopique (voir fig. B.6).

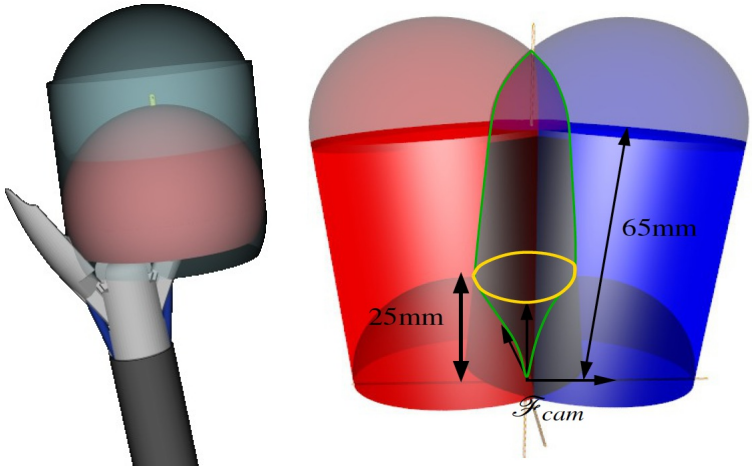

Fig. B.6. Espace de travail de STRAS.

À partir du modèle géométrique direct, il est possible de calculer la matrice Jacobienne du robot qui représente la relation entre les vitesses Cartésiennes et articulaires. Le Jacobien complet du robot est une matrice avec 6 lignes (les 6 composantes Cartésiennes) et 9 colonnes (les DDL du système à l'exclusion de l'ouverture et fermeture de la pince). Étant donné que STRAS a une structure arborescente, un mouvement de l'endoscope affecte la position des deux instruments en même temps. L'endoscope est donc principalement utilisé pour le positionnement initial. De plus, les instruments n'ont que 3 DDL chacun, ce qui veut dire que leurs orientations dans l'espace Cartésien sont déterminées par leurs positions. Par conséquent, il peut être utile de simplifier le calcul du Jacobien considérant chaque instrument séparément : le Jacobien relatif à un instrument est une matrice 3 x 3 de la forme

$$J_I(\boldsymbol{q}_I) = \begin{bmatrix} \frac{\partial X}{\partial \beta} & -Y & 0 \\ \frac{\partial Y}{\partial \beta} & X & 0 \\ \frac{\partial Z}{\partial \beta} & 0 & 1 \end{bmatrix} \tag{B.2}$$

avec :

$$\boldsymbol{q}_I = \begin{bmatrix} \beta & \phi & t_I \end{bmatrix}^T \tag{B.3}$$

et

$$\begin{bmatrix} X \\ Y \\ Z \end{bmatrix} =_{JH} T^{IT} = \begin{bmatrix} d_{HT}\cos(\phi)\sin(\beta) + \frac{\ell\cos(\phi)(1-\cos(\beta))}{\beta} \\ d_{HT}\sin(\phi)\sin(\beta) + \frac{\ell\sin(\phi)(1-\cos(\beta))}{\beta} \\ d_{HT}\cos(\beta) + t_I + \frac{\ell\sin(\beta)}{\beta} \end{bmatrix} \tag{B.4}$$

où d_{HT} est la longueur de l'outil rigide attaché au bout de la partie flexible de l'instrument.

Avec cette formulation du Jacobien il est possible de trouver la position des singularités dans l'espace de travail de l'instrument en calculant le déterminant : dans chaque position singulière sa valeur est égale à zéro.

Notamment, dans l'espace de travail de chaque instrument on peut retrouver deux singularités (voir fig. B.7) :

- en correspondance d'une valeur de déflexion égale à zéro, la rotation propre de l'instrument n'a aucun effet sur la position Cartésienne de l'outil ;
- en correspondance du diamètre de l'ellipsoïde qui représente l'espace de travail de l'instrument, le bout de l'instrument se trouve à la distance maximale de l'axe central de l'instrument ; dans cette situation, aucun mouvement sur le plan XY peut être fait sans utiliser les DDL de l'endoscope.

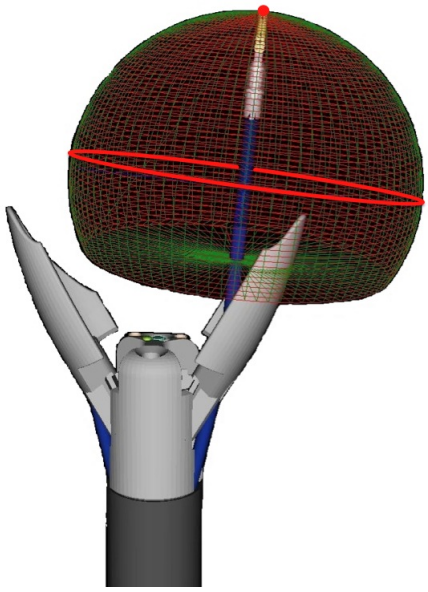

Fig. B.7. Positions des singularités dans l'espace de travail de l'instrument.

B.4 Téléopération

STRAS a été développé sous forme de robot téléopéré, c'est-à-dire d'un système mécatronique esclave commandé par une interface-maître. Le système esclave est composé d'un endoscope et d'instruments robotisés, présentés dans la partie B.2 (voir fig. B.2). Il y a plusieurs possibilités de contrôle pour ce système :

- Contrôle en vitesse en boucle ouverte (voir fig. B.8) : l'entrée de l'utilisateur est exprimée comme une référence de vitesse Ω_{ref}, qui est directement multipliée par l'inverse du Jacobien J^{-1} pour obtenir les références de vitesse articulaire $\dot{q}_{ref}$.

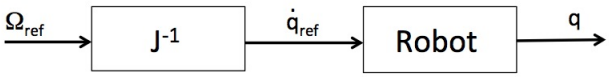

Fig. B.8. Schéma de contrôle en vitesse en boucle ouverte.

- Contrôle articulaire en boucle fermée (voir fig. B.9) : avec l'inversion du modèle géométrique direct il est possible de calculer les références de positions articulaires qui permettent d'atteindre une position Cartésienne désirée. Dans ce cas l'utilisateur donne une référence de position X_{ref}, le modèle géométrique inverse fourni la configuration articulaire q_{ref} correspondante qui est comparée avec l'état actuel du robot, afin d'obtenir une erreur de positionnement articulaire e.

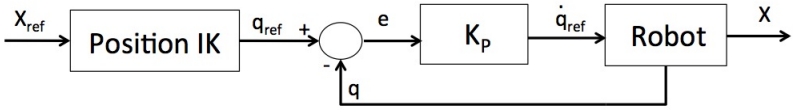

Fig. B.9. Schéma de contrôle articulaire en boucle fermée.

- Contrôle en position en boucle fermée (voir fig. B.10) : l'entrée de l'utilisateur, exprimée comme une position de référence Cartésienne X_{ref}, est comparée à la positionne Cartésienne estimée du robot et une erreur e est calculée. L'estimation peut être obtenue en utilisant le modèle géométrique direct du robot ou un capteur externe, qui peut typiquement exploiter des propriétés électromagnétiques, optiques ou inertielles.

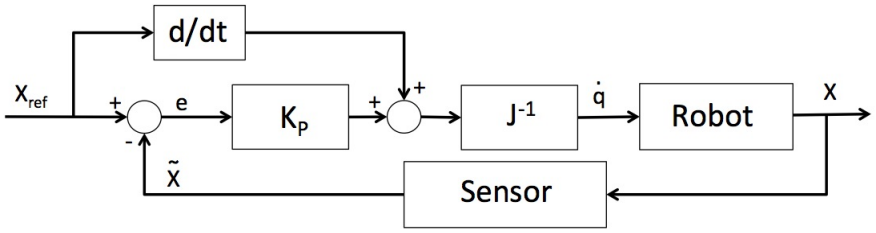

Fig. B.10. Schéma de contrôle en position en boucle fermée.

L'interface-maître de STRAS se compose de deux interfaces haptiques omega.7 (Force Dimension, Nyon, Suisse), qui fournissent 7 DDL chacune : 3 translations, 3 rotations et une gâchette (voir fig. B.11).

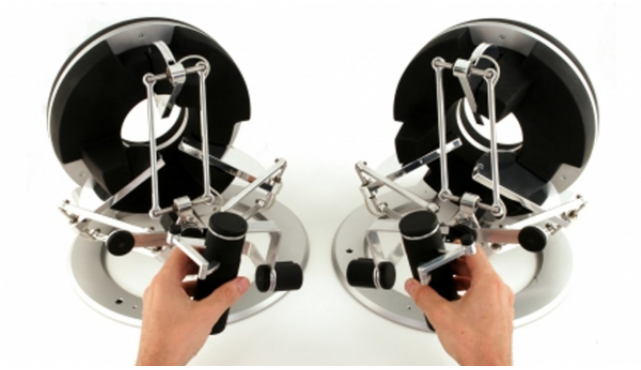

Fig. B.11. Interfaces haptiques omega.7 de Force Dimension.

Les systèmes maître et esclave ont des structures cinématiques complètement différentes: du côté maître 14 DDL sont disponibles, tandis que le robot esclave offre 10 DDL, donc un mappage adéquat entre eux doit être mis en place. En outre, les deux interfaces haptiques doivent contrôler les trois sous-systèmes esclaves pour permettre à un seul utilisateur de faire fonctionner le robot entier. La solution que nous avons adoptée pour résoudre ce problème consiste à assigner le contrôle de l'instrument gauche à l'interface gauche et de l'instrument droit à l'interface droite. Quand un mouvement de l'endoscope est requis, la pression d'une pédale permet de contrôler l'endoscope avec une des interfaces.

Pour notre robot, nous proposons quatre mappages différents :

1. « Direct joint control » : chaque articulation du système esclave est directement contrôlée par un mouvement élémentaire de l'interface-maître. Le but de cette modalité est de reproduire une expérience de manipulation proche au système manuel Anubiscope tout en évitant les effets indésirables, comme le ressenti des frottements de l'actionnement et la mauvaise ergonomie. Dans ce mappage un sous-ensemble des degrés de liberté de l'interface-maître est utilisé : la gâchette, la translation selon Z t_Z et la rotation autour de Z θ_Z contrôlent respectivement la déflexion, la translation et la rotation de l'instrument (voir fig. B.12).
2. « Orientation guidance » : cette modalité offre une sorte de contrôle articulaire où les mouvements de l'interface-maître sont limités à ceux de l'instrument à partir de la configuration actuelle. Comme dans le mappage « Direct joint control », la rotation de l'interface θ_Z contrôle la rotation de l'instrument. En revanche, la référence pour la déflexion de l'instrument est donnée par la poignée de l'interface haptique. Les mouvements de celle-ci sont limités sur une ligne droite, qui passe à travers la position centrale de l'interface, dans le plan $X_M Y_M$ (voir fig. B.13). Étant donné que l'orientation de la poignée est alignée avec celle de l'instrument, la ligne droite représente la trajectoire, projetée sur un plan, que l'instrument parcourt lorsque sa déflexion change.
3. « Cartesian control » : le contrôle cartésien de STRAS peut être réalisé soit en utilisant le modèle géométrique inverse ou le Jacobien du système (voir figs. B.9 et B.10). Dans les deux cas, les références de l'utilisateur sont représentées

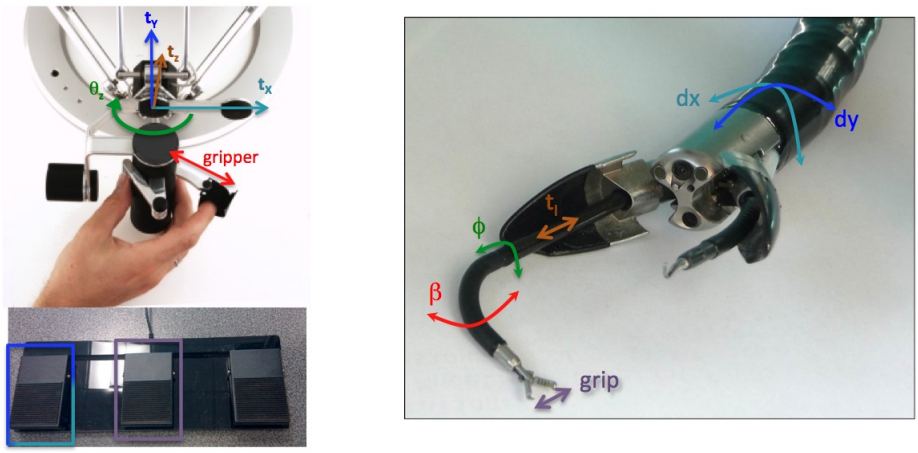

Fig. B.12. Mappage ≪ Direct joint control ≫.

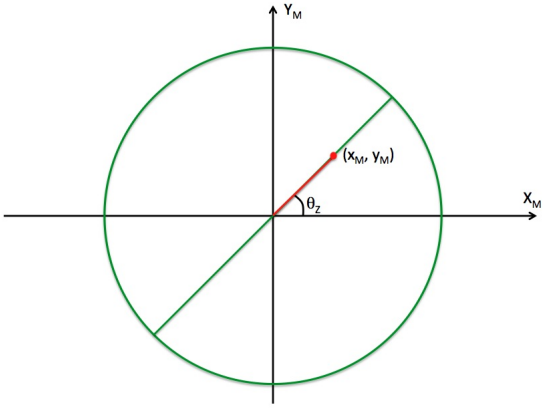

Fig. B.13. Mappage ≪ Orientation guidance ≫.

par des positions Cartésiennes souhaitées pour les instruments. Elle sont transmises par les translations des deux manettes de l'interface-maître.

4. ≪ Pseudo-Cartesian control ≫ : nommé "Pseudo" car elle donne à peu près les mêmes sensations de contrôle qu'une stratégie Cartésienne, cette modalité n'utilise pas un modèle cinématique pour commander le système. Dans cette stratégie, les mouvements de l'interface-maître dans le plan $X_M Y_M$ contrôlent en même temps la déflexion et la rotation des instruments, tandis que la translation t_Z le long de Z de l'interface haptique contrôle directement la translation de l'instrument (voir fig. B.14) :

$$\phi = \arctan 2(y_M,\, x_M) \tag{B.5}$$

$$t_I = z_M \tag{B.6}$$

$$\beta = \lambda \sqrt{x_M^2 + y_M^2} \tag{B.7}$$

où (x_M, y_M, z_M) est la position courante de la manette de l'interface, et λ est un facteur d'échelle qui adapte l'espace de travail de l'interface à celui de l'instrument.

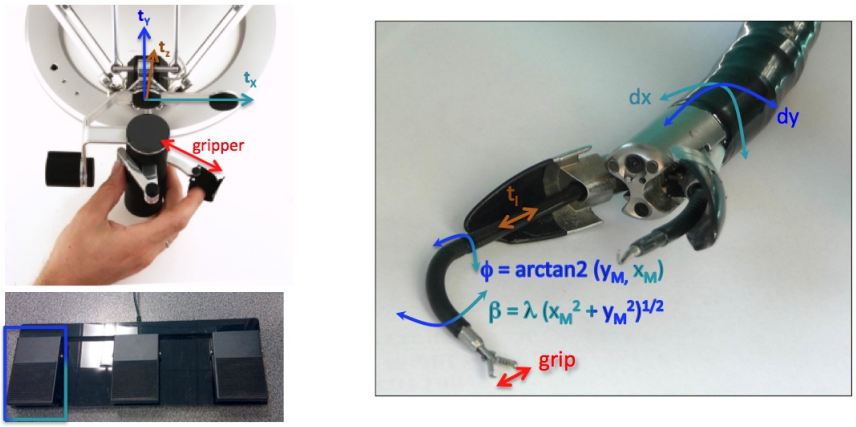

Fig. B.14. Mappage ≪ Pseudo-Cartesian control ≫.

Les quatre mappages proposés ne permettent pas d'exploiter la totalité des degrés de liberté que ce système nous offre, puisque chaque sous-système du robot esclave est contrôlé directement par l'utilisateur et les références calculées pour un instrument ne tiennent pas compte de la position de l'autre instrument. En outre, l'endoscope est activé uniquement lorsqu'un repositionnement de la caméra ou des instruments est nécessaire. Afin d'exploiter toute la mobilité de STRAS de manière coordonnée, un modèle de l'ensemble du système est nécessaire. Le Jacobien est une solution commune en robotique pour résoudre le problème géométrique inverse en terme de vitesse. Dans le cas d'une matrice rectangulaire et lorsque le système n'est pas en position singulière, la matrice Jacobienne inverse $J^{\#}$ peut être calculée avec la formule de la pseudo-inverse de Moore-Penrose :

$$J^{\#} = J^T (J J^T)^{-1}. \tag{B.8}$$

Contrairement aux manipulateurs robotiques standards qui ont un seul organe terminal à contrôler, STRAS a une structure arborescente avec deux organes terminaux différents. Cette structure implique qu'un mouvement de l'endoscope affecte la position des deux instruments. De plus, il pourrait y avoir un conflit entre les tâches assignées aux instruments, notamment quand un mouvement de l'endoscope est nécessaire. Nous avons essayé d'explorer plusieurs solutions différentes à ce problème :

- **Repositionnement automatique de l'endoscope** : puisque le champ de vision de la camera endoscopique ne contient pas complètement l'espace de travail des instruments, un mouvement de l'endoscope peut être requis quand un instrument sort de l'image. Mais étant donné que les instruments sont solidaires de l'endoscope, leurs positions absolues seraient affectées dans le cas où seuls les degrés de liberté de l'endoscope sont utilisés. Une solution à ce problème serait de recalculer une configuration articulaire en utilisant le modèle cinématique inverse qui prenne en compte la totalité des DDL du système.
- **Matrice de pondération** : dans le cas de tâches conflictuelles entre les instruments, une solution de compromis consiste à assigner des poids relatifs aux instruments. De cette manière, l'instrument qui a le poids le plus élevé sera privilégié dans le calcul de la solution finale qui, dans tous les cas, ne satisfera pas complètement toutes les tâches.
- **Tâche prioritaire** : plutôt que d'assigner des poids relatifs, une autre solution pour résoudre un conflit entre tâches consiste à indiquer la tâche qui a la priorité principale et qui, par conséquent, doit absolument être réalisée. Une fois que la première tâche est réalisée, on essaie de procéder à l'exécution de la deuxième sans affecter la position de l'instrument à priorité plus élevée. Ceci est possible en exploitant la redondance du système ou les degrés de liberté non utilisés au cours de la première tâche.

B.5 Simulateur virtuel

La simulation virtuelle est une technique qui consiste à utiliser des systèmes informatiques pour créer des mondes synthétiques. Il y a de nombreux avantages à l'utilisation de la simulation virtuelle en chirurgie, notamment la possibilité pour un chirurgien débutant de s'entraîner sur des tâches de base, ou même de simuler des opérations complexes en évaluant les gestes chirurgicaux. Si pour la laparoscopie plusieurs simulateurs commerciaux existent, des difficultés liées à la spécificité des instruments et à la complexité des opérations ont empêché jusqu'à présent la disponibilité de tels simulateurs pour la technique de chirurgie sans cicatrice.

L'idée de développer un simulateur virtuel de STRAS a déjà été proposée au début du projet : l'objectif était d'avoir une reproduction cinématique virtuelle du robot avec laquelle tester les stratégies de contrôle. Un des avantages de cette approche est la possibilité de tester soit le modèle théorique du système, soit de simuler des non-linéarités qui affectent le robot. De cette manière, on peut étudier séparément l'effet des non-linéarités et voir en même temps les réactions de l'utilisateur par rapport aux différentes stratégies de contrôle. Par conséquent, une première version du simulateur a été développée (voir fig. B.15) en utilisant le langage C# et la bibliothèque graphique VtkDotNet, un wrapper non-officiel du Visualization Toolkit (VTK) de Kitware.

La fenêtre principale du simulateur contient les contrôles pour interagir avec les degrés de libertés du robot, et également pour accéder à toutes les fonctionnalités de l'application. Deux modalités visuelles sont disponibles (voir fig. B.16) : la *vue externe*, qui permet de voir le modèle 3D du robot d'une perspective externe, et la

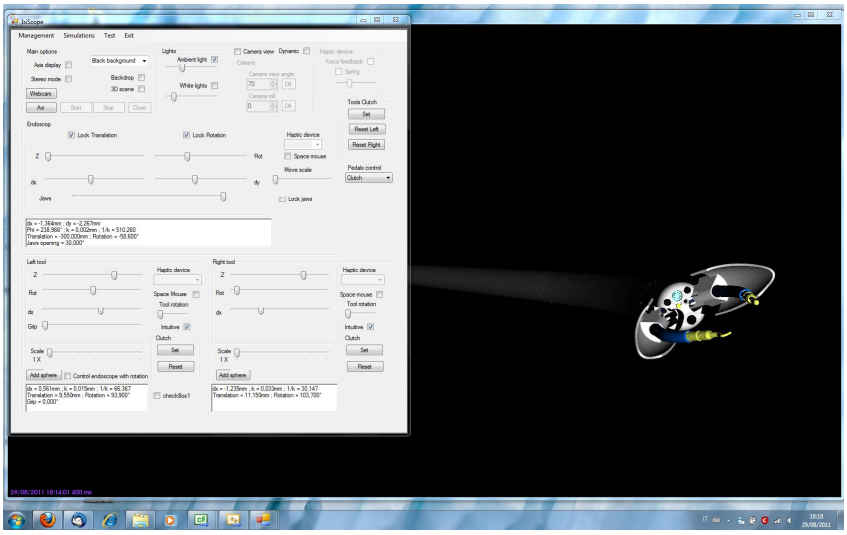

Fig. B.15. Première version du simulateur virtuel de STRAS.

vue caméra, qui reproduit l'image endoscopique provenant de la caméra embarquée dans la tête de l'endoscope.

Comme pour le système réel, le simulateur communique avec les interfaces haptiques afin de recevoir les consignes de l'utilisateur : en fonction de la stratégie choisie, les références pour les moteurs virtuels sont calculées et l'environnement graphique est mis à jour. Afin de s'assurer de l'exactitude des références calculées, il faut faire la mise à jour du modèle cinématique très fréquemment (dans l'ordre de 5 ms) pour que le modèle même soit correct et représente l'état courant du robot. Par contre, du côté graphique le rafraîchissement des modèles 3D nécessite des capacités de calcul accrues de l'ordinateur. Par ailleurs, un frame-rate de 30 fps (frames per second, soit 33 ms) est plus que suffisant pour produire une animation graphique fluide et en temps réel. Il est donc nécessaire de séparer les deux rafraîchissements (cinématique et graphique) en deux boucles différentes qui communiquent de façon asynchrone (voir fig. B.17).

Dans ce premier simulateur toutes les stratégies Cartésiennes ont été implémentées, et une modélisation des non-linéarités du système (notamment le jeu des câbles qui produisent la déflexion) a été proposée. La plus grande limite de cette version du simulateur est l'absence d'interactions physiques dans l'environnement virtuel : étant donné l'absence d'un moteur physique dans le cycle de calcul graphique, il est impossible de détecter les collisions des instruments avec les objets virtuels et, donc, les tâches qui comportent l'utilisation des instruments sont impossibles à réaliser. Afin de réaliser également un système d'entraînement pour les futurs utilisateurs du robot, une deuxième version du simulateur a été développée. Cette version, implémentée comme une extension de l'application principale de contrôle du robot, est basée sur Blender, un logiciel open source de modélisation graphique 3D. Blender intègre un « Game engine » (Moteur de jeu) qui comprend une bibliothèque pour les calculs physiques (Bullet). De cette façon, tous

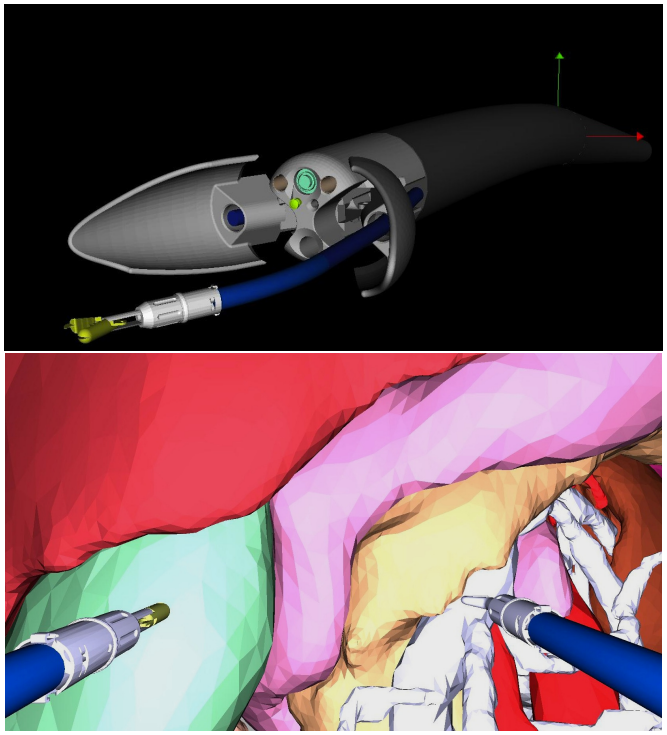

Fig. B.16. Vue externe (haut) et vue caméra (bas) dans le simulateur virtuel de STRAS.

les objets 3D qui font partie de la scène virtuelle sont liés au moteur de jeu et leurs interactions peuvent être détectées à partir des briques logiques « Sensor-Controller-Actuator » (« Capteur-Contrôleur-Actionneur ») :

- Les capteurs détectent l'activation d'un dispositif de saisie (comme une touche pressée ou un mouvement de la souris) ou créent un capteur extéroceptif (comme un radar ou un détecteur de rayons) capable de déclencher un évènement à son activation.
- Les contrôleurs collectent les évènements déclenchés par les capteurs et, selon les fonctions Booléennes qu'ils implémentent, ils les transmettent aux actionneurs. Un contrôleur peut aussi être un script Python qui est exécuté à l'activation d'un capteur.
- Les actionneurs changent l'état courant des objets 3D en termes de position, vitesse ou paramètres propres à chaque objet.

Comme mentionné précédemment, la deuxième version du simulateur n'est pas une application autonome, mais elle s'appuie sur le contrôleur haut-niveau du robot. Cela veut dire que le simulateur est seulement responsable du rafraîchissement graphique, tandis que la mise à jour du modèle cinématique et le calcul des références sont réalisées par l'application principale de contrôle (voir fig. B.18).

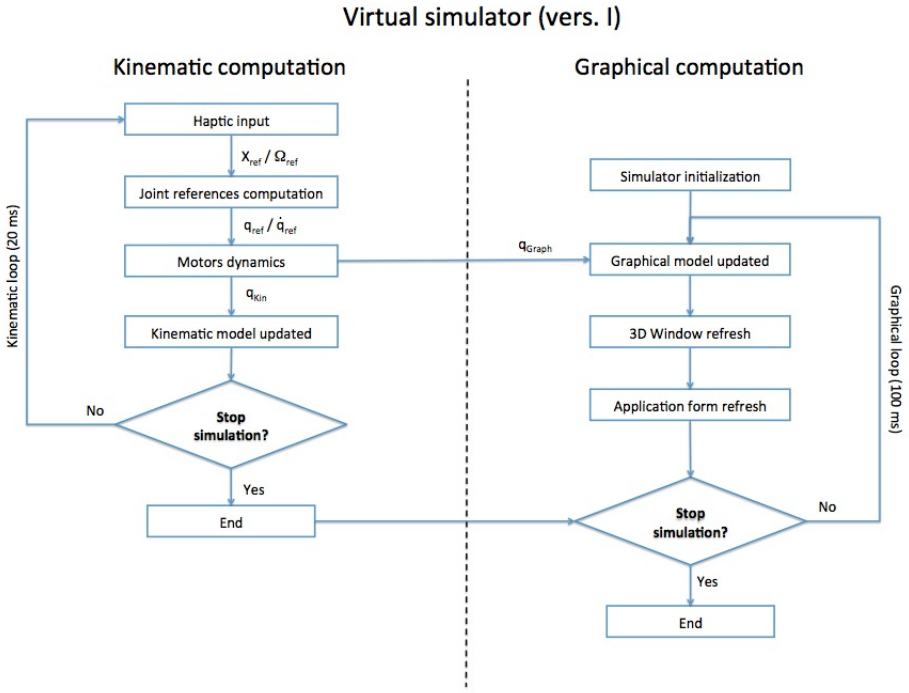

Fig. B.17. Flux de travail de la première version du simulateur virtuel de STRAS.

La communication entre le contrôleur et le simulateur est possible grâce à un socket UDP (User Datagram Protocol). Ce simulateur peut fonctionner avec deux modes différents :

- « Slave mode » : le simulateur reçoit les mêmes références articulaires que le robot dont il suit les mouvements. Cette modalité peut être utile pour avoir une représentation visuelle de la position théorique du système par rapport à sa configuration articulaire.
- « Arcade mode » : le contrôleur haut-niveau communique exclusivement avec le simulateur, et les mouvements du modèle virtuel du robot correspondent aux consignes de l'utilisateur.

Des scènes virtuelles qui reproduisissent des tâches typiques d'entraînement ont été implémentées dans ce simulateur :

- « Rings » : trois anneaux, qui se trouvent sur des clous, doivent être saisis avec l'instrument de droite, passés à l'instrument de gauche et ensuite posés sur le bâton qui se colore en rouge (voir fig. B.19). La position du bâton rouge est choisie au hasard, et des mouvements de l'endoscope sont nécessaires pour atteindre tous les objets de la scène. Au cours de la tâche, plusieurs paramètres sont collectés (temps d'exécution, nombre d'anneaux tombés, nombre de saisies manquées) afin de donner une évaluation du geste à la fin de la simulation.

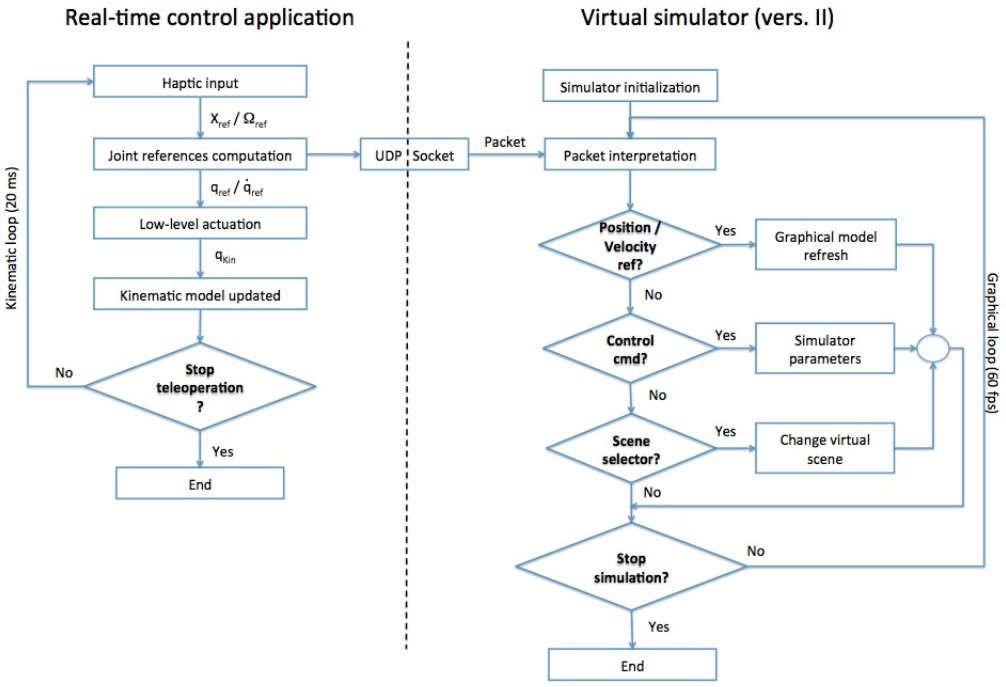

Fig. B.18. Flux de travail de la deuxième version du simulateur virtuel de STRAS.

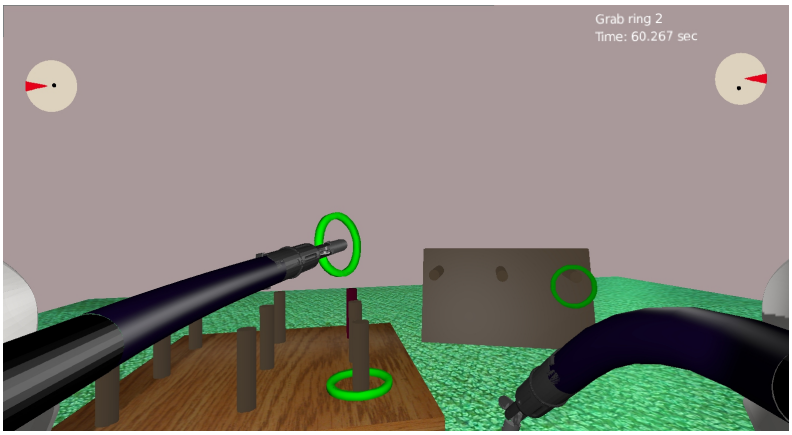

Fig. B.19. Capture d'écran pendant la tâche « Rings ».

- « Rings 2 » : trois anneaux sont cachés à l'intérieur d'une boîte recouverte par un couvercle à charnière qui peut être soulevé par sa poignée sphérique. L'utilisateur doit soulever le couvercle, saisir les trois anneaux un par un et les laisser sur un clou placé sur la droite (voir fig. B.20). Les mêmes paramètres que dans la scène « Rings » sont collectés au cours de la simulation, et la tâche se termine lorsque le troisième anneau est correctement mis autour du clou.

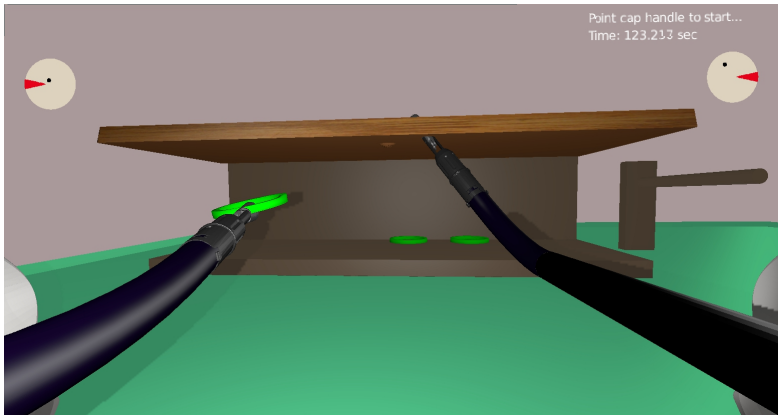

Fig. B.20. Capture d'écran pendant la tâche « Rings 2 ».

- « Surgery » : le but de cette tâche est d'effectuer une cholécystectomie simplifiée. L'utilisateur doit soulever le cinquième segment d'un foie, montré dans la scène, de manière à exposer la vésicule biliaire (voir fig. B.21). Ensuite, la vésicule doit être sectionnée en cautérisant le canal cystique avec l'outil électrique. La tâche se termine avec la récupération de la vésicule, qui doit être déposée dans une boîte de récupération située sur le côté droit de la scène.

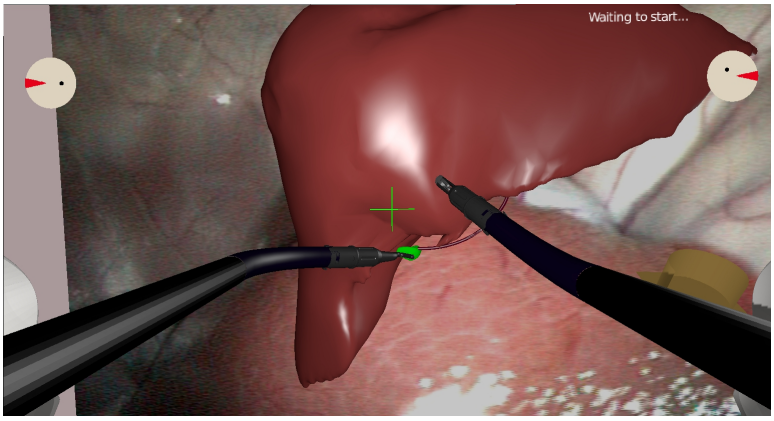

Fig. B.21. Capture d'écran pendant la tâche « Surgery ».

B.6 Résultats

B.6.1 Simulateurs

Lorsque STRAS était encore en cours de développement, nous avons mené des expériences avec la première version du simulateur virtuel afin de comparer les stratégies de contrôle Cartésien que nous proposons. Dans le but de tester la précision et la vitesse de réponse du système, deux tâches spécifiques ont été implémentées (voir fig. B.22) :

- « Precision task » : l'utilisateur doit suivre un chemin tortueux, imitant le mouvement lors d'une suture, avec un instrument, en cherchant à rester le plus proche possible du parcours préétabli.
- « Simple task » : dans ce cas, le chemin à suivre est linéaire et une erreur de suivi, représentée comme un cylindre autour du parcours, est tolérée. Le but est d'effectuer le mouvement le plus rapidement possible en restant à l'intérieur du cylindre avec la pointe de l'instrument.

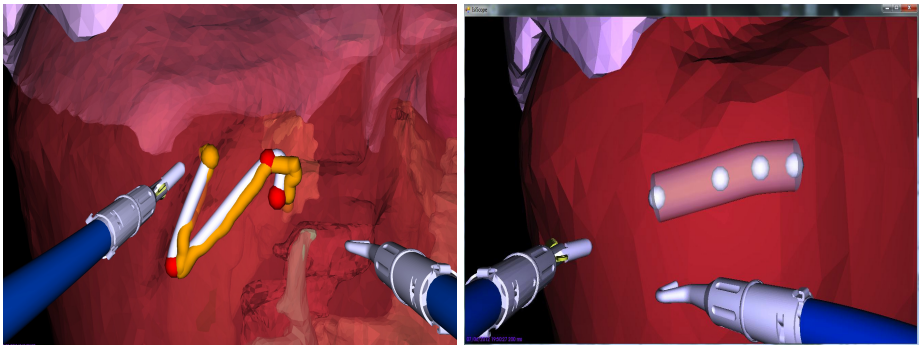

Fig. B.22. Captures d'écran pendant les tâches « Precision task » (gauche) et « Simple task » (droite).

Les deux tâches ont été proposées à deux groupes de dix personnes, qui les ont effectuées dans un premier temps en utilisant le modèle idéal du robot et ensuite en introduisant des non-linéarités. Les avantages d'une telle étude étaient multiples : avec le modèle cinématique idéal on peut évaluer le comportement du système sans la nécessité de prendre en compte les non-linéarités qui l'affectent ; ensuite, en introduisant progressivement des perturbations dans la simulation on peut évaluer leurs effets sur le comportement du système et sur les réactions de l'utilisateur. Pour évaluer les tâches, une fonction de score, qui prend en compte le temps d'exécution T et l'erreur entre le parcours préétabli et celui effectué par l'utilisateur, a été définie :

$$Score = \phi_T T + \phi_e \sqrt{e_X^2 + e_Y^2 + e_Z^2}. \tag{B.9}$$

Les poids ϕ_T e ϕ_e sont différents pour les deux tâches et soulignent la différente contribution des erreurs : pour le « Precision task » $\phi_T = 1$ et $\phi_e = 10$, tandis

que pour le « Simple task » $\phi_T = 10$ et $\phi_e = 5$. Les résultats obtenus, qui doivent être évalués séparément pour chaque tâche, sont résumés dans le tableau B.1.

Precision task						
Slave Control	**Master Output**	**Slave Input**	**Force Feedback**	**Mean Score (no error)**	**Mean Score (rot error)**	**Mean Score (backlash)**
Open Loop	Position	Velocity	Spring	75.268	143.265	151.029
	Velocity	Velocity	Gravity comp	77.056	117.600	507.05
CL Joint	Position	Position	Error	87.317	89.141	184.342
CL Cartesian	Position	Position	Error	83.345	104.262	110.255
	Velocity	Position	Gravity comp	84.110	88.683	199.71

Simple task						
Slave Control	**Master Output**	**Slave Input**	**Force Feedback**	**Mean Score (no error)**	**Mean Score (rot error)**	**Mean Score (backlash)**
Open Loop	Position	Velocity	Spring	80.451	81.726	92.577
	Velocity	Velocity	Gravity comp	91.879	149.493	101.64
CL Joint	Position	Position	Error	77.131	92.958	153.863
CL Cartesian	Position	Position	Error	72.268	99.290	88.591
	Velocity	Position	Gravity comp	78.754	129.780	143.820

Table B.1. Résultats des tâches effectuées en conditions idéales avec le premier simulateur.

Dans des conditions idéales, une stratégie de contrôle en vitesse pour le système esclave, avec des consignes en position pour le système maître, donne de meilleurs résultats pour le « Precision task ». Cette modalité de contrôle permet d'obtenir des mouvements précis des outils, parce que l'entrée de l'utilisateur est donnée sous la forme de petites variations de vitesse. En contrepartie, cela se traduit par une réactivité plus faible des instruments lorsque des grands mouvements sont requis. C'est la raison pour laquelle les stratégies de commande en position fournissent de meilleurs résultats pour le « Simple task ». Les observations changent significativement quand une erreur est introduite dans la simulation (voir tableau B.2).

Dans ce cas, l'erreur introduite simule un jeu au niveau des câbles actionnant la déflexion de l'instrument. Cette non-linéarité donne l'impression que rien ne se passe quand on demande un changement de direction de l'instrument, donc l'utilisateur tend à déplacer davantage l'interface. Cette situation pourrait conduire à l'instabilité du système puisque :

- dans une loi de commande en vitesse, une grande référence de vitesse Cartésienne est envoyée au système esclave qui réagit brusquement quand il sort de la zone morte du jeu;
- dans une loi de commande en position, le vecteur d'erreur calculé par la boucle de contre-réaction augmente rapidement pendant l'effet du jeu ; la boucle de contrôle tente de réduire cette erreur, mais cela peut provoquer de grandes vitesses lors de la sortie de la zone morte du jeu.

	Precision task			Simple Task		
Slave Input **Master Output**	Open Loop Position	CL Cartesian Position	CL Joint Position	Open Loop Position	CL Cartesian Position	CL Joint Position
Mean	81.637	82.321	88.138	79.01	68.196	78.57
(with error)	151.029	110.255	184.342	92.577	88.591	153.863
Median	69.626	67.705	78.08	73.225	52.93	46.94
(with error)	106.465	83.72	128.57	78.622	63.195	105.105
Min / Max	54.08/124.69	50.59/152.29	51.77/123.35	36.34/142.54	32.365/173.89	31.82/176.37
(with error)	84.15/324.94	63.99/290.53	63.17/564.24	50.134/175.23	46.205/203.515	46.09/455.485
Best results (# users)	3	3	4	2	4	4
(with error)	2	5	3	3	5	2

Table B.2. Résultats du deuxième groupe pour les tâches réalisées avec l'introduction d'erreurs dans la simulation.

De nos tests on peut voir qu'une stratégie de contrôle Cartésien avec une référence en position de l'interface-maître permet d'obtenir les meilleurs résultats pour la majorité des personnes impliquées dans les simulations. Le mappage direct entre les espaces de travail de l'instrument et de l'interface haptique, prévu dans cette loi de commande, donne un bon sens de contrôle pour presque tous les utilisateurs, parce que la position de l'interface haptique représente directement la position de l'instrument dans la scène virtuelle.

Avec la deuxième version du simulateur virtuel il était possible de tester le comportement de STRAS avec trois tâches réalistes (cf. section B.5) qui nécessitent l'ensemble des DDL du système et une coopération entre les instruments. Les tâches proposées ont été effectuées par huit utilisateurs répartis en trois groupes : experts (3 utilisateurs qui ont de l'expérience à la fois avec le robot et le simulateur), intermédiaires (3 utilisateurs avec de l'expérience sur le robot) et débutants (2 utilisateurs sans aucune connaissance du système et de son simulateur). Chaque utilisateur devait exécuter les tâches avec les quatre différents mappages proposés (voir section B.4) : « Direct axis control », « Orientation guidance », « Cartesian control » et « Pseudo-Cartesian control ». Les simulations ont été réalisées en utilisant le modèle idéal du système, sans introduire de perturbations. Au cours de chaque tâche, tous les paramètres les plus importants sont enregistrés : les positions Cartésiennes et articulaires du robot, les positions des interfaces haptiques, les temps d'exécution et les erreurs des utilisateurs pendant leurs exécutions. Les résultats de l'expérience sont représentés en fig. B.23. On peut immédiatement remarquer que une modalité de contrôle Cartésien (soit le Pseudo-Cartésien ou le Cartésien réel) donne en moyenne le meilleur résultat pour la majorité des utilisateurs. Cela est probablement à mettre en lien avec la modalité d'entrée de l'utilisateur, plus naturelle et intuitive que celle d'un contrôle non-Cartésien. Les interfaces haptiques utilisées ont une architecture cinématique assez flexible pour permettre plusieurs mappages différents. Cependant, dans chaque stratégie les degrés de liberté non utilisés (notamment les rotations passives de la manette pour les stratégies Cartésiennes) perturbent les utilisateurs pendant l'exécution des tâches. Des interfaces haptiques spécifiquement conçues pour un mappage particulier pourraient être avantageuses pour l'utilisateur en terme de courbe d'apprentissage.

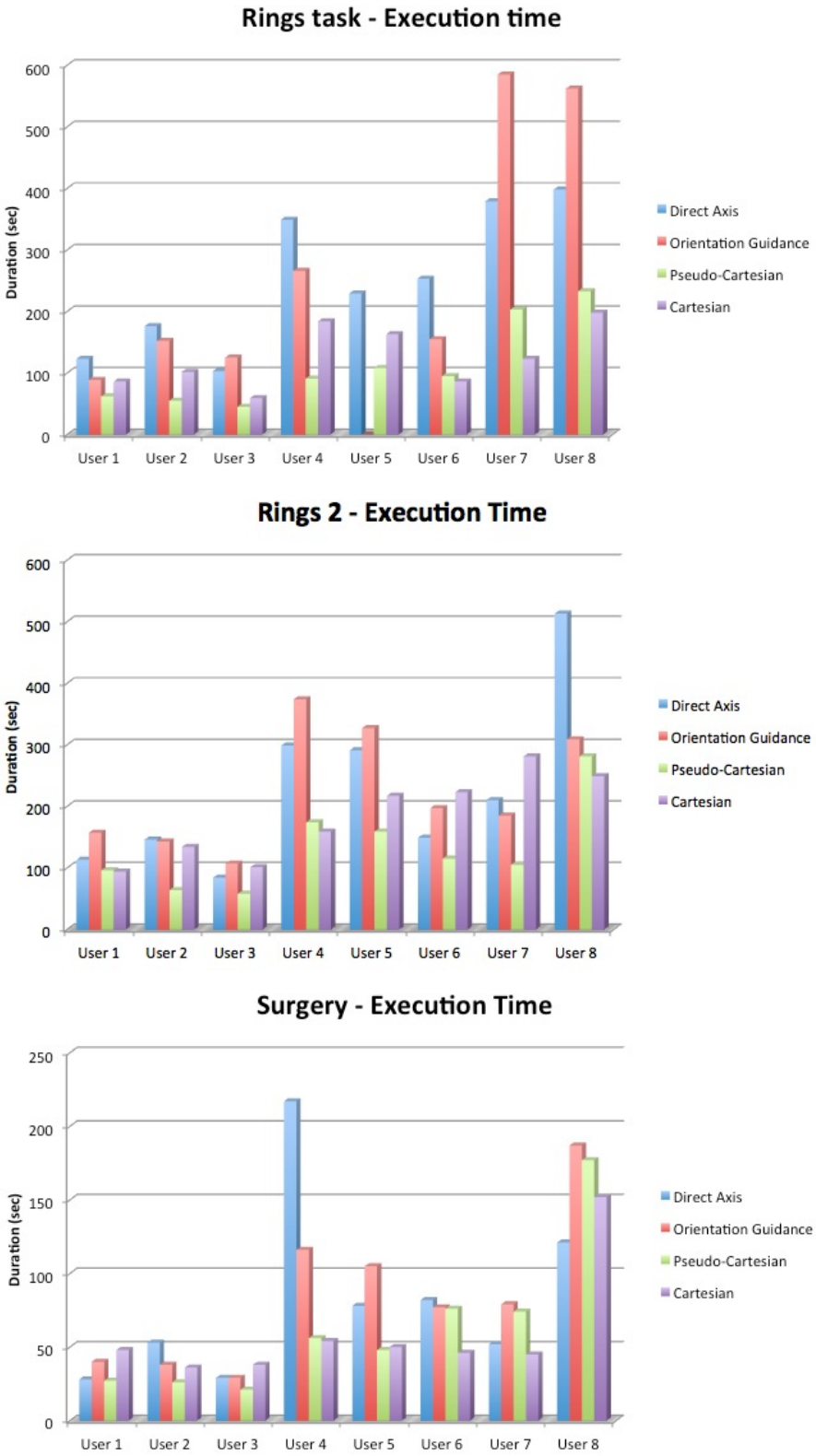

Fig. B.23. Temps d'exécutions pour les trois tâches effectuées avec la deuxième version du simulateur.

B.6.2 Système robotique

Dans la section B.3 nous avons introduit une hypothèse qui nous permet de décrire cinématiquement les parties flexibles de STRAS avec les paramètres de Denavit-Hartenberg. Pour valider cette hypothèse, nous avons procédé à un essai dans lequel on compare les positions de l'instrument sur un chemin imposé et les positions calculées correspondantes données par le modèle géométrique. Les positions de l'instrument ont été capturées par une caméra externe, placée perpendiculairement au plan de déflexion de l'instrument à une distance fixe de 20 cm. Deux marqueurs visuels ont été placés sur l'instrument, un à la base et l'autre à l'extrémité de la partie flexible. Les mouvements de l'instrument ont été effectués dans son plan de déflexion, sans effectuer de rotations. Les images provenant de la caméra ont été traitées afin d'extraire les positions des marqueurs. Le résultat est représenté en fig. B.24.

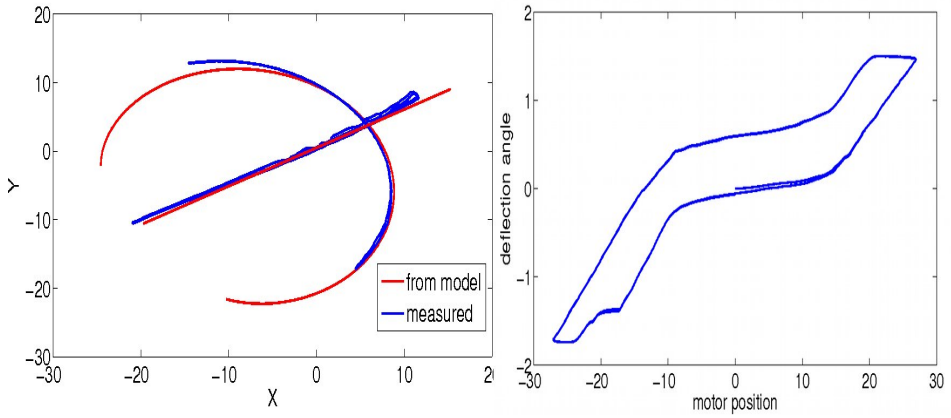

Fig. B.24. Gauche : Comparaison des positions d'un instrument obtenues avec des mesures (en bleu) et avec le modèle géométrique (en rouge). Droite : caractéristique quasi-statique représentant la valeur de déflexion de l'instrument en fonction de la position du moteur correspondant.

Les mouvements de déflexion et translation suivent bien les trajectoires idéales fournies par le modèle cinématique. Cependant, lors d'un changement de sens de déflexion, le jeu des câbles d'actionnement introduit une zone morte qu'il est difficile de compenser analytiquement dans le modèle cinématique, étant donné qu'elle dépend de plusieurs facteurs (forme de l'endoscope, type de câbles, frottements, etc.).

Pour confirmer les résultats obtenus en simulation, nous avons successivement mené des expériences similaires avec STRAS. Dans un premier temps, nous avons reproduit les tests de suivi d'un chemin préétabli et de pointage en utilisant les mappages proposés. Afin d'évaluer la réaction du système, les mouvements requis dans les tâches incluent les singularités. Un seul instrument a été utilisé sans l'assistance des DDL de l'endoscope pour effectuer trois tâches (voir fig. B.25) :

un suivi de parcours et deux pointages (le premier dans l'image et le deuxième en évaluant la profondeur réelle).

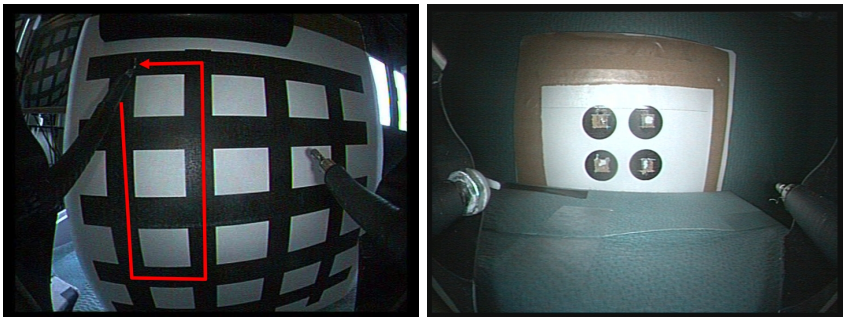

Fig. B.25. Tâches de suivi de chemin et pointage effectuées avec STRAS.

Trois utilisateurs experts ont effectué les tâches en utilisant tous les mappages. Les résultats, représentés en fig. B.26, montrent en moyenne de meilleurs temps d'exécution avec les stratégies Cartésiennes, jugées plus intuitives par les utilisateurs pour l'exécution de tâches dans l'espace Cartésien. Deux types principaux d'erreurs ont été constatés dans la tâche de suivi de chemin : de légers écarts du parcours imposé ou de grands mouvements hors du parcours. Dans le premier cas, les dérives de quelques millimètres sont principalement causées par les singularités cinématiques qui produisent des rotations incontrôlées de l'instrument ; par contre, les écarts de plus d'un centimètre du chemin se produisent typiquement lorsque la limite de l'espace de travail a été atteinte et une reconfiguration articulaire est nécessaire pour continuer la tâche. Les tâches de pointage ont été exécutées plus facilement par rapport à la première tâche puisque le chemin entre les points n'était pas fixé, donc les utilisateurs peuvent choisir des parcours alternatifs pour atteindre la cible.

Après les tests d'évaluation des stratégies proposées, une comparaison du robot avec la version courte du système Anubiscope, produit par Karl Storz GmbH (Tüttlingen, Allemagne), a été effectuée. Le but de cette comparaison est de voir si le système robotique apporte des avantages par rapport à son homologue manuel, notamment en ce qui concerne les temps d'exécutions, la facilité d'emploi et l'ergonomie. Pour cette expérience nous avons développé, avec la collaboration des chirurgiens partenaires du projet, un banc d'essai contenant trois tâches élémentaires (voir fig. B.27) :

- Tâche 1: déplacement d'anneaux entre clous proches en utilisant seulement la pince. Le mouvement requis est à l'intérieur de l'espace de travail de l'instrument et la tâche est réalisable sans nécessité de bouger l'endoscope.
- Tâche 2 : déplacement d'anneaux entre clous éloignés avec l'assistance des DDL de l'endoscope. Étant donné que l'endoscope est commandé par l'interface gauche et la pince avec l'interface droite, pour cette tâche l'utilisateur a les deux mains occupées.

Fig. B.26. Temps d'exécutions pour les tâches de suivi de chemin et pointage.

- Tâche 3 : cette tâche consiste à récupérer un anneau couvert par une gaze et le placer autour d'un clou placé sur la gauche. Dans ce cas, la coopération entre les instruments est fondamentale, aussi bien que les mouvements de l'endoscope.

Fig. B.27. Tâches proposées pour la comparaison STRAS - Anubiscope.

Les essais ont été effectués avec dix utilisateurs : trois chirurgiens (un expérimenté dans l'utilisation de l'Anubiscope) et sept ingénieurs (deux expérimentés avec STRAS). Pour STRAS, tous les mappages proposés ont été testés. Le système Anubiscope manuel a été fixé sur table avec un bras rigide afin d'éviter la présence d'une autre personne pour le maintenir (comme cela se produit au cours de son utilisation clinique). La comparaison entre les deux systèmes a été basée sur les temps d'exécution des tâches, le nombre d'erreurs et le succès ou l'échec dans chaque épreuve. A la fin de leurs essais, les utilisateurs ont reçu un questionnaire pour l'évaluation subjective de l'expérience. Les résultats de cette expérience sont représentés en fig. B.28.

Presque tous les utilisateurs ont été capables de réaliser les tâches dans la durée maximale autorisée. Cependant, dans les tâches 1 et 2 certains utilisateurs ont eu des difficultés pour positionner correctement les anneaux sur les clous en raison de l'impossibilité de changer la rotation propre de l'outil sans modifier sa position. Dans leurs questionnaires, les utilisateurs ont indiqué STRAS comme plus intuitif et simple par rapport à l'Anubiscope. De plus, l'absence de frictions dans l'interface de contrôle et la meilleure ergonomie ont amené une préférence pour le robot. La difficulté dans la perception de la profondeur, commune aux deux systèmes et causée par l'utilisation d'une caméra monoscopique, reste une forte limitation pour les utilisateurs débutants. Dans cette expérience le mappage « Pseudo-Cartesian control » a fourni les meilleurs temps d'exécutions, mais les préférences des utilisateurs ont été reparties entre tous les mappages proposés. Cela dénote le caractère très subjectif d'une telle préférence. L'avantage important de STRAS est donc d'offrir plusieurs modalités de contrôle qui permettent des courbes d'apprentissage plus courtes pour les nouveaux utilisateurs.

B.6.3 Tests ex vivo

Afin de tester STRAS dans des conditions réalistes, nous avons effectué quelques tests *ex vivo* en collaboration avec nos partenaires chirurgiens, dans le but de

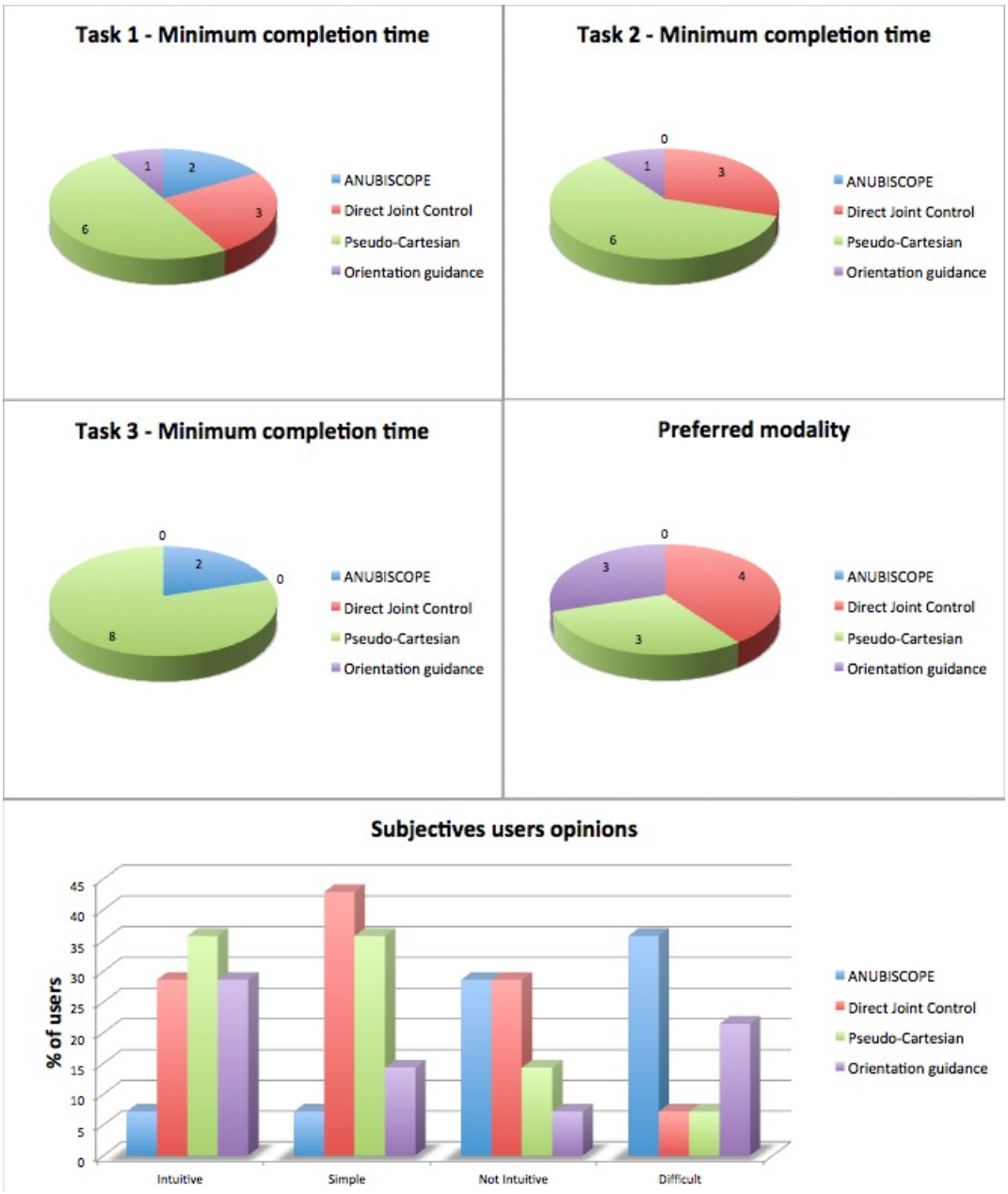

Fig. B.28. Résultats de la comparaison STRAS - Anubiscope.

reproduire une dissection de la sous-muqueuse gastrique (ESD, *Endoscopic Submucosal Dissection* en anglais). Nous avons utilisé un estomac de porc, suturé pour maintenir l'insufflation et attaché autour de la tête de l'endoscope, afin de simuler une approche transgastrique (voir fig. B.29). Nous avons trouvé plusieurs limitations du système dans l'exécution de cette procédure, notamment en ce qui concerne la taille inappropriée des instruments utilisés (une pince et un crochet électrique). Les mâchoires à préhension de la pince étaient trop minces pour saisir correctement le tissu visqueux, et l'effet du crochet électrique était faible par rapport à la taille de la coupe nécessaire, ce qui impose beaucoup de temps pour couper la couche de muqueuse. En effet, les instruments manuels employés dans ce type de chirurgie sont plus larges que ceux de notre dispositif et, par conséquent, ils permettent une meilleure préhension et une ablation du tissu plus efficace. Un autre inconvénient détecté est l'impossibilité de contrôler l'insufflation et d'évacuer la fumée produite pendant l'ablation à partir de la console de l'utilisateur : les contrôles correspondants sont sur le corps de l'endoscope, mais ils n'ont pas été actionnés de manière robotisée sur le prototype courant. En revanche, la mobilité du système était adéquate, ce qui permet une exploration complète de l'estomac. Nous avons également été en mesure d'extraire le crochet électrique pour le nettoyer sans compromettre la fonctionnalité du système. L'installation de STRAS et sa configuration ont été effectuées en moins de 15 minutes : l'intégration du robot dans la salle d'opération n'a pas posé de problèmes par rapport aux équipements déjà présents. De plus, étant donné la petite taille globale du robot, les mouvements des instruments ne représentent pas un risque potentiel pour les personnels qui pourraient être à côté. Nous sommes convaincus qu'avec des instruments plus appropriés STRAS pourrait être utilisé pour une opération chirurgicale complète.

B.7 Conclusions

La prochaine frontière en chirurgie mini-invasive est représentée par la chirurgie sans cicatrice, qui a pour objectif ambitieux d'éviter toutes cicatrices visibles sur la peau du patient après une opération chirurgicale. Dans ce contexte, nous avons présenté STRAS (Single access and Transluminal Robotic Assistant for Surgeons), un nouveau robot pour la chirurgie sans cicatrice développé en collaboration avec Karl Storz GmbH (Tüttlingen, Allemagne) et l'Institut de Recherche contre les Cancers de l'Appareil Digestif (IRCAD, Strasbourg, France). STRAS a été développé comme un robot téléopéré, avec une interface-maître qui contrôle le robot esclave. Étant flexible dans sa structure, STRAS ne peut pas être décrit cinématiquement avec les méthodes classiques de la robotique : nous avons utilisé une formulation spécifiquement développée pour les robots continus afin de calculer son modèle cinématique. Un effort a été fait afin d'obtenir le modèle géométrique inverse du robot, qui permet de calculer toutes les configurations articulaires relatives à une position cartésienne souhaitée des instruments. Nous avons effectué une évaluation numérique de l'espace de travail du robot et nous avons calculé ses singularités. En ce qui concerne le robot esclave, trois schémas de contrôle peuvent être envisagées :

Fig. B.29. Test ex vivo effectué avec STRAS. Haut : le robot est monté sur la table opératoire et un estomac de porc est suturé autour de la tête de l'endoscope. Bas : Poste de travail utilisateur avec les interfaces haptiques, le retour vidéo de la caméra endoscopique et de l'application principale de contrôle.

- contrôle en vitesse en boucle ouverte, dans lequel une référence de vitesse Cartésienne est directement transformée en référence de vitesse articulaire en utilisant le modèle cinématique inverse ;
- contrôle articulaire en boucle fermée, dans lequel le modèle géométrique inverse est exploité pour calculer les références de positions articulaires correspondantes aux positions Cartésiennes souhaitées ;
- contrôle en position en boucle fermée, dans lequel la position Cartésienne souhaitée est comparée avec la position réelle du robot et le vecteur d'erreur calculé est ensuite transformé en référence de vitesses articulaires à travers le modèle cinématique inverse.

Les cinématiques des systèmes maître et esclave sont très différentes, donc plusieurs mappages sont possibles pour les relier. A côté des schémas de contrôle, nous avons proposé quatre mappages pour lier les DDL des deux sous-systèmes :

- « Direct joint control », qui corrèle chaque mouvement élémentaire des interfaces haptiques avec les DDL du robot esclave ;
- « Orientation guidance », dans lequel les mouvements de l'interface haptique sont limités à ceux que l'instrument peut effectuer à partir de la configuration courante ;
- « Cartesian control », qui utilise un des schémas de contrôle en boucle fermée pour transformer des consignes de position Cartésiennes en références articulaires pour le robot ;
- « Pseudo-Cartesian control », dans lequel les mouvements de l'interface haptique dans le plan $X_M Y_M$ déterminent les références pour la déflexion et la rotation de l'instrument. La translation de l'instrument est commandée directement par le mouvement de l'interface le long de Z_M.

Les interfaces-maîtres utilisées offrent une bonne flexibilité d'utilisation, mais les DDL non utilisés sont généralement perturbants pour l'utilisateur. Le développement d'une interface spécifique faciliterait le contrôle du robot, surtout dans les phases d'apprentissage des nouveaux utilisateurs.

Afin d'avoir un environnement de test sûr dans lequel évaluer les mappages proposés et les stratégies de contrôle, nous avons développé un simulateur virtuel de STRAS. Dans sa première version, le simulateur a été conçu pour être une réplique cinématique du robot réel, y compris ses principales non-linéarités et imperfections. Avec ce simulateur nous avons effectué quelques expériences, afin de comparer le comportement du système par rapport aux différentes stratégies proposées. Ces expériences ont montré qu'en conditions idéales le contrôle en vitesse permet d'obtenir une meilleure précision, tandis que le contrôle en position assure une réponse plus rapide du système. Au contraire, lorsque les non-linéarités sont introduites dans le modèle, une stratégie de commande en position permet de mieux compenser leurs effets. La principale limitation de la première version du simulateur virtuel était l'absence d'un moteur physique pour gérer les interactions entre les objets virtuels. Cela implique l'impossibilité d'effectuer la plupart des exercices d'entraînement, comme la saisie d'objets avec la pince ou la dissection de tissus avec l'outil électrique. Nous avons choisi, par conséquent, de développer une nouvelle version du simulateur capable d'interactions physiques. Trois tâches

complexes, qui nécessitent la coopération des instruments, ont été mises en oeuvre à l'intérieur du simulateur. Nous avons organisé une session de test avec huit utilisateurs, choisis selon leur expérience précédente avec STRAS et avec le simulateur virtuel. À la fin de la session de test, nous avons constaté que les mappages Cartésiens donnent en moyenne des meilleurs temps d'exécution pour la majorité des utilisateurs, indépendamment de leur expérience antérieure. Quoi qu'il en soit, le choix d'une modalité de contrôle spécifique dépend largement de préférences subjectives de chaque utilisateur. Dans tous les cas, après une période de formation les résultats avec les différentes modalités ont tendance à s'égaliser, comme on peut le voir en moyenne avec les utilisateurs les plus expérimentés.

Des résultats similaires ont été reportés lors des expériences menées avec STRAS : une stratégie de contrôle Cartésienne est plus intuitive pour la plupart des utilisateurs et permet d'obtenir de meilleurs résultats en termes de temps d'exécution. En outre, l'architecture des interfaces-maîtres est trop générique et empêche une immédiate compréhension des mouvements demandés. Ces résultats communs nous donnent une première validation de notre simulateur virtuel, montrant qu'il représente un bon outil d'évaluation et d'entraînement. Enfin, la comparaison directe entre STRAS et la version courte de l'Anubiscope a montré une préférence des utilisateurs pour le premier, jugé plus simple et plus intuitive que son homologue manuel. L'avantage principal de STRAS est que l'ensemble du système peut être commandé par un seul utilisateur, d'une manière ergonomique et avec la possibilité de choisir parmi plusieurs solutions de contrôle.

C

Abstract in Italian

Sviluppo e controllo di un sistema robotico per la chirurgia senza cicatrici

Contents

C.1 Contesto medico

Dopo un lungo periodo di sperimentazioni e scetticismo tra la fine degli anni '80 e l'inizio degli anni '90, la chirurgia mini-invasiva (CMI) rappresenta oggi lo standard *de facto* per le operazioni chirirgiche. I vantaggi di un approccio mini-invasivo sono numerosi, focalizzati principalmente sul paziente. A differenza della chirurgia denominata "aperta" (o *laparotomia*), le equivalenti operazioni chirurgiche condotte in laparoscopia riducono il trauma causato dalle cicatrici, permettono di diminuire il volume di sangue perso durante l'intervento, riducono il dolore post-operatorio dovuto alla cicatrizzazione e permettono un'ospitalizzazione più corta, così come una riabilitazione più rapida. Tuttavia, le procedure di CMI impongono nuove difficoltà al chirurgo. Non vi è più contatto diretto tra chirurgo e paziente, e la palpazione manuale degli organi e dei tessuti è sostituita dalla loro manipolazione per mezzo di strumenti chirurgici. Inoltre, la visione delle strutture anatomiche è possibile solo grazie ad una telecamera miniaturizzata, inserita all'interno del corpo del paziente, che trasmette delle immagini bidimensionali ad uno schermo.

Oggigiorno la chirurgia senza cicatrici (*no-scar surgery* in inglese) rappresenta l'avanguardia nel campo della CMI. Il suo scopo è di permettere ai chirurghi di operare senza lasciare cicatrici visibili. Questa nuova tecnica include due approcci (vedere fig. C.1) :

- NOTES (Natural Orifice Transluminal Endoscopic Surgery), nella quale gli orifizi naturali sono sfruttati come porte d'accesso al corpo umano; in questo caso non vengono praticate incisioni esterne sulla pelle del paziente, e l'unica cicatrice è all'interno del corpo.
- LESS (Laparo-Endoscopic Single-site Surgery), nella quale gli strumenti chirurgici sono inseriti nel corpo del paziente attraverso una porta d'accesso comune, scelta in una zona nascosta del corpo (tipicamente l'ombelico) in maniera tale che la cicatrice non sia visibile alla fine dell'operazione.

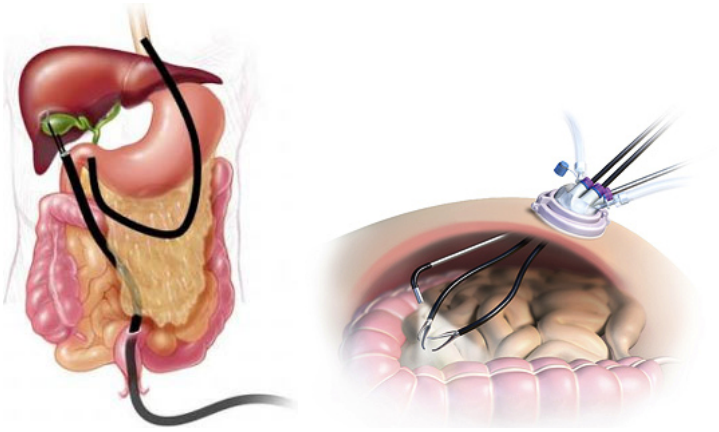

Fig. C.1. Approcci NOTES (sinistra) et LESS (destra) nella chirurgia senza cicatrici.

Rispetto alla laparoscopia standard, questi due approcci implicano un vantaggio supplementare per il paziente, che consiste in un miglior risultato estetico al termine dell'operazione. Tuttavia, le nuove limitazioni imposte al fine di minimizzare il carattere invasivo dell'operazione chirurgica rendono la sua esecuzione più difficile. La triangolazione, la destrezza e la dimensione degli strumenti sono in gran parte limitate dalla porta d'accesso unica, transluminale o ricavata chirurgicamente. Della nuova strumentazione è quindi necessaria, in maniera tale da compensare, in parte o integralmente, le limitazioni d'accesso legate a questa tecnica particolare. Idealmente, gli strumenti perfetti per la chirurgia senza cicatrici dovrebbero essere capaci di passare attraverso una porta d'accesso stretta, raggiungere il punto di destinazione (che potrebbe trovarsi decine di centimetri lontano rispetto al punto d'accesso) e infine riconfigurarsi per l'esecuzione dell'operazione. Tutto ciò implica dei compromessi: innanzitutto, gli strumenti devono essere sufficientemente flessibili per adattare la loro forma ai vincoli anatomici, ma allo stesso tempo rigidi abbastanza per permettere una corretta trasmissione delle forze dal lato prossimale a quello distale. Inoltre, in base alla porta d'accesso scelta, la

lunghezza degli strumenti potrebbe variare ed essere più lunga di quella degli strumenti di laparoscopia (in particolare nelle operazioni transluminali). E' quindi necessario utilizzare un sistema di azionamento appropriato, capace di trasferire in maniera trasparente i movimenti dell'utente agli strumenti. La destrezza potrebbe essere migliorata impiegando delle sezioni flessibili nella struttura degli strumenti, allo scopo di renderli adattabili ad ambienti tortuosi.

La robotica può apportare numerosi vantaggi in chirurgia: rispetto ad una procedura manuale, la stessa operazione effettuata grazie all'assistenza di un sistema robotico può essere realizzata con una migliore precisione, ripetitività ed ergonomia. L'intervento di un sistema robotico all'interno di un'operazione chirurgica può manifestarsi in diversi modi. Ad esempio, il robot può guidare le mani del chirurgo al fine di evitare tutti i movimenti degli strumenti chirurgici all'interno di zone considerate pericolose. Allo stesso modo, l'interfaccia interposta tra il chirurgo e gli strumenti può permettere di filtrare i movimenti delle mani del chirurgo, allo scopo di compensarne il tremore naturale, oppure può ridurre o amplificare il gesto per una migliore destrezza. Tuttavia, le dimensioni di un robot chirurgico devono essere tali da permettergli di adattarsi nella sala operatoria, il robot stesso non deve costituire un pericolo sia per i medici sia per il paziente e deve poter essere rimosso in tutta sicurezza in caso d'emergenza.

C.2 STRAS : Single access and Transluminal Robotic Assistant for Surgeons

In questo contesto, noi proponiamo un nuovo robot flessibile, denominato STRAS (Single access and Transluminal Robotic Assistant for Surgeons), sviluppato specificatamente per la chirurgia LESS e per le operazioni transluminali eseguite in prossimità dell'orifizio di accesso (vedere fig. C.2). STRAS è una guida endoscopica, basata sul sistema Anubiscope prodotto da Karl Storz GmbH (Tuttlingen, Germania), che permette di introdurre due strumenti flessibili (una pinza ed un bisturi elettrico) all'interno del corpo passando da una porta di accesso unica.

L'endoscopio e i due strumenti sono dotati di sezioni distali articolate, le quali permettono la loro deflessione aumentando quindi lo spazio di lavoro del sistema e ottenendo una migliore destrezza. Gli strumenti sono inseriti all'interno dell'endoscopio principale dal suo lato prossimale e, grazie a due alette inclinabili integrate sulla testa dell'endoscopio, i loro canali sono deviati dal lato distale in maniera tale da ottenere la triangolazione. STRAS dispone globalmente di 10 Gradi Di Libertà (GDL) azionati, organizzati come segue:

- 3 GDL dell'endoscopio principale, che può avanzare e indietreggiare, e la sua sezione distale può essere flessa in due direzioni ortogonali;
- 3 GDL per ogni strumento, il quale può traslare, ruotare e flettersi in una direzione;
- 1 GDL supplementare per l'apertura e la chiusura della pinza.

Siccome STRAS ha un'architettura arborescente, la posizione degli strumenti dipende anche dai movimenti dell'endoscopio. La presenza di sezioni flessibili nella struttura del robot impedisce la sua descrizione cinematica per mezzo dei metodi

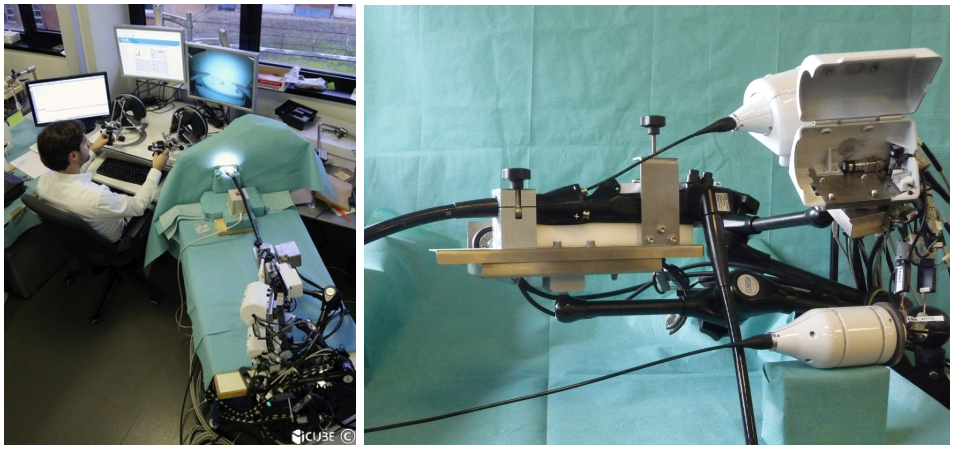

Fig. C.2. Vista di insieme di STRAS (sinistra) e dettaglio del robot (destra).

classici della robotica. Una modellizzazione specifica dovrà perciò essere adottata. Abbiamo sviluppato STRAS come un robot teleoperato, nel quale l'endoscopio e gli strumenti robotizzati sono il sistema slave (vedere fig. C.2). Il sistema master è composto da due interfacce aptiche che offrono 7 GDL ciascuna. Perciò, il primo problema che si pone consiste nel trovare una mappatura appropriata che metta in relazione le cinematiche differenti dei sistemi master e slave. Questa problematica è strettamente legata alla scelta di una strategia di controllo per il robot slave, cioè la legge di controllo che permette di trasformare i riferimenti desiderati, trasmessi dall'utente per mezzo dell'interfaccia master, nei corrispondenti riferimenti di basso livello per gli azionamenti del robot. Numerose mappature e strategie di controllo possono essere proposte, e la scelta particolare di una di queste dipenderà in gran parte dall'applicazione specifica e dalle preferenze personali dell'utente.

C.3 Cinematica

La convenzione di Denavit-Hartenberg, utilizzata in robotica per descrivere cinematicamente un manipolatore seriale, pone l'ipotesi di bracci rigidi connessi da giunti standard (prismatici o rotoidali). Per questo, essa non offre una rappresentazione valida per i robot flessibili. Un approccio semplificato che conduce a dei risultati validi consiste nell'assumere la sezione continua come composta da una serie di archi a curvatura costante. Questo metodo, denominato "piecewise constant curvature kinematics" (cinematica di curvatura costante a tratti), considera che la sezione continua sia composta da un numero finito di bracci curvi, ciascuno descritto da un insieme finito di parametri: la curvatura κ, l'orientazione ϕ del piano contenente l'arco e la lunghezza dell'arco ℓ (vedere fig. C.3).

In questo modo, è possibile rappresentare la parte flessibile per mezzo di una trasformazione rigida tra un sistema di riferimento situato alla base della sezione continua e il corrispondente situato in cima:

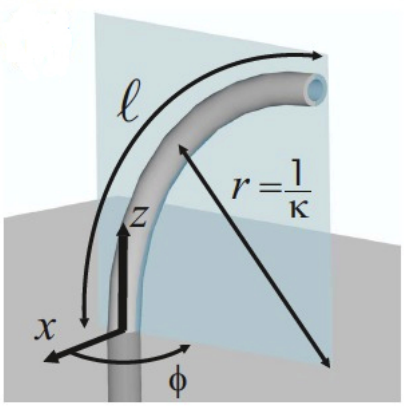

Fig. C.3. Notazione per la descrizione cinematica di un arco flessibile.

$$\mathscr{T}_{FS} = \begin{bmatrix} \cos(\phi)\cos(\kappa\ell) & -\sin(\phi) & \cos(\phi)\sin(\kappa\ell) & \frac{\cos(\phi)(1-\cos(\kappa\ell))}{\kappa} \\ \sin(\phi)\cos(\kappa\ell) & \cos(\phi) & \sin(\phi)\sin(\kappa\ell) & \frac{\sin(\phi)(1-\cos(\kappa\ell))}{\kappa} \\ -\sin(\kappa\ell) & 0 & \cos(\kappa\ell) & \frac{\sin(\kappa\ell)}{\kappa} \\ 0 & 0 & 0 & 1 \end{bmatrix} \tag{C.1}$$

Per ottenere il modello cinematico diretto del robot, che permette di calcolare la posizione Cartesiana degli strumenti rispetto ad un sistema di riferimento fisso di base, bisogna calcolare la trasformazione globale tra i sistemi di riferimento interni identificati sul robot. Abbiamo definito cinque sistemi di riferimento principali per l'endoscopio:

1. "Endoscope Base" (indicato con F_{EB}, vedere fig. C.4), situato alla base della parte flessibile azionata dell'endoscopio.
2. "Endoscope Head" (indicato con F_{EH}, vedere fig. C.4), situato in cima alla parte flessibile azionata dell'endoscopio.
3. "Camera" (indicato con F_{C}, vedere fig. C.4), situato in corrispondenza della telecamera endoscopica.
4. "Left and Right Jaws Heads" (per una maggiore chiarezza, nella fig. C.4 è rappresentato unicamente il sistema di riferimento di destra, indicato con F_{JH}), situati in corrispondenza delle uscite dei canali che contengono gli strumenti.

Tre sistemi di riferimento sono invece stati identificati per ogni strumento:

1. "Instrument Base" (indicato con F_{IB}, vedere fig. C.4), sitato alla base della parte flessibile azionata dello strumento.
2. "Instrument Head" (indicato con F_{IH}, vedere fig. C.4), sitato in cima alla parte flessibile azionata dello strumento.
3. "Instrument Tip" (indicato con F_{IT}, vedere fig. C.4), situato in cima allo strumento.

Come anticipato nella sezione C.2, STRAS dispone di 10 GDL (vedere fig. C.5):

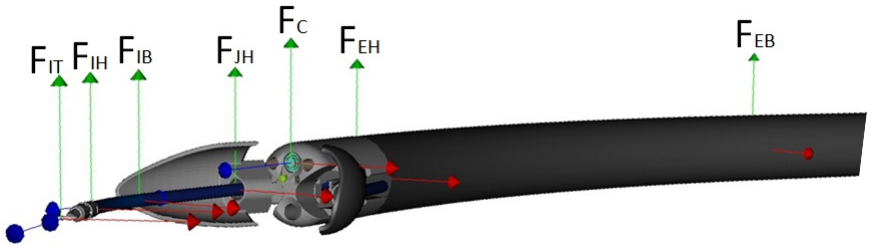

Fig. C.4. Sistemi di riferimento principali di STRAS.

- 3 GDL dell'endoscopio: traslazione longitudinale t_E (indicata con 1, vedere fig. C.5) e due deflessioni ortogonali dx e dy (indicate con 2 e 3, vedere fig. C.5);
- 3 GDL per ogni strumento: translazione longitudinale t_I (indicata con 4, vedere fig. C.5), rotazione θ_I (indicata con 5, vedere fig. C.5) e deflessione β (indicata con 6, vedere fig. C.5);
- un GDL supplementare per l'apertura e la chiusura degli strumenti azionati come la pinza (indicato con 7, vedere fig. C.5).

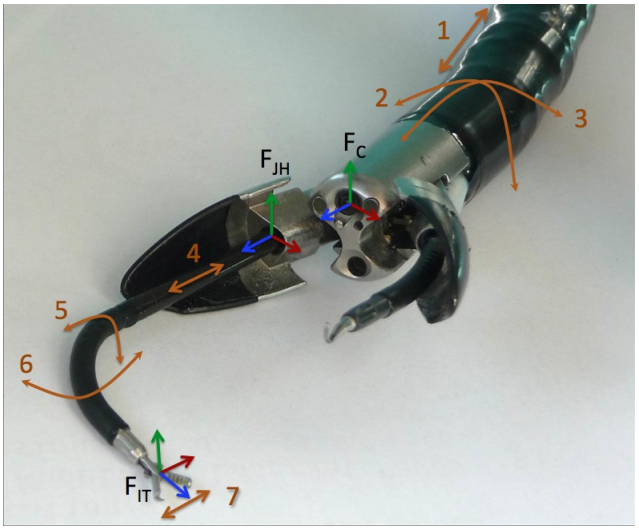

Fig. C.5. Gradi di libertà di STRAS.

Uno studio numerico dello spazio di lavoro del robot ha mostrato che ogni strumento copre una superficie ellissoidale quando vengono utilizzati unicamente i movimenti di deflessione e rotazione. Quando lo strumento è traslato, la superficie ellissoidale viene anch'essa traslata rigidamente nello spazio formando un cilindro (vedere fig. C.6). Gli spazi di lavoro dei due strumenti si incrociano in una zona centrale comune che ha una forma conica. Questa zona ha un'estensione massima situata a 25 mm dalla telecamera endoscopica (vedere fig. C.6).

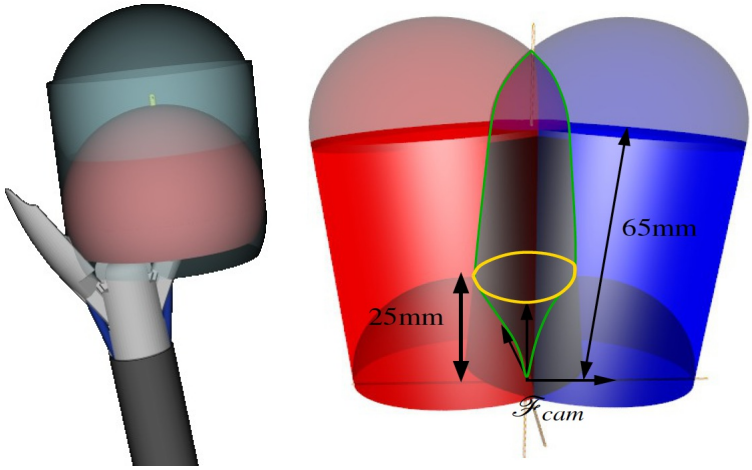

Fig. C.6. Spazio di lavoro di STRAS.

Partendo dal modello cinematico diretto, è possibile calcolare la matrice Jacobiana del robot, la quale rappresenta la relazione tra le velocità Cartesiane e articolari. Lo Jacobiano completo del robot è una matrice con 6 righe (le 6 componenti Cartesiane) e 9 colonne (i GDL del sistema, con l'esclusione dell'apertura e chiusura della pinza). Siccome STRAS ha una struttura arborescente, un movimento dell'endoscopio influenza allo stesso tempo la posizione di entrambi gli strumenti. L'endoscopio è quindi principalmente utilizzato per il posizionamento iniziale. Inoltre, gli strumenti dispongono esclusivamente di 3 GDL ciascuno, quindi la loro orientazione nello spazio Cartesiano è determinata dalla loro posizione. Può essere perciò utile semplificare il calcolo dello Jacobiano considerando ogni strumento separatamente: lo Jacobiano relativo ad uno strumento è una matrice 3 x 3 della forma

$$J_I(\boldsymbol{q}_I) = \begin{bmatrix} \frac{\partial X}{\partial \beta} & -Y & 0 \\ \frac{\partial Y}{\partial \beta} & X & 0 \\ \frac{\partial Z}{\partial \beta} & 0 & 1 \end{bmatrix} \tag{C.2}$$

con:

$$\boldsymbol{q}_I = \begin{bmatrix} \beta & \phi & t_I \end{bmatrix}^T \tag{C.3}$$

e

$$\begin{bmatrix} X \\ Y \\ Z \end{bmatrix} =_{JH} T^{IT} = \begin{bmatrix} d_{HT}\cos(\phi)\sin(\beta) + \frac{\ell\cos(\phi)(1-\cos(\beta))}{\beta} \\ d_{HT}\sin(\phi)\sin(\beta) + \frac{\ell\sin(\phi)(1-\cos(\beta))}{\beta} \\ d_{HT}\cos(\beta) + t_I + \frac{\ell\sin(\beta)}{\beta} \end{bmatrix} \tag{C.4}$$

dove d_{HT} è la lunghezza dello strumento rigido collegato all'estremità della parte flessibile.

Con questa formulazione dello Jacobiano è possibile trovare la posizione delle singolarità nello spazio di lavoro dello strumento calcolandone il determinante: in

ogni posizione singolare il suo valore è uguale a zero. In particolare, nello spazio di lavoro di ogni strumento possiamo trovare due singolarità (vedere fig. C.7):

- in corrispondenza di un valore di deflessione uguale a zero, la rotazione dello strumento non produce alcun effetto sulla sua posizione Cartesiana;
- in corrispondenza del diametro dell'ellissoide che rappresenta lo spazio di lavoro dello strumento, la punta dello strumento si trova alla distanza massima dall'asse dello strumento stesso; in questa situazione, nessun movimento sul piano XY può essere effettuato senza l'impiego dei GDL dell'endoscopio.

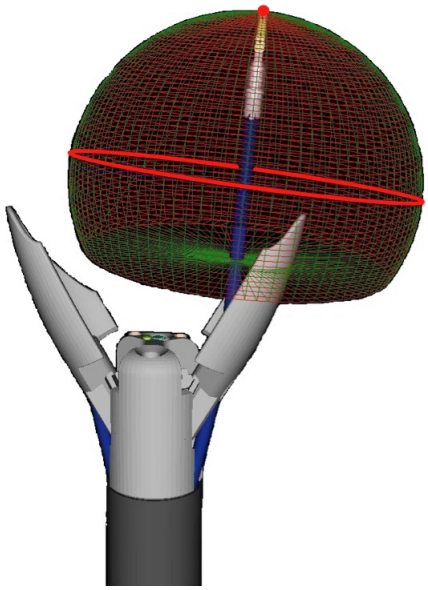

Fig. C.7. Posizione delle singolarità nello spazio di lavoro dello strumento.

C.4 Teleoperazione

STRAS è stato sviluppato come un robot teleoperato, cioè come un sistema meccatronico slave comandato da un'interfaccia master. Il sistema slave è composto da un'endoscopio e due strumenti robotizzati, presentati nella sezione C.2 (vedere fig. C.2). Si possono proporre più modalità di controllo per questo sistema:

- Controllo in velocità ad anello aperto (vedere fig. C.8): l'input dell'utente è espresso come un riferimento di velocità Ω_{ref}, che viene direttamente moltiplicato per lo Jacobiano inverso J^{-1} in maniera tale da ottenere i riferimenti di velocità articolare $\dot{q}_{ref}$.
- Controllo articolare ad anello chiuso (vedere fig. C.9): invertendo il modello cinematico diretto è possibile calcolare i riferimenti di posizione articolari che

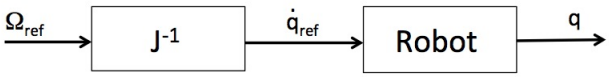

Fig. C.8. Schema di controllo in velocità ad anello aperto.

permettono di collocare lo strumento ad una posizione Cartesiana desiderata. In questo caso l'utente invia un riferimento di posizione X_{ref}, mentre il modello inverso fornisce la corrispondente configurazione articolare q_{ref} che viene confrontata con lo stato attuale del robot, al fine di ottenere un errore di posizionamento articolare e.

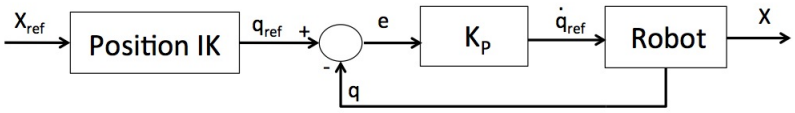

Fig. C.9. Schema di controllo articolare ad anello chiuso.

- Controllo in posizione ad anello chiuso (vedere fig. C.10): l'input dell'utente, espresso come una posizione di riferimento Cartesiana X_{ref}, viene confrontato con la stima della posizione Cartesiana corrente del robot, ottenendo un errore e. La stima può essere ottenuta utilizzando il modello cinematico diretto del robot o un tracker esterno, il quale sfrutta tipicamente delle proprietà elettromagnetiche, ottiche o inerziali.

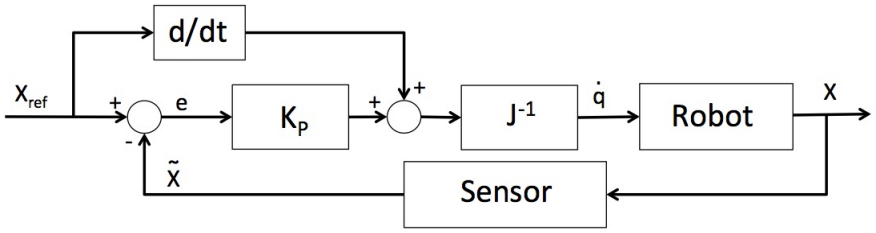

Fig. C.10. Schema di controllo in posizione ad anello chiuso.

Il sistema master di STRAS è composto da due interfacce aptiche omega.7 (Force Dimension, Nyon, Svizzera), che forniscono 7 GDL ciascuna: 3 traslazioni, 3 rotazioni e un grilletto analogico (vedere fig. C.11).

I sistemi master e slave hanno delle strutture cinematiche completamente differenti: sul lato master sono disponibili 14 GDL, mentre il robot slave è dotato di 10 GDL, quindi deve essere stabilita una mappatura tra i due sistemi. Inoltre, le

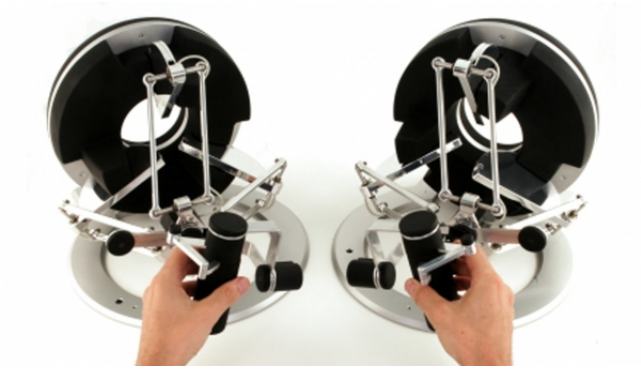

Fig. C.11. Interfacce aptiche omega.7 di Force Dimension.

due interfacce aptiche devono controllare i 3 sotto-sistemi slave per permettere ad un solo utente di far funzionare l'intero robot. La soluzione che abbiamo adottato per risolvere questo problema consiste nell'assegnare il controllo dello strumento sinistro all'interfaccia sinistra e dello strumento destro all'interfaccia destra. Quando è necessario muovere l'endoscopio, la pressione di un pedale permette di controllare l'endoscopio con una delle due interfacce.

Per il nostro robot proponiamo quattro mappature diverse:

1. "Direct joint control": ogni GDL del sistema slave è direttamente controllato da un movimento elementare dell'interfaccia master. Lo scopo di questa modalità è di riprodurre un'esperienza di manipolazione prossima al sistema manuale Anubiscope, evitando gli effetti indesiderati come gli attriti nell'azionamento e la cattiva ergonomia. In questa mappatura viene utilizzato un sotto-insieme dei GDL dell'interfaccia master: il grilletto, la traslazione lungo Z t_Z e la rotazione intorno a Z θ_Z controllano rispettivamente la deflessione, la traslazione e la rotazione dello strumento (vedere fig. C.12).
2. "Orientation guidance": questa modalità offre una sorta di controllo articolare nel quale i movimenti dell'interfaccia master sono limitati a quelli che lo strumento può effettuare a partire dalla configurazione corrente. Come nella mappatura "Direct joint control", la rotazione dell'interfaccia θ_Z controlla la rotazione dello strumento. Di contro, il riferimento per la deflessione dello strumento è dato dall'impugnatura dell'interfaccia aptica: i suoi movimenti sono limitati su una linea retta che passa attraverso la posizione centrale dell'interfaccia nel piano $X_M Y_M$ (vedere fig. C.13). Dato che l'orientazione dell'impugnatura è allineata con quella dello strumento, la linea retta rappresenta la traiettoria, proiettata su un piano, che lo strumento percorre quando la sua deflessione varia.
3. "Cartesian control": il controllo Cartesiano di STRAS può essere realizzato utilizzando il modello cinematico inverso o lo Jacobiano del sistema (vedere fig. C.9 e C.10). In entrambi i casi, l'input dell'utente consiste in posizioni Cartesiane desiderate per gli strumenti, trasmesse per mezzo dell'interfaccia master.

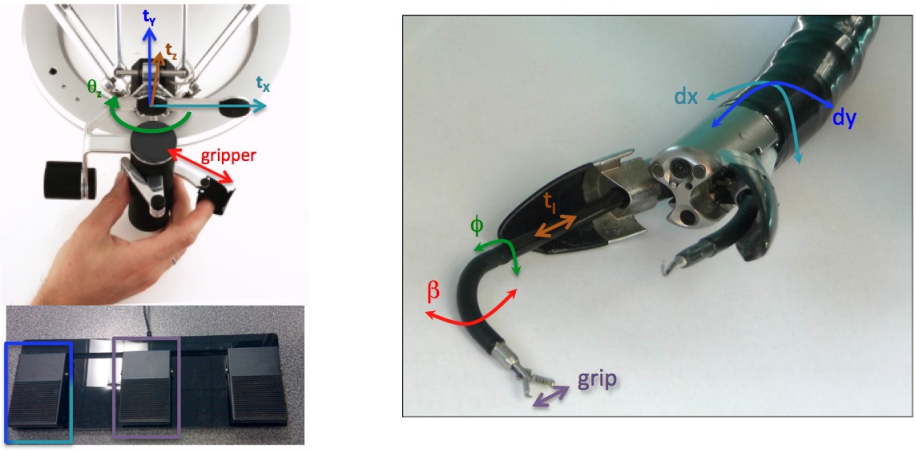

Fig. C.12. Mappatura "Direct joint control".

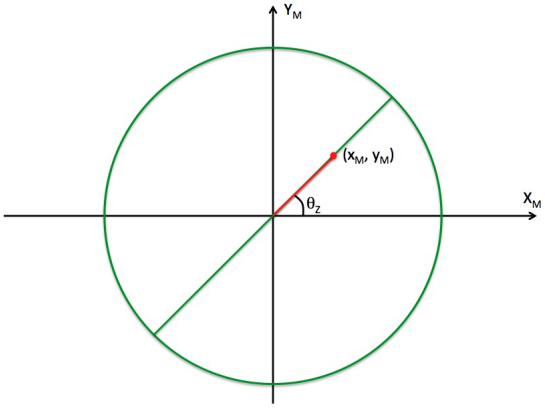

Fig. C.13. Mappatura "Orientation guidance".

4. "Pseudo-Cartesian control": denominata "Pseudo" poiché offre una sensazione di controllo molto simile ad una strategia Cartesiana, questa modalità non utilizza un modello cinematico per controllare il sistema. In questa mappatura, i movimenti dell'interfaccia master nel piano $X_M Y_M$ controllano contemporaneamente la deflessione e la rotazione degli strumenti, mentre la traslazione t_Z dell'interfaccia aptica lungo la direzione Z controlla direttamente la traslazione dello strumento (vedere fig. C.14):

$$\phi = \arctan 2(y_M,\, x_M) \tag{C.5}$$

$$t_I = z_M \tag{C.6}$$

$$\beta = \lambda \sqrt{x_M^2 + y_M^2} \tag{C.7}$$

dove (x_M, y_M, z_M) rappresenta la posizione corrente dell'impugnatura dell'interfaccia aptica, e λ è un fattore di scala che permette di adattare lo spazio di lavoro dell'interfaccia a quello dello strumento.

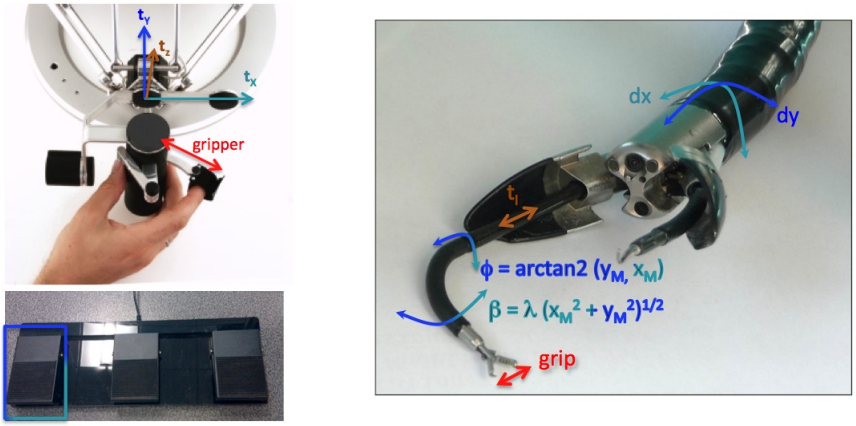

Fig. C.14. Mappatura "Pseudo-Cartesian control".

Le quattro mappature proposte non permettono di sfruttare la totalità dei gradi di liberta che STRAS offre, poiché ogni sotto-sistema del robot slave è controllato direttamente dall'utente e i riferimenti calcolati per uno strumento non tengono conto della posizione dell'altro strumento. Inoltre, l'endoscopio è attivato unicamente nel momento in cui è necessario riposizionare la telecamera endoscopica o la base degli strumenti. Al fine di sfruttare tutta la mobilità di STRAS in maniera coordinata, è necessario utilizzare un modello globale del sistema. Lo Jacobiano rappresenta la soluzione più comune in robotica per risolvere il problema cinematico inverso in termini di velocità. Nel caso di una matrice rettangolare, e quando il sistema non si trova in posizione singolare, lo Jacobiano inverso $J^{\#}$ può essere calcolato con la formula della pseudo-inversa di Moore-Penrose:

$$J^{\#} = J^T(JJ^T)^{-1}. \tag{C.8}$$

Contrariamente ai manipolatori robotici standard, i quali dispongono di un solo organo terminale da controllare, STRAS ha una struttura arborescente con due organi terminali diversi. Questa struttura implica che un movimento dell'endoscopio influenza la posizione dei due strumenti. Inoltre, i compiti assegnati separatamente ai due strumenti potrebbero entrare in conflitto, in maniera particolare quando essi richiedono un movimento dell'endoscopio. Abbiamo provato ad esplorare diverse soluzioni a questo problema:

- **Riposizionamento automatico dell'endoscopio**: poiché il campo di visione della telecamera endoscopica non contiene completamente lo spazio di lavoro degli strumenti, un movimento dell'endoscopio può essere richiesto quando uno strumento esce dall'immagine. Ma siccome gli strumenti sono solidali

con l'endoscopio, le loro posizioni assolute saranno influenzate nel caso in cui vengano utilizzati i soli gradi di libertà dell'endoscopio. Una soluzione a questo problema consiste nel ricalcolare una nuova configurazione articolare, utilizzando il modello cinematico inverso, che prenda in considerazione tutti i GDL del sistema.

- **Matrice di ponderazione**: nel caso di task conflittuali tra gli strumenti, una soluzione di compromesso consiste nell'assegnare dei pesi relativi agli strumenti. In questo modo, lo strumento che ha il peso più elevato sarà privilegiato durante il calcolo della soluzione finale la quale, in ogni caso, non soddisferà completamente nessuno dei task.
- **Task prioritario**: piuttosto che assegnare dei pesi relativi, un'altra soluzione per risolvere un conflitto tra task differenti consiste nell'indicare quale dei task ha la priorità principale e che, quindi, dovrà essere assolutamente completato. Una volta che il compito a priorità maggiore è eseguito, si cerca di effettuare quello a priorità minore senza modificare la posizione del primo strumento. Ciò è possibile sfruttando la ridondanza del sistema o i gradi di libertà non utilizzati duranti il primo task.

C.5 Simulatore virtuale

La simulazione virtuale è una tecnica che consiste nell'utilizzare dei sistemi informatici per creare dei mondi sintetici. I vantaggi nell'utilizzo della simulazione virtuale in chirurgia sono numerosi, in particolar modo la possibilità per un chirurgo principiante di fare pratica con dei compiti elementari, ma anche di simulare delle operazioni complesse nelle quali vengono valutati i gesti effettuati. Mentre per la laparoscopia sono disponibili diversi simulatori commerciali, delle difficoltà legate alla specificità degli strumenti ed alla complessità delle operazioni hanno impedito sinora la disponibilità di tali simulatori per la tecnica della chirurgia senza cicatrici.

L'idea di sviluppare un simulatore virtuale di STRAS era stata già proposta all'inizio del progetto: l'obiettivo iniziale era di avere una riproduzione cinematica virtuale del robot con la quale testare le strategie di controllo. Uno dei vantaggi di questo approccio consiste nella possibilità di testare sia il modello teorico del sistema, sia di simulare le non-linearità che incidono sul robot. In questa maniera, è possibile studiare separatamente l'effetto di ogni non-linearità e vedere allo stesso tempo le reazioni dell'utente rispetto alle diverse strategie di controllo. Per questo motivo, una prima versione del simulatore è stata sviluppata (vedere fig. C.15) utilizzando il linguaggio di programmazione C# e la libreria grafica VtkDotNet, un wrapper non ufficiale del Visualization Toolkit (VTK) di Kitware.

La finestra principale del simulatore contiene i controlli per interagire con i gradi di libertà del robot, così come i comandi per accedere a tutte le funzionalità dell'applicazione. Due modalità di visualizzazione sono disponibili (vedere fig. C.16) : la *vista esterna*, che permette di vedere il modello 3D del robot da una prospettiva esterna, e la *vista telecamera*, che riproduce l'immagine endoscopica proveniente dalla telecamera integrata nella testa dell'endoscopio.

Così come nel sistema reale, il simulatore comunica con le interfacce aptiche in modo tale da ricevere i comandi dell'utente: in funzione della strategia scelta,

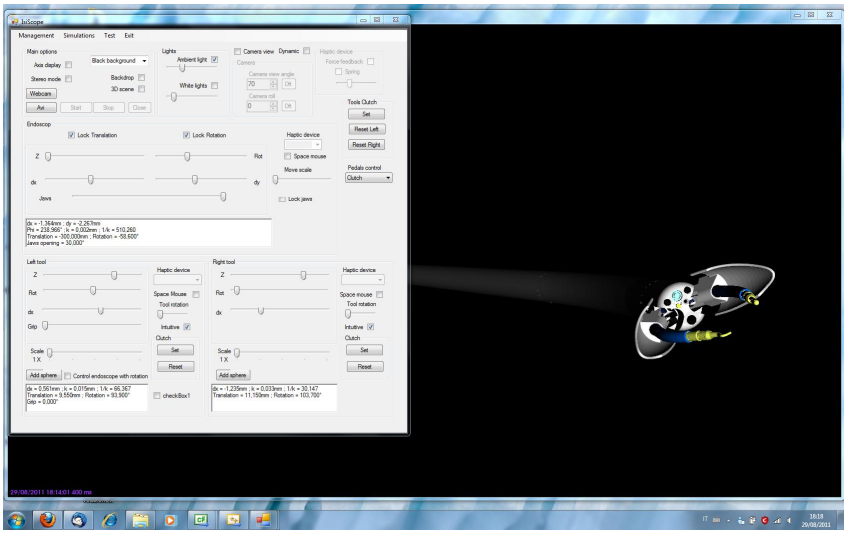

Fig. C.15. Prima versione del simulatore virtuale di STRAS.

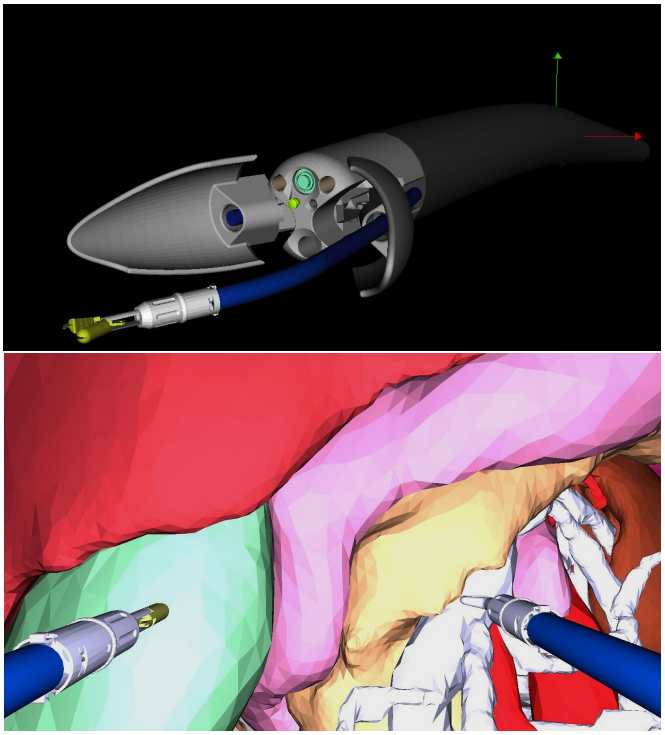

Fig. C.16. Vista esterna (in alto) e vista telecamera (in basso) nel simulatore virtuale di STRAS.

vengono calcolati i riferimenti per i motori virtuali e l'ambiente grafico viene aggiornato. Al fine di ottenere dei riferimenti esatti durante i calcoli, è necessario aggiornare il modello cinematico molto frequentemente (il tempo di refresh deve essere dell'ordine dei 5 ms), in maniera tale che esso sia corretto e rappresenti lo stato corrente del robot. Tuttavia, sul lato grafico il refresh dei modelli 3D richiede delle ingenti capacità di calcolo del computer. In questo caso, un framerate di 30 fps (frames per second, cioè 33 ms) è più che sufficiente per riprodurre un'animazione grafica fluida ed in tempo reale. E' quindi necessario separare i due refresh (cinematico e grafico) in due cicli differenti che comunicano in maniera asincrona (vedere fig. C.17).

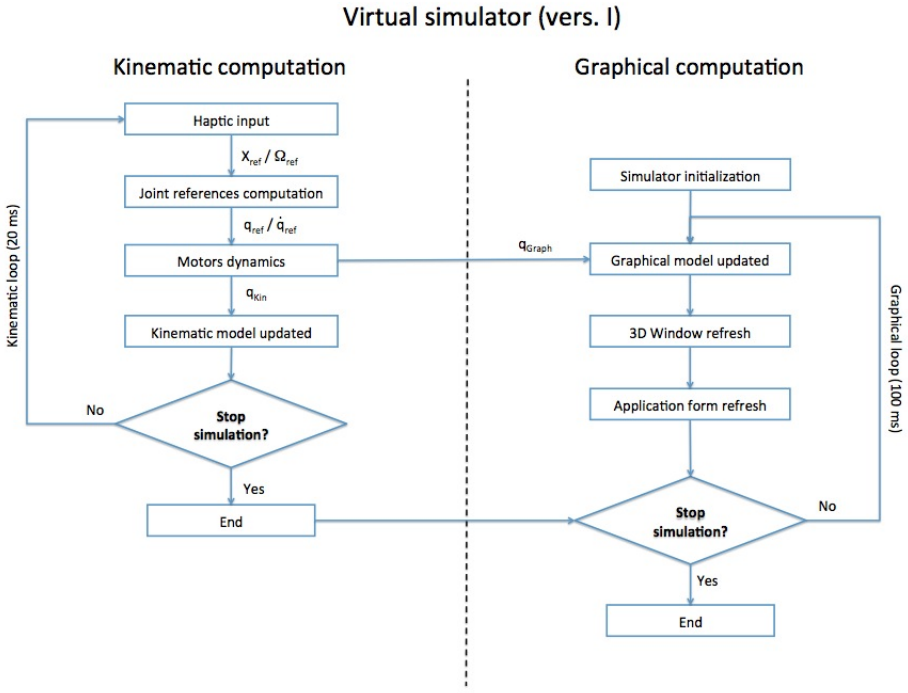

Fig. C.17. Flusso di lavoro della prima versione del simulatore virtuale di STRAS.

In questa prima versione del simulatore sono state implementate tutte le strategie Cartesiane, così come è stata proposta una modellizzazione delle non-linearità del sistema (in particolar modo il gioco dei cavi che producono la deflessione). Il limite principale di questo simulatore è l'assenza di interazioni fisiche nell'ambiente virtuale: data l'assenza di un motore fisico nel ciclo di calcolo grafico, è impossibile rilevare le collisioni degli strumenti con gli oggetti virtuali e, quindi, i task che comportano l'utilizzo degli strumenti sono impossibili da realizzare. Una seconda versione del simulatore è stata perciò sviluppata, con lo scopo aggiuntivo di estendere le funzioni del simulatore e renderlo un sistema di addestramento per gli utenti futuri del robot. Questa versione, realizzata come un'estensione dell'applicazione

principale di controllo del robot, è basata su Blender, un software open source di modellizzazione grafica 3D. Blender integra al suo interno un "Game engine" (Motore di gioco) che comprende una libreria per i calcoli fisici (Bullet). In questo modo, tutti gli oggetti 3D che fanno parte della scena virtuale sono connessi al motore di gioco, e le loro interazioni possono essere rilevate a partire dai blocchi logici "Sensor-Controller-Actuator" ("Sensore-Controllore-Attuatore"):

- I sensori rilevano l'attivazione di un dispositivo di input (come un tasto premuto o un movimento del mouse) o creano un rilevatore esterocettivo (come un radar o un rilevatore laser) capace di innescare un evento alla sua attivazione.
- I controllori riuniscono gli eventi innescati dai sensori e, in base alla funzione Booleana che implementano, li trasmettono agli attuatori. Un controllore può consistere anche in uno script Python che viene eseguito all'attivazione di un sensore.
- Gli attuatori cambiano lo stato corrente degli oggetti 3D in termini di posizione, velocità o parametri specifici ad ogni oggetto.

Come citato in precedenza, la seconda versione del simulatore non è un'applicazione autonoma, ma si integra nel controllore di alto livello del robot. Ciò significa che questo simulatore è responsabile unicamente del refresh grafico, mentre l'aggiornamento del modello cinematico e il calcolo dei riferimenti sono realizzati dall'applicazione principale di controllo (vedere fig. C.18).

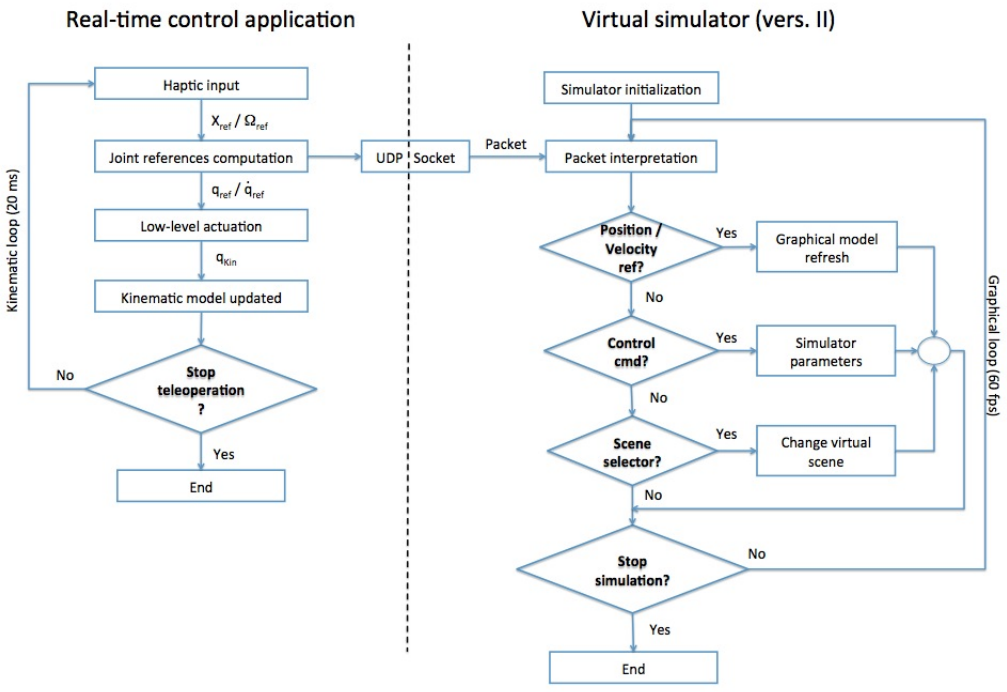

Fig. C.18. Flusso di lavoro della seconda versione del simulatore virtuale di STRAS.

La comunicazione tra il controllore di alto livello ed il simulatore è possibile grazie ad un socket UDP (User Datagram Protocol). Questo simulatore può funzionare in due modalità differenti:

- "Slave mode": il simulatore riceve gli stessi riferimenti articolari del robot, seguendone i movimenti. Questa modalità può essere utile per avere una rappresentazione visiva della posizione teorica del sistema in funzione della sua configurazione articolare.
- "Arcade mode": il controllore di alto livello comunica esclusivamente con il simulatore, e i movimenti del modello virtuale del robot corrispondono all'input dell'utente.

In questo simulatore sono state implementate delle scene virtuali che riproducono dei task tipici di addestramento:

- "Rings": tre anelli, che si trovano su dei pioli, devono essere afferrati con lo strumento di destra, passati allo strumento di sinistra ed infine posati intorno al supporto che si colora di rosso (vedere fig. C.19). La posizione del supporto rosso è scelta casualmente, ed è necessario utilizzare i movimenti dell'endoscopio per poter raggiungere tutti gli oggetti della scena. Durante l'esercizio vengono registrati diversi parametri (tempo d'esecuzione, numero di anelli caduti, numero di prese mancate) in maniera tale da ottenere una valutazione del gesto alla fine della simulazione.

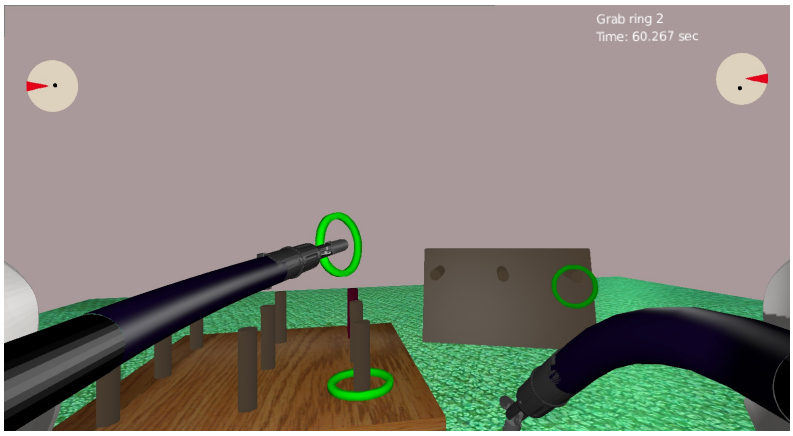

Fig. C.19. Screenshot durante il task "Rings".

- "Rings 2": tre anelli sono nascosti all'interno di una scatola, chiusa da un coperchio a cerniera che può essere sollevato a partire dalla sua maniglia sferica. L'utente deve sollevare il coperchio, afferrare i tre anelli e depositarli su un supporto collocato sulla destra della scena (vedere fig. C.20). Durante la simulazione vengono registrati gli stessi parametri della scena "Rings", e l'esercizio termina quando il terzo anello è collocato correttamente intorno al supporto.
- "Surgery": lo scopo di questo esercizio è di effettuare una colecistectomia semplificata. L'utente deve sollevare il quinto segmento di un fegato, riprodotto

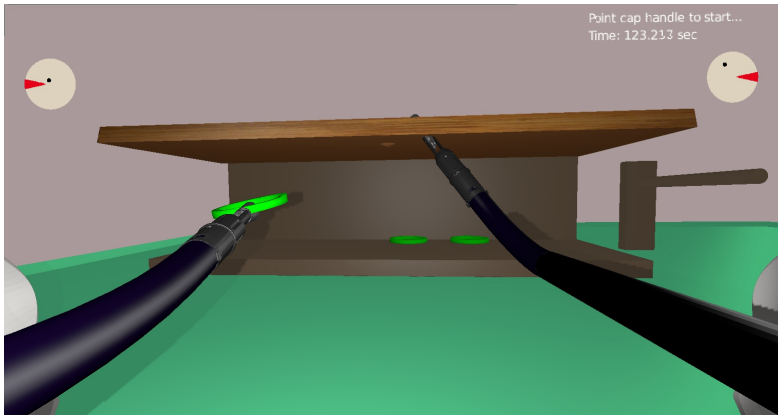

Fig. C.20. Screenshot durante il task "Rings 2".

nella scena, in maniera da esporre la cistifellea (vedere fig. C.21). In seguito, la cistifellea deve essere sezionata cauterizzando il dotto cistico con il bisturi elettrico. L'esercizio termina con il recupero della vescicola, la quale deve essere depositata in una scatola di recupero situata sul lato destro della scena.

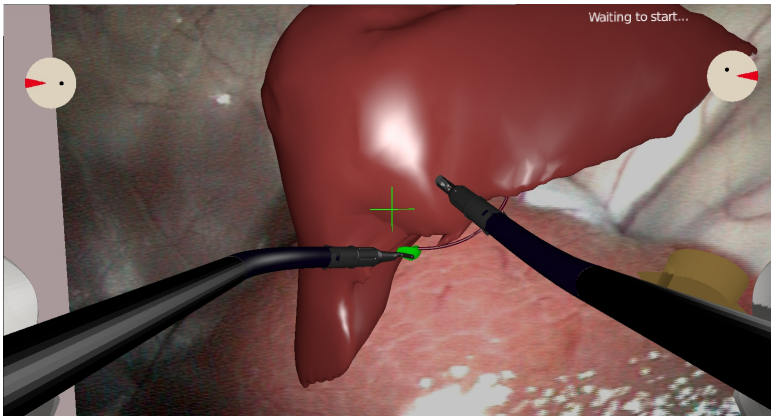

Fig. C.21. Screenshot durante il task "Surgery".

C.6 Risultati

C.6.1 Simulatori

Durante la fase di sviluppo di STRAS abbiamo condotto degli esperimenti con la prima versione del simulatore virtuale, allo scopo di confrontare le strategie di controllo Cartesiano che abbiamo proposto. Al fine di testare la precisione e la velocità di risposta del sistema, sono stati implementati due task specifici (vedere fig. C.22):

- "Precision task": l'utente deve seguire un cammino tortuoso (che imita i movimenti durante una sutura) con uno degli strumenti, cercando di restare il più vicino possibile al percorso prestabilito.
- "Simple task": in questo caso, il cammino da seguire è lineare ed un errore di traiettoria, rappresentato come un cilindro concentrico al percorso, è tollerato. Lo scopo è di effettuare il movimento il più rapidamente possibile, cercando di restare all'interno del cilindro con la punta dello strumento.

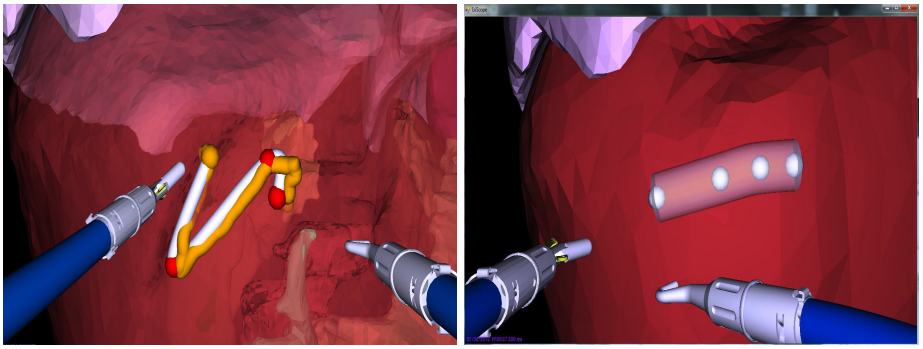

Fig. C.22. Screenshot durante il "Precision task" (sinistra) e il "Simple task" (destra).

I due task sono stati proposti a due gruppi di dieci persone, che li hanno effettuati in un primo tempo utilizzando il modello ideale del robot e successivamente introducendo delle non-linearità. I vantaggi di tale studio sono numerosi: tramite il modello cinematico ideale si può valutare il comportamento del sistema senza la necessità di considerare l'effetto delle non-linearità; successivamente, introducendo progressivamente delle perturbazioni all'interno della simulazione se ne può valutare il loro effetto sul comportamento del sistema e sulle reazioni dell'utente. Per valutare i diversi task abbiamo definito una funzione di punteggio, che prende in conto il tempo di esecuzione T e l'errore tra il percorso prestabilito e quello effettuato dall'utilizzatore:

$$Score = \phi_T T + \phi_e \sqrt{e_X^2 + e_Y^2 + e_Z^2}. \tag{C.9}$$

I pesi ϕ_T e ϕ_e differiscono a seconda del task, in maniera da sottolineare il contributo differente degli errori: per il "Precision task" $\phi_T = 1$ e $\phi_e = 10$, mentre per il "Simple task" $\phi_T = 10$ e $\phi_e = 5$. I risultati ottenuti, che devono essere valutati separatamente per ogni task, sono riassunti nella tabella C.1.

In condizioni ideali, una strategia di controllo in velocità per il sistema slave, insieme ad un input di posizione per il sistema master, dà dei risultati migliori per il "Precision task". Questa modalità di controllo permette di ottenere dei movimenti precisi degli strumenti, poiché l'input dell'utente è dato sotto forma di piccole variazioni di velocità. Di contro, ciò si traduce in una minore reattività degli strumenti qualora siano richiesti dei movimenti più ampi. Per questo motivo le strategie di controllo in posizione forniscono dei risultati migliori per il "Sim-

Precision task						
Slave Control	**Master Output**	**Slave Input**	**Force Feedback**	**Mean Score (no error)**	**Mean Score (rot error)**	**Mean Score (backlash)**
Open Loop	Position	Velocity	Spring	75.268	143.265	151.029
	Velocity	Velocity	Gravity comp	77.056	117.600	507.05
CL Joint	Position	Position	Error	87.317	89.141	184.342
CL Cartesian	Position	Position	Error	83.345	104.262	110.255
	Velocity	Position	Gravity comp	84.110	88.683	199.71

Simple task						
Slave Control	**Master Output**	**Slave Input**	**Force Feedback**	**Mean Score (no error)**	**Mean Score (rot error)**	**Mean Score (backlash)**
Open Loop	Position	Velocity	Spring	80.451	81.726	92.577
	Velocity	Velocity	Gravity comp	91.879	149.493	101.64
CL Joint	Position	Position	Error	77.131	92.958	153.863
CL Cartesian	Position	Position	Error	72.268	99.290	88.591
	Velocity	Position	Gravity comp	78.754	129.780	143.820

Table C.1. Risultati dei task effettuati in condizioni ideali con la prima versione del simulatore.

ple task". Le osservazioni cambiano significativamente quando un errore viene introdotto nella simulazione (vedere tab. C.2).

	Precision task			**Simple Task**		
Slave Input	Open Loop	CL Cartesian	CL Joint	Open Loop	CL Cartesian	CL Joint
Master Output	Position	Position	Position	Position	Position	Position
Mean	81.637	82.321	88.138	79.01	68.196	78.57
(with error)	151.029	110.255	184.342	92.577	88.591	153.863
Median	69.626	67.705	78.08	73.225	52.93	46.94
(with error)	106.465	83.72	128.57	78.622	63.195	105.105
Min / Max	54.08/124.69	50.59/152.29	51.77/123.35	36.34/142.54	32.365/173.89	31.82/176.37
(with error)	84.15/324.94	63.99/290.53	63.17/564.24	50.134/175.23	46.205/203.515	46.09/455.485
Best results (# users)	3	3	4	2	4	4
(with error)	2	5	3	3	5	2

Table C.2. Risultati del secondo gruppo per i task realizzati a seguito dell'introduzione di imperfezioni nella simulazione.

In questo caso, l'errore introdotto simula un gioco a livello dei cavi che permettono la deflessione dello strumento. Questa non-linearità dà l'impressione che nulla accada quando viene richiesto un cambiamento di direzione dello strumento, quindi l'utente tende a muovere ulteriormente l'interfaccia. Questa situazione potrebbe condurre all'instabilità del sistema poiché:

- in una legge di controllo in velocità, un riferimento elevato di velocità Cartesiana viene inviato al sistema slave, il quale reagisce bruscamente all'uscita dalla zona morta del gioco;

- in una legge di controllo in posizione, il vettore di errore calcolato dall'anello di contro-reazione aumenta rapidamente durante l'effetto del gioco; l'anello di controllo cerca di ridurre questo errore, ma, analogamente al caso precedente, ciò può provocare delle velocità elevate all'uscita dalla zona morta del gioco.

Dai nostri test abbiamo potuto rilevare che una strategia di controllo Cartesiano con un riferimento in posizione per l'interfaccia master permette di ottenere i migliori risultati per la maggioranza delle persone implicate nelle simulazioni. La mappatura diretta tra gli spazi di lavoro dello strumento e dell'interfaccia aptica, prevista in questa legge di controllo, dà un buon senso di controllo per la maggior parte degli utenti, poiché la posizione dell'interfaccia aptica rappresenta direttamente la posizione dello strumento nella scena virtuale.

Con la seconda versione del simulatore virtuale abbiamo potuto testare il comportamento di STRAS in tre task realistici (cf. sezione C.5) che richiedono l'insieme dei GDL del sistema ed una cooperazione tra gli strumenti. I task proposti sono stati effettuati da otto utenti ripartiti in tre gruppi: esperti (3 utenti con esperienza sia sul robot sia sul simulatore), intermedi (3 utenti con esperienza sul robot) e principianti (2 utenti senza alcuna conoscenza del sistema e del suo simulatore). Ogni utente ha eseguito i task con le quattro diverse mappature proposte (vedere sezione C.4): "Direct axis control", "Orientation guidance", "Cartesian control" e "Pseudo-Cartesian control". Le simulazioni sono state realizzate utilizzando il modello ideale del sistema, senza introdurre perturbazioni. Durante l'esecuzione di ogni task sono stati registrati i parametri più importanti: le posizioni Cartesiane e articolari del robot, le posizioni delle interfacce aptiche, i tempi di esecuzione e gli errori degli utenti. I risultati di questo esperimento sono rappresentati in fig. C.23. Si può immediatamente notare che una modalità di controllo (Pseudo-)Cartesiano dà in media il miglior risultato per la maggior parte degli utenti. Ciò è da mettere in relazione probabilmente con la modalità di input dell'utente, più naturale ed intuitiva che quella di un controllo non-Cartesiano. Le interfacce aptiche utilizzate hanno un'architettura cinematica sufficientemente flessibile per permettere molteplici mappature. Tuttavia, in ogni strategia i gradi di libertà non utilizzati (in modo particolare le rotazioni passive dell'impugnatura per le strategie Cartesiane) perturbano gli utenti durante l'esecuzione dei task. Delle interfacce aptiche specificatamente concepite per una mappatura particolare potrebbero rappresentare un vantaggio per l'utente nella comprensione del funzionamento del sistema.

C.6.2 Sistema robotico

Nella sezione C.3 abbiamo introdotto un'ipotesi che ci ha permesso di descrivere cinematicamente le sezioni flessibili di STRAS per mezzo dei parametri di Denavit-Hartenberg. Per validare questa ipotesi, abbiamo eseguito un test nel quale sono state confrontate le posizioni dello strumento che si muoveva su un percorso prestabilito con le corrispondenti posizioni calcolate per mezzo del modello cinematico a partire dalle varie configurazioni articolari. Le posizioni dello strumento sono state rilevate mediante una telecamera esterna, collocata perpendicolarmente al piano di deflessione dello strumento ad una distanza fissa di 20 cm. Due marker visivi sono stati piazzati sullo strumento, uno alla base e l'altro all'estremità della parte flessibile. I movimenti dello strumento sono stati effettuati nel suo piano di

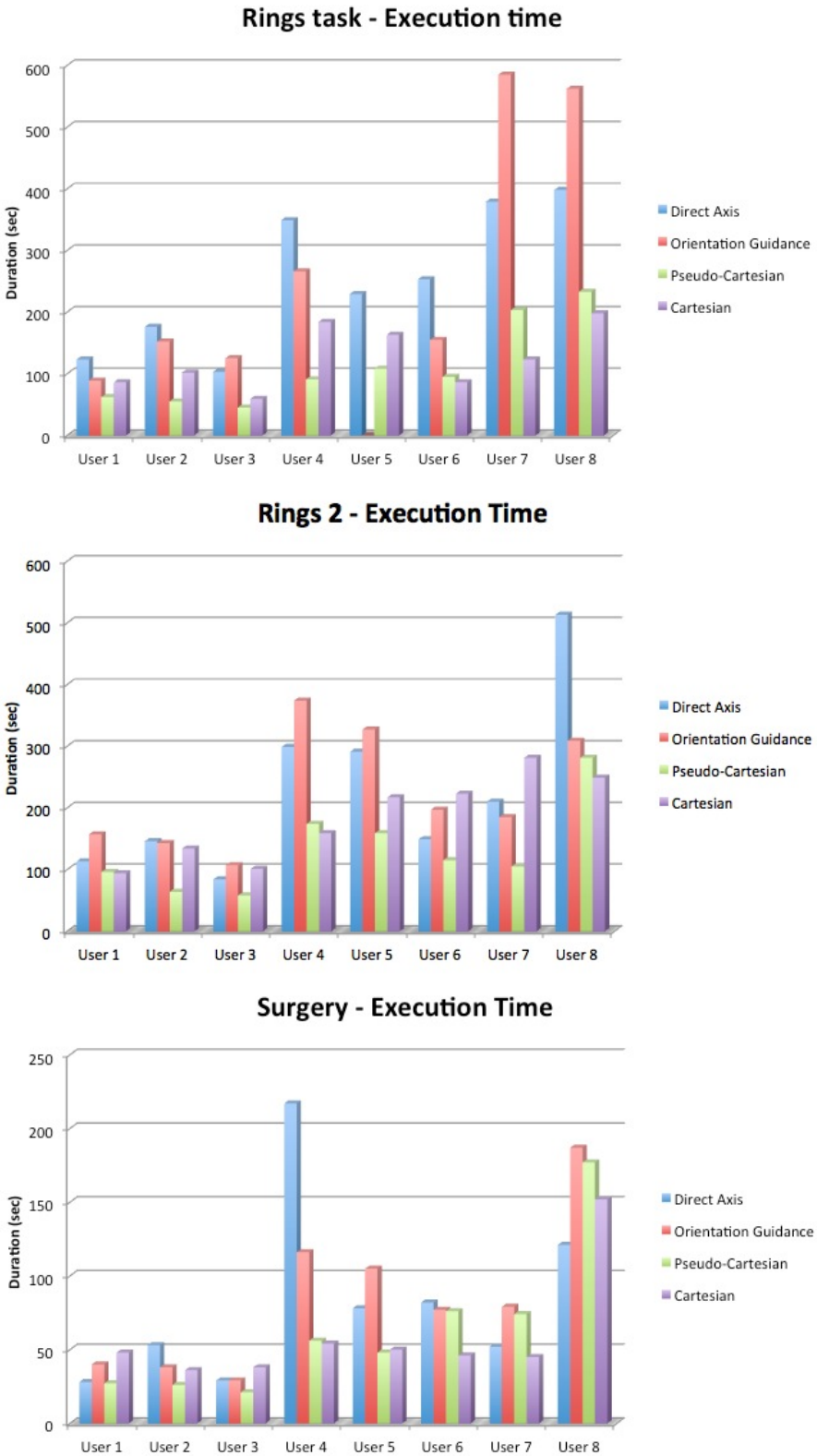

Fig. C.23. Tempi di esecuzione per i tre task effettuati con la seconda versione del simulatore.

deflessione, senza effettuare delle rotazioni. Le immagini provenienti dalla telecamera sono state elaborate allo scopo di estrarre la posizione dei marker. Il risultato è rappresentato in fig. C.24.

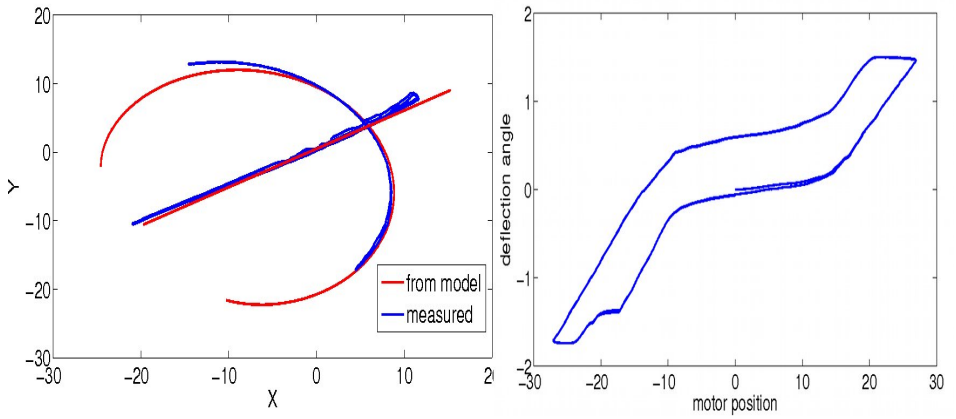

Fig. C.24. Sinistra: Confronto tra le posizioni dello strumento ottenute tramite misure (in blu) e mediante il modello cinematico (in rosso). Destra: caratteristica quasi-statica rappresentante il valore di deflessione dello strumento in funzione della posizione del motore corrispondente.

I movimenti di deflessione e traslazione seguono bene le traiettorie ideali fornite dal modello cinematico. Tuttavia, a seguito di un cambiamento del senso di deflessione, il gioco dei cavi di azionamento introduce una zona morta che è difficile da compensare analiticamente nel modello cinematico, dato che dipende da più fattori (forma dell'endoscopio, tipo di cavi, attriti ecc.).

Per confermare i risultati ottenuti in simulazione, abbiamo successivamente condotto delle esperienze simili con STRAS. In un primo tempo, abbiamo riprodotto i test di inseguimento di un cammino prestabilito e di puntamento utilizzando le mappature proposte. Allo scopo di valutare la reazione del sistema, i movimenti richiesti nei task includevano le singolarità. E' stato utilizzato un solo strumento, senza l'assistenza dei GDL dell'endoscopio, per effettuare i tre task (vedere fig. C.25): un inseguimento di percorso e due puntamenti (il primo nell'immagine e il secondo valutando la profondità reale).

Tre utenti esperti hanno effettuato i task utilizzando tutte le mappature. I risultati, rappresentati in fig. C.26, mostrano in media dei migliori tempi di esecuzione con le strategie Cartesiane, giudicate più intuitive dagli utenti per l'esecuzione di task nello spazio Cartesiano. Durante il task di inseguimento di percorso sono stati rilevati due tipi principali di errore: dei piccoli scarti rispetto al percorso imposto oppure degli ampi movimenti al di fuori del percorso. Nel primo caso, le derive di qualche millimetro sono dovute principalmente alle singolarità cinematiche che producono delle rotazioni incontrollate dello strumento; gli scarti di più di un centimetro dal cammino, invece, avvengono tipicamente quando si raggiunge il limite dello spazio di lavoro, nel qual caso è necessaria una riconfigurazione articolare per poter continuare il movimento. I task di puntamento sono stati eseguiti più facil-

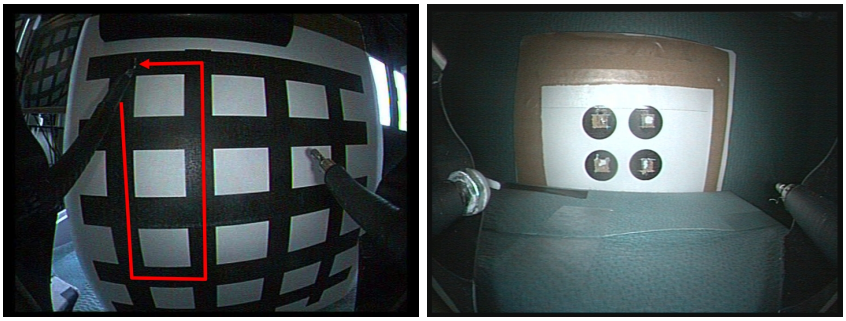

Fig. C.25. Task di inseguimento di percorso e puntamento effettuati con STRAS.

mente rispetto al task di inseguimento di percorso, poiché il cammino tra i punti non era imposto e gli utenti, quindi, potevano scegliere dei percorsi alternativi per raggiungere l'obiettivo.

A seguito dei test di valutazione delle strategie proposte, è stato effettuato un confronto tra il robot e la versione corta del sistema Anubiscope, prodotto da Karl Storz GmbH (Tuttlingen, Germania). Lo scopo di questo confronto consiste nel valutare se il sistema robotico apporta dei vantaggi rispetto al suo omologo manuale, particolarmente per quanto riguarda i tempi di esecuzione, la facilità d'uso e l'ergonomia. Per questo esperimento abbiamo sviluppato, in collaborazione con i chirurghi partner del progetto, un banco di prova contenente tre task elementari (vedere fig. C.27):

- Task 1: spostamento di anelli tra pioli vicini utilizzando esclusivamente la pinza. Il movimento richiesto è all'interno dello spazio di lavoro dello strumento, quindi il task è realizzabile senza la necessità di muovere l'endoscopio.
- Task 2: spostamento di anelli tra pioli lontani con l'assistenza dei GDL dell'endoscopio. Siccome l'endoscopio viene controllato dall'interfaccia sinistra e la pinza da quella destra, per questo task l'utente ha entrambe le mani occupate.
- Task 3: questo esercizio consiste nel recuperare un anello coperto da una garza e nel posizionarlo intorno ad un piolo collocato sulla sinistra. In questo caso, la cooperazione tra gli strumenti è fondamentale, così come i movimenti dell'endoscopio.

I test sono stati condotti con dieci utenti: tre chirurghi (uno dei quali esperto nell'utilizzo di Anubiscope) e sette ingegneri (due esperti nell'utilizzo di STRAS). Per STRAS, sono state testate tutti le mappature proposte. Il sistema manuale Anubiscope è stato fissato su un tavolo mediante un braccio rigido, allo scopo di evitare la presenza di un assistente per mantenerlo (come accade nell'utilizzo clinico di questo sistema). Il confronto tra i due sistemi è stato basato sui tempi di esecuzione dei task, sul numero di errori e sul successo o il fallimento in ogni prova. Al termine dei task, gli utenti hanno ricevuto un questionario per la valutazione soggettiva dell'esperienza. I risultati di questo esperimento sono rappresentati in fig. C.28.

Fig. C.26. Tempi di esecuzione per i task di inseguimento di percorso e puntamento.

Fig. C.27. Task proposti per il confronto STRAS - Anubiscope.

Quasi tutti gli utenti sono stati capaci di realizzare i task in un tempo minore della durata massima autorizzata. Nonostante ciò, durante i task 1 e 2 alcuni utenti hanno avuto delle difficoltà nel posizionare correttamente gli anelli sui pioli a causa dell'impossibilità di variare la rotazione dello strumento senza modificarne la posizione. Nei loro questionari, gli utenti hanno indicato STRAS come più intuitivo e semplice rispetto ad Anubiscope. Inoltre, l'assenza di attriti nell'interfaccia di controllo e la migliore ergonomia hanno posto la preferenza generale per il robot. La difficoltà nella percezione della profondità, comune ai due sistemi e dovuta all'utilizzo di una telecamera monoscopica, resta una forte limitazione per gli utenti principianti. In questo esperimento la mappatura "Pseudo-Cartesian control" ha permesso di ottenere i migliori tempi di esecuzione. Tuttavia, le preferenze degli utenti sono state ugualmente ripartite tra le mappature proposte. Ciò denota il carattere molto soggettivo di una tale scelta. Il vantaggio importante di STRAS è perciò la possibilità di offrire più modalità di controllo che permettono curve di apprendimento più corte per i nuovi utenti.

C.6.3 Test ex vivo

Al fine di testare STRAS in condizioni realistiche, abbiamo effettuato dei test *ex vivo*, in collaborazione con i nostri partner medici, con lo scopo di riprodurre una dissezione della sub-mucosa gastrica (ESD, *Endoscopic Submucosal Dissection* in inglese). Abbiamo adoperato uno stomaco di maiale, suturato in maniera tale da mantenere l'insufflazione e collocato intorno alla testa dell'endoscopio, in modo da simulare un approccio transgastrico (vedere fig. C.29). Abbiamo riscontrato diverse limitazioni del sistema nell'esecuzione di questa procedura, specialmente a causa della dimensione inadeguata degli strumenti utilizzati (una pinza ed un bisturi elettrico). Le ganasce della pinza erano troppo sottili per poter afferrare correttamente il tessuto viscoso, e l'effetto del bisturi elettrico era debole rispetto all'entità della dissezione richiesta per questo tipo di intervento, necessitando quindi di molto tempo per poter tagliare lo strato di mucosa. In effetti, gli strumenti manuali impiegati in questo tipo di chirurgia sono più larghi di quelli a nostra disposizione, permettendo quindi una migliore presa ed un'ablazione più efficace del tessuto. Un altro inconveniente rilevato è l'impossibilità di controllare l'insufflazione e di evacuare il fumo prodotto durante l'ablazione a partire dalla console dell'utente: i corrispondenti controlli, presenti sul corpo dell'endoscopio, non sono stati azionati

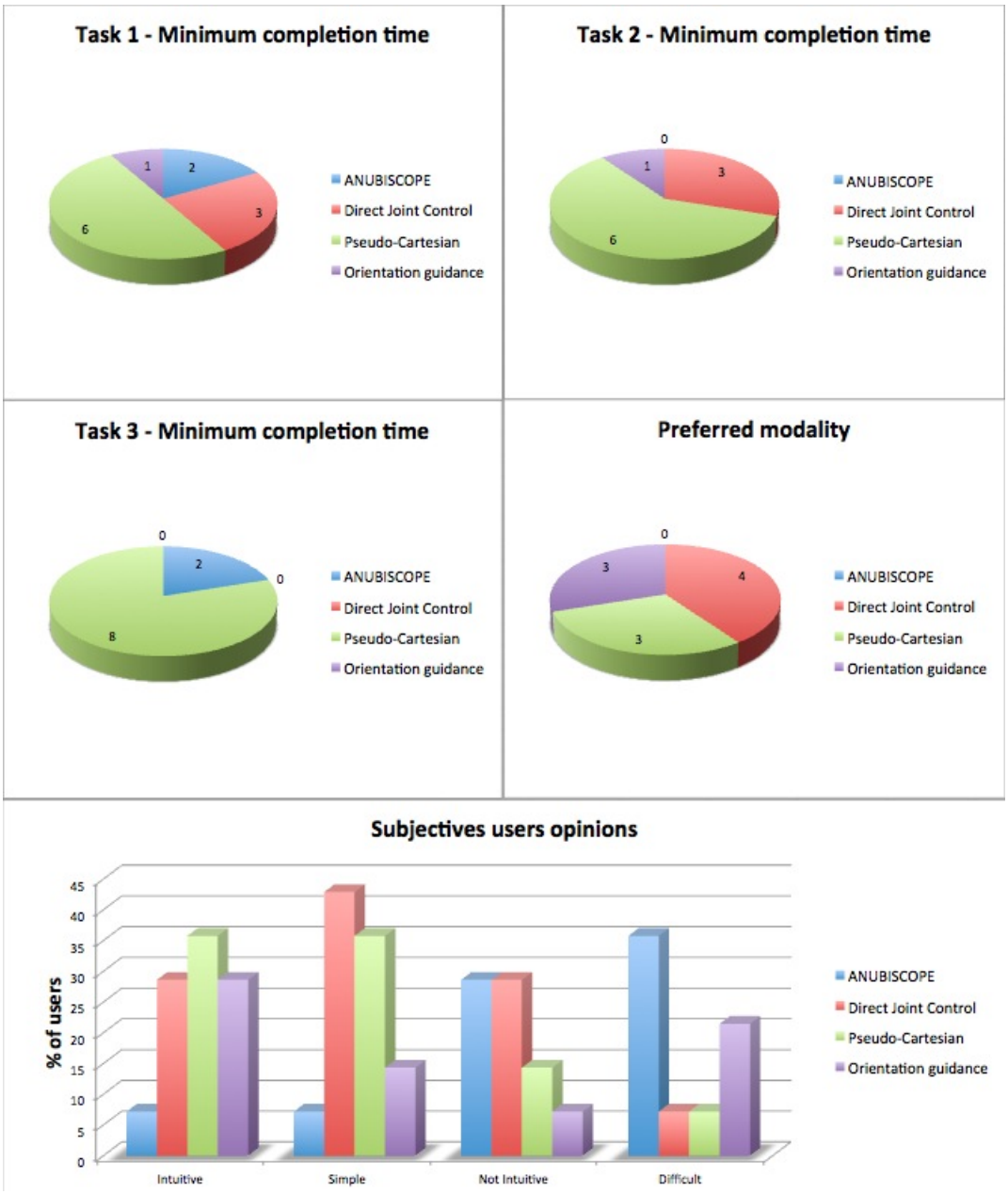

Fig. C.28. Risultati del confronto STRAS - Anubiscope.

roboticamente nel prototipo corrente. Di contro, la mobilità del sistema è stata adeguata, permettendo un'esplorazione completa dello stomaco. Siamo stati altresì in grado di estrarre il bisturi elettrico per pulirlo senza compromettere la funzionalità del sistema. L'installazione di STRAS e la sua configurazione sono state effettuate in meno di 15 minuti: l'integrazione del robot nella sala operatoria non ha posto particolari problemi rispetto ai dispositivi già presenti. Inoltre, data la dimensione ridotta del robot, i movimenti degli strumenti non rappresentano un rischio potenziale per le persone che potrebbero essere in prossimità del robot. Siamo convinti che, utilizzando degli strumenti più appropriati, STRAS potrà essere impiegato per un'operazione chirurgica completa.

C.7 Conclusioni

La prossima frontiera nella chirurgia mini-invasiva è rappresentata dalla chirurgia senza cicatrici, che ha come obiettivo ambizioso quello di evitare ogni tipo di cicatrice visibile sulla pelle del paziente a seguito di un'operazione chirurgica. In questo contesto, abbiamo presentato STRAS (Single access and Transluminal Robotic Assistant for Surgeons), un nuovo robot per la chirurgia senza cicatrici sviluppato in collaborazione con Karl Storz GmbH (Tuttlingen, Germania) e l'Institut de Recherche contre les Cancers de l'Appareil Digestif (IRCAD, Strasbourg, Francia). STRAS è stato sviluppato come un robot teleoperato, con un'interfaccia master che controlla il robot slave. Essendo flessibile nella sua struttura, STRAS non può essere descritto cinematicamente con i metodi classici della robotica: per calcolare il modello cinematico abbiamo quindi adoperato una formulazione sviluppata specificatamente per i robot continui. Uno sforzo è stato fatto al fine di ottenere il modello cinematico inverso del robot, che permette di calcolare tutte le configurazioni articolari relative ad una posizione Cartesiana desiderata degli strumenti. Abbiamo effettuato una valutazione numerica dello spazio di lavoro del robot e abbiamo calcolato le sue singolarità. Per quanto riguarda il robot slave, abbiamo proposto tre schemi di controllo:

- controllo in velocità ad anello aperto, nel quale un riferimento di velocità Cartesiana è direttamente trasformato in riferimento di velocità articolare utilizzando lo Jacobiano inverso;
- controllo articolare ad anello chiuso, nel quale viene adoperato il modello cinematico inverso per calcolare i riferimenti di posizione articolare corrispondenti alle posizioni Cartesiane desiderate;
- controllo in posizione ad anello chiuso, nel quale la posizione Cartesiana desiderata è confrontata con la posizione reale del robot, ed il vettore di errore calcolato è in seguito trasformato in riferimento di velocità articolare per mezzo dello Jacobiano inverso.

Le cinematiche dei sistemi master e slave sono molto differenti, quindi più mappature sono possibili per metterle in relazione. Accanto agli schemi di controllo, abbiamo proposto quattro mappature:

- "Direct joint control", che correla ogni movimento elementare delle interfacce aptiche con i GDL del robot slave;

Fig. C.29. Test ex vivo effettuati con STRAS. In alto: il robot è montato sul tavolo operatorio ed uno stomaco di maiale è suturato intorno alla testa dell'endoscopio. In basso: console dell'utente con le interfacce aptiche, il ritorno video della telecamera endoscopica e dell'applicazione principale di controllo.

- "Orientation guidance", nel quale i movimenti dell'interfaccia aptica sono limitati a quelli che lo strumento può effettuare a partire dalla configurazione corrente;
- "Cartesian control", che utilizza uno degli schemi di controllo ad anello chiuso per trasformare i comandi di posizione Cartesiana in riferimenti articolari per il robot;
- "Pseudo-Cartesian control", nel quale i movimenti dell'interfaccia aptica nel piano $X_M Y_M$ determinano i riferimenti per la deflessione e la rotazione dello strumento. La traslazione dello strumento è invece controllata direttamente dal movimento dell'interfaccia lungo la direzione Z_M.

Le interfacce master utilizzate offrono una buona flessibilità d'uso, ma i GDL non utilizzati sono in genere perturbanti per l'utente. Lo sviluppo di un'interfaccia specifica faciliterebbe il controllo del robot, soprattutto nelle fasi di apprendimento dei nuovi utenti.

Allo scopo di avere un ambiente di test sicuro nel quale valutare le mappature proposte e le strategie di controllo, abbiamo sviluppato un simulatore virtuale di STRAS. Nella sua prima versione, il simulatore è stato concepito per essere una replica cinematica del robot reale, comprese le sue principali non-linearità ed imperfezioni. Con questo simulatore abbiamo effettuato qualche esperimento, al fine di confrontare il comportamento del sistema rispetto alle differenti strategie proposte. Questi esperimenti hanno mostrato che in condizioni ideali il controllo in velocità permette di ottenere una migliore precisione, mentre il controllo in posizione assicura una risposta più rapida del sistema. In condizioni reali, quando cioè delle non-linearità vengono introdotte nel modello, una strategia di controllo in posizione permette di compensare meglio gli effetti delle perturbazioni. Il limite principale della prima versione del simulatore virtuale era l'assenza di un motore fisico per la gestione delle interazioni tra oggetti virtuali. Ciò implica l'impossibilità di effettuare la maggior parte degli esercizi di addestramento, come la presa di oggetti con la pinza o la dissezione di tessuti con il bisturi elettrico. Abbiamo scelto, quindi, di sviluppare una nuova versione del simulatore capace di interazioni fisiche. Tre task complessi, che necessitano della cooperazione tra gli strumenti, sono stati implementati in questo simulatore. Abbiamo organizzato una sessione di test con otto utenti, scelti in base alla loro esperienza precedente con STRAS e con il simulatore virtuale. Alla fine della sessione di test abbiamo constatato che le strategie Cartesiane permettono di ottenere in media dei migliori tempi di esecuzione per la maggior parte degli utilizzatori, indipendentemente dalla loro esperienza precedente. In ogni caso, a seguito di un periodo di formazione i risultati con le diverse modalità tendono ad uguagliarsi, come si può vedere in media con i risultati degli utenti esperti.

Dei risultati simili a quelli ottenuti in simulazione sono stati riportati durante gli esperimenti condotti con STRAS: una strategia di controllo Cartesiana è più intuitiva per la maggior parte degli utenti e permette di ottenere migliori risultati in termini di tempi di esecuzione. Inoltre, l'architettura delle interfacce master è troppo generica ed impedisce una comprensione immediata dei movimenti richiesti. Questi risultati ci forniscono una prima validazione del nostro simulatore virtuale, mostrando che esso rappresenta un buon strumento di valutazione e addestramento. Infine, il confronto diretto tra STRAS e la versione corta dell'Anubiscope

ha evidenziato una preferenza degli utenti per il primo, giudicato più semplice e più intuitivo che il suo omologo manuale. Il vantaggio principale di STRAS è costituito dal fatto che il sistema complessivo può essere controllato da un solo utilizzatore, in maniera ergonomica e con la possibilità di scegliere tra molteplici soluzioni di controllo

References

1. D. J. Abbott, C. Becke, R. I. Rothstein, and W. J. Peine. Design of an endoluminal NOTES robotic system. In *2007 IEEE/RSJ Int. Conf. Intell. Robot. Syst.*, pages 410–416. IEEE, Oct. 2007.
2. V. Agrawal, W. J. Peine, and B. Yao. Modeling of Transmission Characteristics Across a Cable-Conduit System. *IEEE Trans. Robot.*, 26(5):914–924, Oct. 2010.
3. P. Arcara and C. Melchiorri. Control schemes for teleoperation with time delay: A comparative study. *Rob. Auton. Syst.*, 38(1):49–64, Jan. 2002.
4. K. Au, S. Cho, B. Dong, S. Gorkhali, S. Lee, and J. Leung. da Vinci Surgical System. `http://biomed.brown.edu/Courses/BI108/BI108_2005_Groups/04/davinci.html`, Last access: October 2013, 2005.
5. F. Auerbach. *The Zeiss Works and the Carl Zeiss Foundation in Jena. (English Translation by R. Kanthack).* London: W&G Foyle Ltd, 1925.
6. R. Autorino, J. A. Cadeddu, M. M. Desai, M. Gettman, I. S. Gill, L. R. Kavoussi, E. a. Lima, F. Montorsi, L. Richstone, J. U. Stolzenburg, and J. H. Kaouk. Laparoendoscopic single-site and natural orifice transluminal endoscopic surgery in urology: a critical analysis of the literature. *Eur. Urol.*, 59(1):26–45, Jan. 2011.
7. R. Autorino, J. H. Kaouk, J.-U. Stolzenburg, I. S. Gill, A. Mottrie, A. Tewari, and J. A. Cadeddu. Current status and future directions of robotic single-site surgery: a systematic review. *Eur. Urol.*, 63(2):266–280, Feb. 2013.
8. R. Autorino, F. J. Kim, A. Rane, M. De Sio, R. J. Stein, R. Damiano, S. Micali, J. Correia-Pinto, J. H. Kaouk, and E. Lima. Low-cost reusable instrumentation for laparoendoscopic single-site nephrectomy: assessment in a porcine model. *J. Endourol.*, 25(3):419–24, Mar. 2011.
9. A. Bajo, R. E. Goldman, L. Wang, D. Fowler, and N. Simaan. Integration and preliminary evaluation of an Insertable Robotic Effectors Platform for Single Port Access Surgery. In *2012 IEEE Int. Conf. Robot. Autom.*, pages 3381–3387. IEEE, May 2012.
10. J. Banks, J. S. C. II, B. L. Nelson, and D. M. Nicol. *Discrete-Event System Simulation (5th Edition).* Prentice Hall, 2009.
11. S. Bar-Meir. A new endoscopic simulator. *Endoscopy*, 32(11):898–900, Nov. 2000.
12. S. J. Bardaro and L. Swanström. Development of advanced endoscopes for Natural Orifice Transluminal Endoscopic Surgery (NOTES). *Minim. Invasive Ther. Allied Technol.*, 15(6):378–83, Jan. 2006.
13. C. Benmessaoud, H. Kharrazi, and K. F. MacDorman. Facilitators and barriers to adopting robotic-assisted surgery: contextualizing the unified theory of acceptance and use of technology. *PLoS One*, 6(1):e16395, Jan. 2011.

14. B. M. Bernheim. IV. Organoscopy: Cystoscopy of the Abdominal Cavity. *Ann. Surg.*, 53(6):764–7, June 1911.
15. Blender Foundation. Blender 2.65a. `www.blender.org`, Last Access: January 2013.
16. O. Bottema and B. Roth. *Theoretical Kinematics*. Dover Publications, 1979.
17. W. S. Boyle and G. E. Smith. Charge-coupled devices: A new approach to MIS device structures. *IEEE Spectr.*, 8(7):18–27, July 1971.
18. P. Bozzini. Lichtleiter, eine Erfindung zur Anschauung innerer Theile und Krankheiten nebst der Abbildung. *Hufelands neues J Pr. Heikd.*, 17:107–124, 1806.
19. A. W. Branco, A. J. Branco Filho, R. W. Noda, M. A. de George, A. H. L. A. de Camargo, and W. Kondo. New Minimally Invasive Surgical Approaches: Transvaginal and Transumbilical. *Brazilian J. Videoendoscopic Surg.*, 1(1):29–36, 2008.
20. R. Buckingham and A. Graham. Reaching the unreachable - Snake arm robots. In *Int. Symp. Robot.*, 2003.
21. Business Editors. Intuitive Surgical and IBM Corporation Jointly Sue Computer Motion for Patent Infringement. `http://www.thefreelibrary.com/Intuitive+Surgical+and+IBM+Corporation+Jointly+Sue+Computer+Motion...-a072736704`, Last access: October 2013.
22. J. Cadeddu, R. Fernandez, M. Desai, R. Bergs, C. Tracy, S.-J. Tang, P. Rao, M. Desai, and D. Scott. Novel magnetically guided intra-abdominal camera to facilitate laparoendoscopic single-site surgery: initial human experience. *Surg. Endosc.*, 23(8):1894–9, Aug. 2009.
23. S. Can, A. Fiolka, H. Mayer, A. Knoll, A. Schneider, D. Wilhelm, A. Meining, and H. Feussner. The mechatronic support system "HVSPS" and the way to NOTES. *Minim Invasive Ther Allied Technol*, 17(6):341–345, Jan. 2008.
24. R. S. Chamberlain and S. V. Sakpal. A comprehensive review of single-incision laparoscopic surgery (SILS) and natural orifice transluminal endoscopic surgery (NOTES) techniques for cholecystectomy. *J. Gastrointest. Surg.*, 13(9):1733–40, Sept. 2009.
25. S. Chiaverini. Singularity-robust task-priority redundancy resolution for real-time kinematic control of robot manipulators. *IEEE Trans. Robot. Autom.*, 13(3):398–410, June 1997.
26. G. Chirikjian. A continuum approach to hyper-redundant manipulator dynamics. In *Proc. 1993 IEEE/RSJ Int. Conf. Intell. Robot. Syst. (IROS '93)*, volume 2, pages 1059–1066. IEEE, 1993.
27. M. R. Cohen. Laparoscopy, Culdoscopy and Gynecography. Technique and Atlas. *Ann. Intern. Med.*, 74(1):156, Jan. 1971.
28. M. A. Cuesta, F. Berends, and A. A. F. A. Veenhof. The "invisible cholecystectomy": A transumbilical laparoscopic operation without a scar. *Surg. Endosc.*, 22(5):1211–3, May 2008.
29. P. G. Curcillo, S. A. King, E. R. Podolsky, and S. J. Rottman. Single Port Access (SPA) Minimal Access Surgery Through a Single Incision. *Surg. Technol. Int.*, 18:19–25, Apr. 2009.
30. B. Dallemagne, S. Perretta, P. Allemann, M. Asakuma, and J. Marescaux. Transgastric hybrid cholecystectomy. *Br. J. Surg.*, 96(10):1162–6, Oct. 2009.
31. P. Dario, R. Dillman, and H. I. Christensen. EURON Research Roadmaps - Key Area 1 on Research Coordinations. 2004.
32. A. Darzi, V. Datta, and S. Mackay. The challenge of objective assessment of surgical skill. *Am. J. Surg.*, 181(6):484–486, 2001.
33. V. Datta, S. Mackay, M. Mandalia, and A. Darzi. The use of electromagnetic motion tracking analysis to objectively measure open surgical skill in the laboratory-based model1 1No competing interests declared. *J. Am. Coll. Surg.*, 193(5):479–485, 2001.

34. V. Datta, M. Mandalia, S. Mackay, and A. Darzi. The PreOp flexible sigmoidoscopy trainer. Validation and early evaluation of a virtual reality based system. *Surg. Endosc.*, 16(10):1459–63, Oct. 2002.
35. B. L. Davies. A Discussion of Safety Issues for Medical Robots. In R. H. Taylor, S. Lavallée, G. Burdea, and R. Mosges, editors, *Comput. Surg. Technol. Clin. Appl.*, page 756. The MIT Press, 1996.
36. B. L. Davies, S. J. Harris, W. J. Lin, R. D. Hibberd, R. Middleton, and J. C. Cobb. Active compliance in robotic surgery - the use of force control as a dynamic constraint. *Proc. Inst. Mech. Eng. Part H J. Eng. Med.*, 211(4):285–292, Apr. 1997.
37. S. L. Delp, J. P. Loan, M. G. Hoy, F. E. Zajac, E. L. Topp, and J. M. Rosen. An interactive graphics-based model of the lower extremity to study orthopaedic surgical procedures. *IEEE Trans. Biomed. Eng.*, 37(8):757–67, Aug. 1990.
38. J. Denavit and R. Hartenberg. A kinematic notation for lower-pair mechanisms based on matrices. *Trans. ASME. J. Appl. Mech.*, 22:215 – 221, 1955.
39. P. Desbats, F. Geffard, G. Piolain, and A. Coudray. Force-feedback teleoperation of an industrial robot in a nuclear spent fuel reprocessing plant. *Ind. Robot An Int. J.*, 33(3):178–186, Jan. 2006.
40. P. W. Dhumane, M. Diana, J. Leroy, and J. Marescaux. Minimally invasive single-site surgery for the digestive system: A technological review. *J. Minim. Access Surg.*, 7(1):40–51, 2011.
41. B. Dickens and R. Cook. Legal and ethical issues in telemedicine and robotics. *Int. J. Gynecol. Obstet.*, 94(1):73–78, 2006.
42. Digia Plc. Qt Framework 4.7.1. `http://qt-project.org`, , Last access: September 2013.
43. A. Dolgert. .NET Wrappers for VTK 5. `vtkdotnet.sourceforge.net`, Last access: September 2013.
44. X. Dray and A. N. Kalloo. History of NOTES. In A. N. Kalloo, J. Marescaux, and R. Zorrón, editors, *Nat. Orifice Translumenal Endosc. Surg. Textb. Video Atlas*, chapter 1, page 328. Wiley-Blackwell, 2012.
45. B. J. Dunkin. Flexible Endoscopy Simulators. *Surg. Innov.*, 10(1):29–35, Mar. 2003.
46. G. Echeverria, N. Lassabe, A. Degroote, and S. Lemaignan. Modular open robots simulation engine: MORSE. In *2011 IEEE Int. Conf. Robot. Autom.*, pages 46–51. IEEE, May 2011.
47. A. Eickhoff, J. van Dam, R. Jakobs, V. Kudis, D. Hartmann, U. Damian, U. Weickert, D. Schilling, and J. F. Riemann. Computer-assisted colonoscopy (the NeoGuide Endoscopy System): results of the first human clinical trial ("PACE study"). *Am. J. Gastroenterol.*, 102(2):261–6, Feb. 2007.
48. M. Einhorn. *Diseases of the stomach*. William Wood and Company, 1903.
49. D. Eisenberg, E. Storne, and A. Belson. Use of a flexible robotic transgastric natural orifice translumenal endoscopic surgery (NOTES) platform in a cadaver to test access, navigation, maneuverability, and stability. *Surg. Endosc.*, 24(9):2323, Sept. 2010.
50. I. A. Emhoff, G. C. Lee, and P. Sylla. Transanal colorectal resection using natural orifice translumenal endoscopic surgery (NOTES). *Dig. Endosc.*, Aug. 2013.
51. Epic Games, Inc. Unreal Developer's Kit (UDK). `http://www.unrealengine.com/udk/`, Last access: October 2013.
52. Y. Fan, S.-D. Wu, and J. Kong. Single-port access transaxillary totally endoscopic thyroidectomy: a new approach for minimally invasive thyroid operation. *J. Laparoendosc. Adv. Surg. Tech. A*, 21(3):243–7, Apr. 2011.
53. FLS Program. Fundamental of Laparoscopic Surgery. `www.flsprogram.org`, Last access: September 2013.

54. Force Dimension. Haptic and Robotic SDKs. `http://forcedimension.com`, , Last access: September 2013.
55. M. Fourestier, A. Gladu, and J. Vulmiere. Perfectionnements à l'endoscopie médicale. Réalisation bronchoscopique. *Presse Med.*, 60:1292–1294, 1952.
56. N. K. Francis. The Performance of Master Surgeons on the Advanced Dundee Endoscopic Psychomotor Tester - Contrast Validity Study. *Arch. Surg.*, 137(7):841–844, July 2002.
57. R. J. Franzino. The Laprotek surgical system and the next generation of robotics. *Surg. Clin. North Am.*, 83(6):1317–20, Dec. 2003.
58. A. Fritscher-Ravens. Transgastric endoscopy–a new fashion, a new excitement! *Endoscopy*, 39(2):161–7, Feb. 2007.
59. K.-H. Fuchs and W. Breithaupt. Transgastric small bowel resection with the new multitasking platform EndoSAMURAI for natural orifice transluminal endoscopic surgery. *Surg. Endosc.*, 26(8):2281–7, Aug. 2012.
60. Game Physics Simulation. Bullet Physics Library. `http://bulletphysics.org/wordpress/`, Last access: September 2013.
61. F. V. Gassel. Design of a machine which rotates hoist elements around its vertical axis. In G. H. Watson, R. L. Tucker, and J. K. Walters, editors, *ISARC Proc.*, pages 277–284. Elsevier, 1993.
62. M. Gauthier and S. Regnier. *Robotic Micro-Assembly.* Wiley-IEEE Press, Oct. 2010.
63. G. P. Georghiou, M. Berman, V. Bobovnikov, B. A. Vidne, and M. Saute. Minimally invasive thoracoscopic sympathectomy for palmar hyperhidrosis via a transaxillary single-port approach. *Interact. Cardiovasc. Thorac. Surg.*, 3(3):437–41, Sept. 2004.
64. R. Goertz and R. Thompson. Electronically controlled manipulator. *Nucleonics*, 12(11):46–47, 1954.
65. O. Goetze. Ein neues Verfahren zur Gasfullung fur das Pneumoperitoneum. *Munich Med Wochenschr*, 51:233–236, 1921.
66. A. Gorden. The history and development of endoscopic surgery. In C. Sutton and M. P. Diamond, editors, *Endosc. Surg. Gynaecol.*, pages 3–7. London: WB Saunders, 1993.
67. G.-P. Haber, R. Autorino, H. Laydner, B. Yang, M. A. White, S. Hillyer, F. Altunrende, R. Khanna, G. Spana, I. Wahib, K. Fareed, R. J. Stein, and J. H. Kaouk. SPIDER surgical system for urologic procedures with laparoendoscopic single-site surgery: from initial laboratory experience to first clinical application. *Eur. Urol.*, 61(2):415–22, Feb. 2012.
68. A. Hackethal, J. Sucke, F. Oehmke, K. Münstedt, W. Padberg, and H.-R. Tinneberg. Establishing transvaginal NOTES for gynecological and surgical indications: benefits, limits, and patient experience. *Endoscopy*, 42(10):875–8, Oct. 2010.
69. H. Hanafusa, T. Yoshikawa, and Y. Nakamura. Analysis and control of articulated robot arms with redundancy. *Prepr. 8th Trienn. IFAC World Congr.*, 14:78–83, 1981.
70. M. W. Hannan and I. D. Walker. Kinematics and the Implementation of an Elephant's Trunk Manipulator and Other Continuum Style Robots. *J. Robot. Syst.*, 20:45–63, 2003.
71. A. Hassan-Zahraee, B. Herman, and J. Szewczyk. Mechatronic design of a handheld instrument with active trocar for laparoscopy. In *2011 IEEE Int. Conf. Robot. Autom.*, pages 1890–1895. IEEE, May 2011.
72. A. Hassan-Zahraee, J. K. Paik, J. Szewczyk, and G. Morel. Toward the Development of a Hand-Held Surgical Robot for Laparoscopy. *IEEE/ASME Trans. Mechatronics*, 15(6):853–861, Dec. 2010.

73. M. Hatzinger, K. Badawi, S. Langbein, and A. Häcker. The seminal contribution of Georg Kelling to laparoscopy. *J. Endourol.*, 19(10):1154–6, Dec. 2005.
74. V. H. Hausmann. Maximilian Nitze (1848-1906) Seine Bedeutung fiir die Entwicklung der Urologie. *Z Urol Nephrol*, 80:539, 1987.
75. J. Himpens, G. Leman, and G. B. Cadiere. Telesurgical laparoscopic cholecystectomy. *Surg. Endosc.*, 12(8):1091, Aug. 1998.
76. D. Hirano, S. Minei, K. Yamaguchi, T. Yoshikawa, T. Hachiya, T. Yoshida, H. Ishida, Y. Takimoto, T. Saitoh, S. Kiyotaki, and K. Okada. Retroperitoneoscopic adrenalectomy for adrenal tumors via a single large port. *J. Endourol.*, 19(7):788–92, Sept. 2005.
77. S. Hirose. *Biologically Inspired Robots: Snake-like Locomotors and Manipulators*. Oxford University Press, USA, 1993.
78. S. Hirose and M. Mori. Biologically Inspired Snake-like Robots. In *2004 IEEE Int. Conf. Robot. Biomimetics*, pages 1–7. IEEE, 2004.
79. B. I. Hirschowitz, L. E. Curtiss, C. W. Peters, and H. M. Pollard. Demonstration of a new gastroscope, the fiberscope. *Gastroenterology*, 35(1):50–53, July 1958.
80. K.-Y. Ho, S. J. Phee, A. Shabbir, S. C. Low, V. A. Huynh, A. P. Kencana, K. Yang, D. Lomanto, B. Y. J. So, Y. Y. J. Wong, and S. C. S. Chung. Endoscopic submucosal dissection of gastric lesions by using a Master and Slave Transluminal Endoscopic Robot (MASTER). *Gastrointest. Endosc.*, 72(3):593–9, Sept. 2010.
81. P. F. Hokayem and M. W. Spong. Bilateral teleoperation: An historical survey. *Automatica*, 42(12):2035–2057, Dec. 2006.
82. H. H. Hopkins. On the Diffraction Theory of Optical Images. *Proc. R. Soc. A Math. Phys. Eng. Sci.*, 217(1130):408–432, May 1953.
83. H. H. Hopkins and N. S. Kapani. A flexible fiberscope, using static scanning. *Nature*, 173:39–41, 1954.
84. R. D. Howe and Y. Matsuoka. Robotics for surgery. *Annu. Rev. Biomed. Eng.*, 1:211–40, Jan. 1999.
85. C.-K. Huang, J.-C. Tsai, C.-H. Lo, J.-Y. Houng, Y.-S. Chen, S.-C. Chi, and P.-H. Lee. Preliminary surgical results of single-incision transumbilical laparoscopic bariatric surgery. *Obes. Surg.*, 21(3):391–6, Mar. 2011.
86. J. Hugh. *Dynamic System Modeling and Control*. 2013.
87. H. C. Jacobaeus. Ueber die möglichkeit die zystoskopie bei untersuchung seröser höhlungen anzuwenden. *Munich Med Wochenschr*, 57:2090–2092, 1910.
88. H. C. Jacobaeus. Kurze übersicht über meine Erfahrungen der Laparo-Thorakoskopie. *Munich Med Wochenschr*, 58:2017–2019, 1911.
89. M. Jakopec, S. Harris, F. Rodriguez y Baena, P. Gomes, and B. Davies. Acrobot: a "hands-on" robot for total knee replacement surgery. In *7th Int. Work. Adv. Motion Control. Proc. (Cat. No.02TH8623)*, pages 116–120. IEEE, 2002.
90. B. A. Jones and I. D. Walker. Kinematics for multisection continuum robots. *IEEE Trans. Robot.*, 22(1):43–55, Feb. 2006.
91. H. Kalk. Indikationsstellung und Gefahrenmoment bei der Laparoskopie. *DMW - Dtsch. Medizinische Wochenschrift*, 61(46):1831–1833, Sept. 1935.
92. H. Kalk, W. Brühl, and W. Burgmann. *Leitfaden der Laparoskopie und Gastroskopie [Gebundene Ausgabe]*. Thieme Stuttgart, 1951.
93. H. O. Kalk. Erfafungen mit der laparoskopie. *Z Klin Med*, 111:303–348, 1929.
94. A. N. Kalloo, V. K. Singh, S. B. Jagannath, H. Niiyama, S. L. Hill, C. A. Vaughn, C. A. Magee, and S. V. Kantsevoy. Flexible transgastric peritoneoscopy: a novel approach to diagnostic and therapeutic interventions in the peritoneal cavity. *Gastrointest. Endosc.*, 60(1):114–7, July 2004.
95. P. Kanumuri, S. Ganai, E. M. Wohaibi, R. W. Bush, D. R. Grow, and N. E. Seymour. Virtual reality and computer-enhanced training devices equally improve laparoscopic surgical skill in novices. *JSLS*, 12(3):219–26, 2008.

96. G. Kelling. Ueber oesophagoskopie, gastroskopie un kolioscopie. *Munich Med Wochenschr*, 1:21–24, 1902.
97. P. A. Kenney, M. F. Wszolek, J. J. Gould, J. A. Libertino, and A. Moinzadeh. Face, Content, and Construct Validity of dV-Trainer, a Novel Virtual Reality Simulator for Robotic Surgery. *Urology*, 73(6):1288–1292, 2009.
98. Kitware Inc. Visualization Toolkit (VTK). `www.vtk.org`, Last access: September 2013.
99. Y. Kobayashi, Y. Tomono, Y. Sekiguchi, H. Watanabe, K. Toyoda, K. Konishi, M. Tomikawa, S. Ieiri, K. Tanoue, M. Hashizume, and M. G. Fujie. A surgical robot with vision field control for single port endoscopic surgery. *Int. J. Med. Robot.*, 6(4):454–64, Dec. 2010.
100. R. Korbsch. Die Laparoskopie Nach Jakobaeus. *Berl Klin Wochenschr*, 38:696–700, 1921.
101. S. V. Kotsis and K. C. Chung. Application of the "see one, do one, teach one" concept in surgical training. *Plast. Reconstr. Surg.*, 131(5):1194–201, May 2013.
102. D. M. Krpata and T. A. Ponsky. Instrumentation and equipment for single-site umbilical laparoscopic surgery. *Semin. Pediatr. Surg.*, 20(4):190–5, Nov. 2011.
103. Y. S. Kwoh, J. Hou, E. A. Jonckheere, and S. Hayati. A robot with improved absolute positioning accuracy for CT guided stereotactic brain surgery. *IEEE Trans. Biomed. Eng.*, 35(2):153–60, Mar. 1988.
104. D. Lawrence. Stability and transparency in bilateral teleoperation. *IEEE Trans. Robot. Autom.*, 9(5):624–637, 1993.
105. A. C. Lehman, N. A. Wood, S. Farritor, M. R. Goede, and D. Oleynikov. Dexterous miniature robot for advanced minimally invasive surgery. *Surg. Endosc.*, 25(1):119–23, Jan. 2011.
106. G. S. Litynski. *Highlights in the history of laparoscopy: the development of laparoscopic techniques– a cumulative effort of internists, gynecologists, and surgeons.* Barbara Bernert Verlag, 1996.
107. G. S. Litynski. Erich Mühe and the rejection of laparoscopic cholecystectomy (1985): a surgeon ahead of his time. *JSLS*, 2(4):341 – 6, 1998.
108. G. S. Litynski. Profiles in laparoscopy: Mouret, Dubois, and Perissat: the laparoscopic breakthrough in Europe (1987-1988). *JSLS*, 3(2):163–7, 1999.
109. A. Loeve, P. Breedveld, and J. Dankelman. Scopes too flexible...and too stiff. *IEEE Pulse*, 1(3):26–41, 2010.
110. V. Long and A. N. Kalloo. AccuTouch Endoscopy Simulator: development, applications and early experience. *Gastrointest. Endosc. Clin. N. Am.*, 16(3):479–87, July 2006.
111. A. A. Maciejewski and C. A. Klein. Obstacle Avoidance for Kinematically Redundant Manipulators in Dynamically Varying Environments. *Int. J. Rob. Res.*, 4(3):109–117, Sept. 1985.
112. A. J. Madhani, G. Niemeyer, and K. J. Salisbury. The Black Falcon: A Teleoperated Surgical Instrument for Minimally Invasive Surgery. In *IEEE/RSJ Int. Conf. Intell. Robot. Syst.*, volume 2, pages 936–944, 1998.
113. J. Marescaux, B. Dallemagne, S. Perretta, A. Wattiez, D. Mutter, and D. Coumaros. Surgery without scars: report of transluminal cholecystectomy in a human being. *Arch. Surg.*, 142(9):823–6; discussion 826–7, Sept. 2007.
114. J. Marescaux, J. Leroy, M. Gagner, F. Rubino, D. Mutter, M. Vix, S. E. Butner, and M. K. Smith. Transatlantic robot-assisted telesurgery. *Nature*, 413(6854):379–80, Sept. 2001.
115. J. A. Martin, G. Regehr, R. Reznick, H. MacRae, J. Murnaghan, C. Hutchinson, and M. Brown. Objective structured assessment of technical skill (OSATS) for surgical residents. *Br. J. Surg.*, 84(2):273–278, Feb. 1997.

116. Microsoft. XNA Game Studio. http://msdn.microsoft.com/it-it/library/bb200104%28v=xnagamestudio.40%29.aspx, Last access: October 2013.
117. J. Mikulicz-Radecki. Ueber Gastroskopie und Oesophagoskopie. *Verh Dtsch Ges Chir*, 10:81–85, 1882.
118. I. M. Modlin, M. Kidd, and K. D. Lye. From the lumen to the laparoscope. *Arch. Surg.*, 139(10):1110–26, Oct. 2004.
119. W. G. Mouton, J. R. Bessell, and G. J. Maddern. Looking back to the advent of modern endoscopy: 150th birthday of Maximilian Nitze. *World J. Surg.*, 22(12):1256–8, Dec. 1998.
120. M. T. Moyer, R. S. Haluck, J. Gopal, E. M. Pauli, and A. Mathew. Transgastric organ resection solely with the prototype R-scope and the self-approximating transluminal access technique. *Gastrointest. Endosc.*, 72(1):170–6, July 2010.
121. R. R. Mummadi and P. J. Pasricha. The eagle or the snake: platforms for NOTES and radical endoscopic therapy. *Gastrointest. Endosc. Clin. N. Am.*, 18(2):279–89; viii, Apr. 2008.
122. O. Nadeau and O. Kampmeier. Endoscopy of the abdomen; abdominoscopy. A preliminary study, including a summary of the literature and a description of the technique. *Surg Gynecol Obs.*, 41:259–271, 1925.
123. Y. Nakamura and H. Hanafusa. Inverse Kinematic Solutions With Singularity Robustness for Robot Manipulator Control. *J. Dyn. Syst. Meas. Control*, 108(3):163, Sept. 1986.
124. Natural Orifice Surgery Consortium for Assessment and Research (NOSCAR). White paper. www.noscar.org/resources/, Last access: September 2013.
125. H. Neuhaus, G. Costamagna, J. Devière, P. Fockens, T. Ponchon, and T. Rösch. Endoscopic submucosal dissection (ESD) of early neoplastic gastric lesions using a new double-channel endoscope (the "R-scope"). *Endoscopy*, 38(10):1016–23, Oct. 2006.
126. C. Nezhat. *Nezhat's History of Endoscopy: A Historical Analysis of Endoscopy's Ascension Since Antiquity*. CNezhatMD, 2011.
127. C. Nezhat, S. R. Crowgey, and C. P. Garrison. Surgical treatment of endometriosis via laser laparoscopy. *Fertil. Steril.*, 45(6):778–83, June 1986.
128. NICTA. Armadillo. http://arma.sourceforge.net, Last access: September 2013.
129. M. Nitze. Beobachtung-und Untersuchungsmethode fur Harnohre, Harnblase und Rectum. *Wien Med Wochenschr*, 29:649, 1879.
130. D. Oetomo, D. Daney, K. Harada, J.-P. Merlet, A. Menciassi, and P. Dario. Topology design of surgical reconfigurable robots by interval analysis. In *2009 IEEE Int. Conf. Robot. Autom.*, pages 3085–3090. IEEE, May 2009.
131. Open source project. Xenomai 2.6.0. http://www.xenomai.org, Last access: September 2013.
132. B. H. Orndoff. The peritoneoscope in diagnosis of diseases of the abdomen. *J Radiol*, 1:307–325, 1920.
133. T. Ota, A. Degani, D. Schwartzman, B. Zubiate, J. McGarvey, H. Choset, and M. A. Zenati. A highly articulated robotic surgical system for minimally invasive surgery. *Ann. Thorac. Surg.*, 87(4):1253–6, Apr. 2009.
134. W. K. Otis. Concerning the new electrocystoscope. *NY Med. J*, 1881:625–628, 1905.
135. N. Pappalepore, S. Tursini, N. Marino, G. Lisi, and P. Lelli Chiesa. Transumbilical laparoscopic-assisted appendectomy (TULAA): a safe and useful alternative for uncomplicated appendicitis. *Eur J Pediatr Surg*, 12(6):383–6, Dec. 2002.
136. S. Park, R. A. Bergs, R. Eberhart, L. Baker, R. Fernandez, and J. A. Cadeddu. Trocar-less instrumentation for laparoscopy: magnetic positioning of intra-abdominal camera and retractor. *Ann. Surg.*, 245(3):379–84, Mar. 2007.

137. L. E. Parker and J. V. Draper. Robotics applications in maintenance and repair. In S. Y. Nof, editor, *Handb. Ind. Robot.*, page 1378. Wiley, 2nd edition, 1998.
138. G. Petroni, M. Niccolini, A. Menciassi, P. Dario, and A. Cuschieri. A novel intracorporeal assembling robotic system for single-port laparoscopic surgery. *Surg. Endosc.*, 27(2):665–70, Feb. 2013.
139. S. J. Phee, S. C. Low, V. A. Huynh, A. P. Kencana, Z. L. Sun, and K. Yang. Master and slave transluminal endoscopic robot (MASTER) for natural orifice transluminal endoscopic surgery (NOTES). In *IEEE Int. Conf. Eng. Med. Biol. Soc. (EMBC), 2009*, pages 1192–1195, Jan. 2009.
140. R. Platteborse. [Laparoscopy, laparophotography, punch biopsy of the liver, gallbladder punch biopsy and collection of specimens of the peritoneal organs through a single trocar]. *Acta Gastroenterol. Belg.*, 24:696–700, Dec. 1961.
141. E. R. Podolsky, S. J. Rottman, H. Poblete, S. A. King, and P. G. Curcillo. Single port access (SPA) cholecystectomy: a completely transumbilical approach. *J. Laparoendosc. Adv. Surg. Tech. A*, 19(2):219–22, Apr. 2009.
142. J. D. Raman, K. Bensalah, A. Bagrodia, J. M. Stern, and J. A. Cadeddu. Laboratory and clinical development of single keyhole umbilical nephrectomy. *Urology*, 70(6):1039–42, Dec. 2007.
143. J. D. Raman, D. J. Scott, and J. A. Cadeddu. Role of magnetic anchors during laparoendoscopic single site surgery and NOTES. *J. Endourol.*, 23(5):781–6, May 2009.
144. A. Rané, P. Rao, and P. Rao. Single-port-access nephrectomy and other laparoscopic urologic procedures using a novel laparoscopic port (R-port). *Urology*, 72(2):260–3; discussion 263–4, Aug. 2008.
145. P. P. Rao, P. P. Rao, and S. Bhagwat. Single-incision laparoscopic surgery - current status and controversies. *J. Minim. Access Surg.*, 7(1):6–16, Jan. 2011.
146. P. Rather. Max Nitze (1848-1906). *Invest Urol*, 5:327, 1976.
147. N. Reddy and P. Rao. Per oral transgastric endoscopic appendectomy in human. In *45th Annu. Conf. Soc. Gastrointest. Endosc. India, Jaipur*, pages 28–29, 2004.
148. M. A. Reuter. *Reinhold H. Wappler and the American Cystoscope Makers, Inc.* Max Nitze Museum, 1996.
149. J. E. Rioux. Operative laparoscopy. *J. Reprod. Med.*, 10(5):249–55, May 1973.
150. C. M. Rivera-Serrano, P. Johnson, B. Zubiate, R. Kuenzler, H. Choset, M. Zenati, S. Tully, and U. Duvvuri. A transoral highly flexible robot. *Laryngoscope*, 122(5):1067–1071, May 2012.
151. G. Robinson and J. Davies. Continuum robots - a state of the art. In *Proc. 1999 IEEE Int. Conf. Robot. Autom.*, volume 4, pages 2849–2854. IEEE, 1999.
152. R. D. Rosin. History. In R. D. Rosin, editor, *Minimal Access Med. Surg. Princ. Tech.*, pages 1–9. Radcliffe Medical Press, Oxford, 1993.
153. S. Ross, A. Rosemurgy, M. Albrink, E. Choung, G. Dapri, S. Gallagher, J. Hernandez, S. Horgan, W. Kelley, M. Kia, J. Marks, J. Martinez, Y. Mintz, D. Oleynikov, A. Pryor, D. Rattner, H. Rivas, K. Roberts, E. Rubach, S. Schwaitzberg, L. Swanstrom, J. Sweeney, E. Wilson, H. Zemon, and N. Zundel. Consensus statement of the consortium for LESS cholecystectomy. *Surg. Endosc.*, 26(10):2711–6, Oct. 2012.
154. J. C. Ruddock. Peritoneoscopy. *West J Surg*, 42:392, 1934.
155. J. C. Ruddock. Peritoneoscopy. *Surg Gynecol Obs.*, 65:623–639, 1937.
156. J. C. Ruddock. Peritoneoscopy: a critical clinical review. *Surg Clin North Am*, 37(5):1249–1260, Oct. 1957.
157. R. M. Satava. Virtual reality surgical simulator. The first steps. *Surg. Endosc.*, 7(3):203–5, 1993.

158. R. M. Satava. Surgical robotics: the early chronicles: a personal historical perspective. *Surg. Laparosc. Endosc. percutaneous Tech.*, 12(1):6–16, Feb. 2002.
159. R. M. Satava. Historical Review of Surgical Simulation - A Personal Perspective. *World J. Surg.*, 32(2):141–8, Feb. 2008.
160. T. Schollmeyer, A. S. Soyinka, M. Schollmeyer, and I. Meinhold-Heerlein. Georg Kelling (1866-1945): the root of modern day minimal invasive surgery. A forgotten legend? *Arch. Gynecol. Obstet.*, 276(5):505–9, Nov. 2007.
161. I. Schwegler and R. Schlumpf. Single-trocar-access thoracoscopy for fully optical controlled routine chest drainage: a technical report and feasibility study. *Surg Laparosc Endosc Percutan Tech*, 10(6):387–90, Dec. 2000.
162. P. S. Ségalas. Description of an instrument for inspecting the urethra and bladder. *Lancet*, ii:603–604, 1826.
163. Y. Sekiguchi, Y. Kobayashi, H. Watanabe, Y. Tomono, T. Noguchi, Y. Takahashi, K. Toyoda, M. Uemura, S. Ieiri, T. Ohdaira, M. Tomikawa, M. Hashizume, and M. G. Fujie. In vivo experiments of a surgical robot with vision field control for Single Port Endoscopic Surgery. In *IEEE Int. Conf. Eng. Med. Biol. Soc. (EMBC), 2011*, volume 2011, pages 7045–7048, Jan. 2011.
164. J. Shah. Endoscopy through the ages. *BJU Int.*, 89(7):645–652, May 2002.
165. S. N. Shaikh and C. C. Thompson. Natural orifice translumenal surgery: Flexible platform review. *World J Gastrointest Surg*, 2(6):210–216, June 2010.
166. J. Shang, D. Noonan, C. Payne, J. Clark, M. Sodergren, A. Darzi, and G.-Z. Yang. An articulated universal joint based flexible access robot for minimally invasive surgery. In *2011 IEEE Int. Conf. Robot. Autom.*, pages 1147–1152. IEEE, May 2011.
167. J. Shang, C. J. Payne, J. Clark, D. P. Noonan, K.-W. Kwok, A. Darzi, and G.-Z. Yang. Design of a multitasking robotic platform with flexible arms and articulated head for Minimally Invasive Surgery. In *2012 IEEE/RSJ Int. Conf. Intell. Robot. Syst.*, pages 1988–1993. IEEE, Oct. 2012.
168. T. Sheridan. Telerobotics. *Automatica*, 25(4):487–507, July 1989.
169. W. R. Sherman and A. B. Craig. *Understanding Virtual Reality: Interface, Application, and Design (The Morgan Kaufmann Series in Computer Graphics)*. Morgan Kaufmann, 2002.
170. M. Shoham, M. Burman, E. Zehavi, L. Joskowicz, E. Batkilin, and Y. Kunicher. Bone-mounted miniature robot for surgical procedures: concept and clinical applications. *IEEE Trans. Robot. Autom.*, 19(5):893–901, Oct. 2003.
171. A. Shushan. How long does laparoscopic surgery really take? Lessons learned from 1000 operative laparoscopies. *Hum. Reprod.*, 14(1):39–43, Jan. 1999.
172. A. Singla, Y. Li, S. C. Ng, N. G. Csikesz, J. F. Tseng, and S. A. Shah. Is the growth in laparoscopic surgery reproducible with more complex procedures? *Surgery*, 146(2):367–374, 2009.
173. D. C. Smith, L. R. Donohue, and S. J. Waszak. A hospital review of advanced gynecologic endoscopic procedures. *Am. J. Obstet. Gynecol.*, 170(6):1635–40; discussion 1640–2, June 1994.
174. L. Soler. Réalité Virtuelle et Télérobotique: les révolutions chirurgicales à l'aube du XXIème siècle. In *2ème Journ. Inform. Imag. MEDICALE "Présent Avenir"*, Nancy, France, 2000.
175. L. Soler and J. Marescaux. Patient-specific surgical simulation. *World J. Surg.*, 32(2):208–12, Feb. 2008.
176. A. Soulas, J. M. Dubois de Montreynaud, R. J. Edwards, and A. Gladu. Bronchoscopy and Television. In *22nd Annu. Meet. Am. Coll. Chest Physicians, Chicago*, pages 580–584, 1955.

177. B. Stanberry. Telemedicine: barriers and opportunities in the 21st century. *J. Intern. Med.*, 247(6):615–628, June 2000.
178. N. Sugano. Computer-assisted orthopaedic surgery and robotic surgery in total hip arthroplasty. *Clin. Orthop. Surg.*, 5(1):1–9, Mar. 2013.
179. SurgRob Blog. Report on the historical Intuitive Surgical vs. Computer Motion case. `http://surgrob.blogspot.fr/2010/03/vintage-report-on-intuitive-vs-computer.html`, Last access: October 2013, 2010.
180. L. Swanström, P. Swain, and P. Denk. Development and validation of a new generation of flexible endoscope for NOTES. *Surg. Innov.*, 16(2):104–10, June 2009.
181. M. Tan, N. Prufer, N. Chinosornvatana, C. Park, and P. Woo. Application of natural orifice transluminal endoscopic surgery (NOTES) instrumentation to the endolarynx. *Ann. Otol. Rhinol. Laryngol.*, 121(7):435–41, July 2012.
182. S. Tanaka, S. Oka, I. Kaneko, M. Hirata, R. Mouri, H. Kanao, S. Yoshida, and K. Chayama. Endoscopic submucosal dissection for colorectal neoplasia: possibility of standardization. *Gastrointest. Endosc.*, 66(1):100–107, 2007.
183. R. H. Taylor. Robots as surgical assistants: Where we are, wither we are tending, and how to get there. In E. Keravnou, C. Garbay, R. Baud, and J. Wyatt, editors, *Artif. Intell. Med.*, volume Lecture No of *Lecture Notes in Computer Science*, pages 1–11, Berlin/Heidelberg, 1997. Springer-Verlag.
184. S. Tognarelli, M. Salerno, G. Tortora, C. Quaglia, P. Dario, and A. Menciassi. An endoluminal robotic platform for Minimally Invasive Surgery. In *2012 4th IEEE RAS EMBS Int. Conf. Biomed. Robot. Biomechatronics*, pages 7–12. IEEE, June 2012.
185. M. Tompsett, G. Amelio, W. Bertram, R. Buckley, W. McNamara, J. Mikkelsen, and D. Sealer. Charge-coupled imaging devices: Experimental results. *IEEE Trans. Electron Devices*, 18(11):992–996, Nov. 1971.
186. C. R. Tracy, J. D. Raman, J. A. Cadeddu, and A. Rane. Laparoendoscopic single-site surgery in urology: where have we been and where are we heading? *Nat. Clin. Pract. Urol.*, 5(10):561–8, Oct. 2008.
187. J. Troccaz, M. Peshkin, and B. Davies. Guiding systems for computer-assisted surgery: introducing synergistic devices and discussing the different approaches. *Med. Image Anal.*, 2(2):101–119, June 1998.
188. E. Udd. An overview of fiber-optic sensors. *Rev. Sci. Instrum.*, 66(8):4015, Aug. 1995.
189. T. Uji, T. Shirotokoro, and T. Hayashida. The gastrocamera. *Tokyo Med J*, 61:135–142, 1952.
190. Unity Technologies. Unity 3D. `http://www.unity3d.com`, Last access: October 2013.
191. V. T. Vasconcelos. *Blender 2.5 Character Animation Cookbook*. Packt Publishing Limited, 2011.
192. J. Veress. Neues Instrument zur Ausführung von Brust-oder Bauchpunktionen und Pneumothoraxbehandlung. *Deutsch Med Wochenschr*, 41:1480–1481, 1938.
193. V. Vitiello, S.-L. Lee, T. P. Cundy, and G.-Z. Yang. Emerging robotic platforms for minimally invasive surgery. *IEEE Rev. Biomed. Eng.*, 6(c):111–26, Jan. 2013.
194. D. von Ott. Illumination of the abdomen (ventroscopia). *J Akush Zhensk Boliez*, 15:1045–1049, 1901.
195. D. von Ott. Die direkte Beleuchtung der Bauchhole, der Harnblase, des Dickdarms und des Uterus zu diagnostiche Zwecken. *Rev Med Tcheq.*, 2:27–30, 1909.
196. I. D. Walker and M. W. Hannan. A novel 'elephant's trunk' robot. In *1999 IEEE/ASME Int. Conf. Adv. Intell. Mechatronics (Cat. No.99TH8399)*, pages 410–415. IEEE, 1999.

197. X. Wang and M. Meng. Robotics for Natural Orifice Transluminal Endoscopic Surgery: A Review. *J. Robot.*, 2012.
198. Y. Wang, D. R. Uecker, K. P. Laby, J. Wilson, S. Jordan, and J. Wright. Method and apparatus for performing minimally invasive cardiac procedures. Patent US6244809 B1, June 2001.
199. R. J. Webster and B. A. Jones. Design and Kinematic Modeling of Constant Curvature Continuum Robots: A Review. *Int. J. Rob. Res.*, 29(13):1661–1683, June 2010.
200. D. Whitney. Resolved Motion Rate Control of Manipulators and Human Prostheses. *IEEE Trans. Man Mach. Syst.*, 10(2):47–53, June 1969.
201. J. E. A. Wickham. The new surgery. *BMJ*, 295(6613):1581–1582, Dec. 1987.
202. M. S. Wilson, A. Middlebrook, C. Sutton, R. Stone, and R. F. McCloy. MIST VR: a virtual reality trainer for laparoscopic surgery assesses performance. *Ann. R. Coll. Surg. Engl.*, 79(6):403–4, Nov. 1997.
203. G. W. Yim, Y. W. Jung, J. Paek, S. H. Lee, H. Y. Kwon, E. J. Nam, S. Kim, J. H. Kim, Y. T. Kim, and S. W. Kim. Transumbilical single-port access versus conventional total laparoscopic hysterectomy: surgical outcomes. *Am. J. Obstet. Gynecol.*, 203(1):26.e1–6, July 2010.
204. Y. Yokokohji and T. Yoshikawa. Bilateral control of master-slave manipulators for ideal kinesthetic coupling-formulation and experiment. In *Proc. 1992 IEEE Int. Conf. Robot. Autom.*, pages 849–858. IEEE Comput. Soc. Press, 1992.
205. J. F. Zhu. Scarless endoscopic surgery: NOTES or TUES. *Surg. Endosc.*, 21(10):1898–9, Oct. 2007.
206. M. A. Zmuda, A. Elesev, and Y. T. Morton. Robot Localization Using RE and Inertial Sensors. In *2008 IEEE Natl. Aerosp. Electron. Conf.*, pages 343–348. IEEE, July 2008.
207. R. Zorron, M. Filgueiras, L. C. Maggioni, L. Pombo, G. Lopes Carvalho, and A. Lacerda Oliveira. NOTES. Transvaginal cholecystectomy: report of the first case. *Surg. Innov.*, 14(4):279–83, Dec. 2007.